ELECTRON TRANSFER THROUGH THE DNA DOUBLE HELIX:

SPECTROSCOPIC AND ELECTROCHEMICAL STUDIES

Thesis by

Shana O. Kelley

Submitted in Partial Fulfillment
of the Requirements
for the Degree of Doctor of Philosophy

California Institute of Technology

Pasadena, California

1999

(Submitted December 17, 1998)

ACKNOWLEDGEMENTS

There are so many people who provided essential intellectual and emotional support throughout my time at Caltech. I could not imagine a more supportive and enthusiastic mentor than my advisor, Jackie Barton. She gave me a well-balanced combination of intellectual freedom and guidance that helped me to develop creativity and high scientific standards. The fact that our work was perceived as controversial and not readily accepted often discouraged me, but Jackie always pulled important lessons out of difficult circumstances and pushed us to do better science. I had other important interactions with professors who I consider intellectual mentors, including the members of my thesis committee. In particular, being involved with the Laboratory of Molecular Sciences under the direction of Prof. Ahmed Zewail was a stimulating experience that I truly enjoyed. My undergraduate advisors, Prof. Rory Murphy and Prof. Jim Hanson, were also essential in my Caltech experience, as they steered me here and prepared me well to succeed. In addition, Prof. Matt Petersheim was an important figure in my undergraduate education - his excitement about chemistry stays with me to this day, despite his passing away one month ago.

Michelle Arkin, Eric Stemp, and Erik Holmlin all contributed to my development as a scientist by showing me the ropes as a young graduate student, and participating in countless discussions (about science and life) over the years. The excellence that they attained while at Caltech set an outstanding example for me to follow. In addition, past and present Barton group members have provided a pleasant environment in which to work. I would also like to thank the members of the BI community, including Bob Houser, Sonya Franklin, Christine Stinner, and Scott Carter for all their help over the years. Tom Wilhelm, Aaron Batista, Heather Maynard, and Christine were good friends who always supplied much-needed outside perspective through countless lunch outings. I also thank Torsten Fiebig - an important collaborator at LMS and a good friend.

My parents and stepparents, Mom, Russ, Dad, and Barbara, were always incredibly supportive. They believed in me even in times that I did not believe in myself, and through their unconditional love, I now have the same confidence in myself that they always seemed to have in me.

Last, but in no way least, I thank Michael for his support, love, and companionship. Our relationship is a source of great strength for me, and I am grateful everyday for the bond we share. Through road trips, long walks, the antics of his dancing cat and another truly obnoxious cat, he has helped me retain my sanity and humor through this process and has contributed joy and deep meaning to my life.

ABSTRACT

The DNA helix, containing a stacked array of aromatic base pairs, presents a novel medium in which electron transfer mediated by a molecular π-stack can be investigated. To probe electron transfer through DNA, we have constructed duplex assemblies modified with photo- and redox-active probes and applied spectroscopic and electrochemical approaches to the study of DNA-mediated charge transport.

Photoinduced electron transfer between intercalators was examined as a function of distance in a series of small DNA duplexes covalently modified with ethidium (Et) and $Rh(phi)_2bpy^{3+}$. At distances up to 35 Å, electron transfer occurs on the subnanosecond time scale ($k \gtrsim 10^{10}$ s^{-1}). In duplexes containing disruptive base mismatches, large decreases in electron-transfer yields are observed, confirming that the electron transfer pathway proceeds through the stacked base pairs. Hence, it was demonstrated for the first time that DNA-mediated electron transfer between intercalators is exceptionally efficient, only weakly dependent on distance, but highly sensitive to perturbations in base stacking.

To investigate a DNA base within the π-stack as a reactant, ethidium-modified duplexes containing the base analogue deazaguanine were synthesized. The photooxidation of deazaguanine by ethidium also proceeds on a subnanosecond time scale ($k \gtrsim 10^{10}$ s^{-1}) and exhibits a shallow distance dependence. The efficiency and overall distance dependence is sensitive to the stacking of deazaguanine as determined by flanking sequence. These studies again showed that the DNA base stack can mediate extremely fast, long-range charge transport, and further elucidated that stacking interactions are critical in modulating the efficiency of this phenomenon.

Using base-base photochemistry, electron transfer through DNA was probed directly without external donors and acceptors. Using fluorescent analogues of adenine that selectively oxidize guanine, electron transfer through the DNA π-stack was investigated as a function of reactant stacking and energetics. Small variations in each of these factors lead to remarkable changes in the kinetics of DNA-mediated electron transfer and values of β, a parameter reflecting the exponential dependence of electron transfer on

distance, were measured ranging from 0.1 Å^{-1} to 1.0 Å^{-1}. The DNA base stack was shown to exhibit insulator to "wire"-like properties, depending on the structure and energetics of reactants employed to probe this medium.

To investigate DNA-mediated electron transfer using electrochemical methods, we assembled DNA films and incorporated intercalating redox-active molecules into the monolayers. Surface characterization techniques were employed to determine the orientation of the DNA helices within the films. With the intercalator daunomycin crosslinked to DNA duplexes immobilized on gold, efficient electron transfer over distances greater than 30 Å was observed. Base mismatches also attenuate this long-range reaction, providing a new method for the electrochemical detection of genomic mutations.

These studies have provided essential measurements of electron transfer in DNA over known, fixed distances. It is now apparent that stacking interactions modulate the efficiency of this phenomenon, an observation that may explain the range of conflicting results reported within this field. Moreover, as experimental evidence increasingly supports the notion that ultrafast charge transport can occur through the DNA helix over long distances, the implications for biological systems can now be considered. Our findings point to the DNA π-stack as not only a carrier of genetic information, but also a pathway which is conducive to charge transport.

TABLE OF CONTENTS

LIST OF FIGURES

Chapter 3

Chapter 4

Chapter 5

Chapter 6

LIST OF TABLES

Chapter 1

Electron Transfer Through the DNA Helix[‡]

1.1 Introduction

Electron transfer constitutes one of the most fundamental types of chemical reactions, and is a ubiquitous mechanism driving biological function. Redox reactions within proteins facilitate essential physiological processes including energy production and oxygen metabolism. Electron transfer within nucleic acids is much more destructive, as redox reactions of the DNA bases with radical species generated by radiation, carcinogens, or oxidative stress can lead to mutagenic damage.[1] Therefore, as the fidelity of the genetic code can potentially be disrupted by redox reactions occurring within DNA, the efficiency and dynamics of radical transport through this medium hold profound biological implications.

The presence of an extended, π-stacked arrangement of base pairs at the core of the essential genetic material is intriguing. Structurally similar solid-state materials are conductive when oxidatively doped.[2] However, double helical nucleic acids may be a unique example of a *molecular* π-stacked array. Although electron-transfer reactions through the σ-bonded matrices found in proteins have been extensively investigated both experimentally and theoretically,[3-4] this phenomenon has not been characterized in detail for π-stacked media. Hence, the DNA double helix, structurally well-characterized and synthetically accessible, may represent a valuable medium in which to study the migration of radicals from a fundamental perspective.

This introductory chapter will outline the relevance of DNA-mediated charge transport to biological function, and will describe the previous and present efforts of researchers investigating this phenomenon. As studies of electron transfer within DNA at the molecular level have provided conflicting assessments of the ability of the DNA base stack to facilitate charge transport,[5-48] it is important to review all available data, so that the conclusions presented within this thesis may be considered in terms of mechanisms that not only explain the results obtained in each system, but also address
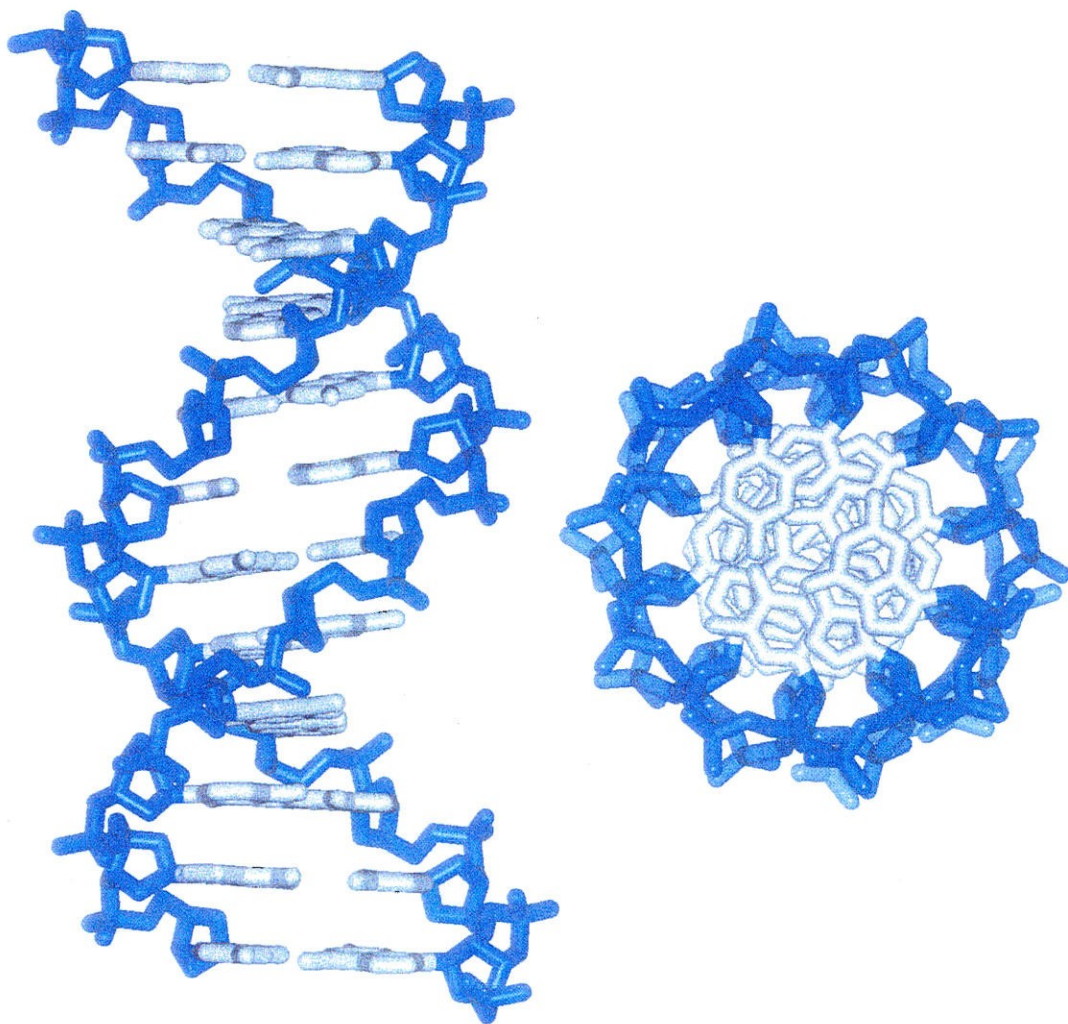
Figure 1.1 Structure of the DNA double helix.

the many differing results obtained by various researchers. In particular, this thesis focuses on experiments employing probes intercalated or stacked within the double helix of DNA. Stacking, both among the DNA bases and between reactants and the DNA bases, is identified throughout studies of diverse systems as a key parameter dictating the efficiency of this phenomenon. As such, discussions of the role of reactant and base stacking are interwoven throughout the descriptions of past and present studies in this field as a means of understanding this body of work as a whole.

1.2 Electron transfer in DNA: relevance to biological function and biosensing

Within the cell, reactive oxygen species and other radicals are byproducts of normal aerobic metabolism. In addition, reactive free radicals can be generated by ionizing radiation or chemical agents. These radicals can change the chemical composition and hence the identity of the DNA bases, leading to pathogenic mutations. Oxidative damage is increasingly recognized as a molecular mechanism contributing to debilitating human diseases and aging.[5-6] Indeed, highly elevated levels of 8-oxo-guanine, a lesion produced by the oxidation of guanine, have been detected in the DNA of patients with Alzheimer's disease, Parkinson's disease, Huntington's disease and other neurodegenerative conditions.[5] Moreover, the "free radical theory of aging" suggests that the accumulation of oxidative damage incurred through normal physiological function drives the aging process.[6] The efficiency of charge migration may therefore determine whether redox-initiated base damage is ultimately a localized event, or can be promoted across long distances. Hence, the electronic structure of the DNA helix may therefore be intimately linked to the ability of this molecule to accurately store genetic information and supply the instructions necessary for healthy cellular function.

There are other interesting observations that may relate the electronic structure of DNA to the biological roles of this material. Redox-active transcription factors can be activated through electron-transfer reactions,[7] and the DNA–binding properties of numerous proteins involved in tumor suppression are modulated by redox reactions.[8] Moreover, DNA-cleavage reactions of many anticancer drugs are triggered by cellular reductants,[9] while some chemotherapeutics must be introduced into the cell in a specific oxidation state for maximum efficacy.[10] Although relationships between these functional mechanisms and any long-range electron transfer events mediated by DNA are purely speculative at this juncture, they provide intriguing motives for the investigation of charge-transport phenomena within the double helix.

Besides the biological ramifications and fundamental implications of DNA-mediated electron-transfer reactions, this chemistry may have great utility in DNA-based biosensors. If this sensitivity of charge transfer to changes in DNA sequences and structure can be systematically evaluated, a new means to assay the genetic information within the double helix may be developed. As links between genetic makeup and disease are increasingly elucidated, new highly-sensitive methods will be required for the routine diagnosis of DNA-based disorders.

Hence, using a chemical approach, fundamental questions concerning charge migration through DNA can be addressed. Does radical migration through DNA occur over long molecular distances? How is it modulated by DNA sequence and the structural variations in DNA? Is it physiologically important? How general is this phenomenon? These are issues that need to be addressed in the context of delineating mechanisms of DNA damage and to form an understanding of π-stacked media as electron-transfer pathways.

1.3 Structural and electronic properties of DNA

The discovery of the double-helical structure of DNA (Figure 1.1) by Watson and Crick in 1953[49] provided a structural basis for the role of this molecule as the genetic material. From that point forward, the three-dimensional structure of DNA has been investigated extensively as an ordered array of functional groups encoding information vital for cellular function. Besides providing a scaffolding for molecular handles involved in recognition, the arrangement of the DNA bases within the double helix presents an interesting structure with respect to the electronic properties of this material: a π-stacked array. The interplanar distance, 3.4 Å, is close to that of stacked solids (*i.e.,* graphite) known to mediate significant levels of conductivity.[50]

Indeed, the stacking interactions between adjacent base steps represent a force essential to the formation of the double helix.[51] The existence of interactions among the stacked bases is evident from the spectral properties of DNA. The nucleic acid bases within the intact double helix absorb at least 30% less light than when present as monomers or in denatured polymers. This effect is attributed to hypochromism, a result of dipole interactions among interacting chromophores.[51] The hypochromism of the stacked bases has been used extensively to monitor the thermodynamic properties of nucleic acids.

The extended π-stack of aromatic heterocycles within the DNA helix attracted the interest of chemists, biologists, and physicists soon after the discovery of this unique structure. However, as described in the following section, researchers within each of these disciplines have obtained many seemingly contradictory results, impeding the formation of a definitive picture with respect to the efficiency of DNA-mediated charge transport.

1.4 Charge transport in DNA: biological and chemical history

Early experiments: DNA conductivity. The first glimpse of the structure of DNA prompted an almost immediate flurry of experimentation to determine whether the array of π-stacked bases within the double helix had the same capabilities for electron conduction as one-dimensional aromatic crystals.[52] The first experiments addressing this issue relied on the measurement of the bulk conductivity and photoelectric effects in DNA (Figure 1.2A). In 1961, Eley and Spivey measured the d.c. conductivity of dry DNA, observed high levels of electron mobility, and predicted that anisotropic effects would be observed if single-fiber measurements could be made.[11] However, a variety of subsequent studies by other researchers both supported and disputed these conclusions. Liang and Scalo concluded in 1964 that the observed conduction resulted from electrons associated with impurities,[12] while Snart provided evidence for conduction involving the π-electrons of the DNA bases in 1968 by correlating photocurrent profiles with the absorption properties of the bases.[13] These early experiments provided some intriguing evidence that DNA could facilitate significant levels of charge transport, but the difficulties of obtaining reliable results from poorly-defined samples of DNA in an experiment where the response can be influenced by different mechanisms of charge transport certainly impeded the formation of definitive conclusions. Nonetheless, the early efforts of chemists drawn to this problem only by the unique structural features of the double helix highlight the historical origin of the exploration of charge migration phenomena in nucleic acids.

Pulse radiolysis studies. The next generation of experiments addressing charge migration in nucleic acids relied on pulse radiolysis (Figure 1.2B).[14-20] By monitoring the migration of radical species generated by ionizing radiation (either within DNA directly or in aqueous solution, *e.g.,* OH˙, hydrated electrons, SO_4˙⁻, and COO˙⁻), the fate of radicals within the DNA helix could be determined, and DNA damage inflicted from

8
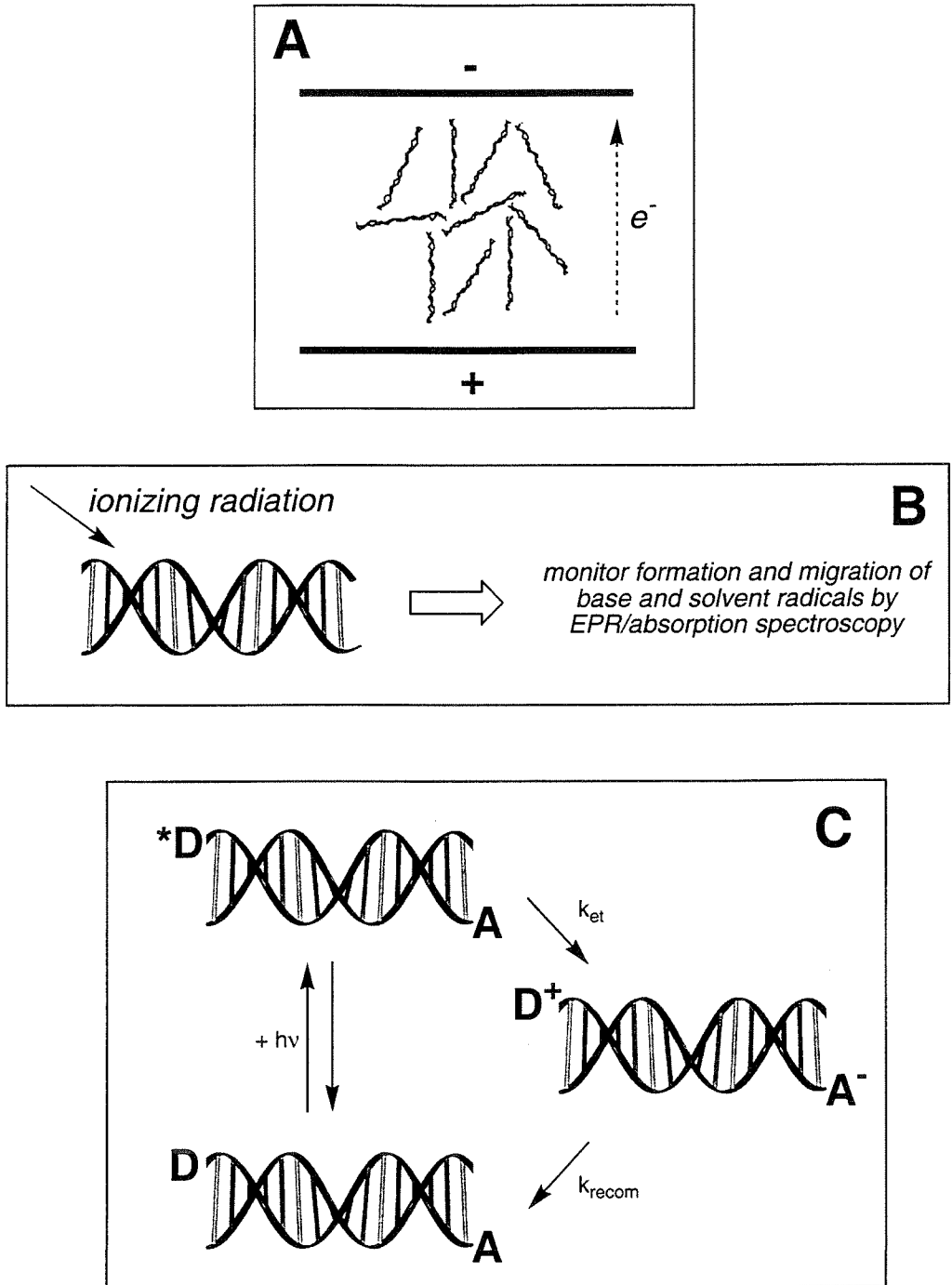
Figure 1.2 Experimental approaches addressing charge transport through DNA.
(**A**) bulk conductivity measurements; (**B**) pulse radiolysis; (**C**) photoinduced
electron transfer between DNA bound donors (D) and acceptors (A).

this source could be assessed. Based on pulse radiolysis studies, estimates have been made that radicals can travel anywhere from 1-200 base pairs within DNA. In 1970, Gregoli *et al.* monitored the EPR spectrum of proflavine bound to irradiated DNA and concluded that radical migration was feasible over 50 base pairs in freeze-dried DNA samples.[15] However, a subsequent study by Whillans where absorption spectroscopy was used to monitor this same system in aqueous solution prompted the conclusion that 5 base pairs was a "firm upper limit" for the migration of electrons.[16] The debate concerning migration distances has continued through the four decades since these initial measurements,[17-19] with various researchers obtaining different estimates of the efficiency of this process in DNA. A variety of experimental conditions have been employed, and it is not clear how best to reconcile the range of distance limits obtained. However, many of the studies employing intercalators as spin traps have produced data consistent with charge migration over > 25 Å. [15,18-19] In addition, electron-spin resonance measurements specifically monitoring the reduced form of the intercalating antitumor agent daunomycin provided evidence for the disproportionation of this radical over 100 base pairs.[20]

Studies of photoinduced electron transfer. Most recently, chemists have focused their efforts on studying photoinduced electron-transfer events between donors and acceptors bound to DNA (Figure 1.2C).[21-33] The ability to probe discrete reactions between molecular reactants bound to DNA in solution provides a powerful means to assess the electronic coupling provided by the DNA helix. Analyzed within the theoretical framework outlined by Marcus,[4] experimental studies of photoinduced electron transfer reactions in different media have provided essential measurements of electronic coupling in proteins and synthetic model systems.[3] Marcus theory predicts that electron-transfer rates should reflect variations in nuclear parameters, the free

energy differential between reactants and products, and the electronic coupling provided by the medium intervening between donor and acceptor as follows:

$$k_{et} = \left(\sqrt{\frac{4\pi^3}{h^2 \lambda k_B T}} \right) H_{AB}^2 \, e^{-\left(\frac{\Delta G^*}{RT} \right)}$$
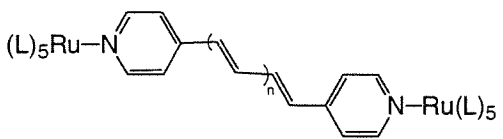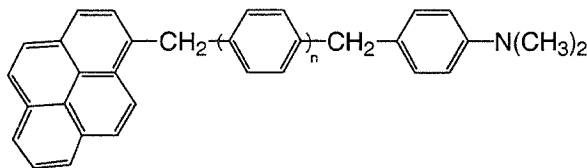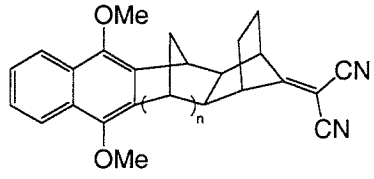
$$H_{AB}^2 \propto e^{-\beta r}$$

$$k_{et} = k_{et}^o \, e^{-\beta r}$$

where λ is the reorganizational energy of the donor, acceptor, and solvent, H_{AB} is the matrix coupling element, and ΔG^* is the free energy of activation. According to this model, electronic coupling (as dictated by wavefunction overlap) decays exponentially with distance (r) as described by the parameter β. Therefore, the nature of a particular medium as a bridge for electron transfer is typically investigated through the measurement of reaction kinetics as a function of distance, and described by a characteristic β value. Using this approach, β values of $\sim 0.8 - 1.2$ Å^{-1} have been measured for σ-bonded pathways in proteins and organic molecules, and increased levels of coupling are observed in conjugated systems, with $\beta \leq 0.2$ Å^{-1} (Table 1.1).[4] In most media, various independent measurements of this parameter are comparable. However, attempts to determine the value of β in DNA have produced a surprisingly wide range of results, with measurements of this parameter varying by a full order of magnitude (Table 1.2).
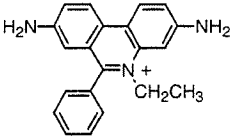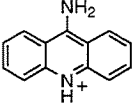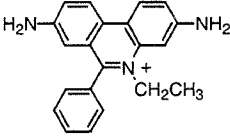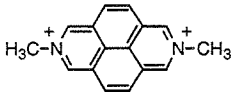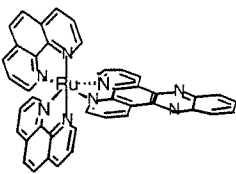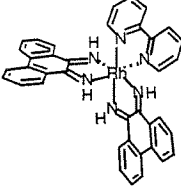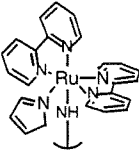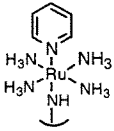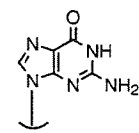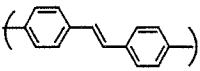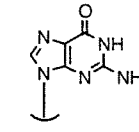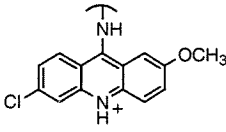
In designing systems for the study of DNA-mediated photoinduced electron transfer reactions, small molecules binding to DNA in a variety of ways depending on their structural properties are available. Studies using molecular probes have taken advantage of molecules which bind to DNA through electrostatic association with the anionic phosphate backbone, hydrophobic interaction with the grooves of the helix, or via intercalation of a planar, aromatic, heterocyclic moiety between the DNA bases

Table 1.1 Values of β in σ-bonded and conjugated systems[a]

	β
(L)$_5$Ru—N⟨pyridine⟩(CH=CH)$_n$⟨pyridine⟩N—Ru(L)$_5$	**0.14 Å^{-1}**
pyrene—CH$_2$(C$_6$H$_4$)$_n$CH$_2$—C$_6$H$_4$—N(CH$_3$)$_2$	**0.50 Å^{-1}**
OMe...(CN)$_2$ structure	**0.85 Å^{-1}**
myoglobin	**0.8 - 0.9 Å^{-1}**

[a]adapted from reference 4.

Table 1.2 Studies of photoinduced electron transfer in DNA

Donor	Acceptor	Observations	ref.
H_2N ... NH_2 ; N+ ; CH_2CH_3	NH_2 ; N+ H	Rapid, sequence-dependent electron transfer at low donor/acceptor loadings (noncovalently bound reactants)	21
H_2N ... NH_2 ; N+ ; CH_2CH_3	H_3C-N+ ... N+$-CH_3$	Slower, distance dependent electron transfer $\beta \sim 1\ \text{Å}^{-1}$ (noncovalently bound reactants)	23
(Ru complex structure)	(Rh complex structure)	Fast electron transfer at low donor/acceptor loadings; sensitive to reactant chirality (noncovalently bound reactants)	29,31
		Efficient electron transfer over 40 Å $\beta \leq 0.2\ \text{Å}^{-1}$ (covalently bound reactants)	30
(Ru complex structure)	H_3N, H_3N Ru NH_3, NH_3, NH	Slower "protein-like" electron transfer (covalently bound reactants)	25
(guanine structure) O, N, NH, N, NH_2	( )$_n$ stilbene structure	Distance-dependent electron transfer $\beta = 0.6\ \text{Å}^{-1}$ (covalently bound reactants)	24
(guanine structure) O, N, NH, N, NH_2	NH ; OCH_3 ; Cl ; N+ H	Highly distance-dependent electron transfer $\beta = 1.4\ \text{Å}^{-1}$ (covalently bound reactants)	26
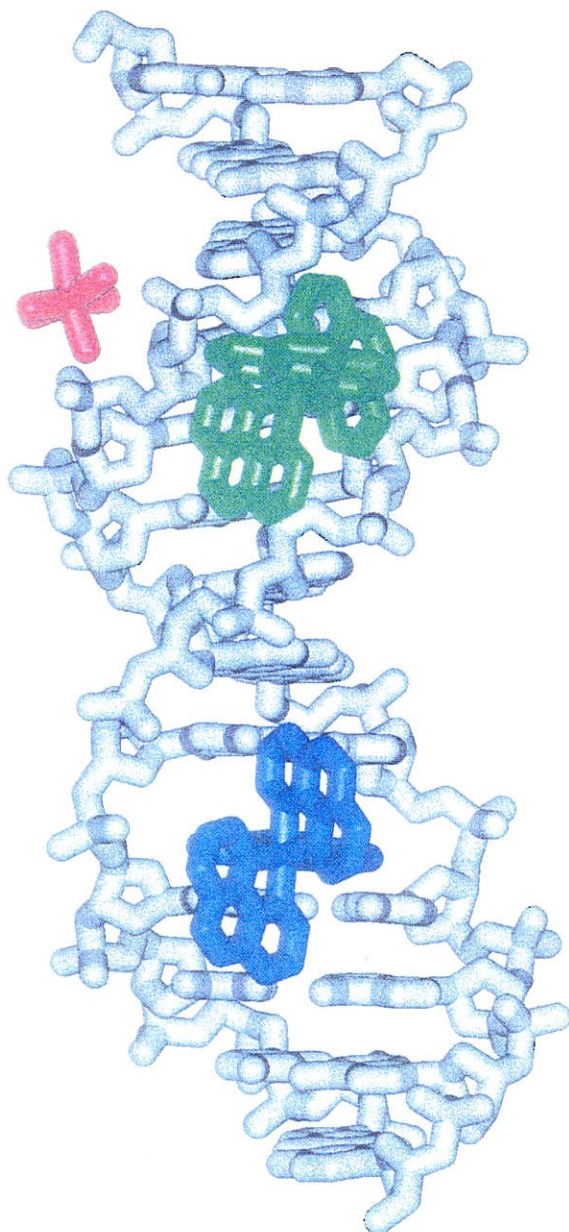
Figure 1.3 Illustration of small molecule-DNA binding interactions: intercalation of Ru(phen)$_2$dppz^{2+} (blue), groove-binding of Ru(phen)$_3$$^{2+}$ (green), and electrostatic binding of Ru(NH$_3$)$_6$$^{3+}$.

which entails electrostatic, hydrophobic, and dipolar interactions (Figure 1.3). Many DNA-binding molecules are both positively charged and contain hydrophobic or aromatic functionalities, so a mixture of these binding modes may also prevail under a given set of conditions.

One of the first studies of photoinduced electron transfer through DNA employed ethidium (Et), a classical organic intercalator, as an electron donor, and acridine antitumor drugs as acceptors.[21] Efficient quenching of the fluorescent singlet excited state of ethidium was observed, presumably due to reduction of the excited chromophore by the acceptors. This reaction appeared to take place on a time scale that precluded diffusional contact, and gave perhaps the first indication that intercalated species were afforded strong electronic coupling through the base stack. In a different study where the groove-binding acceptor methyl viologen was utilized in conjunction with this same donor,[22] rates of electron transfer representing an enhancement over those in the absence of DNA were obtained. However, for this set of reactants, the time scale of this quenching reaction was slower than that observed with intercalating acridine acceptors, indicating that diffusional contact was involved in the quenching reaction with the more mobile viologen acceptor.

At about this time, our laboratory was investigating the relationship between the structural features and the DNA-binding properties of small transition metal complexes of the formula $M(phen)_3^{2+}$ (M=Ru, Co, Rh, Cr). In the course of these studies, it was discovered that the presence of DNA greatly accelerated the quenching reaction between these complexes.[27-28] Since the architecture of these molecules allows both intercalation and binding to the surface of the DNA grooves, there were also diffusional components in the quenching profiles. In order to assess selectively the role of the DNA helix in modulating electronic coupling between intercalated species, a new family of probes was required.

The metallointercalators $Ru(phen)_2dppz^{2+}$ and $Rh(phi)_2bpy^{3+}$ represented the next generation of coordination complexes employed to study the DNA base stack as a medium for electron transfer.[29-33] These molecules exhibit large DNA binding constants ($K \geq 10^6$ M^{-1}), and highly favor intercalative binding.[53-54] Moreover, the MLCT excited state of $Ru(phen)_2dppz^{2+}$, localized on the intercalated dppz ligand, is energetically suited (E^o ($Ru^{3+}/*Ru^{2+}$) = -0.6 V) to undergo electron transfer with $Rh(phi)_2bpy^{3+}$, which features a low potential reduction (E^o (Rh^{3+}/Rh^{2+}) = +0.03 V) localized on the intercalated phi ligand.[29] The spectroscopic properties of this pair and the donor analogue $Os(phen)_2dppz^{2+}$ also provide handles for the characterization of charge-separated intermediates during the electron transfer and the monitoring of reaction dynamics *via* transient absorption.[31-32]

Indeed, remarkably fast electron-transfer kinetics ($k_{et} \geq 10^{10}$ s^{-1}) at dilute donor/acceptor loadings (1 (Ru(II)/Rh(III))/50 bp) have been observed for this reactant pair in the presence of calf thymus (CT) DNA.[31] In addition, the reaction is extremely sensitive to the interaction of these molecules with the DNA base stack. Much lower efficiencies were measured for Λ-enantiomers, presumably due to poorer intercalation for complexes with chiralities that are not complementary to right-handed DNA. Surprisingly, the reaction kinetics monitored *via* transient absorption were not affected by variations in the loading of the intercalators, and hence appear to be remarkably insensitive to distance. It was subsequently suggested that this insensitivity does not reflect the ability of the DNA base stack to mediate long-range electron transfer, but instead reflects a cooperative clustering between the intercalators.[54-55] Although theoretical modeling of the quenching data in terms of cooperative binding was put forth and putative experimental support for this mechanism was obtained by monitoring perturbations in the circular dichroism spectra of the intercalated complexes, the sensitivity of the reaction kinetics for electron transfer between $Ru(phen)_2dppz^{2+}$ and

$Rh(phi)_2bpy^{3+}$ to sequence and donor/acceptor chirality was still inconsistent with this model. Moreover, a recent reinvestigation of these circular dichroism experiments and an NMR study of the intercalated complexes revealed no indication of cooperative binding and instead confirmed the reasonable expectation that the preferred arrangement of these cationic metal complexes on a DNA helix was one in which the complexes were spatially separated.[56] It appears then that the ultrafast electron transfer kinetics observed in this system actually reflect efficient charge transport through the DNA base stack over long molecular distances.

During the course of these investigations, electron transfer across a fixed distance was also studied in a 15-mer DNA duplex with derivatives of the metallointercalators $Ru(phen)_2dppz^{2+}$ and $Rh(phi)_2phen^{3+}$ attached to the 5' termini of complementary strands.[30] In this system, the luminescence of $Ru(phen)_2dppz^{2+}$ was quantitatively quenched on a subnanosecond time scale in the presence of the acceptor located 40 Å down the helix. Here, where the locations of the reactants were indisputable, results consistent with long-range electron transfer were again observed between these two intercalators.

Substantially different conclusions about DNA as an electron-transfer medium have been drawn from other systems that would appear to be quite similar in design. For instance, where the intercalator ethidium was used as a photoreductant in the presence of DAP (DAP = N,N'-dimethyl-2,7-diazapyrenium dichloride), electron transfer rates of $\sim 10^6$-10^8 s^{-1} were measured at high intercalator loadings where donor/acceptor distances were estimated from a nonrandom binding distribution as 10-17 Å.[23] Although the reactant separations were not well-known, a value for β was reported as 1 Å^{-1}. This value indicates a significantly greater sensitivity to distance than the intercalator systems described above. Since ethidium was previously observed to undergo much more efficient electron transfer with the intercalated acridine acceptors

mentioned previously, it is possible that the binding mode of the DAP acceptor used in this study, which may be a combination of weak intercalation and groove binding, precludes fast reaction dynamics because of poor intercalation into the base stack.

Slower electron-transfer kinetics and steeper distance dependences have also been observed in other systems with reactants bound at fixed positions. In an octamer duplex modified with two transition metal complexes through σ-linkages, an electron-transfer rate constant of 10^6 s^{-1} was measured over a ~ 20 Å through-space separation,[25] indicating a much steeper dependence on distance than was observed in any of the previously described systems with intercalated probes. In a series of stilbene-bridged DNA hairpins, the electron-transfer kinetics for the oxidation of guanine by this chromophore ranged from 10^{12} s^{-1} at a donor/acceptor separation of 3.4 Å to 10^8 s^{-1} at a distance of 17 Å, and a value of $\beta = 0.6$ Å^{-1} was calculated.[24] Furthermore, recent studies of electron-transfer between acridine covalently bound to the DNA backbone and guanine report a value for β even greater than that observed in σ-bonded systems ($\beta = 1.4$ Å^{-1}).[26]

Although all of the systems have sought to obtain information on electron transport through the same DNA medium, it is remarkable that such different evaluations have been put forth. Clearly, from the very broad range of experimental results obtained, it is evident that other parameters besides distance must also affect electron transfer through the DNA helix. In addition, as summarized in Table 1.2, a variety of systems have been used to explore the efficiency of DNA-mediated charge transport, but very few of the assemblies are chemically well-defined. The systematic variation of structural and energetic factors may ultimately reconcile these apparently conflicting results.

Long-range base damage and repair. As the electron-transfer reactions involving DNA that are proposed to occur in the biological milieu result in the

formation of irreversible base damage, the possibility of long-range oxidative damage has been explored with intercalating oxidants.[57] In addition, a particularly prevalent lesion, the thymine dimer, is not only formed but can be repaired by electron transfer *in vivo*.[58] The investigation of the role of long-range charge transport in these reactions therefore has direct relevance to mechanisms of carcinogenesis and mutagenesis.

Guanine is the most easily oxidized DNA base ($E^\circ \sim +1.3$ V versus NHE), and is presumed to be the primary target for oxidative damage in the cell.[57] Many investigations of base damage *in vitro* have confirmed this expectation.[59-62] In fact both theoretical[62] and empirical[59-61] studies have uncovered the fact that 5'-GG-3' doublets are preferentially oxidized, with damage concentrated at the 5'-G of the pair.

Complexes of Rh(III) containing phi ligands have been employed extensively in our laboratory as structural probes of nucleic acids and have been utilized in designing strategies for the recognition of specific base sequences.[54] These complexes intercalate from the major groove of the double helix using the phi ligand and display very high affinity for B-form DNA. The position and extent of binding can be easily assayed for these complexes, as their photochemical properties lead to strand scission upon irradiation at wavelengths in the near-ultraviolet region.[63] Perhaps, of greater interest in this context, $Rh(phi)_2bpy^{3+}$ has been shown not only to promote direct strand scission upon photolysis at 313 nm but also to oxidize guanine bases when irradiated at 365 nm.[64] This rhodium complex is a potent photooxidant, with an excited state reduction potential ($E(Rh^{3+*}/Rh^{2+})$) of ~ 2.0 V vs. NHE, and hence can inflict permanent damage at guanine sites as shown in Figure 1.4. Because both position of intercalation and site of oxidation can be probed in discrete photochemical reactions using this complex, this intercalator could be harnessed as an ideal probe of long-range base oxidation in DNA.

$$\{GG, {}^*Rh^{3+}\} \xrightarrow{k_{et}} \{GG^+, Rh^{2+}\}$$

{GG, *Rh^{3+}}

k_{et}

hv k_d

{GG$^+$, Rh^{2+}}

chemical modification
of guanine

k_{back} O$_2$

{GG, Rh^{3+}}

{GG^{Ox}, Rh^{2+}}
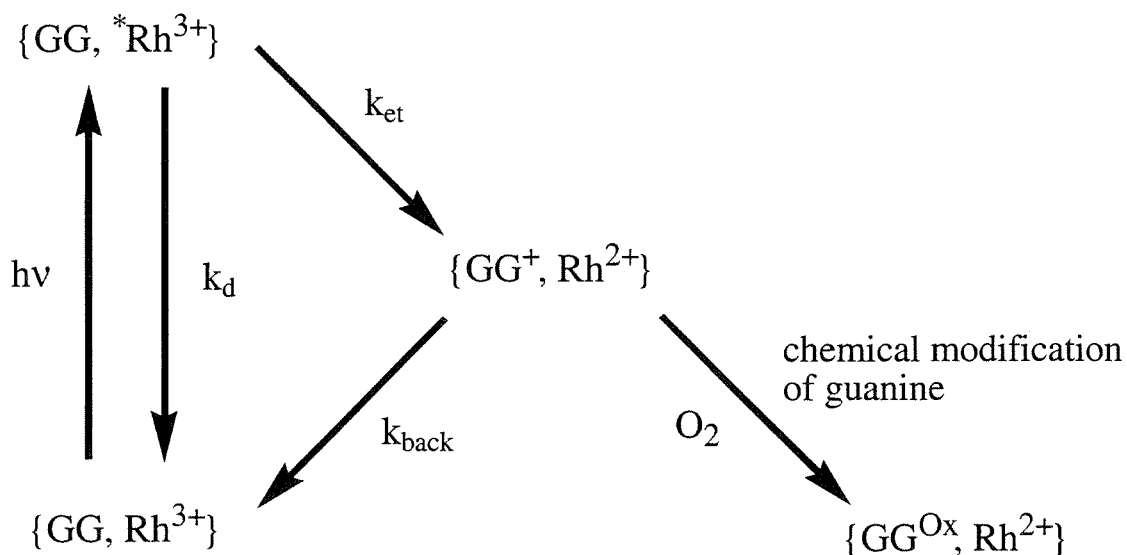
Figure 1.4 Electron transfer reaction between *Rh(phi)$_2$bpy^{3+} and
guanine leading to irreversible base damage.

In an assembly containing an intercalating Rh(III) photooxidant covalently

tethered to one end of a DNA duplex damage of remote 5'-GG-3' sites, revealed as

piperidine-sensitive strand breaks, was observed (Figure 1.5).[34] These data indicated

for the first time in a chemically well-defined system that the migration of an injected

hole can promote oxidative damage to DNA from a distance. Interestingly, no

attenuation in the yield of damage was observed for a distal relative to a proximal

guanine doublet, suggesting that the hole migration through DNA is not dramatically

affected by distance. Moreover, the primary oxidative lesion, established by digestion

without piperidine treatment was found to be 8-oxo-guanine, a common oxidative lesion

to DNA *in vivo*. Comparable results are obtained with ground-state Ru(III) and

photoexcited anthraquinone oxidants,[36,61,65] demonstrating the generality of this

reaction. Thus, a physiologically relevant and important oxidative lesion in DNA can

be initiated by the facile transport of electrons through the DNA base stack over long
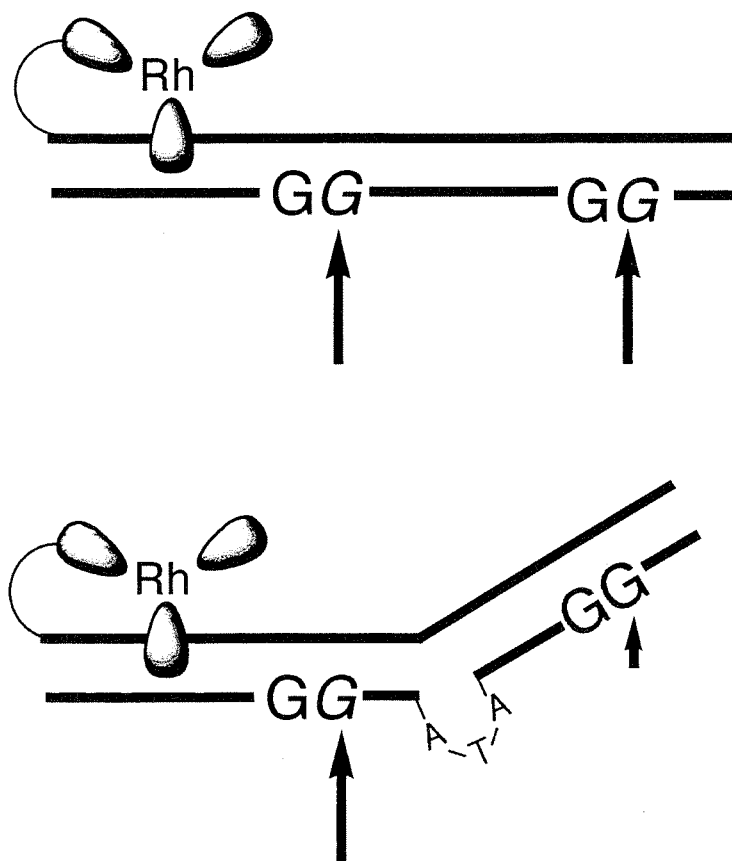
Figure 1.5 Schematic illustration of long-range guanine oxidation by *Rh(phi)$_2$bpy^{3+} and the effect of an intervening bulge on this reaction. Arrows indicates sites of guanine damage with sizes proportional to damage yield.

molecular distances. Therefore, DNA damage may result not only from localized events but may also be promoted from remote sites along the DNA helix.

The results obtained confirm that components of the DNA base stack can participate in electron transfer as reactants, but here again, the integrity of the DNA bridge is still crucial. When bulged regions were introduced to disrupt the base stacking between the Rh(III) intercalator and guanine doublets, the yield of guanine damage at the distal site was significantly diminished (Figure 1.5).[35] This observation

demonstrates that the extent of stacking between the DNA bases is an important parameter which modulates the efficiency of DNA-mediated charge transport.

Another attractive target for DNA-mediated electron transfer chemistry is the repair of a base lesion. The primary photochemical lesion in DNA is the cyclobutyl thymine dimer, which results from a [2+2] photocycloaddition between adjacent thymine bases on the same polynucleotide strand. In *E. Coli*, the thymine dimer is repaired by photolyase in an electron-transfer reaction involving a flavin cofactor.[58] This reaction repairs the dimer through a reductive event, but model studies have revealed that this lesion can also be repaired oxidatively (E° (T<>T) ~ + 2 V). Hence the repair of a thymine dimer represents a physiologically important reaction that can be triggered cleanly by electron or hole transfer and involves no subsequent atom transfer reactions.

Using a Rh(III) intercalator tethered to the end of a DNA duplex containing a thymine dimer, the products of a chemical reaction, occurring as a result of charge migration over extraordinary distance, were detected.[37] As we had observed in tests of oxidative damage to DNA from a distance, the efficiency of DNA repair was relatively insensitive to distance. In fact, the repair yield increased slightly when the dimer was moved down the helix away from the intercalator. Additionally, the stacking of the DNA bases was found to be an important factor in modulating this reaction. In the presence of bulged regions within the DNA base stack intervening between the intercalator and the dimer, the yield of repair is drastically diminished, suggesting that the pathway for this reaction has been significantly affected by the perturbation in base stacking.
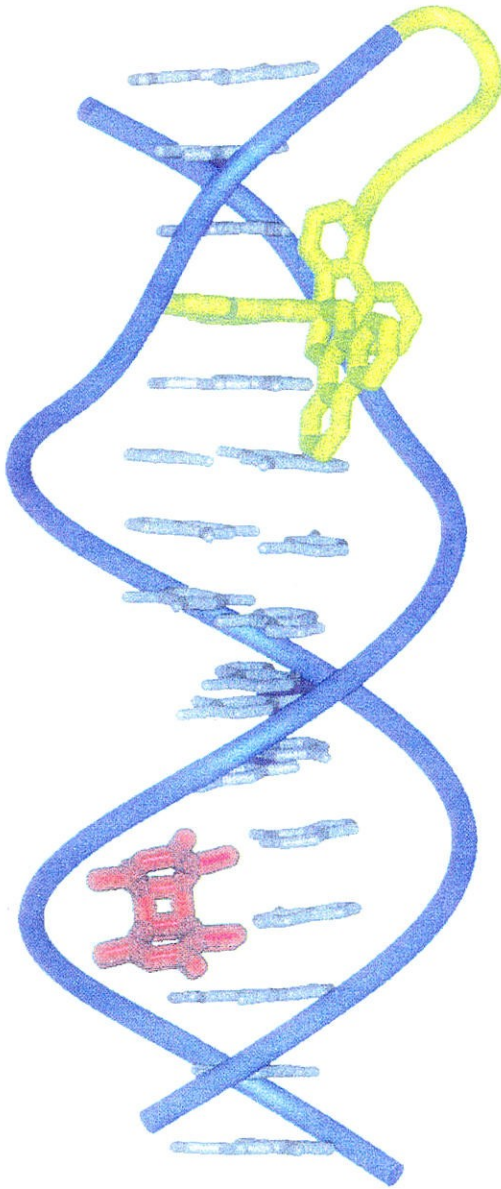
Figure 1.6 DNA duplex containing tethered Rh(III) intercalator
and thymine dimer lesion.

Additional photophysical, photochemical, and electrochemical studies. Other recent reports concerning DNA-mediated charge transport offer additional methods for studying this phenomenon. Holmlin *et al.* studied triplet energy transfer, putatively a two-electron transfer, between metallointercalators tethered to synthetic DNA duplexes.[39] Here, a shallow distance dependence was observed, and the efficiency of this reaction was remarkably sensitive to perturbations in the base stack intervening between donor and acceptor.

Giese and coworkers have developed an assay where the migration distance of a radical generated by the photoactivation of a modified deoxyribose unit is monitored.[40] By quantitating the extent of damage as a function of distance, and relating this yield of product to the rate of an electron transfer event, a β value of ~ 1 Å^{-1} was obtained.

In addition, a recent study by Okahata *et al.* revisits the early experiments exploring DNA conductivity.[41] Here, conductivity comparable to conducting organic polymers is observed in DNA films oriented with the helical axes perpendicular to the electrodes. Importantly, the conductivity was highly orientation-dependent, with significantly lower currents measured when the DNA strands were arranged parallel to the electrode. These results fulfill the expectation of Eley and Spivey[11] almost four decades ago concerning the anisotropy of conductivity through DNA.

Theoretical Studies of DNA-Mediated Charge Transport. A variety of theoretical studies have sought to describe the features of DNA-mediated electron transfer reactions.[42-47] The first calculations of charge transport in DNA in 1974 by Dee and Baur utilized a quantum mechanical model that considered electron hopping through DNA.[42] This study predicted base-to-base migration on the femtosecond timescale, allowing long-range migration (>100 Å) in picoseconds, albeit in discrete steps.

Beratan and coworkers have applied the semi-empirical self-consistent field methods used in theoretical studies of proteins to predict electron-transfer rates in experimental systems.[43] For donor/acceptor assemblies where slow electron-transfer kinetics consistent with significant distance dependences ($\beta \sim 1$ Å^{-1}) were observed,[23,25] this approach yields good agreement between experiment and theory. However, the very fast kinetics of electron transfer between intercalated donors and acceptors[30] are underestimated by six orders or magnitude by the calculations, and therefore dismissed as arising from "a misunderstanding of the intercalation geometry or an alternative quenching mechanism." It is worth noting, however, that the magnitude of the DNA HOMO-LUMO gap employed in this study is overestimated by at least 4 eV. The position of these orbitals with respect to reactant orbitals are expected to affect long-range electronic coupling,[48] hence this study may be prone to error because these energetic factors were neglected.

The application of Redfield theory has been most successful in explaining the experimental observations of ultrafast long-range charge transport through DNA.[44-45] The first theoretical study of this type by Freisner and coworkers treated the DNA base stack as a delocalized bridge system dissapatively coupled to a thermal bath.[44] The energetic proximity of donor orbitals on intercalating reactants to those of the bridging bases is recognized, which therefore presents a transfer mechanism other than superexchange. Here, the possibility is discussed that electron transfer proceeds by thermal promotion of electrons into the bridge followed by delocalization into bridge states facilitated by dephasing bath fluctuations, thereby leading to efficient long-range electron transfer. An exponential dependence on temperature is expected because of the requirement of thermal energy for bridge access. Moreover, non-adiabatic superexchange is predicted to dominate electron transfer at shorter distances, with a

critical number of bridging residues required for transfer through the efficient adiabatic channel to be observed.

Recently, Mukamel and coworkers have elaborated on this approach by including the effects of solvent reorganization on DNA-mediated electron transfer.[45] In addition to incorporating this important parameter, a variety of other pertinent issues are presented. A distinction is made between a coherent (non-adiabatic tunneling) channel for electron transfer through DNA, termed the *transfer* regime, and an incoherent (hopping) sequential channel which is associated with a *transport* regime. The terms transfer and transport are used interchangeably by experimentalists (as they will be here), but the definition of these regimes illustrates that multiple mechanisms may be considered in explaining experimental observations. This theoretical study investigates the parameters governing the crossover point between these two regimes, and identifies temperature, reorganizational energy, and energy gap as modulators of the mechanistic pathway. However, the discussion of these mechanisms does not offer any explanation for the reports of differing distance dependences in systems where these parameters do not deviate significantly. Jortner *et al.* also recently attempted to invoke mechanistic differences as an explanation reconciling disparate electron transfer distance dependences.[46] However, only systems with relatively steep distance dependences (0.6 – 1.4 $Å^{-1}$) and donor orbitals lower in energy than bridge orbitals were included as examples of reactions dominated by superexchange, while the representative examples of systems with shallow or undetectable distance dependences had reactant orbitals higher in energy than bridge states, where it was concluded that a hopping mechanism would be most efficient. In reality, there are examples of shallow distance dependences when the reactant energies are below the bridge, and steep distance dependences even though the reactions were initiated by species with potentials higher than those of the

bridge. Hence, the mechanistic arguments by theoreticians offered to date based on energetic factors do not reconcile the conflicting experimental results.

An obvious deficiency in the theoretical treatments of DNA-mediated charge transfer reactions are considerations of DNA *structure*. As will be presented in the following chapters, subtle changes in the stacking of reactants or the DNA bases are amplified as significant decreases in the efficiency of electron transfer. A recent set of calculations reported by Chen and Chen predicts rapid charge transfer through DNA based on the consideration of the ionization potentials (IP) and electron affinities (EA) of charge-transfer complexes formed transiently by adjacent base pairs upon the addition of electrons or holes into the base stack.[47] This model argues that the small energetic differences among the ionization potentials and electron affinities of the base pairs (~ 4 kcal/mol) will facilitate efficient electron transfer enhanced by conformational "flapper effects" that result in enhanced coupling, but only for *properly aligned, stacked species*. Although this theory may prove to be difficult to test experimentally, it is one of the only theoretical treatments offered to date that considers the unique structural properties of the DNA base stack.

1.5 DNA-mediated electron transfer: experimental challenges

Although all of the experiments described have sought to understand charge transport through the same medium, the DNA helix, widely varying dynamics and distance dependences have been reported. In many cases, however, the reactants employed (solution-borne radicals, non-intercalated probes) do not interact strongly with the base stack, and it is these systems which show the largest sensitivity to distance and provide the most conservative estimates of the efficiency of radical migration within DNA. On the other hand, in the majority of systems where intercalators are employed as reactants or radical scavengers, reactions occurring over extended

distances are observed on fast time scales. These trends indicate that the interactions between reactants and the DNA base stack cannot be neglected in interpreting experimental data, and that π-stacking may strongly influence the kinetics and distance dependences of DNA-mediated electron-transfer reactions. It is therefore imperative that structurally well-defined systems be used for the study of electron transfer through DNA. This is the main challenge of this developing field, as the synthetic manipulation of nucleic acids requires careful consideration of the structural and chemical intricacies of this material.

Our first studies of electron transfer between intercalating probes within the DNA base stack provided promising indications that exceptionally efficient electron transfer can be mediated by this macromolecular structure. However, to explore the effects of distance and structural perturbations within the DNA helix in an unequivocal fashion, we turned our attention almost exclusively towards studies of reactants covalently attached to synthetic DNA duplexes, where electron transfer can be monitored within structurally well-characterized assemblies. The study of photoinduced electron transfer in such well-defined assemblies where intercalators serve as reactants is described in Chapter 2, while Chapter 3 describes the results obtained from the study of a reaction between an intercalator and a modified base. Electron transfer through DNA is probed without external donors and acceptors by using only DNA bases as reactants as described in Chapter 4. In order to expand the range of methodologies employed in studying DNA-mediated electron transfer, and to provide a route towards biosensing applications, we also employed electrochemical methods to study long-range redox processes at gold surfaces modified with DNA duplexes. These studies, the subjects of Chapters 5 and 6, have provided important complementary information concerning this medium as a bridge for electron transfer.

The work that will be described in this thesis includes an important focus on the role of stacking in modulating the efficiency of charge transport in DNA. Taken together, these studies not only may provide a cohesive picture of the nature of DNA as an electron-transfer medium but also may help to reconcile the controversy surrounding previous disparate results. These studies serve to demonstrate that stacking within the DNA bridge is essential for efficient, long-range charge transfer.

1.6 References

1. Cadet, J. in *DNA Adducts: Identification and Significance* (K. Hemminki, A. Dipple, D.E.G. Shuker, F.F. Kadlubar, D. Segerback, and H. Bartsch, eds.), IARC Publications, Lyon (1994).

2. Marks, T.J. *Science* **1985**, *227*, 881.

3. Bowler, B.E.; Raphael, A.L.; Gray, H.B. *Prog. Inorg. Chem.* **1990**, *38*, 259.

4. Marcus, R.A.; Sutin, N. *Biochim. Biophys. Acta* **1985**, *811*, 265.

5. Beal, M.F. *The Neuroscientist* **1997**, *3*, 21.

6. Beckman, K.B.; Ames, B.N. *Phys. Rev.* **1998**, *78*, 547.

7. Hildalgo, E.; Ding, H.G.; Demple, B. *Trens. Biochem. Sci.* **1997**, *22*, 207.

8. Sen, C.K.; Packer, L. *FASEB J.* **1996**, *10*, 709.

9. Nicolaou, K.C.; Dai, W.M. *Angew. Chem.* **1991**, *30*, 1387.

10. Arcamone, F., *Doxorubicin: Anticancer Antibiotics*, Academic Press, New York (1981).

11. Eley, D.D.; Spivey, D.I. *Trans. Faraday Soc.* **1961**, *58*, 411.

12. Liang, C.Y.; Scalo, E.G. *J. Chem. Phys.* **1964**, *40*, 919.

13. Snart, R.S. *Biopolymers* **1968**, *6*, 293.

14. Whillans, D.W. *Biochim. Biophys. Acta.* **1975**, *414*, 193.

15. Gregoli, S.; Taverna, C.; Bertinchamps, A. *Int. J. Radiat. Biol.* **1970** *18*, 577.

16. Cullius, P.M.; McClymont, J.D.; Symons, M.C.R. *J. Chem. Soc. Faraday Trans.,* **1990**, *86*, 591.

17. van Lith, D.; Warman, J.M.; de Haas, M.P.; Hummel, A. *J. Chem. Soc., Faraday Trans. 1* **1986**, *82*, 2933.

18. Miller, J.H.; Swenberg, C.E. *Can J. Phys.* **1990**, *68*, 962.

19. Razskazovskii, Y.; 'Swarts, S.G.; Falcone, J.M.; Taylor, C.; Sevilla, M.D. *J. Phys. Chem.* **1997**, *101*, 1460.

20. Houee-Levin, C.; Gardes-Albert, M.; Rouscilles, A.; Ferradini, C.; Hickel, B. *Biochemistry*, **1991**, *30*, 8216.

21. Davis, L.M.; Harvey, J.D.; Baguley, B.C. *Chem.-Biol. Interactions* **1987**, *62,* 45.

22. Fromhertz, P.; Rieger, B. *J. Am. Chem. Soc.*, **1986**, *108*, 5361.

23. Brun, A. M.; Harriman, A. *J. Am. Chem. Soc.* **1992**, *114*, 3656.

24. Lewis, F.D.; Wu, Taifeng; Zhang, Y.; Letsinger, R.L.; Greenfield, S.R.; Wasielewski, M.R. *Science* **1997**, *277*, 673.

25. Meade, T. J.; Kayyem, J. F. *Angew. Chem. Int. Ed. Engl.* **1995**, *34*, 352.

26. Fukui, K.; Tanaka, K. *Angew. Chem. Int. Ed.* **1998**, *37*, 158.

27. Barton, J. K.; Kumar; C. V.; Turro, N. J. *J. Am. Chem. Soc.* **1986**, *108*, 6391.

28. Purugganan, D.; Kumar, C. V.; Turro, N. J.; Barton, J. K. *Science* **1986**, *241*, 1645.

29. Murphy, C.J.; Arkin, M.A.; Ghatlia, N.D.; Bossman, S.; Turro, N.J.; Barton, J.K. *Proc. Natl. Acad. Sci. U.S.A.* **1994**, *91*, 5315.

30. Murphy, C. J.; Arkin, M. A.; Jenkins, Y.; Ghatlia, N. D.; Bossman, S.; Turro, N. J.; Barton, J.K. *Science* **1993**, *262*, 1025.

31. Arkin, M.R.; Stemp, E.D.A.; Holmlin, R.E.; Barton, J.K.; Hörmann, A.; Olson, E.J.C.; Barbara, P.A. *Science* **1996**, *273*, 475.

32. Holmlin, R.E.; Stemp, E.D.A.; Barton, J.K. *J. Am. Chem. Soc.* **1996**, *118*, 5236.

33. Holmlin, R.E.; Dandliker, P.J.; Barton, J.K. *Angew. Chem. Int. Ed..* **1998**, *36*, 2714.

34. Hall, D.B.; Holmlin, R.E.; Barton, J.K. *Nature,* **1996**, *382*, 731.

35. Hall, D.B.; Barton, J.K. *J. Am. Chem. Soc.,* **1997**, *119*, 5045.

36. Arkin, M.R.; Stemp, E.D.A.; Barton, J.K. *Chem. & Biol.,* **1997**, *4*, 389.

37. Dandliker, P.J.; Holmlin, R.E.; Barton, J.K. *Science* **1997**, *275*, 1465.

38. Dandliker, P.J.; Nunez, M.E.; Barton, J.K. *Biochemistry* **1998**, *37*, 6491.

39. Homlin, R.E.; Tong, R.; Barton, J.K. *J. Am. Chem. Soc.* **1998**, *120*, 9724.

40. Meggers, E.; Kusch, D.; Spichty, M.; Wille, U.; Giese, B. *Angew. Chem.* **1998**, *37*, 460.

41. Okahata, Y.; Kobayashi, T.; Tanaka, K.; Shimomura, M. *J. Am. Chem. Soc.* **1998** *120*, 6165.

42. Dee, D.; Baur, M.E. *J. Chem. Phys.* **1974**, *60*, 541.

43. Priyadarshy, S.; Risser, S.M.; Beratan, D.N. *J. Phys. Chem.* **1996**, *100*, 17678.

44. Felts, A.K.; Pollard, W.T.; Freisner, R.A. *J. Phys. Chem.* **1995**, *99*, 29291.

45. Okada, A.; Chernyak, V.; Mukamel, S. *J. Phys. Chem. A* **1998**, *102*, 1241.

46. Jortner, J.; Bixon, M.; Langenbacher, T.; Michel-Beyerle, M.E. *Proc. Natl. Acad. Sci, U.S.A.* **1998**, *95*, 12759.

47. Chen, E.S.; Chen, E.C.M. *Bioelectrochem. Bioenerg.* **1998**, *46*, 15. 47.

48. Evenson, J.W.; Karplus, M. *Science* **1993**, *262*, 1247.

49. Watson, J.; Crick, F. *Nature* **1953**, *171*, 737.

50. Shriver, D. F.; Atkins, P.; Langford, C. H. (1994) *Inorganic Chemistry*, 2nd ed. W. H. Freeman and Co., New York, 481.

51. Cantor, C.; Schimmel, P. (1980) *Biophysical Chemistry.*, W.H. Freeman and Co., New York, 381-408.

52. LeBlanc, O.H. *J. Chem. Phys.* **1960**, *119*, 1226.

53. Dupureur, C.M.; Barton J.K. in *Comprehensive Supramolecular Chemistry, Vol. 5* (J.M. Lehn, ed.), Pergamon Press, Oxford (1995).

54. Johann, T. W.; Barton, J. K. *Phil. Trans. Royal Society* **1996**, *354*, 299.

55. (a) Olson, E.J.C.; Hu, D.; Hörmann, A.; Barbara, P.F. *J. Phys. Chem.* **1997**, *101*, 299; (b) Lincoln, P.; Tuite, E.; Norden, B. *J. Am. Chem. Soc.* **1997**, *119*, 1454.

56. Franklin, S.J.; Treadway, C.R.; Barton, J.K. *Inorg. Chem.* **1998**, *37*, 5198.

57. Steenken, S. *Chem. Rev.* **1989**, *89*, 503.

58. Sancar, A.; Sancar, G.B. *Ann. Rev. Biochem.* **1988**, *57*, 29.

59. Kasai, H.; Yamaizumi, Z.; Berger, M.; Cadet, J. *J. Am. Chem. Soc.* **1992**, *114*, 9692.

60. Saito, I.; Takayama, M.; Sugiyama, H.; Nakatani, K.; Tsuchida, A.; Yamamoto, M. *J. Am. Chem. Soc.,* **1995**, *117*, 6406.

61. Breslin, D.T.; Schuster, G.B. *J. Am. Chem. Soc.* **1997**, *119*, 5045.

62. Sugiyama, H.; Saito, I. *J. Am. Chem. Soc.* **1996**, *118*, 7063.

63. Sitlani, A.; Long, E. C.; Pyle, A. M.; Barton, J.K. *J. Am. Chem. Soc.* **1992**, *114*, 2303-2312.

64. Turro, C.; Evenzahav, A.; Bossmann, A.; Barton, J. K.; Turro, N.J. *Inorg. Chim. Acta* **1996**, *243*, 101.

65. Stemp, E.D.A; Arkin, M.R.; Barton, J.K. *J. Am. Chem. Soc.* **1997**, *119*, 2921.

Chapter 2

Photoinduced Electron Transfer Between Intercalators: Sensitivity to Distance and Base Stacking[‡]

2.1 INTRODUCTION

The observation of ultrafast electron transfer between metallointercalators bound to DNA provided intriguing evidence that the base stack can mediate remarkably efficient reactions.[1-5] However, other seemingly similar experiments have prompted very different conclusions.[6-8] To determine whether the fast reactions observed between metallointercalators represent generally the nature of the DNA base stack as a medium for electron transfer, we sought to employ other reactants to study this phenomenon. Moreover, we desired a probe amenable to derivatization and conjugation to DNA, so that we might study electron transfer through DNA as a function of distance. By fixing the positions of donors and acceptors within DNA assemblies, the role of stacking interactions among the intervening bases could also be tested. We previously discovered that electron transfer was extremely sensitive to the integrity of stacking between reactants and the DNA base stack.[2] The degree of interaction between the stacked bases could also therefore be envisioned to affect the efficiency of electron transfer in DNA.

In this chapter, studies examining photoinduced electron transfer between intercalators covalently bound to DNA as a function of distance *and* base stacking are described. The donor employed, ethidium, is a classical intercalator ($K \sim 10^6$ M^{-1}),[9-10] and the acceptor is Rh(phi)$_2$bpy^{3+} (phi = 9,10-diimine phenanthrenequinone), a metallointercalator ($K \gtrsim 10^6$ M^{-1}).[11] This minor-groove binding organic intercalator and metallointercalator undergo fast electron transfer when noncovalently bound to DNA, mirroring results obtained with metallointercalator donors and acceptors. Moreover, both of these molecules have been functionalized with methylene tethers and attached to DNA duplexes 10-14 base pairs in length. We find that fluorescence quenching occurs by electron transfer over distances ranging from 17-36 Å. Although this DNA-mediated electron-transfer reaction is weakly dependent on distance, it

depends sensitively upon base stacking. Indeed, with perturbations in stacking, large decreases in the quenching efficiency are observed. Our findings support the notion that the DNA base stack facilitates direct long-range electron transfer.

2.2 EXPERIMENTAL SECTION

Synthesis and Characterization. Unless otherwise noted, all reagents and starting materials used in synthetic protocols were purchased from Aldrich or Fluka and used without further purification. Reagents for oligonucleotide synthesis were obtained from Glen Research. [Rh(phi)$_2$bpy]Cl$_3$ was prepared and the enantiomers of this complex were resolved as previously described.[11]

Synthesis of N-glycyl ethidium (Et'). Ethidium bromide (1 eq., 1 g) was heated at 70°C in a small volume of DMF (~50 ml) with glutaric anhydride (1 eq.) for 48 hrs. The solvent was removed *via* rotary evaporation and the residue dissolved in H$_2$O/CH$_3$CN. Starting material and the disubstituted product were separated from the desired monosubstituted form on a cation (Sephadex C-25) exchange column. The crude mixture was loaded on the column, the yellow disubstituted product was eluted at neutral pH, and the orange-pink monosubstituted product was eluted upon raising the pH of the mobile phase. This material contains both the 3' and 8'-functionalized isomers, although mainly the desired 8' form, hence the isomer mixture was used directly in conjugate synthesis. Identity of the product was confirmed using FAB mass spec (calc. (found) *m/z* (M^{+1}) = 428 (428)), ^{1}H NMR (300 MHz, CD$_3$OD), δ (ppm): 1.45 (m, 3H, N5-CH$_3$), 2.0-2.4 (m, 6H, side chain CH$_2$), 4.7 (2H, N5-CH$_2$), 7.4 (m, 2H: H$_2$, H$_4$), 7.6-7.8 (m, 6H: φH, H$_9$), 8.6 (m, 2H: H$_1$, H$_{10}$), and ultraviolet-visible (uv-vis) absorption spectroscopy (λ$_{max}$(vis)=460 nm, ε=5.7x10^3 M^{-1}cm^{-1}).

Modification of oligonucleotides. Unmodified oligonucleotides were prepared using standard automated techniques[12] on a 394 ABI synthesizer and purified by

reverse phase HPLC. For conjugate synthesis, oligonucleotides lacking the terminal 5'-dimethoxytrityl group were synthesized on a 2000 Å controlled pore glass (CPG) support. A diaminononane linker was attached to the oligonucleotide on the resin using procedures previously described.[13]

To effect coupling with amino-terminated oligonucleotides, the succinimidyl ester of Et' was first prepared *in situ* by combining Et' in 1:1:1 CH_2Cl_2/DMF/dioxane with 10 eq. N,N'-disuccinimidyl carbonate for 15 min., or alternatively by stirring Et' with 10 eq. O-(N-succinimidyl)-N,N,N',N'-tetramethyluronium tetrafluoroborate (TSTU) in 1:1:1 CH_3CN/CH_3OH/CH_2Cl_2 and 5 eq. diisopropylethylamine for 30 min.. Once activation was confirmed *via* thin layer chromatography (alumina/MeOH, r_f Et'-NHS >> Et'), the amino-derivatized DNA on the CPG support was added to the Et' solution and the mixture was stirred overnight at ambient temperature. The Et'-DNA-CPG was isolated from the reaction mixture by vacuum filtration and washed with H_2O, CH_3CN, and a small amount of CH_3OH. The Et'-DNA was then cleaved from the resin and the protecting groups on the oligonucleotide removed by incubating at 55°C in concentrated (30%) NH_4OH overnight. The NH_4OH solution was subsequently evaporated and the modified oligonucleotides purified in the same manner as unmodified oligonucleotides using reversed phase HPLC. For a gradient of 50 mM ammonium acetate/CH_3CN increasing from 0% to 40% CH_3CN over 40 min. on a C4 column, the modified conjugates have a retention time of ~ 30 min., while underivatized DNA elutes with a retention time ~ 15 min.. The product is identified by a characteristic DNA/Et' hybrid spectrum (λ_{max} = 260 nm, 484 nm). Rhodium-modified oligonucleotides were prepared in an analogous manner;[14] diastereomeric Δ-Rh and Λ-Rh-containing conjugates were resolved using reversed phase HPLC. Quantitation of Et and Rh-modified conjugates was performed using extinction coefficients of $\varepsilon_{(Et,484)}$ =

4.0×10^3 M^{-1} cm^{-1} and $\varepsilon_{(Rh, 390)} = 19.5 \times 10^3$ M^{-1}cm^{-1}, which were evaluated from phosphate analysis[15] and other stoichiometry determinations.

The conjugates have also been characterized by matrix-assisted time-of-flight (MALDI-TOF) and electrospray ionization mass spectrometry and base analysis by enzymatic digestion.[16] In the case of Et'-5'CTATCTATCGT, the 11 base conjugate used in this study, the mass of the conjugate was obtained by MALDI-TOF mass spectrometry (calc. (found) m/z (M(-H)) 3877 (3874±5)). All other masses of Et-modified sequences obtained by MALDI-TOF were within 3 m/z of calculated values. Characterization of Rhodium-modified oligonucleotides are described elsewhere.[14] The base ratios obtained by digestion followed by quantitation *via* HPLC for this conjugate were as follows: dC = 3.03, dG = 0.96, dT = 4.07, dA = 2.03, dT + Et'-linker = 1.0.

Hybridization of DNA duplexes. Based on the extinction coefficients listed above for modified conjugates and calculated extinction coefficients for unmodified sequences (ε_{260} (M^{-1} cm^{-1}) : dC = 7.4 x 10^3; dG = 12.3 x 10^3; dT = 6.7 x 10^3; dA = 15.0 x 10^3), appropriate amounts of complementary materials were combined at 1:1 stoichiometry and dissolved in 5 mM phosphate, 50 mM NaCl (pH 7) to give a final duplex concentration of 5 µM. The resulting solutions were heated to 90°C and slowly cooled to ambient temperature over 2-3 hours to anneal the duplex.

Melting profiles. Thermal denaturation experiments were performed on a HP8452A diode array spectrophotometer with samples at a duplex concentration of 5 µM in 5 mM phosphate, 50 mM NaCl (pH 7). Absorbance at 260 nm was monitored every 2°C with 3 minute equilibration times.

Electrochemical measurements. Reduction potentials for ethidium and Rh(phi)$_2$bpy^{3+} were measured *via* cyclic voltammetry on a BAS CV-50W potentiostat in 0.1 M TBAH/CH$_3$CN. Cyclic voltammetry was carried out at 20°C with a normal three electrode configuration consisting of a glassy carbon working electrode, saturated

calomel reference electrode, and platinum auxiliary electrode. The ethidium excited-state oxidation potential ($E^o(2+/^*)$) was calculated using the expression $E^o(2+/^*) = E_{oo} - E^o(2+/+)$. Values of E_{oo} were approximated both by averaging absorption and emission maxima and examining intersection points of absorption and emission spectra. Both methods yielded equivalent results for ethidium. Potentials are reported *vs.* NHE.

Photophysical measurements. *Preparation of samples with intercalators noncovalenty bound to DNA.* In sample preparation for steady-state and time-resolved fluorescence measurements employing ethidium and Rh(phi)$_2$bpy^{3+} randomly associated with calf thymus (CT) DNA, the following extinction coefficients were employed: $\varepsilon_{(Et, 484)} = 5.7$ x 10^3 M^{-1} cm^{-1}, $\varepsilon_{(Rh, 350)} = 23.6$ x 10^3 M^{-1} cm^{-1}, $\varepsilon_{(CT\ DNA, 260)} = 6.6$ x 10^3 M^{-1} cm^{-1} (nucl.). Appropriate quantities of freshly prepared stock solutions were dissolved in 5 mM phosphate, 50 mM NaCl, pH 7.

Steady-state fluorescence experiments. Steady-state fluorescence polarization measurements were made at 20°C unless otherwise specified with excitation at 480 nm on an SLM 8000 spectrofluorimeter equipped with Glan-Thompson calcite prism polarizers arranged in a T-shaped geometry. Fluorescence intensities were measured on the same apparatus; spectra were integrated from 520 to 800 nm. Typically, samples were measured at a duplex concentration of 5 μM in 5 mM phosphate, 50 mM NaCl (pH 7). In variable viscosity experiments, solutions containing sucrose were prepared and the viscosities determined with a falling ball viscometer. Quenching yields for modified duplexes obtained by steady-state fluorescence measurements were calculated from 2-5 sets of samples from different syntheses of Et/Rh conjugates.

Time-correlated single photon counting (TCSPC). TCSPC was carried out using facilities described previously[17] with $\lambda_{exc} = 335$ nm obtained by doubling the 670 nm (dye = DCM) fundamental line; data fitting was accomplished using least-squares methods in a commercial software program (Axum). Data sets contained 5-10,000

counts, except in cases when small time windows were necessary to ensure constant laser power. Steady-state quenching yields obtained with λ_{exc} = 480 nm were identical to those observed with λ_{exc} = 335 nm. Sample conditions and concentrations were identical in time-resolved and steady-state measurements. No photodegradation was observed, as confirmed by uv-vis absorption spectra taken before and after irradiation.

2.3 RESULTS

2.3.1 Photoinduced electron transfer between ethidium and Rh(phi)$_2$bpy^{3+}

Fluorescence from the ethidium singlet excited state ($E^o(Et^{2+}/Et^*) \sim$ -0.9 V) is quenched by Rh(phi)$_2$bpy^{3+} (E^o(Rh(III)/Rh(II))= -0.03 V) when both molecules are noncovalently bound to double-stranded DNA *via* intercalation (Figure 2.1) as measured by steady-state techniques. For intercalated ethidium, Λ-Rh(phi)$_2$bpy^{3+} is a more efficient quencher than Δ-Rh(phi)$_2$bpy^{3+}. The fluorescence of ethidium is quenched by 47% in the presence of 2 equivalents of the Λ-Rh acceptor and by 75% with 4 equivalents of Λ-Rh. With 2 eq. Δ-Rh(phi)$_2$bpy^{3+} (1 Et/100 bp CT DNA), 31% of the ethidium emission is quenched, while with 4 eq. Δ-Rh(phi)$_2$bpy^{3+}, 54% quenching is observed. This is a surprising result, because with metallointercalator donors, more efficient electron transfer is typically observed with the Δ–Rh enantiomer.[3] The DNA-donor coupling may differ in this system such that the enantioselectivity is reversed, or some minor groove binding of the Λ-Rh isomer may facilitate more diffusional quenching.

The quenching reaction between ethidium and Rh(phi)$_2$bpy^{3+} was also investigated using TCSPC (Figure 2.2). In the presence of DNA, the excited state of ethidium decays with τ = 23 ns. With the addition of Λ-Rh(phi)$_2$bpy^{3+}, the ethidium fluorescence can be analyzed as a biexponential decay (Table 2.1). A small portion of
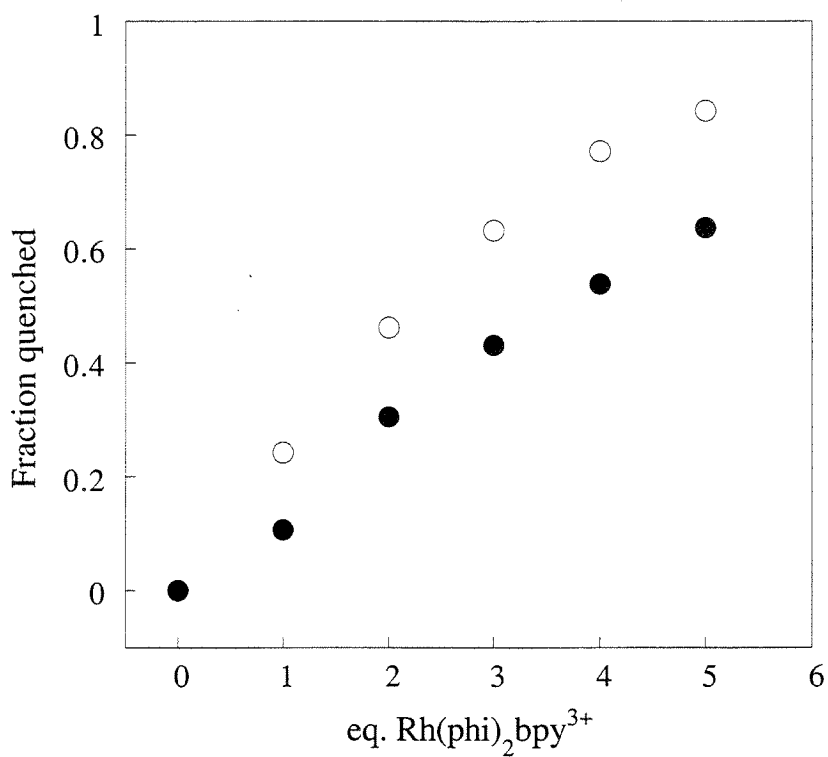
Figure 2.1 Steady-state fluorescence quenching of ethidium (10 μM) by Λ-Rh(phi)$_2$bpy^{3+} (empty circles) or Δ-Rh(phi)$_2$bpy^{3+} (filled circles) noncovalently bound to calf thymus DNA (1 mM nucl.), 5 mM phosphate, 50 mM NaCl, pH 7.
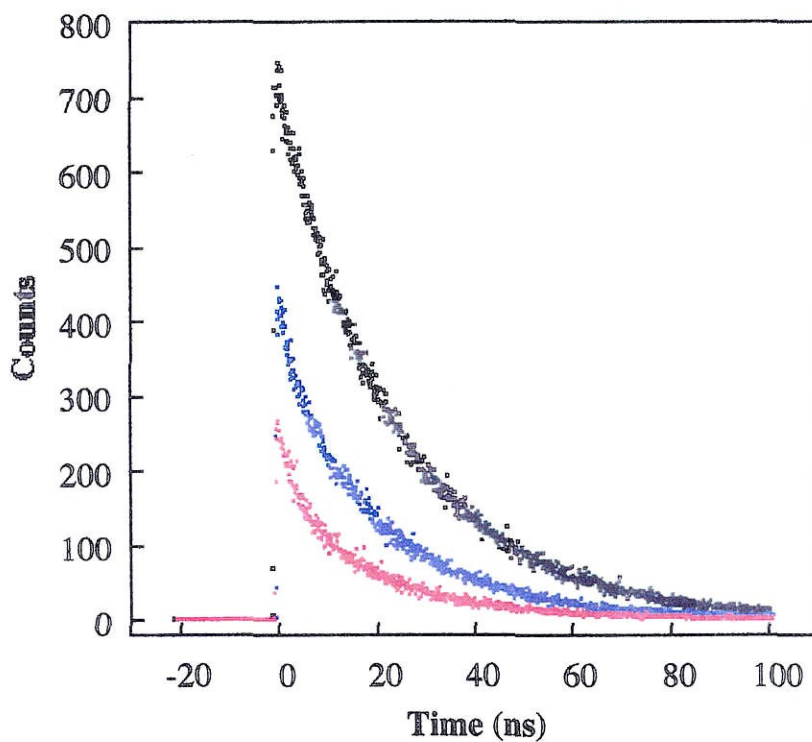
Figure 2.2 TCSPC data for 10 μM Et bound to CT DNA (1 mM nucl.) in the absence (black) of acceptor or with 20 (blue) and 40 μM (red) Λ- Rh(phi)$_2$bpy^{3+}. Data were obtained with steady laser power during 120 s intervals to illustrate the large amounts of static quenching occurring in this system.

Table 2.1 Excited-state quenching of ethidium by Λ/Δ-Rh(phi)$_2$bpy^{3+} [a]

	τ_1 (ns)	τ_2 (ns)	F_q (steady state)
0 eq. Rh(phi)$_2$bpy^{3+}	23.7	---	0
2 eq. Δ−Rh(phi)$_2$bpy^{3+}	5.1(15%)	22 (85%)	0.31
4 eq. Δ−Rh(phi)$_2$bpy^{3+}	3.7 (28%)	19 (72%)	0.54
2 eq. Λ−Rh(phi)$_2$bpy^{3+}	4.4 (18%)	21 (82%)	0.47
4 eq. Λ−Rh(phi)$_2$bpy^{3+}	3.5 (32%)	19 (68%)	0.75

[a]10 µM Et, 1 mM CT DNA, 5 mM Pi, 50 mM NaCl, pH 7. λ_{exc}=324 nm, λ_{em}= 605 nm. Data sets contained 5-10,000 counts and were analyzed using a nonlinear least squares fitting routine.

the steady-state quenching described above is reflected in lifetimes changes; however, the majority of the quenching proceeds within the instrument response (~150 ps) and is reflected in the data shown as a decrease in initial intensity. This fast quenching is referred to as static quenching, and corresponds to the deactivation of a large portion of the donor molecules on a subnanosecond timescale. While the quenching observed in this system is remarkably efficient, the dependence of the quenching yield on the acceptor loading (17 bp/intercalator (2 eq.), 10 bp/intercalator (4 eq.)) indicates that increasing the number of base pairs between donor and acceptor does decrease the efficiency of electron transfer in this system. Importantly, the observed static quenching cannot correspond to displacement of the donor, as ethidium has a lifetime in water (2.3 ns) which would be detected in this experiment.

Time-resolved transient absorption studies of DNA-bound ethidium and Rh(phi)$_2$bpy^{3+} provide spectroscopic evidence for electron transfer as the quenching mechanism between these two intercalated species. For ethidium bound to calf thymus (CT) DNA in the presence of Rh(phi)$_2$bpy^{3+}, long-lived transients consistent with oxidized Et[18] were observed on the microsecond timescale with λ_{max}=425 nm. In addition, the transient signals were correlated with the amount of quenching observed over a range of acceptor concentrations. These transient absorption data parallel previous studies of metallointercalators where residual recombination on microsecond time scales was also observed,[5,19] but measurements using ultrafast spectroscopy showed that the majority of back-electron transfer occurred on a faster time scale (k ~ 10^{10} s^{-1}).[2] For the electron-transfer reaction between ethidium and Rh(phi)$_2$bpy^{3+}, the observed transients account for only ~10% of the quenched donors, thus it appears that here too a faster reaction may account for most of the recombination. Given the weak spectroscopic signatures for Et^{2+} and Rh(phi)$_2$bpy^{2+} and the indication that most of the back-electron transfer appears to occur on a very fast time scale, time-resolved transient

absorption measurements do not provide a sensitive means to study this reaction. Nevertheless, the correlation between transient yields and quenching yields allows the fluorescence quenching mechanism to be assigned as electron transfer.

2.3.2 Synthesis and photophysics of N-glycyl ethidium

The efficient reaction observed between ethidium and $Rh(phi)_2bpy^{3+}$ provides new evidence the DNA base stack promotes facile electron transfer between intercalated species. However, to unequivocally demonstrate that this reactions is mediated by the DNA helix, the positions of reactants must be precisely known. The derivation of small DNA duplexes with these intercalators was therefore undertaken as a means to study DNA-mediated electron transfer over defined distances.

A derivative of ethidium which would allow facile attachment of the intercalator to an oligonucleotide was synthesized. This compound, N-8-(glycyl)-ethidium (Et'), and a disubstituted form (Et") were synthesized as shown in Figure 2.3.
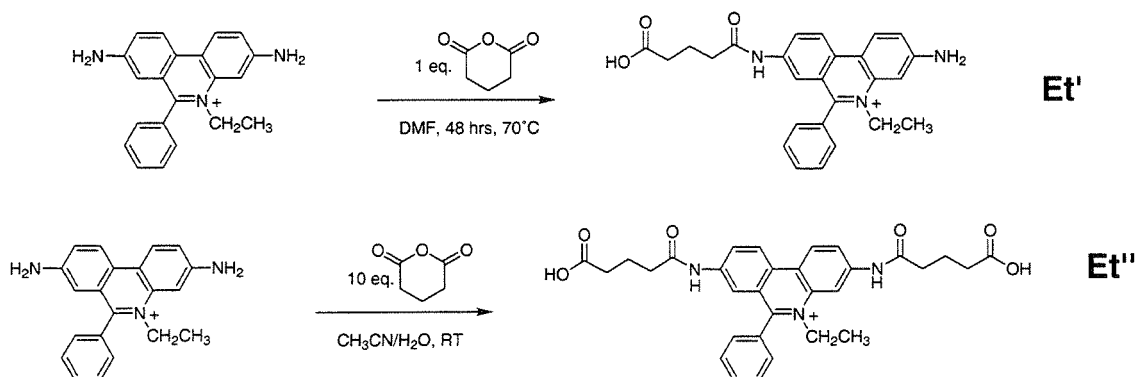
Figure 2.3 Synthesis of ethidium derivatives.

The predominant monosubstituted product is derivatized at the 8'-carbon, presumably due to activation of this position resulting from asymmetric electronic effects. The uv-

vis absorption spectra of the derivatized compounds as compared to the parent molecule reveal that alkylation at the exocyclic amine of ethidium significantly affects the energy of the n-π* transition located at about 480 nm for the unsubstituted analogue (Figure 2.4).

The photophysical properties of ethidium are also affected by the alkylation of the exocyclic amine. Et' has faster excited-state decay kinetics than the parent molecule; while photoexcited ethidium exhibits a lifetime of 2.7 ns in water, photoexcited Et' decays with a lifetime of 440 ps. Upon intercalation, the emission kinetics of these molecules also differ. In the presence of CT DNA (50 bp/Et), ethidium exhibits a monoexponential decay with $\tau = 23$ ns, while the excited state decay for Et' is best described by a biexponential with $\tau_1 = 5.1$ ns (46%), $\tau_2 = 2.3$ ns (54%). Since each of these lifetimes is enhanced compared to the lifetime of Et' free in solution (440 ps), the biexponential decay reflects at least two intercalated geometries rather than a distribution of free and intercalated species. The Et' excited state decay likely contains a distribution of lifetimes reflecting a family of stacking orientations similar to that observed with metallointercalators.[20-21] However, Et' bound to DNA undergoes electron transfer to $Rh(phi)_2bpy^{3+}$ with the same efficiency as the underivatized donor, and is therefore a suitable probe for the investigation of DNA-mediated charge transport.

2.3.3 Synthesis and characterization of Et/Rh-modified duplexes

Using solid-phase coupling methods, N-8-glycl ethidium was conjugated to DNA oligonucleotides (Figure 2.5). The carboxyl group of Et' is activated through conversion to an N-hydroxy-succinimide ester, and upon addition of amino-nonane terminated oligonucleotides, an amide bond is formed to create an ethidium-DNA conjugate. Ethidium-modified oligonucleotides were characterized using base analysis, phosphate analysis, and mass spectrometry (Figure 2.6). Analogous methods had
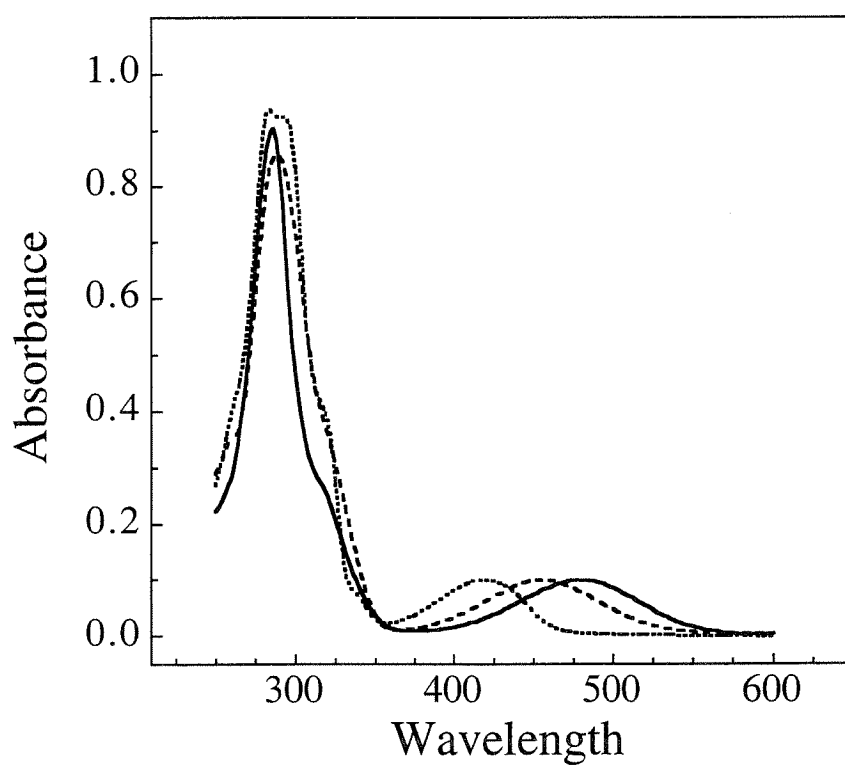
Figure 2.4 Absorption spectra for ethidium (solid line) and modified analogues Et' (dashed line) and Et" (dotted line) obtained in H_2O.
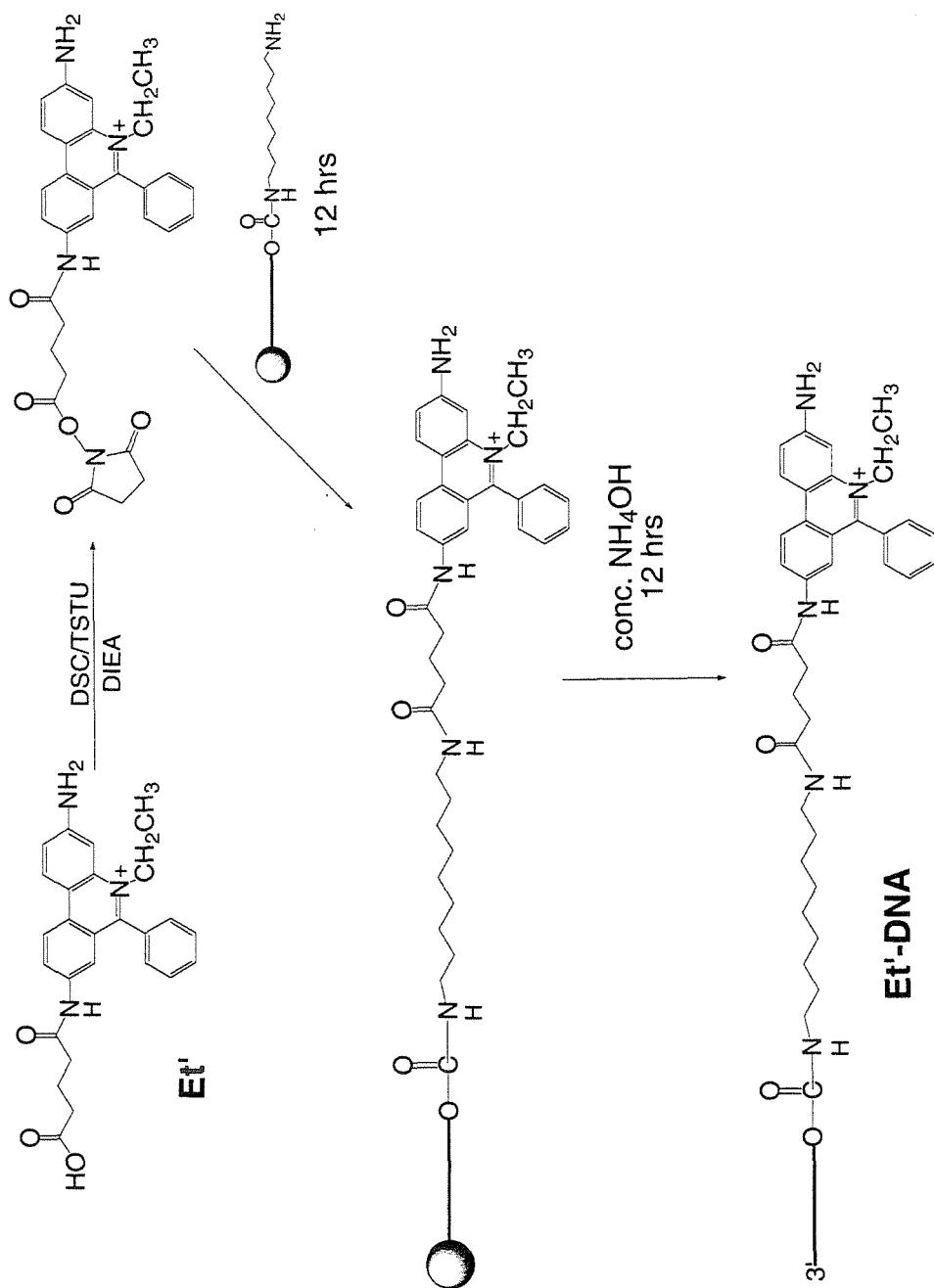
Figure 2.5 Synthesis of Et-DNA.
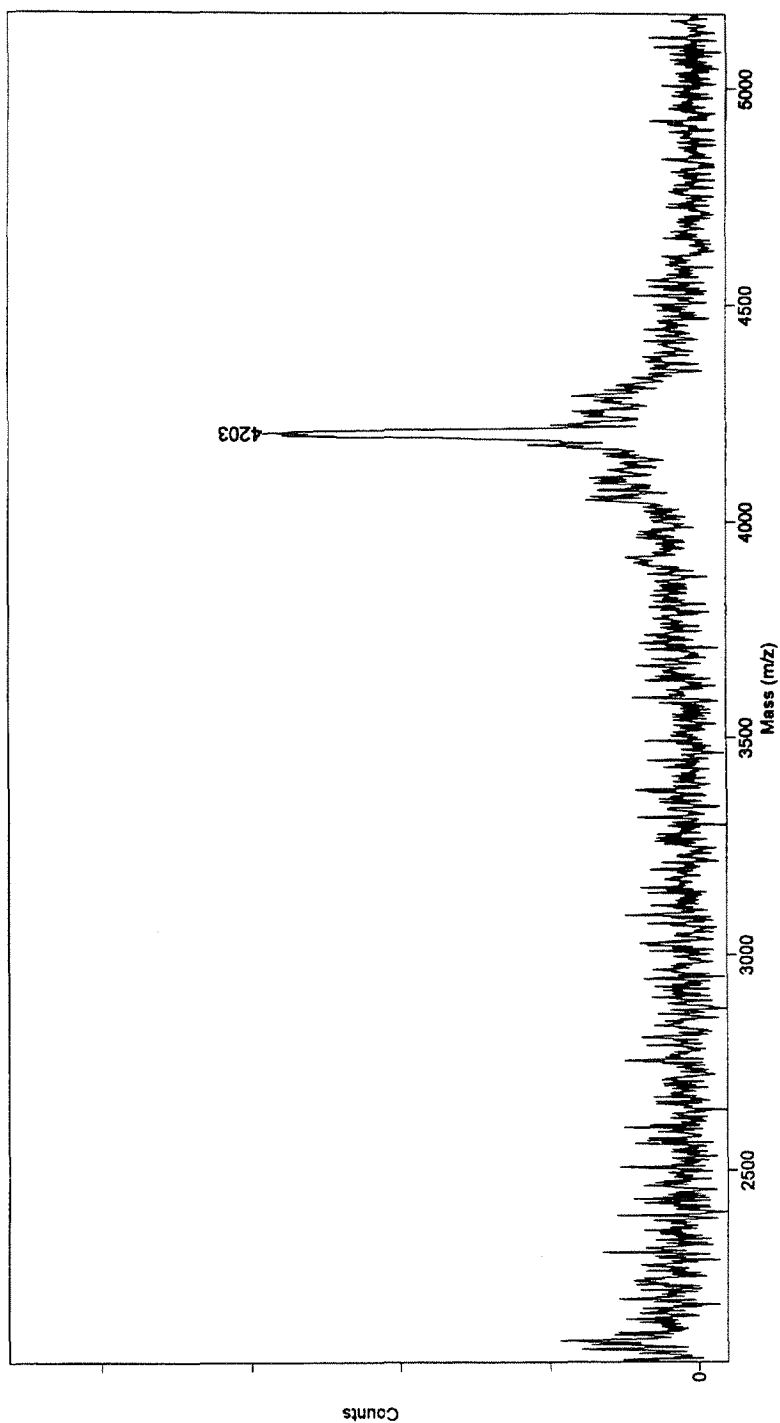
Figure 2.6 MALDI-TOF mass spectrum for Et-DNA conjugate.
Sequence: Et-5'-CTATCTACGTAGCA (calc. mass = 4204).

previously been implemented in our group for the synthesis of oligonucleotides modified with $Rh(phi)_2bpy^{3+}$.

A series of DNA duplexes, ranging from 10-14 base pairs in length, were synthesized by the 5' modification oligonucleotides with N-8-glycyl ethidium or $Rh(phi)_2bpy'^{3+}$ (bpy'=4-butyric acid 4'-methyl bipyridine) (Figure 2.7). In varying the length of the ethidium/rhodium(III)-modified (Et/Rh) oligonucleotides, binding sites were conserved and bases were inserted in the middle of the duplexes. Based on photocleavage experiments, tethered $Rh(phi)_2bpy'^{3+}$ is bound predominantly at the second base step for the Λ-Rh-containing diastereomer, and equally at the second or third base step for the Δ-Rh-containing diastereomer.[14] As the linker is similar for Et', we deduce that this intercalator binds at either the 2nd or 3rd base step. It is probable that ethidium binds at the 2nd base step, as this tether must extend closer to the base stack due to the planarity of this intercalator. Electron-transfer reactions between covalently bound Et' and modified bases also support the assignment of this binding site (see Chapter 3). These binding sites lead to a range of donor-acceptor separations from 17 Å (assuming both intercalators are bound at the 3rd base pair from the respective ends of the 10-mer) to 36 Å (assuming both intercalators are bound at the 2nd base pair from the respective ends of the 14-mer). Distances are therefore listed as ranges in Table 1 reflecting the distribution of possible binding sites, but the variation in donor/acceptor distance with increasing duplex length has a much lower uncertainty; the Et/Rh binding sites are conserved and the linkers are identical across the series of duplexes, thus the donor/acceptor distance changes only by 3.4Å for each base pair added to the duplex.

Thermal denaturation experiments. Thermal denaturation experiments monitored by uv-vis absorbance were performed on all modified assemblies. For all of the duplexes in the series, stabilization of the melting temperatures (T_m) was observed upon

50
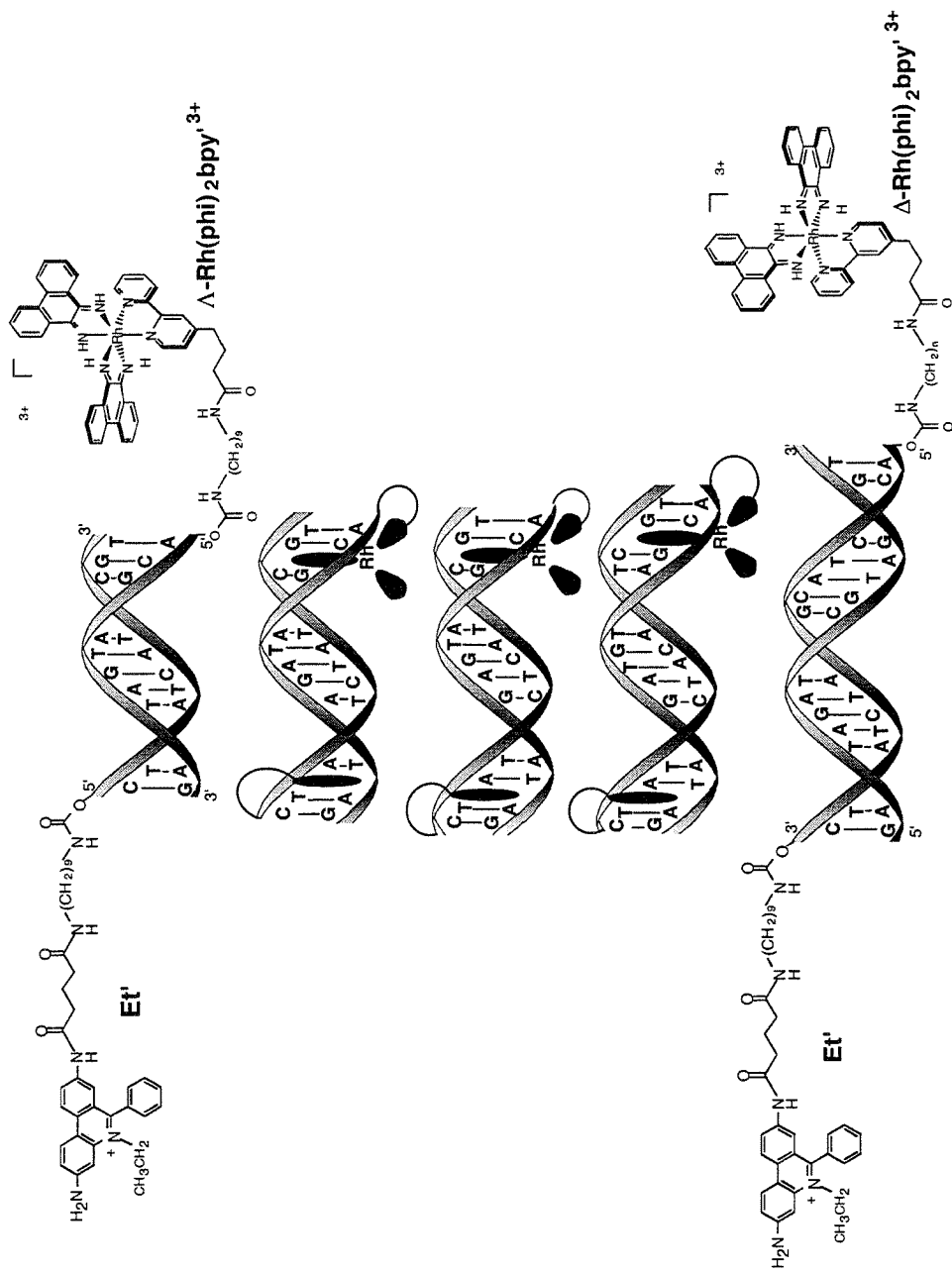
Figure 2.7 Et/Rh modified duplexes.

the incorporation of the intercalators into the duplexes. For example, in an unmodified 10 base pair duplex, $T_m = 32°C$ under the conditions utilized in the quenching experiments. The T_m for the corresponding Et-modified duplex is 34°C, and for the Et/Λ-Rh duplex, $T_m = 39°C$. The degree of stabilization observed in the 10-mer is typical for the series and the melting temperatures also increase with of duplex length, as expected. In all cases, T_m (Et/Rh) > T_m (Et-only) > T_m (unmodified duplex). These data demonstrate the helix stabilization which would be expected upon intercalation of the tethered moiety,[24] as the observed T_m enhancements are comparable to those observed with noncovalently bound intercalators.

Steady-state fluorescence polarization measurements. The Et/Rh assemblies were also characterized with respect to the intercalation environment of the donor using steady-state fluorescence polarization measurements. Measurable increases in polarization were observed upon hybridization of an ethidium-modified conjugate either to an unmodified or Rh-derivatized complement (Table 2.2). The observation of comparable polarizations for Et and Et/Rh-modified duplexes confirms that the donor remains tightly intercalated upon the incorporation of the acceptor into the duplex. Maximum polarization is observed at a ratio of 1:1 Et/Rh strands (Figure 2.8), confirming that the correct stoichiometries of the donor and acceptor-modified strands are present. Duplexes of different lengths showed similar behavior. Titration of Et-modified sequences with 1-1.6 equivalents of Rh-modified conjugates did not cause further increases in polarization or quenching yields, thus it appears that single-stranded Rh-conjugates do not bind to hybridized duplexes.

Temperature and viscosity-dependent polarization studies allow the determination of the duplex volume (Figure 2.8).[25-26] For this calculation, linear regression of data obtained at 20°C was utilized along with excited state lifetimes obtained by TCSPC or calculated from relative steady-state fluorescence intensities.

Table 2.2 Photophysical data for Et/Rh-modified duplexes

Sample	Length (bp)	D-A sep. (Å)[a]	I_{ss}[b]	F_q[c]	P[d]
Et==	10	-	0.37	--	0.185
Et==Λ-Rh	10	17-24	0.26	0.29(2)	0.213
Et==Δ-Rh	10	17-24	0.29	0.28(2)	0.214
Et==	11	-	0.36	--	0.207
Et==Λ-Rh	11	20-27	0.28	0.21(2)	0.232
Et==Δ-Rh	11	20-27	0.27	0.24(1)	0.232
Et==	12	-	0.37	-	0.222
Et==Λ-Rh	12	23-30	0.31	0.16(2)	0.238
Et==Δ-Rh	12	23-30	0.30	0.19(3)	0.239
Et==	13	-	0.35	-	0.234
Et==Λ-Rh	13	26-33	0.31	0.11(1)	0.246
Et==Δ-Rh	13	26-33	0.30	0.14(1)	0.246
Et==	14	-	0.38	-	0.212
Et==Λ-Rh	14	29-36	0.35	0.08(3)	0.221
Et==Δ-Rh	14	29-36	0.35	0.07(3)	0.221

[a]Donor-acceptor separation calculated for intercalators bound at 2nd-3rd base steps. [b]Steady-state fluorescence intensity (I_{ss}) relative to 10 uM Ru(bpy)$_3^{2+}$ (λ_{exc}=480 nm, 20°C, 5 mM phosphate, 50 mM NaCl, pH 7). [c]Fraction quenched (F_q=1-($I_{Et/Rh}/I_{Et}$)) calculated from 2-5 sets of independent samples from different syntheses of Et/Rh conjugates; approximate errors are listed in parentheses [d]Steady-state luminescence polarization (P) data collected at 20°C ; approximate error in polarization values=±0.005.
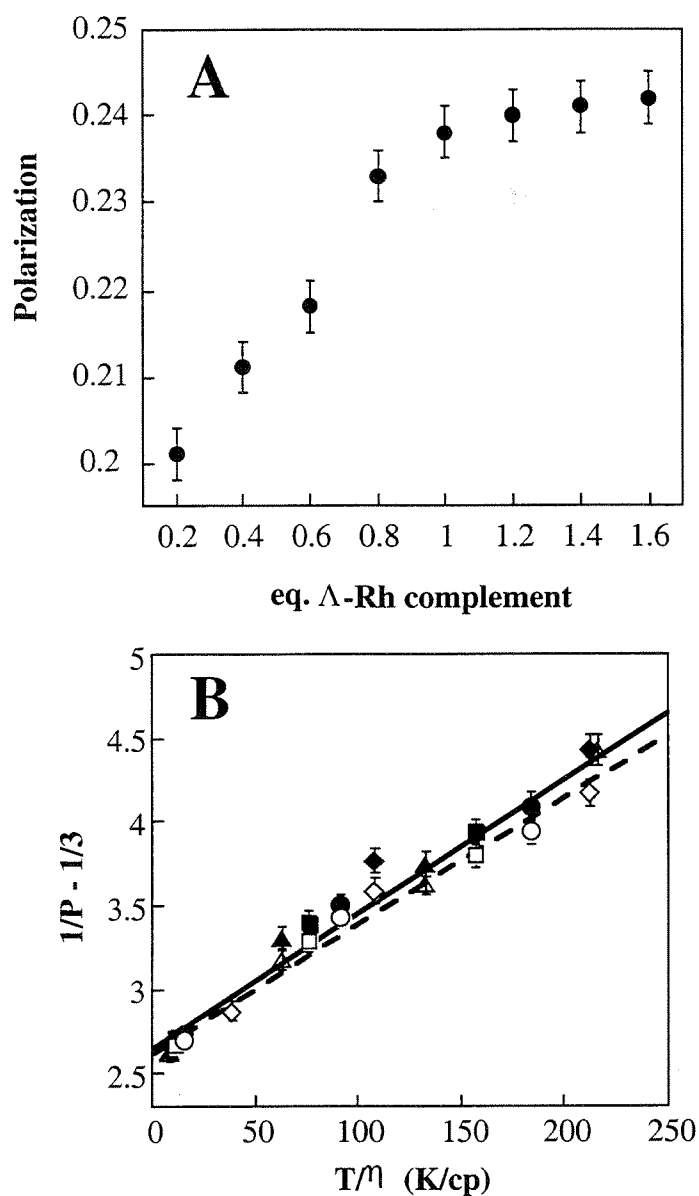
Figure 2.8 Steady-state fluorescence polarization assays for the structural

integrity of Et/Rh-modified duplexes. (**A**) Fluorescence polarization as a

function of hybridization for Et/Λ-Rh-12 mer. (**B**) Determination of duplex

volume from viscosity (η) and temperature (T) dependence of polarization (P)

for Et-modified (solid line) and Et/Rh-modified (dotted line) 11-mer.

From these measurements, volumes of $2.1(2) \times 10^4$ Å^3 and $2.3(2) \times 10^4$Å^3 are obtained

for the Et and Et/Rh modified 11-mer duplexes, respectively, which correlate closely

with the calculated volumes of 2.14×10^4 Å^3 and 2.32×10^4 Å^3.[27-28] Moreover, very

similar temperature and viscosity profiles are observed for both duplexes; the values of

P_0, the limiting polarization, obtained in these studies can be compared and the

difference in angular freedom allowed by both duplexes calculated.[26] This analysis also

confirms that intercalated ethidium is rigidly held in both the Et-modified and the Et/Rh-

modified duplex. In fact, the fluorophore actually experiences less angular freedom

(average angle $\approx 3°$) in the Et/Rh assembly.

2.3.4. Photoinduced electron transfer in Et/Rh duplexes

Quenching as a function of duplex length. Photoinduced electron transfer

between ethidium and Rh(phi)$_2$bpy^{3+} in the modified duplexes was studied by steady-

state and time-resolved fluorescence measurements (Table 2.2). The steady-state

fluorescence intensities observed for the ethidium-only duplexes are essentially constant,

while those for the Et/Rh systems rise with increasing distance between the two

intercalators. Therefore, the amount of quenching decreases with increasing

donor/acceptor separation. In a 10 base pair Et/Rh duplex, 28% of the ethidium

fluorescence is quenched by the intercalated acceptor.

The time scale of the quenching observed in Et/Rh duplexes was investigated

using TCSPC (Figure 2.9). The excited state decay of Et' in both the unquenched and

quenched duplexes was best fit to a triexponential. For example, in the Et-modified 10-

mer: $\tau_1 = 7.6$ ns (28%), $\tau_2 = 2.4$ ns (59%),$\tau_3 = 1.2$ ns (13%), and in the Et/Λ-Rh

analogue: $\tau_1 = 7.8$ ns (18%), $\tau_2 = 2.3$ ns (65%),$\tau_3 = 0.9$ ns (17%). As these lifetimes reflect

only small changes in the decay kinetics, some of the quenching observed in steady-state

measurements is manifested in these TCSPC measurements as a decrease in initial
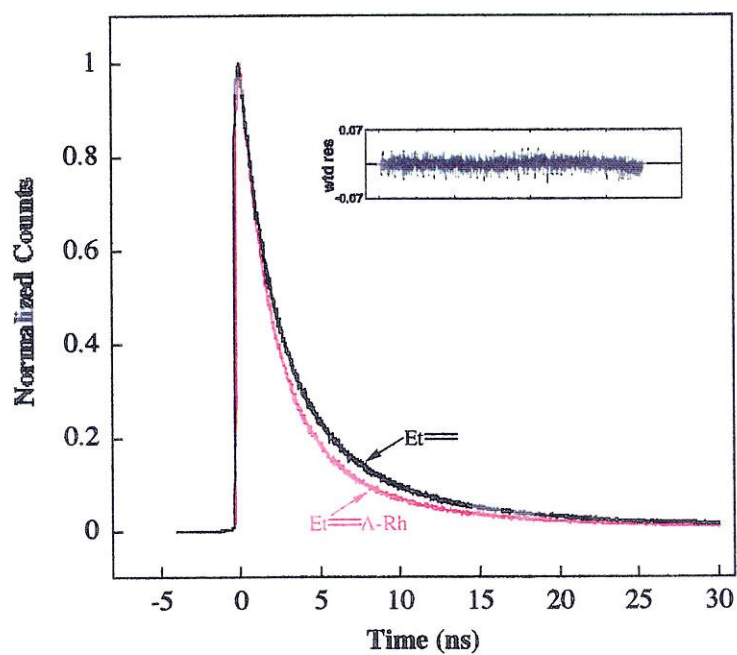
Figure 2.9 Normalized excited state decay profiles for Et and Et/Λ-Rh-modified 10 base pair duplexes by TCSPC. (insert) Residuals for triexpontential fit for Et/Rh 10-mer data.

intensity (static quenching). Hence, substantial quenching occurs on a time scale which is fast compared to the resolution of the instrument (~150 ps). For all of the Et/Rh duplexes studied, small changes in the triexponential excited-state decay profiles are observed relative to the duplexes modified only with ethidium; in the quenched samples, the percentage of the long decay component is decreased, while the percentages of the shorter lifetimes are increased. Other fitting procedures were explored in attempts to isolate a new component corresponding to an electron-transfer rate (*e.g.*, triexponential fit for quenched sample with fixed lifetimes obtained from biexponential fit for unquenched sample), but the triexponentials obtained for both the unquenched and quenched duplexes which contained the same lifetimes in slightly different proportions yielded the most accurate description of the decay profiles. These small changes observed for the decay kinetics may indicate some quenching on the nanosecond timescale or may reflect an apparent redistribution of excited state lifetimes owing to the selective static quenching of the longest decay component. The similar polarization values observed for Et and Et/Rh-modified duplexes also support static quenching as the deactivation mechanism, for if larger changes in the excited state lifetimes were responsible for the observed quenching, greater changes in the polarization values would be apparent.

By comparing time-resolved data to steady-state measurements or by quantitating the buildup of counts in the initial data channel by TCSPC for a fixed period of data collection, a substantial static component is present for the Et/Rh duplexes relative to the Et-duplex. The amount of static quenching approximated from these data exhibits the same variation with distance as the overall quenching, measured by steady state methods. However, since these time-resolved data were obtained on single samples of a given duplex length rather than a sample population as in the steady-state experiments, sample variability is not accounted for in the values obtained from TCSPC

and the uncertainty in this emission intensity estimation is large. Therefore, it is more instructive to consider distance trends based upon the overall quenching observed in steady-state measurements.

The observed static quenching is consistent with fast electron transfer ($k \geq 10^{10}$ s^{-1}) in these modified duplexes, and photoinduced quenching on this time scale parallels that observed with metallointercalators.[1-5] However, this ultrafast quenching does not permit measurements of forward rates of reaction. The multiexponential decays observed in this system warrants a focus on steady-state measurements which can be more accurately analyzed. Thus, the yield of electron transfer can be quantitated by fluorescence quenching and used to evaluate the distance dependence of electron-transfer efficiency. These data offer the first examination of how the yield of an electron-transfer reaction in DNA varies as a function of donor-acceptor distance.

In order to establish that the quenching was intrahelix and not the result of factors outside the π-stack, solution conditions were varied in experiments utilizing the 11 base pair assemblies. In D_2O, where the excited state lifetime of the fluorophore is increased,[29] no decreases in quenching were observed as might be expected for a solvent-mediated process or displacement of the donor from the base stack. Additionally, only very small decreases in quenching yield occurred with increased viscosity (η=3.2 cp) or ionic strength (10-200 mM NaCl). Investigations of the concentration dependence of the reaction revealed that the quenching yields were constant over the concentration range of 2-20 μM. At concentrations of donor-only duplexes above 20 μM, self-quenching of ethidium fluorescence was observed, reflecting interduplex intercalation. Furthermore, in experiments where the ethidium donor and rhodium(III) acceptors were localized on separate duplexes, negligible quenching was observed at 5 μM duplex concentration, eliminating the possibility of an interduplex reaction. These results all confirm that the quenching observed in these

systems is the result of an intrahelix process and therefore must proceed over extended distances mediated by the DNA π-stack.

2.3.5 Effects of base stacking on electron transfer

The sensitivity of the long-range quenching reaction to base-pair stacking was also examined. Figure 2.10 depicts steady-state fluorescence intensity of the covalently-bound fluorophore as a function of temperature for Et-modified and Et/Rh-modified duplexes. Over the temperature range where the duplex melts, the quenching is lost. Importantly, just as the melting process is reversible, the quenching loss is also reversible. When temperature-dependent quenching yields are directly compared to the loss in hypochromicity associated with base stacking (Figure 2.11), it is apparent that the two phenomena are affected identically by the uncoupling of the bases at elevated temperatures. Therefore, the quenching must be occurring across a fully base-paired duplex. It is clear that the π-stack of the double helix, which is tightly stacked only in the helical form, electronically couples the acceptor and donor brought together by the complementary strands to which they are tethered.

The sensitivity of the quenching to base stacking is best illustrated in modified duplexes containing intervening mismatches. In order to maintain a constant donor-acceptor distance while perturbing stacking within the DNA helix at a constant temperature, single-base pair mismatches were introduced into 11 base pair Et/Rh-modified duplexes. Both GA and CA mismatches were incorporated into modified duplexes; NMR and crystallographic studies indicate that CA mispairs significantly perturb the stacked bases, while GA mismatches stack favorably.[30-31] Consistent with the expected perturbations to the π-stack, the CA mismatch leads to a significant decrease in the quenching yield (Table 2.3). However, with a GA mismatch, the quenching reaction is as efficient as in the fully Watson-Crick base-paired duplex.
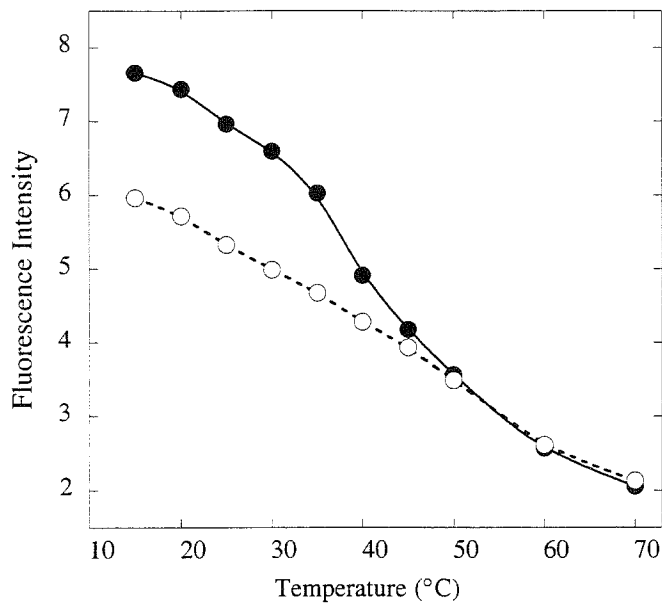
Figure 2.10 Temperature dependence of emission for the

Et (filled circles) and Et/Rh-modified (empty circles) 11-mer.
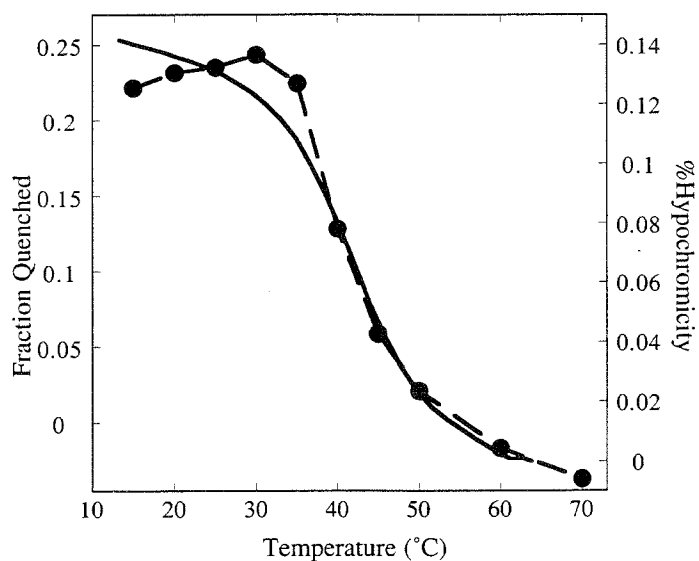
Figure 2.11 Comparison of quenching yield (circles, dotted line)

and % hypochromicity (solid line) for Et/Rh 11-mer.

Table 2.3 Quenching in Et/Rh-modified Mismatch Duplexes[a]

	I_{Et}[b]	$I_{Et/Rh}$	F_q[c]
Et'−5'C T T A T **C** G T 　　　　C T A T C G **T** 　G A T A **A** G C A5'−Λ-**Rh**	0.36	0.28	**0.21**
Et'−5'C T T A T **C** G T 　　　　C T A **C** C G T 　G A T A **A** G C A5'−Λ-**Rh**	0.35	0.34	**0.04**
Et'−5'C T T A T **C** G T 　　　　C T A **G** C G T 　G A T A **A** G C A5'−Λ-**Rh**	0.37	0.25	**0.26**

[a]T_m values were collected for each Et and Et/Rh modified duplex at same conditions used for fluorescence quenching experiments. Et_{TA}= 37°C, Et/Rh $_{TA}$= 43°C; Et_{CA}= 23°C, Et/Rh $_{CA}$= 26°C; Et_{GA}= 28°C, Et/Rh $_{GA}$= 34°C. [b]Intensities for Et (I_{Et}) and Et/Rh-modified ($I_{Et/Rh}$) duplexes are listed relative to 10 μM Ru(bpy)$_3^{2+}$ at 20 °C. [c]The quenching yields (F_q) at 20°C and 10°C were identical within error (5%).

These results highlight the sensitivity of DNA-mediated electron transfer to perturbations in stacking and base-pair stability within the DNA helix.

2.4 DISCUSSION

2.4.1 Ethidium and $Rh(phi)_2bpy^{3+}$ as electron donor and acceptor in DNA

Photoinduced electron transfer between ethidium and $Rh(phi)_2bpy^{3+}$ bound to DNA by intercalation occurs efficiently and on a fast timescale. Fluorescence quenching of DNA-bound ethidium by rhodium is primarily static (with nanosecond resolution), and 50% quenching is apparent at low intercalator/DNA loadings (1 Et/2 Rh/50 bp). The efficiency of the electron-transfer reaction between ethidium and $Rh(phi)_2bpy^{3+}$ is notably lower than that observed with $Ru(phen)_2dppz^{2+}$ as a donor,[2-3] despite a comparable driving force. However, the fast kinetics of the photoinduced quenching (k $\geq$ 10^{10} s^{-1}) parallel those obtained with the metallointercalator donor. Interestingly, when ethidium is intercalated, only the phenyl ring is exposed to the minor groove, and thus, this organic heterocycle would be less likely to participate in the clustering interactions previously proposed to facilitate fast electron transfer between metallointercalators.[30-31] It is also noteworthy that the fast quenching observed in the Et/Rh(III) system contrasts that observed with DAP, possibly owing to the weaker intercalative binding of this acceptor.[6,32] The different trends observed in these studies indicate that the coupling of donor-acceptor pairs into the DNA π-stack is extremely sensitive to the binding properties of the reactants.

2.4.1 Sensitivity of DNA-mediated electron transfer to distance and stacking

DNA oligonucleotide duplexes containing covalently bound ethidium and rhodium intercalators were prepared in order to probe further the characteristics of photoinduced electron transfer mediated by the DNA helix. Measurements of fluorescence quenching in these modified duplexes allow the examination of the fast quenching reaction between ethidium and $Rh(phi)_2bpy^{3+}$ without the possibility of intercalator clustering. Moreover, by systematically varying the length of the oligonucleotide region between the intercalators, we could, for the first time, examine how such photoinduced quenching varies as a function of distance separating the bound donor and acceptor.

Photoinduced electron transfer is also apparent between intercalated ethidium and rhodium in these covalently modified oligonucleotide duplexes. In DNA duplexes with ethidium and rhodium separated by ~20 Å, 30% of the ethidium fluorescence is quenched, while with a separation of ~30 Å, 10% quenching is observed. Time-resolved measurements on the modified oligomers reveal multiexponential decays in ethidium emission in the presence and absence of covalently bound rhodium, and demonstrate that quenching by the rhodium complex at a pronounced donor/acceptor separation is also primarily static on the nanosecond timescale. The amount of quenching observed across the family of modified oligomers shows a shallow dependence on distance. However, the quenching yield is found to be extremely sensitive to base stacking, as is most dramatically evident in comparing quenching in modified duplexes with or without a single intervening DNA mismatch. These results all support the notion that the stacked DNA bases can facilitate long-range electron transfer.

Alternate interpretations considered. Given the striking difference suggested by these data in the distance dependence for electron transfer with DNA as a medium compared to proteins,[33] it is important to consider first whether alternate structural

models might account for these results. It is essential that the integrity of intercalation and of the duplex structures be firmly established for the results presented to be interpreted as long-range electron transfer through the base stack of DNA.

For the electron-transfer reaction to take place through the base stack in this system, both donor and acceptor must be intercalated within the DNA helix. Thermal denaturation studies demonstrate the increased helix stability of duplexes modified with each intercalator; modification with both intercalators yields still greater stabilization. The fluorescence enhancement seen for ethidium tethered to the DNA duplex compared to free ethidium also is fully consistent with intercalation.[10] Fluorescence polarization data indicate that the bound ethidium is rigidly positioned. In addition, direct strand photocleavage, as found in tethered rhodium duplexes,[14] is observed only with tight intercalation of the complex,[11] and this photocleavage chemistry points to a pattern of intercalation sites expected based upon model building.

Might intercalation of the rhodium in DNA duplexes promote fluorescence quenching resulting from the displacement of ethidium? The higher melting temperature found for the doubly-modified duplexes is inconsistent with this notion of displacement. In addition, volumes for the DNA duplexes determined based upon fluorescence depolarization measurements are fully consistent with intercalation of both rhodium and ethidium (leading to the increase in length of the cylinder); indeed these data suggest greater rigidity for ethidium in the presence of rhodium. Moreover, as the lifetime of Et' in H_2O ($\tau = 440$ ps) is significantly enhanced upon intercalation ($\tau_1 = 7.6$ ns (28%), $\tau_2 = 2.4$ ns (59%),$\tau_3 = 1.2$ ns (13%)), the presence of free fluorophore either in the Et or Et/Rh modified duplex could be monitored in single photon counting experiments; no emission lifetime characteristic of the free fluorophore is detected at the concentrations under which these experiments were performed. Lastly, if the presence of bound rhodium led to apparent fluorescence quenching by making ethidium more

accessible to solvent, quenching should be decreased in D_2O,[29] but in this system, the nature of the solvent has little effect on the quenching observed.

The possibility that some deformation or fraying of the duplex could lead to direct contact between the donor and acceptor may also be considered. Again, time-resolved measurements show no indication of free, non-intercalated ethidium. Polarization results rule out a gross structural heterogeneity in the duplexes, as trends observed obey relationships predicted for ellipsoid molecules of one discrete structure.[25] While polarization measurements examine only unquenched material, these data correlate with melting studies monitored by absorbance, which also indicate structurally homogeneous duplex populations. Certainly for the shorter duplexes, where 25-30% quenching occurs, such hetereogeneity in structure would be discernible by these techniques. Importantly, hypochromism as a function of temperature is found to correlate directly with fluorescence quenching, supporting the idea that a quenched population is not structurally distinctive. Moreover, similar percentages of hypochromism are observed in all the duplexes, indicating that analogous duplex structures are present in all of the Et and Et/Rh assemblies utilized in this study. One might also consider that if fraying were responsible for the observed quenching, larger amounts of quenching would be expected at elevated temperatures, where such fraying would be favored. On the contrary, the quenching observed in this system exhibits the same temperature dependence as the melting of the duplex, indicating that the loss of the well-ordered base stack eliminates the pathway for electron transfer.

The effect of an intervening CA mismatch on the quenching yield in the modified duplexes is perhaps the strongest single observation in support of a DNA-mediated reaction. If fraying at the ends were to arise, leading to some direct contact between donor and acceptor, this fraying should also occur in the DNA duplex containing the CA mismatch, yet no quenching in the duplex containing the intervening

mismatch occurs. Indeed, since the mismatch-containing oligomer is less stable than that without the mismatch, based upon arguments requiring a helix opening or bending to occur, greater opening of the duplex would be expected to facilitate more quenching in the mismatched duplex. The observation that quenching is maintained in the duplex containing the GA mismatch, which stacks well within the DNA helix, is consistent with this idea that quenching requires a well-ordered base stack. Thus, the significant loss in quenching observed with an intervening CA mismatch confirms that this reaction proceeds through the intervening base stack, not on the periphery of the helix.

Lastly, we consider whether the quenching arises through electron transfer rather than an alternate mechanism. We assign the mechanism responsible for the quenching reaction as electron transfer based primarily upon transient absorption data for ethidium and rhodium non-covalently bound to DNA. Transient absorption data provide evidence for the electron transfer products, and the yields of electron transfer intermediates, although small on the microsecond timescale, correlate with photoinduced quenching. Electron transfer between photoexcited ethidium and $Rh(phi)_2bpy^{3+}$ is certainly thermodynamically favored ($\Delta G \sim -900$ mV). Little spectral overlap is observed between the donor emission and acceptor absorption, and hence quenching through a singlet energy transfer mechanism would be expected to be negligible. Furthermore, the dependence on distance of the quenching we observe in this system is inconsistent with either the $1/r^6$ dependence expected for a Förster mechanism or any variations on such a $1/r^6$ dependence that may arise owing to the effects of helical orientation observed previously.[62]

Thus, data obtained in this system are fully consistent with fluorescence quenching which arises as a result of long-range electron transfer mediated by the DNA base stack. Given this electron-transfer process within the well-characterized assemblies described, the sensitivity of this reaction to distance and stacking may be examined.

2.4.3 Analysis of distance dependence

The steady-state quenching yield exhibits a logarithmic dependence on the distance separating the donor and the Rh(III) acceptor (Figure 2.12). If this relationship is considered within the framework of Marcus theory,[35] the slope of this line (0.1 Å^{-1}) would reflect the decay of the electronic coupling with distance (β). However, time-resolved measurements of the fluorescence decay reveal that the quenching has a significant static component. Thus, these data allow us only to establish a fastest quenching rate as $\geq 10^9$ s^{-1} over distances varying from ~ 20-35 Å. The variations in quenching observed at different donor/acceptor separations appear to be related to the *yield* of a very fast electron-transfer process, rather than to a large variation in quenching rate. Qualitatively, it is apparent that DNA facilitates remarkably efficient long-range electron transfer with a shallow dependence upon distance distinct from that observed in proteins, but a meaningful value for β cannot be extracted from these data due to the fast time scale of electron transfer at all of the donor/acceptor distances investigated.

Nonetheless, the very shallow dependence of this DNA-mediated reaction on distance is inconsistent with recent theoretical studies which predict distance trends similar to those observed in proteins.[36] Our results indicate that the extended π-stack provides much stronger electronic coupling than observed in many protein systems, where distance dependences are dominated by σ-tunneling.[33] A shallow distance dependence for the observed electron-transfer reaction might be a result of a small energetic difference between the donor excited state and the DNA bridge, in which case donor/acceptor coupling has been predicted to proceed over extended distances.[37-39] However, these energies are not known. Our results underscore the need to determine experimentally the energy gaps for stacked DNA bases and species stacked within the DNA helix.

The distance dependence of this DNA-mediated electron-transfer reaction may in
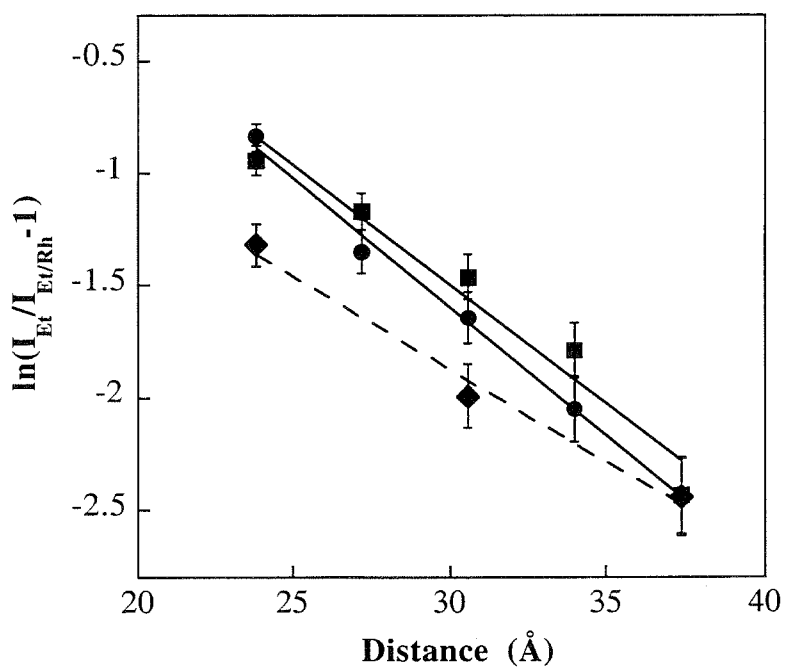
Figure 2.12 Distance dependence of steady-state fluorescence quenching for Et/Rh-modified duplexes. Data shown are for the Δ-Rh diastereomer with a 5'ACGA binding site (squares, long dash), Λ-Rh diastereomer with a 5'ACGA binding site (circles, solid line), and *rac*-Rh with a 5'ACAC binding site (diamonds, short dash).

part reflect a structural property intrinsic to the DNA helix: stacking. It is well known that the double helical structure of DNA is dynamic.[24] Internal motions within the DNA helix have been observed on time scales ranging from milliseconds to picoseconds.[28-40] Therefore, we propose that the quenching process is gated by disruptions in the π-stack-mediated electronic coupling; as the number of intervening base pairs increases, the probability that all base pairs will be stacked on the time scale of the electron-transfer reaction decreases. With a simple model, expressions can be derived to relate the amount of quenching (F_q) observed in the modified duplexes to the probability of full base stacking (P_{st}) which decreases with increasing number of base pairs within the duplex (n).

$$F_q = (P_{st})^n P_D P_A$$
$$\log F_q = n \log(P_{st})^n + \log(P_D P_A)$$

The quenching would also depend on stacking probabilities for the donor (P_D) and acceptor (P_A). Thus, the quenching yield would reflect both the coupling of donor and acceptor into the helix (which remains constant with increasing duplex length) and the probability of base pair stacking (which varies exponentially with the number of intervening DNA base pairs). This expression predicts a logarithmic dependence of the quenching yield on the number of base pairs between donor and acceptor, and the data obtained from this system yields $P_{st} = 0.76$.

The striking correlation between quenching yields and the loss of hypochromism through the thermal activation of base pair opening indicates that the electron transfer requires a well-ordered π-stack. The sensitivity of quenching to a CA mispair, which has a higher destacking probability, also indicates that how well the base pairs are stacked affects electronic coupling between donor and acceptor. Taken together, these

findings all suggest that the probability of an electron-transfer event mediated by the DNA π-stack is modulated in part by stacking and thus, electron-transfer may be a sensitive reporter of base stacking.

2.4.4 Implications with respect to biological electron transfer

It is clear that the system described here differs significantly from donor/acceptor complexes which rely on σ-bonded arrays for electronic coupling. Based on our results for intercalated donors and acceptors, it is apparent that electron transfer through DNA is not protein-like. In classic studies of protein-mediated electron transfer using donors and acceptors at fixed distances of separation, β was found to range from 0.8 to 1.4 Å^{-1}.[33] When the oxidation of guanine by stilbene was measured in a DNA hairpin, β was calculated as 0.6 Å^{-1} for DNA-mediated electron transfer in this system.[8] Here, in the first systematic study of DNA-mediated electron transfer between intercalators as a function of distance, we conclude that β may be much lower, or that in the tunneling energy regime investigated, the distance dependence may be more complex.[39] Indeed, β may not be the sole parameter which characterizes the distance dependence of electron transfer in DNA. For example, stacking parameters, which do not appear to be a primary issue in electron-transfer pathways for folded proteins, may also influence the distance dependence we observe.

As the base stack of DNA is not a medium dominated by σ-connectivities, but instead π-mediated stacking, it is not surprising that the difference between the electronic properties of proteins and DNA arises. Conductivity is observed in π-stacks of doped solid state materials.[41-43] Based on this analogy, as long as the pathway for electron-transfer goes through the π-stacked base pairs of DNA, we might expect the distance dependence to be more shallow than in proteins. Moreover, the structural properties of the double helix, which are dominated by non-covalent stacking of

aromatic heterocycles, must be considered in describing long-range electron transfer across DNA. From our results, it is evident that the electronic coupling provided by DNA is highly sensitive to stacking interactions within the double helix. Indeed, the sensitivity of electron transfer to stacking is dramatically illustrated by our results with single base mismatches.

The discovery of this sensitivity to stacking may also reconcile the varying efficiencies of DNA-mediated electron-transfer reactions reported for different systems.[3,4,7,9-10,13-15] When intercalators are utilized to probe the base stack of DNA as a medium for photoinduced electron transfer, fast kinetics are observed in reactions that proceed over long distances.[1-8] When non-intercalating or poorly stacked probes are employed, much steeper distance dependences and slower electron transfer kinetics result.[8-10] Just as the efficiency of long-range electron transfer in DNA is sensitive to base stacking, it is also now clear that this phenomenon is also affected by stacking interactions between the DNA bases and reporter molecules. Stacking is a crucial parameter in understanding electron-transfer processes in DNA, and distinguishes this medium from proteins. Stacking interactions appear to be essential in facilitating reactant/DNA couplings, while no analogous parameter has been implicated in modulating coupling for σ-bonded systems.

For the electron transfer between ethidium and $Rh(phi)_2bpy^{3+}$, it has been demonstrated that photoinduced electron transfer is fast, modulated by the intervening π-stack, and can take place over distances of ~30 Å. The variety of systems in which the DNA double helix has now been shown to facilitate charge transport over long distances provides a basis for speculation concerning mechanisms existing within cells where long-range electron transfer in DNA is utilized. In addition, electronic delocalization within DNA may allow base damage to be concentrated at low-energy sites where specific repair mechanisms can operate efficiently. As proteins have been specifically

engineered for electron-transfer processes, we might imagine that the evolution of nucleic acids also involved electronic considerations. Our findings point to the DNA π-stack as not only a carrier of genetic information, but also a pathway which is conducive to charge transport.

2.5 REFERENCES

1. Murphy, C. J.; Arkin, M. A.; Jenkins, Y.; Ghatlia, N. D.; Bossman, S.; Turro, N. J.; Barton, J.K. *Science* **1993**, *262*, 1025.

2. Arkin, M.R.; Stemp, E.D.A; Holmlin, R.E.; Barton, J.K.; Hörmann, A.; Olson, E.J.C.; Barbara, P.A. *Science* **1996**, *273*, 475.

3. Murphy, C.J.; Arkin, M.A.; Ghatlia, N.D.; Bossman, S.; Turro, N.J.; Barton, J.K. *Proc. Natl. Acad. Sci. U.S.A.* **1994**, *91*, 5315.

4. Arkin, M.R.; Stemp, E.D.A.; Turro, C.; Turro, N.; Barton, J.K. *J. Am. Chem. Soc* **1996**, *118*, 2267.

5. Holmlin, R.E.; Stemp, E.D.A.; Barton, J.K. *J. Am. Chem. Soc.* **1996**, *118*, 5236.

6. Brun, A. M.; Harriman, A. *J. Am. Chem. Soc.* **1992**, *114*, 3656.

7. Meade, T. J.; Kayyem, J. F. *Angew. Chem. Int. Ed. Engl.* **1995**, *34*, 352.

8. Lewis, F.D.; Wu, Taifeng; Zhang, Y.; Letsinger, R.L.; Greenfield, S.R.; Wasielewski, M.R. *Science* **1997**, in press.

9. Waring, M.J. *J. Mol. Biol.* **1965**, *13*, 269.

10. LePecq, J.B.; Paoletti, C. *J. Mol. Biol.* **1967**, *27*, 87.

11. Pyle, A.M.; Chiang; M.; Barton, J.K. *Inorg. Chem.* **1990**, *29*, 4487.

12. Beaucage, S.L.; Caruthers, M.H.; *Tet. Lett.* **1981**, *23*, 1859.

13. Wachter, L.; Jablonski, J.A.; Ramachandran, K.L. *Nucl. Acids Res.* **1986**, *14*, 7985.

14. Holmlin, R.E., *doctoral thesis*.

15. Lindberg, O.; Ernsten, L. in *Methods of Biochemical Analysis , Vol. 3* (Glick, D. Ed.), Interscience: NY, **1954.**

16. Eritja, R.; Horowitz, D.M.; Walker, P.A.; Ziehler-Martin, J.P.; Boosalis, M.S.; Goodman, M.F.; Itakura, K.; Kaplan, B.E. *Nucl. Acids. Res.* **1986**, *14*, 8135.

17. Holmlin, R.E.; Barton, J.K. *Inorg. Chem.* **1995**, *34*, 7.

18. Atherton, S.J.; Beaumont, P.C. *J. Phys. Chem.* **1987**, *91*, 3993.

19. Stemp, E.D.A.; Arkin, M.R.; Barton, J.K. *J. Am. Chem. Soc.* **1995**, *117*, 2375.

20. Jenkins, Y.; Friedman, A.E.; Turro, N.J.; Barton, J.K. *Biochemistry* **1992**, *31*, 10809.

21. Hartshorn, R.M.; Barton, J.K. *J. Am. Chem. Soc.* **1992**, *114*, 5919.

22. DuPureur, C.M.; Barton, J.K. *J. Am. Chem. Soc.* **1994**, *116*, 10286.

23. DuPureur, C. M.; Barton, J. K. *Inorg. Chem.* **1997**, *36*, 33.

24. Saenger, W. *Principles of Nucleic Acid Structure.* **1984,** Springer-Verlag New York, and references therin.

25. Weber, G. *Biochemistry* **1952**, *51*, 145.

26. Lakowicz, J.R. *Principles of Fluorescence Spectroscopy.* **1983**, Plenum Press, New York, pp. 111-153.

27. LeBret, M. *Biopolymers* **1978**, *17*, 1939.

28. Millar, D.P.; Roberts, R.J.; Zewail, A.H. *Proc. Natl. Acad. Sci.* **1980**, *77*, 5593.

29. Olmsted, J.; Kearns, D.R. *Biochemistry* **1977**, *16*, 3647.

30. Patel, D.J.; Kozlowski, S.A.; Ikuta, S.; Itakura, K. *FASEB* **1984**, *11*, 2664.

31. Brown, T.; Hunter, W.N.; Kneale, G.; Kennard, O. *Proc. Natl. Acad. Sci. U.S.A.* **1986**, *83*, 2402.

32. Brun, A.M.; Harriman, A. *J. Am. Chem. Soc.* **1991**, *113*, 8153.

33. Bowler, B.E.; Raphael, A.L.; Gray, H.B. *Prog. Inorg. Chem.* **1990**, *38*, 259

34. Clegg, R.M.; Murchie, A.I.H.; Zechel, A.; Lilley, D.M.J. *Proc. Natl. Acad. Sci. U.S.A.* **1993**, *90*, 2994.

35. Marcus, R.A.; Sutin, N. *Biochim. Biophys. Acta* **1985**, *811*, 265.

36. Priyadarshy, S.; Risser, S.M.; Beratan, D.N. *J. Phys. Chem.* **1996**, *100*, 17678.

37. Felts, A.K.; Pollard; W.T.; Freisner, R.A. *J. Phys. Chem.* **1995**, *99*, 2929.

38. Reimers, J.R.; Hush, N.S. *J. Photochem. Photobiol. A: Chem.* **1994**, *82*, 31.

39. Evenson, J.W.; Karplus, M. *Science* **1993**, *262*, 1247.

40. Robinson, B.H.; Mailer, C.; Drobny, G. *Ann. Rev. Biophys. Biomol. Sruct.* **1997**, *26*, 629.

41. Graf, D.D.; Campbell, J.P.; Young, V.J.; Miller, L.L; Mann, K.R. *J. Am. Chem. Soc.* **1996**, *118*, 5480.

42. Schouten, P.G.; Warman, J.M.; deHaas, M.P.; Fox, M.A.; Pan, H.-L. *Nature* **1991**, 353, 736.

43. Marks, T.J. *Science* **1985**, *227*, 881.

Chapter 3

Photoinduced Electron Transfer Between an Intercalator and a DNA Base: Π-Stacking as a Modulator of Reactivity[‡]

3.1   INTRODUCTION

In systems employing intercalating reactants,[1-5] we have observed efficient, long-range electron transfer mediated by the DNA bases. However, other investigations using nonintercalated reactants have revealed steeper distance dependences and slower reaction kinetics.[6-8] To address these disparate results and establish the generality of our findings with intercalated systems, we sought to employ a DNA base in a photoinduced electron-transfer reaction. Moreover, using a DNA base as a reactant would link our findings to biological electron-transfer chemistry related to base damage.[9] We therefore investigated the efficiency of the photooxidation of a novel base analogue, 7-deazaguanine (dz-G, Z), by ethidium (Et) (Figure 3.1). As described in the previous chapter, we have extensively characterized ethidium-modified DNA assemblies; moreover, the binding site of ethidium can be established using a high-energy photoreactivity of this intercalator.[10] Since the site of deazaguanine incorporation is determined during oligonucleotide synthesis, precise donor/acceptor distances within Et/Z duplexes can therefore be determined and varied systematically.

Using a DNA base as a reactant not only affords a structurally well-defined system, but allows the investigation of a parameter unique to the DNA helix as a biological macromolecule: stacking. In several studies of charge transport through DNA including the photoinduced electron-transfer reaction described in the previous chapter, the *intervening stacking* within the DNA base stack pathway was identified as a crucial factor modulating the efficiency of these reactions. Here, *reactant stacking* can be varied. By changing the flanking sequence surrounding the electron donor, the local stacking environment can be altered. In addition, by incorporating this base analogue within mismatched pairs, the stacking of deazaguanine within the DNA helix can be perturbed.
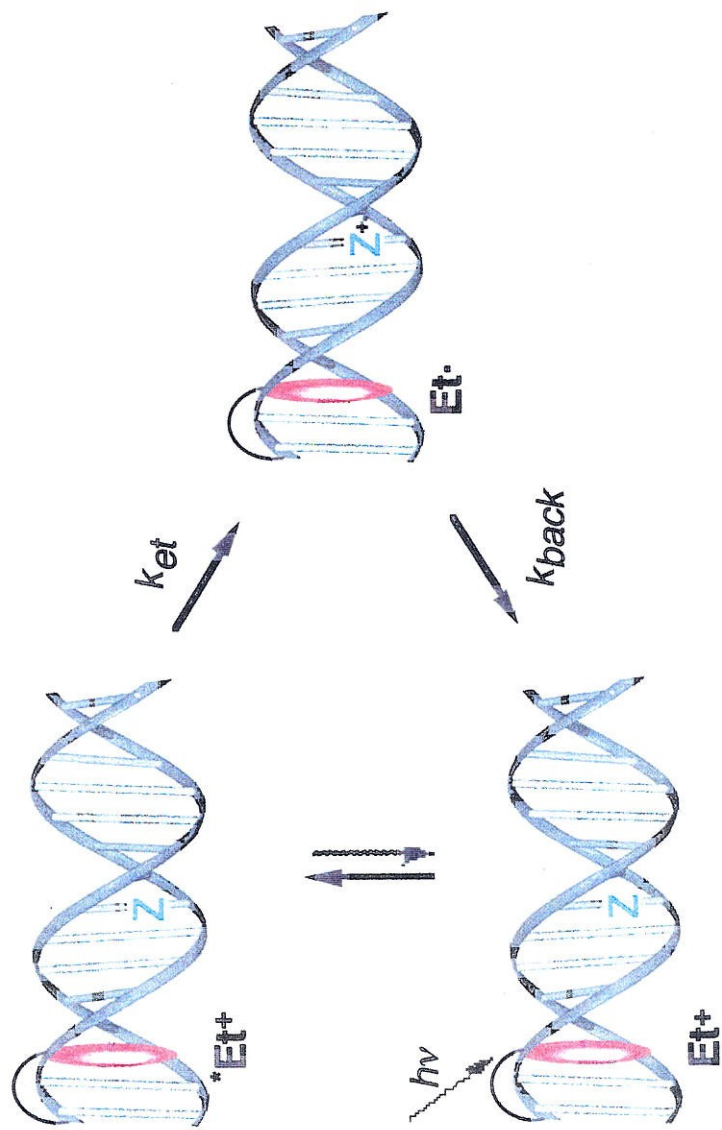
Figure 3.1 Schematic diagram of photooxidation of deazaguanine (Z) by intercalated ethidium

Using this approach, we have observed extraordinarily fast ($k_{ET} \geq 10^{10}$ s^{-1}) electron transfer over a large range of ethidium/deazaguanine separations (14-30 Å). Importantly, the distance *dependence* of this photooxidation reaction is sensitive to sequence and appears to be modulated by base-base interactions. The remarkable efficiency of the photooxidation of deazaguanine by intercalated ethidium over long molecular distances provides new evidence for the existence of pathways for fast electron transfer through DNA. This study represents the first investigation of DNA-mediated electron transfer between a tethered intercalator and a modified base. By varying sequence as well as reactant separation, this work provided the first experimental demonstration of the importance of reactant stacking in the modulation of long-range DNA-mediated electron-transfer reactions.

3.2 EXPERIMENTAL SECTION

Materials. Unless otherwise noted, all reagents were purchased from Aldrich or Fluka and used without further purification. Reagents for oligonucleotide synthesis were obtained from Glen Research. Triphosphate nucleotides were obtained from Pharmacia.

Preparation of Et/dz-G duplexes. N-8-glycyl ethidium and ethidium-modified oligonucleotides (Et-NHCO(CH$_2$)$_3$CONH(CH$_2$)$_n$-5'-DNA (n = 2,6,9)) were prepared as previously described in Chapter 2. Oligonucleotides containing deazaguanine were synthesized on a 394 ABI synthesizer by standard automated techniques,[11] with the exception of a 3 minute oxidation step employing 10-camphorsulfonyl oxaziridine (1g/10 ml CH$_3$CN). All conjugates and unmodified oligonucleotides were purified by reversed phase HPLC. For the hybridization of duplex samples, appropriate amounts of complementary materials based on the extinction coefficient for ethidium-modified sequences (ε_{484}=4000 M^{-1} cm^{-1}) and calculated extinction coefficients for unmodified sequences (ε_{260} (M^{-1} cm^{-1}) : dC = 7.4 x 10^3; dG = 12.3 x 10^3; dzG = 10.5 x 10^3; dT =

6.7×10^3; dA = 15.0×10^3), were combined at 1:1 stoichiometry and dissolved in 5 mM phosphate, 50 mM NaCl (pH 7) to yield a final duplex concentration of 5 μM. The resulting solutions were heated to 90°C and slowly cooled to ambient temperature over 2-3 hours to anneal the duplex.

Characterization of modified duplexes. As previously described,[3] ethidium-modified sequences were characterized as single strands by mass spectrometry, base digestion analysis, phosphate analysis, and ultraviolet-visible absorbance. In double-stranded form, thermal denaturation measurements monitored by absorbance at 260 nm were used to confirm the integrity of modified duplexes (*vide supra*). The fluorescence intensities of the 14-base pair duplexes used in this study were comparable to those observed for the variable-length series previously reported.[3]

Electrochemical measurements. The reduction potential of ethidium was measured *via* cyclic voltammetry on a BAS CV-50W potentiostat in 0.1 M TBAH/CH$_3$CN. Potentials for 2'-deoxyguanosine triphosphate (dGTP) (Pharmacia) and 7-deaza-2'-deoxyguanosine triphosphate (dz-dGTP) (Pharmacia) were obtained on the same apparatus in 0.1 M phosphate buffer, pH 7. Cyclic voltammetry was carried out at 20°C with a normal three electrode configuration consisting of a glassy carbon working electrode, saturated calomel reference electrode, and platinum auxiliary electrode. The ethidium excited-state reduction potential ($E^o(^{*/0})$) was calculated using the expression $E^o(^{*/0}) = E_{oo} - E^o(^{+/0})$. Values of E_{oo} were approximated both by averaging absorption and emission maxima and examining intersection points of absorption and emission spectra. Both methods yielded equivalent results for ethidium. Potentials are reported *versus* NHE.

Steady-state fluorescence experiments. Steady-state fluorescence measurements were made at 20°C with excitation at 480 nm on an SLM 8000 spectrofluorimeter. Fluorescence intensities were integrated from 520 to 800 nm. Samples with identical

absorbance at the wavelength of excitation were measured at a duplex concentration of 5 μM in 5 mM phosphate, 50 mM NaCl (pH 7). Quenching yields for modified duplexes obtained by steady-state fluorescence measurements were calculated from 3-4 samples sets.

Time-correlated single photon counting (TCSPC). TCSPC was carried out using facilities described previously[2] with λ_{exc} = 335 nm obtained by doubling the 670 nm fundamental line; data fitting was accomplished using least-squares methods in a commercial software program (Axum). Data sets contained 5,000-10,000 counts, except in cases when small time windows were necessary to ensure constant laser power. Steady-state quenching yields obtained with λ_{exc} = 480 nm were identical to those observed with λ_{exc} = 335 nm. Sample conditions and concentrations were identical in time-resolved and steady-state measurements. No photodegradation was observed, as confirmed by uv-vis absorption spectra taken before and after irradiation.

Melting profiles. Thermal denaturation experiments were performed on a HP8452A diode-array spectrophotometer with samples at a duplex concentration of 5 μM in 5 mM phosphate, 50 mM NaCl (pH 7). Absorbance at 260 nm was monitored every 2°C with 3 minute equilibration times.

3.3   RESULTS

3.3.1   Redox properties of 7-deazaguanine

7-deazaguanine differs in structure from the natural base by only one atom (Figure 3.2). This small change in structure shifts the oxidation potential from ~ +1.3 V (*vs.* NHE) for guanine to ~ +1.0 V for deazaguanine (Table 3.1). The lowered potential for the modified base is apparent in the reactivity of the nucleotides towards the fluorescent singlet excited state of ethidium in aqueous solution (Figure 3.3). No change
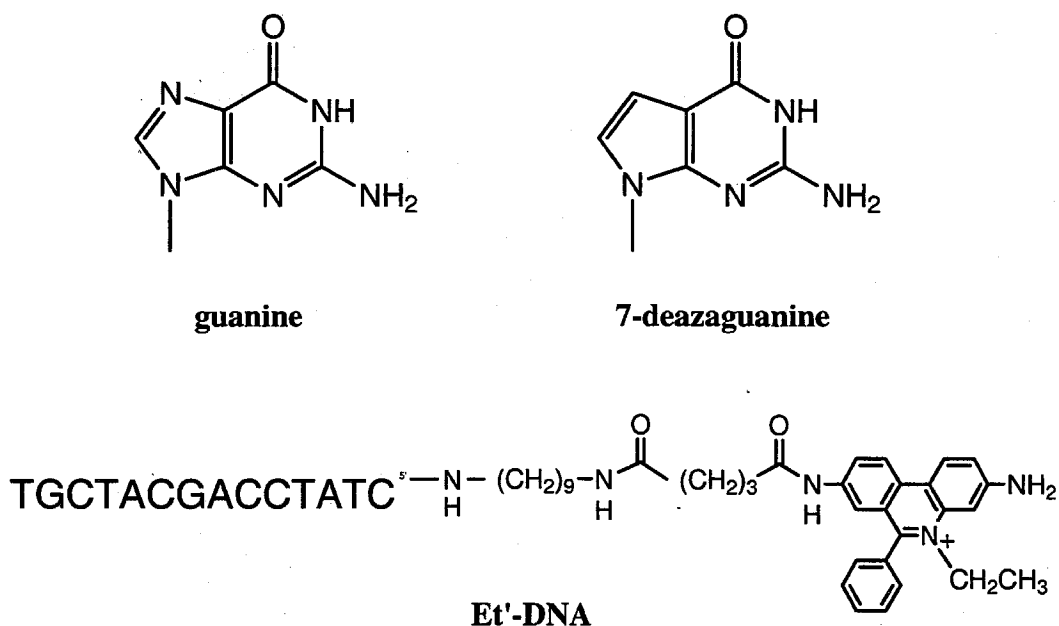
Figure 3.2 Structures of guanine, deazaguanine, and an ethidum-modified oligonucleotide.

Table 3.1 Reduction potentials for *Et, dGTP, and dz-dGTP

	Potential *vs.* NHE[a]
Et$^{*/0}$	+1.2 V[b]
dGTP$^{+/0}$	+1.3 V[c]
dz-dGTP$^{+/0}$	+1.0 V[c]

[a] Potentials were obtained in 100 mM phosphate buffer, pH 7 with a normal three electrode configuration consisting of a glassy carbon working electrode, saturated calomel reference electrode, and platinum auxiliary electrode. [b]Calculated using expression $E^{o(*/0)} = E_{oo} - E^{o(+/0)}$. [c] Irreversible peak potential.
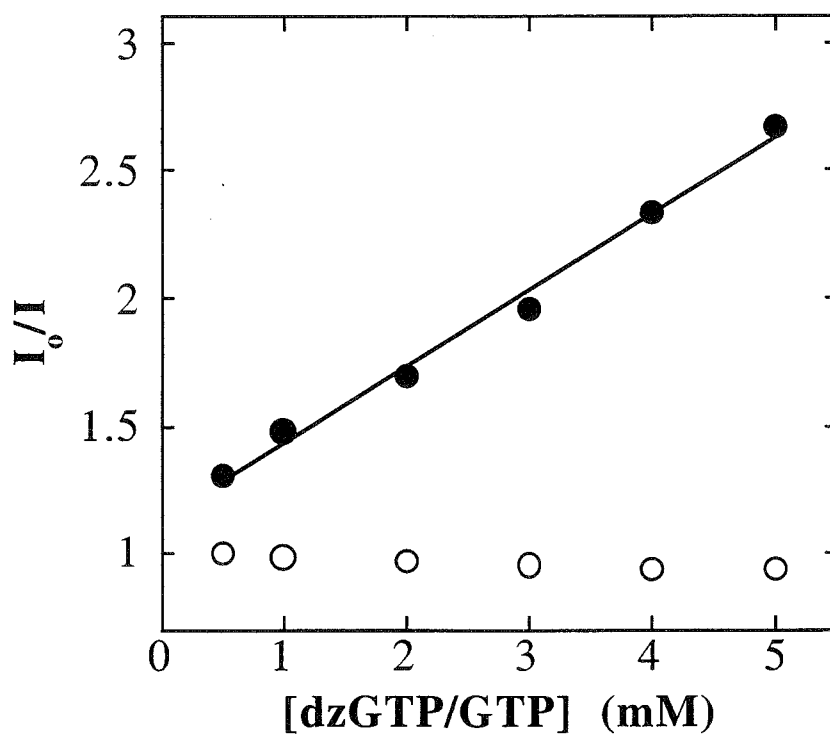
Figure 3.3 Steady-state fluorescence quenching of 10 μM ethidium by dGTP (○) and dz-dGTP (●) in 5 mM phosphate, 50 mM NaCl, pH 7.

in the ethidium quantum yield is observed in the presence of dGTP, whereas addition of dz-dGTP results in efficient fluorescence quenching ($K_{SV} = 3 \times 10^2$ M^{-1}). Neither the absorption of dGTP or of dz-dGTP show any spectral overlap with ethidium emission. Because these molecules differ only in oxidation potential, the mechanism of this quenching most likely proceeds by photoinduced oxidation of deazaguanine by ethidium.

3.3.2 Photooxidation of deazaguanine by ethidium in DNA

When incorporated into DNA duplexes, deazaguanine is also oxidized by the ethidium excited state. Significant decreases in the fluorescence quantum yield are observed for ethidium noncovalently bound to DNA duplexes containing deazaguanine relative to those containing guanine (Figure 3.4). A similar decrease in ethidium fluorescence in the presence of dz-G was found in studies where this modified base was incorporated into large DNA polymers.[12] In that case, the decreased fluorescence relative to natural sequences was not recognized as electron-transfer quenching, but was instead suggested to arise from an alteration in the electronic structure of ethidium upon binding at sites adjacent to deazaguanine.

The redox properties of deazaguanine make this base analogue a suitable reactant for the study of long-range electron transfer in ethidium-modified duplexes of heterogeneous sequence. Since the excited state of ethidium is not sufficiently oxidizing to react with any of the other DNA bases, electron transfer between an intercalator and a localized component of the base stack can be evaluated in the absence of competing reactions. Moreover, since duplexes containing this base differ from those containing guanine by only one out of over 800 atoms, quenching effects can cleanly be attributed to redox processes. Thus, the photooxidation reaction has been studied using fluorescence quenching measurements as a function of distance, flanking sequence, and base pairing. Because the oxidation potential for dz-G differs from G by only ~300 mV and quenching
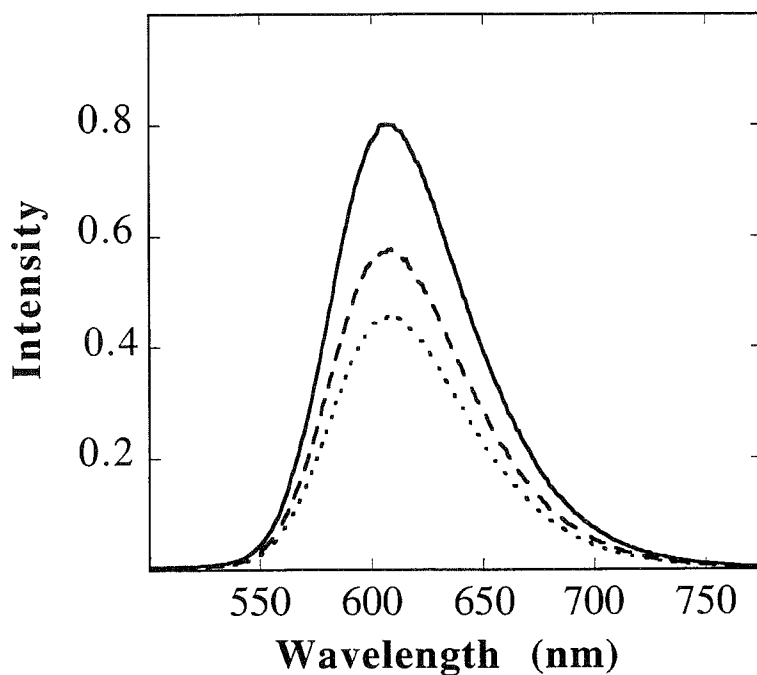
Figure 3.4 Steady state emission spectra for ethidium (5 μM) noncovalently bound to 5'ACACTGCTGACGGTA (solid), 5'ACACTGCTZACGGTA (long-dash), and 5'ACACTZCTZACGGTA (short-dash). Sequences were hybridized with complements and samples contained 5 μM duplex in 5 mM phosphate/50 mM NaCl, pH 7.

is only observed with dz-G, it should be noted that the driving force for this reaction is particularly small.

Duplex characterization and linker length optimization. The investigation of the long-range photooxidation of deazaguanine by ethidium as a function of distance necessitates the construction of a well-defined assembly. Duplexes containing covalently linked ethidium exhibit the structural properties expected for small cylindrical helices.[3] Steady-state polarization studies of ethidium-modified duplexes revealed that the covalently attached fluorophore is bound rigidly within the site of intercalation; these studies indicated little motion of the intercalator independent of the overall duplex dynamics.[3]

Many studies of DNA-mediated electron transfer have indicated that the integrity of intercalative interactions appears to modulate reaction efficiencies and kinetics.[1] In choosing a linkage between ethidium and the DNA duplex, a tether that afforded the strongest intercalative binding mode for the intercalator was sought. Therefore, Et-DNA linkers of differing lengths (Et-NHCO(CH$_2$)$_3$CONH(CH$_2$)$_n$NHCO-5'CTACCAGACATCGT (n = 2 (C2), 6 (C6), 9 (C9)) were investigated.

Consideration of the three-dimensional structure of DNA duplexes containing tethered ethidium using CPK models revealed that only a C9 linker provided unconstrained intercalation for ethidium. These models assume that the DNA duplex remains intact and is not denatured; this is a reasonable assumption given that the covalent attachment of ethidium increases the melting temperature of the duplex by > 2°C. From these models, the preferred intercalation site for ethidium tethered either with a C9 or C6 linker was identified as the second base step; however, it appeared that the C6 linker would encounter greater strain in this conformation. The models also revealed that ethidium attached by the C2 linker was substantially constrained and only intercalated partially at the first base step.

The fluorescence of ethidium was investigated in DNA duplexes featuring the different linkages (Figure 3.5). Et-modified duplexes containing the C9 and C6 linkers give the highest overall fluorescence intensities, indicating efficient protection from solvent through tight binding of the fluorophore within the hydrophobic core of the DNA helix. Ethidium tethered via the C2 linker shows significantly less fluorescence, indicating that this linker must sufficiently constrain the intercalator to limit the extent of protection from solvent. These observations are fully consistent with predictions from the models described above.

The binding mode(s) of the tethered intercalator can also be probed by examining fluorescence as a function of ionic strength (Figure 3.5): electrostatic associations which would stabilize a groove-bound form are expected only at very low ionic strengths and intercalative binding is favored at higher ionic strengths.[13-16] For the duplex containing the C9 linker, only small changes in the ethidium quantum yield are evident with increasing salt (Figure 3.5). Decreases in fluorescence of this magnitude with increasing ionic strength are commonly observed for intercalated ethidium. The binding of ethidium to this duplex therefore appears to reflect only a small contribution from electrostatic interactions.

Ethidium tethered by the C6 linker exhibits a much greater sensitivity to ionic strength compared with the C9 linker, consistent with intercalation being more constrained with this tether and a greater electrostatic component contributing to the binding of ethidium. With the C2 linker, significant decreases in the already diminished quantum yield are also observed. Hence, from this line of experimentation, and previous studies of the photophysical properties of duplexes modified with this linked intercalator,[3] it appears that the C9 linker allows the most favorable intercalative interactions to occur between ethidium and the derivatized duplex.
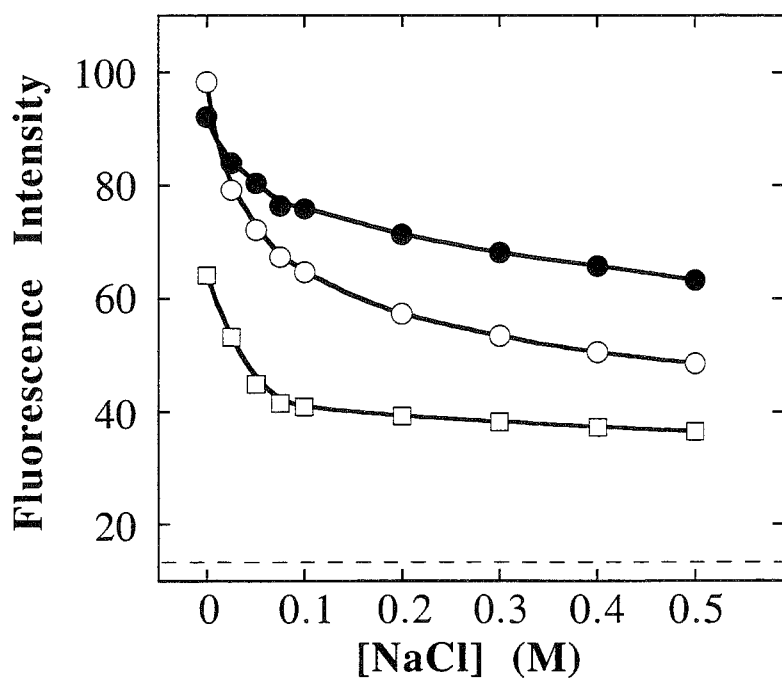
Figure 3.5 Effect of linker and ionic strength on fluoresence of ethidium covalently bound to the duplex (Et-NHCO(CH$_2$)$_3$CONH(CH$_2$)$_n$NHCO-5'CTACCAGACATCGT (n=2 (□), n = 6 (○), and n = 9 (●))). Dotted line represents fluorescence for free N-8-glycyl ethidium.

These results are consistent with recent studies of crosslinking reactions between tethered ethidium and DNA bases. When excited with high-energy light (~310 nm), ethidium inflicts short-range, G-specific direct cleavage.[10] This reactivity therefore allows the identification of the ethidium binding site. Indeed, for ethidium attached to a DNA duplex by a C9 tether, crosslinking is observed predominantly at the first two base steps of the tethered end of the duplex, confirming that the intercalator can only access the terminal bases of the assembly.

Therefore, a C9 linkage was utilized to probe the long-range photooxidation of deazaguanine. Establishing intercalation by ethidium tethered with this long linker is an important issue, for if the linked fluorophore were groove-bound in a fully extended conformation, it could directly contact the first five base pairs of the duplex (~17 Å), albeit with substantial strain. The photooxidation of deazaguanine was studied with the quencher located from four (14 Å) to ten bases (34 Å) from the end of the duplex. Thus, if ethidium were bound in the groove, the fluorophore would be provided direct access to the quencher only in the first duplexes of the series. But in fact, the C9 linkage allows very strong intercalative binding by the tethered ethidium most likely at the first or second base steps, and therefore direct contact with deazaguanine is precluded in all of the assemblies prepared. Instead, with intercalated ethidium, photoinduced reactions must occur over ethidium/deazaguanine separations of 6-27 Å.

3.3.3 Et/Z electron transfer as a function of distance

The ability of the DNA base stack to facilitate the oxidation of deazaguanine over extended distances was investigated in 14 base-pair duplexes covalently modified with N-8-glycyl ethidium (Et'). By the systematic replacement of a guanine residue by deazaguanine along a DNA duplex, fluorescence quenching experiments can be used to

investigate the efficiency and time scale of this base oxidation reaction as a function of donor/acceptor separation through the base stack.

Steady-state fluorescence measurements were employed to determine the yield of ethidium excited-state quenching by the photooxidation of deazaguanine in each of the duplexes shown in Table 3.2. In these 14 base-pair DNA duplexes containing tethered Et, the position of dz-G was systematically moved across the duplex to provide a range of donor-acceptor distances. Based on the structural dimensions of the Et-modified duplex and crosslinking studies, as described earlier, an ethidium binding site located between the second and third base steps is used to calculate donor/acceptor distances. It is worth noting that although a narrow distribution of possible binding sites may exist, the binding site is held constant throughout the series of duplexes used to evaluate the electron-transfer distance dependence, allowing the effect of distance on the photooxidation efficiency and kinetics to be unambiguously evaluated. Therefore, with Et intercalated between the second and third base steps, and with deazaguanine contained within a 5'-TZG site (Table 3.2), the different duplexes have Et/dz-G distances of 10-27 Å.

In this series of duplexes shown in Table 3.2, fluorescence quenching is observed until the donor-acceptor separation exceeds 6 base pairs. Over the range where quenching is detected (10-24 Å), the yield of this process decreases from 70% to 4%.

Fluorescence quenching was also investigated as a function of dz-G flanking sequence, 5'-GZA (bottom, Table 3.2). In this set of duplexes, which differ from those described above only in the sequence flanking deazaguanine, quenching yields varied from 55% to 0% over a Et/dz-G separation range of 6 to 20 Å. Despite less efficient quenching for deazaguanine stacked within this site, the photooxidation still proceeds over long distances.

The quenching yields (Figure 3.6) in both sets of duplexes exhibit a shallow exponential dependence on distance, paralleling trends reported in studies of long-

Table 3.2 Steady-state fluorescence quenching measurements for Et/dzG duplexes[a]

	Et/dz-G separation (Å)[b]	I(Et/G)	I(Et/dzG)	Fraction quenched[c]
5'CT ACCAGACATCGT / GA TGZTCTGTAGCA	10	0.36	0.11	0.70(5)
5'CT ATCCAGCATCGT / GA TAGZTCGTAGCA	14	0.40	0.18	0.56(4)
5'CT AATCCAGCTCGT / GA TTAGZTCGAGCA	17	0.37	0.27	0.28(2)
5'CT AAGTCCAGCTCT / GA TTCAGZTCGACA	20	0.33	0.30	0.10(3)
5'CT AAGCTCCAGTCT / GA TTCGAGZTCACA	24	0.33	0.32	0.04(2)
5'CT AAGCTTCCAGCT / GA TTCGAAGZTCCA	27	0.36	0.37	-0.03(3)
5'CT TCCAGACATCGT / GA AZGTCTGTAGCA	6	0.40	0.18	0.55(3)
5'CT ATCCAGCATCGT / GA TAZGTCGTAGCA	10	0.40	0.23	0.43(4)
5'CT AATCCAGCTCGT / GA TTAZGTCGAGCA	14	0.38	0.25	0.32(2)
5'CT AAGTCCAGCTGT / GA TTCAZGTCGACA	17	0.37	0.30	0.16(4)
5'CT AAGCTCCAGTGT / GA TTCGAZGTCACA	20	0.38	0.38	-0.01(2)

[a]Steady-state fluorescence intensity (I) relative to 10 uM Ru(bpy)$_3^{2+}$ (λ_{exc}=480 nm, 20°C, 5 μM duplex, 5 mM phosphate, 50 mM NaCl, pH 7). [b]Distances calculated with Et intercalated between 2nd and 3rd base step. [c]Fraction quenched (F_q=1-(I_{Et-dzG}/I_{Et-G})) calculated from 3-4 sets of independent samples; approximate errors are listed in parentheses
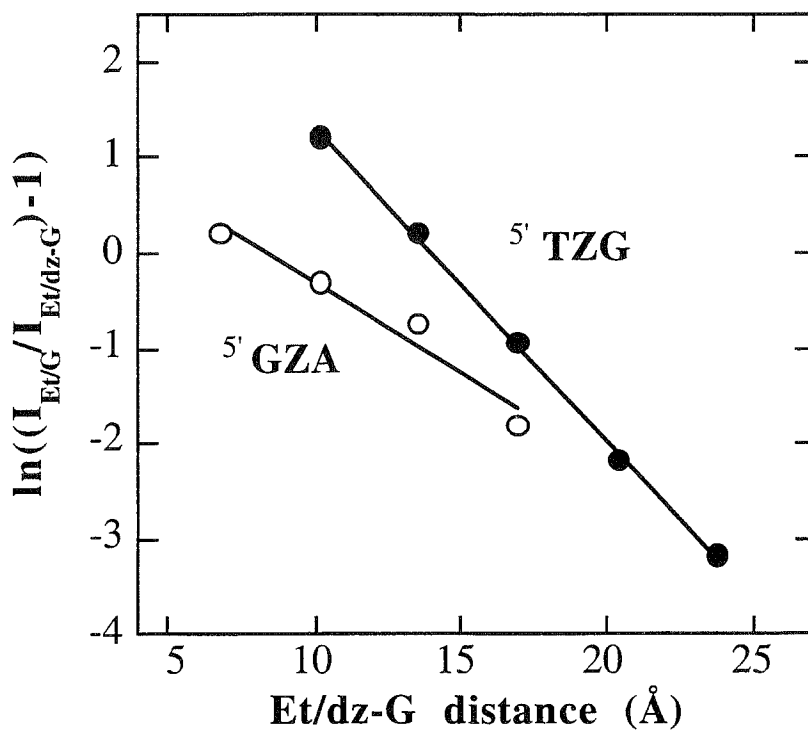
Figure 3.6 Exponential distance dependence for photoinduced

oxidation of ethidium by deazaguanine. Data shown correspond

to two different flanking sequences, 5' TZG (●) and 5' GZA (○).

distance electron transfer between intercalators.[3] Importantly, *the distance dependence of the Et/dz-G quenching reaction is sensitive to the sequence flanking the modified base.* In the 5'-TZG site, the exponential function used to evaluate the dependence of the quenching efficiency on distance yields a slope (γ) of 0.33(3) Å^{-1}. For a 5'-GZA site, a more shallow distance dependence is observed with $\gamma = 0.20(4)$ Å^{-1}. By simply changing the flanking sequence, a change in the variation of quenching yield with distance is detected. The most obvious difference between these two sites is the number of purines flanking deazaguanine, and thus, because the duplexes are otherwise identical, this effect may result from more favorable stacking in the site containing two purines.[17]

It should be noted that these results are fully consistent with an intramolecular processes. In the micromolar (1-15 µM) concentration range, the quenching yield is constant. If ethidium were to intercalate intermolecularly, we would expect essentially equal quenching at all distances. Indeed, when the concentration of ethidium-modified duplexes is raised above 20 µM, the observed quenching varies little with the Et/dz-G separation. For duplexes modified only with Et, self-quenching is also apparent at concentrations higher than 20 µM.[11]

The kinetics of the photoinduced oxidation of deazaguanine in these assemblies was investigated using TCSPC (Figure 3.7). In all of the ethidium/deazaguanine duplexes, fluorescence quenching occurs on a subnanosecond time scale, *i.e.*, all of the observed quenching is manifested only as a decrease in initial intensity (static quenching), and not as a decreased Et excited state (*Et) lifetime. For example, in a duplex where ethidium and the site of modification were separated by ~ 14 Å, the ethidium excited state exhibits a biexponential decay with $\tau_1 = 8.7$ ns (38%) and $\tau_2 = 2.6$ ns (62%) for the duplex containing guanine. In the analogous deazaguanine-modified duplex, where 55% quenching of *Et emission is observed in steady state measurements, the fluorescence decay profile is quite
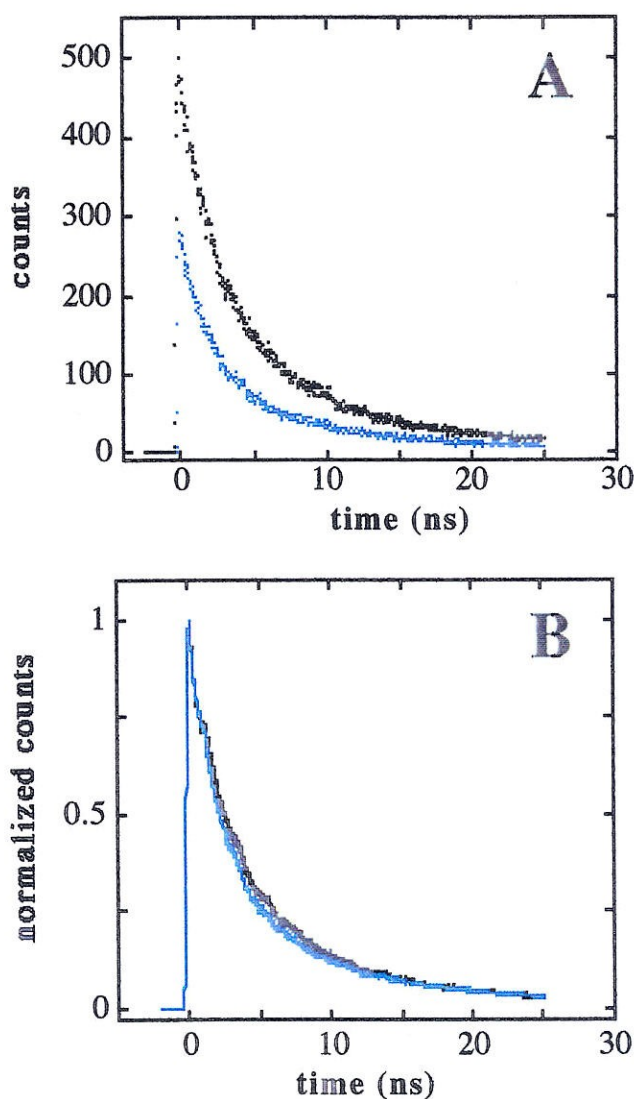
Figure 3.7 (A) Time-correlated single photon counting measurements for Et-5'-CTATC(C/G)AGCATCGT (blue trace) and Et-5' CTATC(C/Z)AGCATCGT (black trace) illustrating static quenching on this time scale (instrument response ~200 ps). Samples contained 5 μM duplex in 5 mM phosphate, 50 mM NaCl, pH 7. (B) Normalized single photon counting for sequences listed above.

Table 3.3 Fluorescence decay lifetimes for Et-G/Z duplexes[a]

Et-G/Z distance[b]	G		Z	
	τ_1 (%)	τ_2 (%)	τ_1 (%)	τ_2 (%)
10 Å	6.4 ns (30%)	2.7 ns (70%)	6.4 ns (25%)	2.3 ns (75%)
14 Å	8.7 ns (38%)	2.6 ns (62%)	9.4 ns (31%)	2.2 ns (69%)
17 Å	8.5 ns (32%)	2.2 ns (68%)	9.0 ns (26%)	2.1 ns (74%)
24 Å	8.4 ns (25%)	2.3 ns (75%)	8.4 ns (25%)	2.3 ns (75%)

[a]Sequences are listed in Table 3.2, top section. [b]Calculated with ethidium intercalated between second and third base pairs.

similar with $\tau_1 = 9.4$ ns (31%) and $\tau_2 = 2.2$ ns (69%) (Table 3.3). Equivalent profiles were measured for all duplexes. Figure 3.7, depicting representative raw and normalized SPC data, graphically illustrates that the quenching is almost entirely static on the time scale of this experiment and is not reflected in large changes in measurable lifetimes or in the percentages of these components. As the resolution of this experiment is ~ 150 ps, these measurements indicate that the quenching process occurs faster than this time response at *all donor/acceptor separations*. Thus, consistent with our earlier studies, electron transfer in DNA can proceed across a range of extended distances on very fast time scales.

It is noteworthy that the excited-state decay profiles we observe are inconsistent with the presence of a significant concentration of free Et. N-8-glycyl ethidium has an excited state lifetime of 440 ps in H_2O (which is shorter than that of ethidium because of the modification at the exocyclic amine), a decay component that would be easily detected in this experiment.

3.3.4 Effects of reactant stacking and environment

Variation of flanking sequence. To explore in more detail the effect of the sequence environment surrounding deazaguanine, duplexes were synthesized containing each of the four bases on either side of the modified base (Table 3.4). In this study, a base adjacent to deazaguanine was varied in each duplex and the effect of these sequence changes on the quenching yield was monitored. Only very small perturbations in the quenching yield are observed when the adjacent base on the 5'-side is varied. However, dramatic changes in the efficiency of photooxidation result when the 3'-sequence is altered. For instance, when deazaguanine is located adjacent to 3'-C, about 26% of the ethidium fluorescence is quenched; changing this 3'-site to G nearly doubles the quenching yield to 48%.

Table 3.4 Effect of flanking sequence on Et/dzG quenching yield[a-c]

5'-variation	
	Fraction quenched
Et ▬▬▬▬▬▬▬▬ 3' ▬▬ **AZA** ▬▬ 5'	0.24(6)
Et ▬▬▬▬▬▬▬▬ 3' ▬▬ **AZT** ▬▬ 5'	0.26(3)
Et ▬▬▬▬▬▬▬▬ 3' ▬▬ **AZG** ▬▬ 5'	0.32(2)
Et ▬▬▬▬▬▬▬▬ 3' ▬▬ **AZC** ▬▬ 5'	0.26(2)
3'-variation	
	Fraction quenched
Et ▬▬▬▬▬▬▬▬ 3' ▬▬ **TZG** ▬▬ 5'	0.35(3)
Et ▬▬▬▬▬▬▬▬ 3' ▬▬ **GZG** ▬▬ 5'	0.48(1)
Et ▬▬▬▬▬▬▬▬ 3' ▬▬ **CZG** ▬▬ 5'	0.26(1)

[a]Quenching yields obtained as described in Table II.
[b]Full sequence used in study: Et'-5'CTAA**X**C**Y**AGCTCGT,
X/Y=T,A,G,C *(C is base-paired with deazaguanine)*.
[c]All sequences displayed very similar amounts of
hypochromicity (23(2)%) at 260 nm .

The trend observed in these quenching yields may reflect small changes in oxidation potential. Theoretical studies have predicted that the ionization potentials for stacked base pairs should increase in the order 5' GG < 5' GA ≤ 5' GT < 5' GC. In this series of duplexes, a parallel trend in quenching efficiency is observed: 5' dz-GG > 5' dz-GT ≥ 5' dz-GA > 5' dz-GC. Interestingly, for the photoinduced electron-transfer reaction studied here, it appears that the 3'- sequence is most crucial in determining the reactivity of deazaguanine, consistent with theoretical prediction.[18] These results provide experimental evidence that stacked DNA bases have redox properties distinct from monomeric species in solution.

Effect of base mismatches . Single-base mutations were incorporated into Et/dz-G duplexes to monitor the effect of different dz-G base pairings on the oxidation efficiency (Table 3.5). In a duplex featuring deazaguanine paired to its natural partner, C, a quenching yield of 28% is observed. However, when the modified base is paired to any other base, the efficiency of the oxidation reaction is significantly diminished (fraction quenched = 7-10%). These results indicate that the photoinduced reaction is mediated by the DNA base stack. If the photooxidation was occurring on the periphery of the helix, the instability of the stacking for deazaguanine introduced by the presence of a mispair would surely enhance the fluorescence quenching.

An analysis of the melting profiles obtained via absorbance spectroscopy reveals that these mismatched duplexes have lower melting temperatures and reduced hypochromicity at 260 nm compared to the full Watson-Crick paired duplex. As hypochromicity is directly related to base-base interactions,[19] it can be inferred that the presence of the mismatch causes a significant perturbation in the stacking of deazaguanine within the duplex. Thus, these results provide further evidence that the efficiency of long-range electron-transfer reactions within DNA is very sensitive to π-stacking effects.

Table 3.5 Effect of base pairing on Et/dzG quenching yield[a]

	Fraction quenched[b]	$T_m{}^c$	% hypochromism (260 nm)[d]
Et 5'════ **C** ════ / ──── **Z** ────	0.28(3)	51.5	24
Et 5'════ **T** ════ / ──── **Z** ────	0.07(2)	41.0	19
Et 5'════ **A** ════ / ──── **Z** ────	0.09(1)	40.1	19
Et 5'════ **G** ════ / ──── **Z** ────	0.10(1)	37.8	19

[a] Full sequence used in study: Et'-5'CTAATCXAGCTCGT, X=C,T,A,G (across from deazaguanine).
[b] Quenching yields calculated as described in Table II. [c] Approximate error for melting temperatures $(T_m) \sim 0.8$ °C. [d] Approximate error for % hypochromism ~ 1.

Effect of linker length on photooxidation. The remarkably fast time scale and shallow distance dependence of the described reaction necessitates a more detailed examination of the interaction of tethered ethidium with the helix. Is there any direct contact possible between the tethered ethidium and deazaguanine? It has been well-established that ethidium binds to DNA primarily via intercalation,[13-15] and based on the physical and photophysical properties of the Et-modified duplexes, it appears that this derivative is similarly intercalated when covalently tethered. However, if tethered ethidium were instead groove-bound, this might allow direct contact between the fluorophore and the modified base, and hence this possibility requires experimental consideration. Here again, the variation of the Et-DNA linker length and ionic strength provides a means to assess the contribution of a non-base stack mediated pathway.

Based on the dimensions of the duplexes employed in this study, the C9 linker was the only tether of sufficient length to allow direct contact between ethidium and deazaguanine incorporated at the fifth base position from the tethered end (on the complementary strand) and *only* if the fluorophore were in a strained, extended position bound in the groove of the duplex. Even with this linker, *no direct contact appears possible between ethidium and any base position on the complementary strand six or more sites from the tethered end*, where quenching yields up to 55% are observed. Moreover, for the C6 and C2 linkers, even if ethidium is fully extended along the DNA groove, no direct contact is permitted with deazaguanine when the modified base is located at the fifth base step and further down the duplex. In fact, although these linkers appear to be quite long when extended, they are attached to the 5' end of the DNA backbone, pointed away from the helix, and in three-dimensional space actually provide access to a very limited region of the duplex.

The quenching of ethidium by deazaguanine is affected by linker length and ionic strength (Figure 3.8). At low ionic strengths (5 mM phosphate, 0 - 25 mM NaCl),
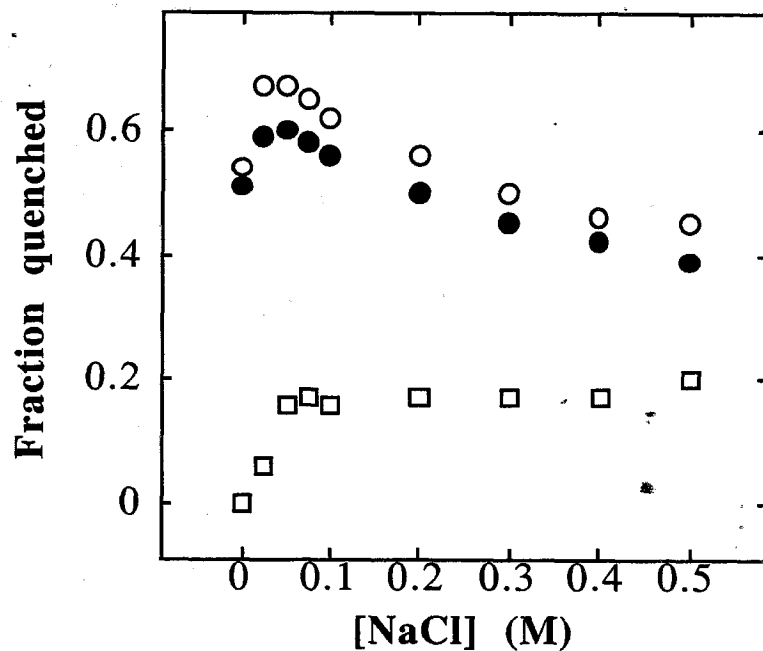
Figure 3.8 Effect of linker and ionic strength on fluorescence

quenching by deazaguanine for ethidium covalently bound to the duplex

(Et-NHCO(CH$_2$)$_3$CONH(CH$_2$)$_n$NHCO-5'CTACCAGACATCGT

(n=2 (□), n = 6 (○), and n = 9 (●))); deazaguanine is located at fifth base

step from Et-modified terminus.

smaller quenching yields are observed relative to those at higher ionic strengths (5 mM phosphate, 25 - 100 mM NaCl). Since groove binding has only been characterized for ethidium at low ionic strengths (< 0.01 M), these results appear to indicate that groove binding inhibits, rather than facilitates, the quenching reaction. It is interesting that in the duplexes containing C6 and C9 linkers, at all ionic strengths, essentially identical levels of quenching are observed, although the shorter linker of this pair cannot directly contact the deazaguanine in the duplex even if fully groove bound. The similar levels of quenching for these two linkers instead suggest that the fluorophore is intercalated at the same site in these two assemblies, a result also consistent with modeling. Ethidium tethered to the duplex by the C2 linker shows no quenching at very low ionic strength and is only quenched by deazaguanine in the presence of sufficient ionic strengths to favor intercalation. Overall, lower levels of quenching are observed with this modified duplex, likely a result of poorer stacking of ethidium within the duplex due to the constraints of the linker and possibly, the location of the intercalation site at the first base step. The lower fluorescence of Et-modified duplexes containing the C2 linker supports this conclusion.

3.4   DISCUSSION

3.4.1 Photoxidation of deazaguanine by ethidium: distance dependence

This study of the long-range photoinduced oxidation of deazaguanine by ethidium represents the first systematic investigation by fluorescence spectroscopy of a DNA-mediated electron-transfer reaction between a tethered intercalator and a modified DNA base in mixed sequence DNA. Here the dynamics, distance, and sequence dependence of a base oxidation reaction can be directly monitored. We find that the reaction between ethidium and deazaguanine occurs over extended distances through DNA on a remarkably fast time scale. Over distances of 6-24 Å, this reaction occurs within 150 ps, demonstrating that the DNA base stack can mediate efficient electron transport with little sensitivity to distance.

Since our probe is a modified base, we can examine electron transfer reactions across a range of sequences using all four of the natural bases. We find that the efficiency of this reaction is remarkably sensitive to the flanking sequence surrounding deazaguanine. Neighboring bases may serve to promote small changes in redox potential of the stacked deazaguanine,[18] and these changes lead to significant variations in quenching yield. The base pairing of deazaguanine also modulates the efficiency of the photooxidation reaction. Paired to any base other than its natural mate, deazaguanine is a much less efficient reductive quencher for the ethidium excited state. These observations indicate that the photooxidation reaction occurs through the base stack and that even very small changes (one base) in the composition of the stack can significantly alter the efficiency of this reaction. Perhaps most dramatically, the distance *dependence* of electron transfer differs depending upon the base(s) neighboring the reactant. This observation requires a more detailed consideration of the electronic coupling in double helical DNA; significant deviations arise with small, but obviously not insignificant, energetic differences within the base pair stack.

In fact, the sensitivity of the photooxidation of deazaguanine to very subtle changes in the structure of the base stack underscores the unique features of this medium. The DNA double helix is unlike any other structure through which long-distance electron transfer has been investigated. Proteins provide primarily σ-bonded pathways for charge transport. Although structurally similar to the base stack of DNA, π-stacked arrays in the solid state[20] do not offer the dynamical fluctuations afforded to DNA molecules in solution. Π-stacking offers significant stabilization to the double helix,[21] and depends upon both sequence and environment. The enthalpic contribution of stacking to the overall stability of DNA arises largely through a combination of dipolar and induced dipolar interactions between heterocyclic base pairs. Because the most direct electron-transfer pathway through DNA proceeds through the π-stacked bases, any model to explain these long-range

processes must take into account how these stacking interactions influence the electronic structure of DNA.

Consideration of alternate mechanisms. Because ethidium is attached to the DNA duplexes under study by a long and flexible tether, a thorough investigation of the binding geometry of ethidium within these duplexes is necessary to establish that this reaction is in fact mediated by the DNA base stack. The interactions of ethidium with DNA have been studied extensively,[13-16] and the intercalation of ethidium is typically the benchmark by which the binding modes of other molecules are determined. Nonetheless, by examining the photophysics of the ethidium-modified duplexes with different linkers and as a function of ionic strength, the interactions between ethidium and the DNA helix in these assemblies can be better understood.

Direct contact between deazaguanine and ethidium in the assemblies is only possible if the tethered fluorophore is not intercalated, but instead, is extended into the groove of the helix. Yet, ionic strength conditions which should maximize groove binding instead inhibit the quenching reaction. Based upon modeling, direct contact is only possible with a C9 linker and even with this tether, only at the smallest donor/acceptor separation investigated in this study. However, significant quenching on a fast time scale is apparent across a range of donor/acceptor separations with this linker, and with a C6 analog (where direct contact with deazaguanine is precluded even at the closest donor/acceptor separation employed) equivalent quenching is observed. Ethidium-modified duplexes containing a C2 linker show substantially lower levels of quenching in the presence of deazaguanine, but also exhibit reduced fluorescence quantum yields, indicating that the binding allowed by this tether does not provide a high degree of protection from solvent. The constrained binding with this tether may also limit the coupling of the fluorophore into the DNA base stack.

In addition, if some percentage of ethidium were groove-bound, a distinct excited-state population should be detected, and this population should likewise be selectively quenched. Photoexcited ethidium bound within these duplexes exhibits a biexponential decay profile with lifetimes on the order of 7 and 2 ns. Both lifetimes reflect significant enhancements relative to free N-8-glycyl ethidium (400 ps), and the average ratio of $\tau(\text{free})/\tau(\text{intercalated}) = 11$ parallels that observed with intercalated ethidium ($\tau(\text{free})/\tau(\text{intercalated}) = 12$). Lifetimes intermediate between free and intercalated are typically observed for groove-bound ethidium[16] with levels of enhancement lower than either of the components described for the covalently bound fluorophore. If the shorter of the observed lifetimes did correspond to groove-bound ethidium, then this component should be selectively quenched, but instead, both lifetimes are equally quenched on a fast time scale.

The contribution of dynamic exchange between a groove-bound and intercalated form of ethidium to the quenching reaction may also be considered as a possible explanation for the results described here. However, the fast kinetics of the quenching observed across the entire range of donor-acceptor distances appears to preclude such a dynamical process. On this picosecond time scale of the quenching, essentially only static conformations of ethidium within the duplexes can be considered. Moreover, previous studies of steady-state fluorescence polarization trends for ethidium tethered to DNA duplexes[3] indicated rigid binding of this species to the duplex.

Based on the experimental evidence presented, it appears that this remarkably fast electron-transfer reaction occurs between *intercalated* ethidium and deazaguanine, and is facilitated by the base stack, not through-space contacts. The significant effects of local sequence within the duplexes also indicate that the photooxidation reaction must occur through this medium, as opposed to on the periphery of the helix.

Models for distance dependence. The photooxidation of deazaguanine is relatively insensitive to distance: it proceeds up to distances of 30 Å and occurs on a subnanosecond time scale over this entire range. The ultrafast time scale of the electron-transfer kinetics observed here over all distances precludes the calculation of β, the decay of electronic coupling with distance described by Marcus.[22] It is nonetheless clear that β must be low (≤ 0.2 Å^{-1}), since over a range of distances (6 - 24 Å), rate constants $\leq 10^9$ sec^{-1} were not observed. Thus, for reactants which are well-stacked within the helix, the distance dependence of electron transfer must be exceedingly shallow.

Moreover, the change in photooxidation *efficiency* with distance without appreciable changes in electron-transfer dynamics indicates that a mechanism is operative which may be unique to the double helix as a stacked array in solution. In studies of electron transfer between intercalators covalently bound to DNA, the same behavior was observed.[3] In that case, the observed distance dependence was proposed to result from conformational heterogeneity arising from the internal dynamics of the DNA helix. This heterogeneity within the base stack could be envisioned to give rise to disruptions in π-stack mediated coupling and determine the yield of electron transfer at a given distance. Since the probability of having a properly stacked duplex on the time scale of the photoinduced experiment would depend exponentially on the number of intervening base pairs, this model provides a reasonable explanation for the distance dependences of the quenching yields in these DNA-mediated reactions. Thus, if such motions serve to gate electron transfer through the base pair stack, this mechanism may offer a new measurement of base pair dynamics.

The remarkable characteristics of DNA-mediated electron transfer have often prompted discussion of DNA as a molecular "wire."[23] From the work described here and elsewhere,[1-5] it is increasingly clear that the DNA base pair stack can facilitate long-range, ultrafast reactions. However, given the apparent sensitivity to base-pair stacking

dynamics, if double-helical DNA can function as a "wire," it does so transiently. Thus, the base-pair stack provides remarkable long-range coupling, but also limits the range over which this type of reactivity may proceed because of its dynamical nature.

Other factors may also modulate the trends observed in this study. This DNA-mediated reaction is slightly more sensitive to distance ($\gamma = 0.20$-0.35 Å^{-1}) than the oxidative quenching reaction observed between Et and Rh(phi)$_2$bpy^{3+} ($\gamma = 0.10$ Å^{-1}),[11] but other differences between these reactions exist. The Et/dz-G reaction may proceed through a HOMO state of the DNA bridge, as Et is being reductively quenched, whereas the Et/Rh reaction may involve a LUMO state for the oxidative quenching reaction. These states have different electronic structures and different energy gaps relative to the ethidium excited state. In addition, the driving forces for these two reactions vary significantly (Et/dz-G: $\Delta G \sim -200$ mV, Et/Rh: $\Delta G \sim -800$ mV). In addition, it is worth noting that these systems employ reactants (metallointercalator versus DNA base) which may interact with the base stack differently, and this may also affect the efficiency of the reaction. More systematic studies exploring the effects of these parameters on DNA-mediated electron transfer reactions will be necessary to determine the origin of the different distance dependences observed in these systems.

3.4.2 Effect of stacking on the efficiency of charge transport in DNA

Certainly, how the donor and acceptor are coupled into the DNA base stack is a critical issue, and the application of a modified base as probe of long range electron transfer has permitted us directly to monitor the effect of subtle changes in stacking on the reactivity of this molecule within the helix. The incorporation of deazaguanine in a base mismatch, for example, significantly decreases the yield of fluorescence quenching. Generally base mismatches do not result in gross structural changes within the DNA helix,[37] but instead are known to cause only local disruptions in stacking. Hence this result underscores the

exquisite sensitivity of this phenomenon to small perturbations in stacking. Here, the presence of the mismatch also causes a measurable decrease in the hypochromicity of these duplexes, confirming that stacking of deazaguanine within the base stack is significantly altered. Therefore, although the reactants still retain the same through-space separation, *the change in stacking for deazaguanine results in a dramatic decrease in the efficiency of this electron-transfer reaction.*

Stacking also appears to dramatically modulate the distance dependence of DNA-mediated electron transfer. For the photooxidation of deazaguanine, the variation in the yield with donor-acceptor separation (γ) clearly depends upon the sequence surrounding the modified base. A more shallow distance dependence is observed for deazaguanine stacked within a purine-purine site, perhaps indicating that greater stacking stabilization within a given sequence provides more favorable electronic coupling for this long-range reaction. Importantly, this result provides the first demonstration that *the distance dependence of a DNA-mediated electron transfer reaction is not only sensitive to the identity of donor and acceptor, but is also affected by the stacking environment of the donor and acceptor.*

3.4.3 Reconciliation of previous studies: π-stacking modulates reactivity

As evident from the above discussion, base stacking affects many aspects of the photooxidation of deazaguanine by ethidium. This parameter may determine the electron-transfer yield at a given distance, may influence the ability of this modified base to serve as an electron donor within base mismatches, and may also modulate the overall distance dependence for this reaction. The stacking interactions available within the DNA helix distinguish this medium structurally from any other examined in systematic studies of electron transfer.

Different studies of electron-transfer processes within DNA have reached conclusions very distinct from those discussed with respect to this system.[6-8] Much

slower electron-transfer kinetics and steeper distance dependences have been observed, leading to a great deal of controversy concerning the nature of DNA as an electron-transfer medium. It is now clear that there are factors other than donor/acceptor distance that must be considered in order to make any conclusions concerning the efficiency of charge transport in DNA. The results described here underscore that point.

When intercalators or components of the base stack are used to probe DNA-mediated electron transfer, fast reactions can be observed over extended distances.[1-5] In systems employing groove-bound reactants, or partially stacked molecules, the time scales and reaction distances are diminished significantly.[6-8] In our own studies, we have observed very different reactivities for intercalating versus groove-bound species, and even among intercalators of different chiralities.[1] The electron-transfer kinetics in a stilbene-modified DNA hairpin must depend in part upon the interaction of this chromophore with the DNA bases.[7] As stilbene is not a molecule which naturally binds to DNA without being covalently constrained, it is likely that this molecule is not favorably stacked in a conformation analogous to intercalation; in fact, no hypochromism is associated with the interaction between stilbene and the DNA base stack. Significantly, still slower electron-transfer kinetics were observed with reactants attached to DNA only through σ-bonded linkages.[6] Most recently, a β value of 1.4 Å^{-1} was obtained for a DNA-mediated electron-transfer reaction between an acridine-based fluorophore and guanine.[8] The level of electronic coupling through DNA indicated by this experiment is extremely poor, even when compared to the stilbene hairpin assembly. Biophysical studies[24] have indicated that substantial changes in fluorescence, hypochromicity, and thermal stability arise with small changes in this assembly. How the acridine derivative is actually accommodated within the base stack and what local base pair disruptions arise need still to be established for the proper interpretation of this result.

Our recent investigations have not only focused on stacked reactants but have also included tests of whether the DNA base stack represents the intervening pathway. Other studies have not addressed this issue. In fact, in cases where reactants are not directly interacting with the base stack, electron transfer may proceed through alternate pathways with higher intrinsic values of β. Indeed, even in fully stacked systems, we see here that very small sequence changes which alter local stacking interactions cause marked changes in the overall distance dependence. It is therefore reasonable that reactants which do not have direct contact with the base stack, or limited interactions, would display drastically different behavior. Our own results indicate that *subtle variations in stacking lead to significant change in reactivity*. The results obtained in all of these systems may therefore be reconciled if the detailed interactions between the reactants and the base stack, as well as the structure of the base stack, are considered. The structural complexity of DNA, and the now apparent sensitivity of electron transfer through this medium to the stacking of reactants with the DNA bases, necessitates that careful consideration be given to all factors which may affect experimental results obtained in this field.

The base stack of the DNA helix is again implicated in facilitating long-range charge transport reactions. This study of the photooxidation of deazaguanine by ethidium not only provides another example of a reaction which occurs on a fast time scale over remarkable distances mediated by the DNA helix, but also underscores the importance of another parameter besides distance: stacking. Base-stacking interactions determine the efficiency of long-range electron transfer in this system and may also determine the overall distance dependence of this process. This work establishes that the behavior of the DNA helix as a bridge and reactant in electron-transfer processes is contingent upon stacking interactions within this structure. Previous studies which suggest DNA to be a poor mediator for charge transport can be reconciled within this context. Reactants which are not well-stacked within the DNA helix have repeatedly revealed much less efficient electron transfer

than those which interact with the base stack via intercalation. Here, it is demonstrated that changing the stacking of a given reactant attenuates the reaction efficiency. Therefore, it becomes apparent that the interaction of reactants with the DNA base stack must be carefully considered when conclusions concerning DNA-mediated electron transfer are drawn. It is increasingly clear that to assess properly the nature of charge transfer in nucleic acids and apply this knowledge to an understanding of base damage and repair mechanisms, the structure of this biopolymer must be considered.

3.5 REFERENCES

1.   a) Murphy, C. J.; Arkin, M. A.; Jenkins, Y.; Ghatlia, N. D.; Bossman, S.; Turro, N. J.; Barton, J.K. *Science* **1993**, *262*, 1025. b) Murphy, C.J.; Arkin, M.A.; Ghatlia, N.D.; Bossman, S.; Turro, N.J.; Barton, J.K. *Proc. Natl. Acad. Sci. U.S.A.* **1994**, *91*, 5315. c) Arkin, M.R.; Stemp, E.D.A.; Turro, C.; Turro, N.; Barton, J.K. *J. Am. Chem. Soc* **1996**, *118,* 2267. d) Arkin, M.R.; Stemp, E.D.A; Holmlin, R.E.; Barton, J.K.; Hörmann, A.; Olson, E.J.C.; Barbara, P.A. *Science* **1996**, *273*, 475.

2.   Holmlin, R.E.; Stemp, E.D.A.; Barton, J.K. *J. Am. Chem. Soc.* **1996**, *118*, 5236.

3.   Kelley, S.O.; Holmlin, R.E.; Stemp, E.D.A; Barton, J.K. *J. Am. Chem. Soc.* **1997**, *119*, 9861-9870.

4.   Kelley, S.O.; Jackson, N.M.; Barton, J.K.; Hill, M.G. *Bioconj. Chem.* **1997**, *8*, 31.

5.   Kelley, S.O.; Jackson, N.M.; Hill, M.G.; Barton, J.K. **1998**, *submitted.*

6.   Meade, T. J.; Kayyem, J. F. *Angew. Chem. Int. Ed. Engl.* **1995**, *34*, 352.

7.   a) Lewis, F.D.; Wu, Taifeng; Zhang, Y.; Letsinger, R.L.; Greenfield, S.R.; Wasielewski, M.R. *Science* **1997**, *277*, 673; b) Lewis F.D.; Letsinger, R.L *JBIC* **1998**, *3*, 215-221.

8.   Fukui, K.; Tanaka, K. *Angew. Chem. Int. Ed.* **1998**, *37*, 158.

9.   Steenken, S. *Chem. Rev.* **1989**, *89*, 503.

10.   Hall, D. B.; Kelley, S.O.; Barton, J.K. *Biochemistry* **1998**, *in press.*

11.   Beaucage, S.L.; Caruthers, M.H.; *Tet. Lett.* **1981**, *23*, 1859.

12.   Latimer, L.J.P.; Lee, J.S. *J. Biol. Chem.* **1991**, *266*, 13849.

13.   Waring, M.J. *J. Mol. Biol.* **1965**, *13*, 269.

14.   LePecq, J.B.; Paoletti, C. *J. Mol. Biol.* **1967**, *27*, 87.

15. Burns, V. W. F. *Arch. Biochem. Biophys.* **1969**, *133*, 420-424.

16. Olmsted, J.; Kearns, D.R. *Biochemistry* **1977**, *16*, 3647.

17. Petersheim, M.; Turner, D.H. *Biochemistry* **1983**, *22*, 256.

18. Sugiyama, H.; Saito, I. *J. Am. Chem. Soc.* **1996**, *118*, 7063.

19. Cantor, C.; Schimmel, P. (1980) *Biophysical Chemistry*, W.H. Freeman and Co., New York, 381-408.

20. Marks, T.J. *Science* **1985**, *227*, 881.

21. Saenger, W. (1984) *Principles of Nucleic Acid Structure*, Springer-Verlag New York.

22. Marcus, R.A.; Sutin, N. *Biochim. Biophys. Acta* **1985**, *811*, 265.

23. a) Beratan, D.N.; Priyadarshy, S.; Risser, S.M. *Chem. & Biol.* **1997**, *4*, 3-8; b) Netzel, T.L. *JBIC*, **1998**, *3*, 210-214.

24. Fukui, K.; Tanaka, K., *Nucl. Acids. Res.*, **1996**, *24*, 3926-3967.

Chapter 4

Electron Transfer Between DNA Bases in Double Helical DNA[‡]

4.1   INTRODUCTION

Experiments addressing electron transfer through DNA employing pendant donors and acceptors have provided remarkably different assessments of the electronic coupling provided by DNA.[1-8] Values for β, the decay of electronic coupling with distance,[9] ranging from ≤ 0.1 Å^{-1} to 1.4 Å^{-1} have been reported. In Chapters 2 and 3, ultrafast electron-transfer reactions with shallow distance dependences ($\beta \leq 0.1 - 0.4$ Å^{-1}) between intercalating or well-stacked reactants were described. A profound sensitivity to stacking was observed in these systems, as the presence of base mismatches was demonstrated to essentially shut down long-range electron transfer.[2-4] These results appear to provide strong evidence that electronic coupling is efficiently mediated by the stacked bases within the DNA helix, but other studies have prompted the opposite conclusion. Indeed, in systems employing donors and acceptors interacting with the DNA base stack through σ-linkages or limited stacking, much slower electron transfer kinetics and steeper distance dependences ($\beta = 0.6 - 1.4$ Å^{-1}) have been observed.[5-8] The large range of values obtained despite DNA as a common bridge has slowed progress towards a detailed understanding of charge transport through DNA, and has pointed out the great need for a well-defined system where electron transfer through DNA can be studied without the structural ambiguity associated with extrinsic donors and acceptors.

Figure 4.1 Base-base electron transfer.

Hence, to directly evaluate the efficiency of electron transfer through DNA, we have studied photoinduced electron transfer between DNA bases incorporated within synthetic duplexes (Figure 4.1). Base-base electron-transfer chemistry provides a means

to probe directly electron transfer through DNA without external donors and acceptors. This chapter therefore describes the use of fluorescent analogues of adenine that selectively oxidize guanine to study photoinduced electron transfer through the DNA π-stack as a function of reactant properties and orientation. A systematic series of measurements within structurally identical DNA assemblies were performed which illustrate the great range of reactivity that results from subtle changes in the stacking or orientation of reactants within the helix. Moreover, results are presented indicating that reactant energetics also affect the distance dependence of electron transfer through DNA, potentially providing the first experimental demonstration of tunneling-barrier effects in DNA-mediated electron-transfer reactions. These experiments, illustrating that a range of reactivity can be observed for reactants similar or identical in structure through small changes in structural and energetic parameters, provide clear insight into the origin of conflicting assessments of DNA as a medium for electron transfer.

4.2 EXPERIMENTAL SECTION

Preparation of oligonucleotide samples. Aminopurine, ethenoadenine, inosine, and deazaguanine phosphoramidites were obtained from Glen Research. Oligonucleotides were prepared using standard automated techniques (with the exceptions described below) on a 394 ABI synthesizer and purified by reverse phase HPLC. For deazaguanine, the oxidation step was carried out with 10-camphorsulfonyl oxaziridine as previously described.[3] Base deprotection of ethenoadenine-containing oligonucleotides was carried out for 24 hours at room temperature. Oligonucleotides containing modified bases were characterized using electrospray mass spectroscopy.

Samples were prepared as follows: based on the calculated extinction coefficients for DNA sequences (ε_{260} (M^{-1} cm^{-1}): dC = 7.4 x 10^3; dG = 12.3 x 10^3; dT = 6.7 x 10^3; dA = 15.0 x 10^3; dz-G = 10.5 x 10^3; dI = 11.0 x 10^3 ; d(A$_\varepsilon$) = 4.5 x 10^3; d(A$_2$) = 2.5 x 10^3) appropriate amounts of complementary materials were combined at 1:1

stoichiometry and dissolved in 100 mM sodium phosphate (pH 7) to give a final duplex concentration of 100 μM. The resulting solutions were heated to 90°C and slowly cooled to ambient temperature over 2-3 hours to anneal the duplex. The uv-vis spectra of the duplex samples were carefully measured to ensure that the absorbance at the excitation wavelength was identical for every sample.

Steday-state fluorescence measurements. Emission spectra were collected on an ISS K2 spectrofluorimeter. For A_2-containing samples, excitation was performed at 325 nm and emission spectra were integrated from 340-500 nm unless otherwise noted. For A_ε-containing samples, excitation was performed at 335 nm and emission spectra were integrated from 335-525 nm unless otherwise noted. All fluorescence measurements were made at 20°C with air-equilibrated samples.

TCSPC measurements. Measurements were performed on a TCSPC apparatus previously described.[2] Excitation was performed at 325 nm, and emission was monitored at 350 nm for A_2, 400 nm for A_ε. Two data sets were obtained for each sample, one containing > 10,000 counts for the determination of decay lifetimes, and another taken over a 120 second time interval to quantitate static quenching. Experiments were otherwise performed under the same conditions as steady-state experiments (100 μM duplex, 100 mM sodium phosphate, pH 7).

Thermal denaturation experiments. Thermal denaturation experiments were performed on a HP8452A diode array spectrophotometer with samples at a duplex concentration of 25 μM in 100 mM phosphate (pH 7). Absorbance was monitored every 2°C with 3 minute equilibration times. All duplexes used in these experiments exhibited cooperative thermal denaturation profiles with melting temperatures > 25°C with 25 μM duplex, and therefore were fully hybridized under the conditions of all fluorescence experiments (100 μM, 20°C).

4.3 RESULTS AND DISCUSION

4.3.1 Reactivity of fluorescent adenine analogues with DNA bases

The reactivity of two fluorescent analogues of adenine, 2-aminopurine[10] (A_2) and 1,N^6-ethenoadenine[11] (A_ε), with DNA nucleotides was first explored in quenching titrations in aqueous solution (Figure 4.3). A_2 and A_ε both emit strongly from π-π^* excited states not populated in the natural DNA bases,[12-13] and have similar excited-state energies (as approximated using the expression $E^o(^{*/-}) = E_{oo} - E^o(^{0/-})$ where E_{oo} = intersection points of absorption and emission spectra and $E^o(^{0/-})$ = electrochemical reduction potentials) of +1.5 for A_2 and +1.4 V for A_ε *versus* NHE.

A_ε A_2
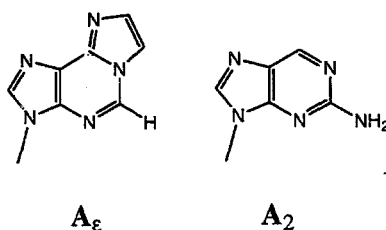
Figure 4.2 Structures of ethenoadenosine and aminopurine.

The fluorescence of both of these bases is efficiently quenched by deazaguanine and guanine, with only small amounts of quenching observed with inosine (I) and the other DNA bases with significantly higher redox potentials.[14] For A_2, Stern-Volmer quenching rates (k_q) of 2.2(4) x 10^9 $M^{-1}s^{-1}$ for guanine triphosphate (GTP) and 5.2(3) x 10^9 $M^{-1}s^{-1}$ for deazaguanine triphosphate (ZTP) were derived from these titrations. For A_ε and GTP, k_q = 1.9(2) x 10^9 $M^{-1}s^{-1}$, and for A_ε and ZTP, k_q = 4.6(4) x 10^9 $M^{-1}s^{-1}$. Both fluorophores react with these nucleotides in the order anticipated based on driving force for electron transfer (E^o_{ZTP} (~+1.0 V) < E^o_{GTP} (~+1.3 V) < E^o_{ITP} (~+1.5 V)).

In these titrations, the A_2 free base and A_ε nucleotide triphosphate were utilized. For the nucleotide triphosphate form of A_2, smaller k_q values would be expected due to higher electrostatic repulsions with the nucleotide triphosphate quenchers, and an increase in the reduction potential of the alkylated base.
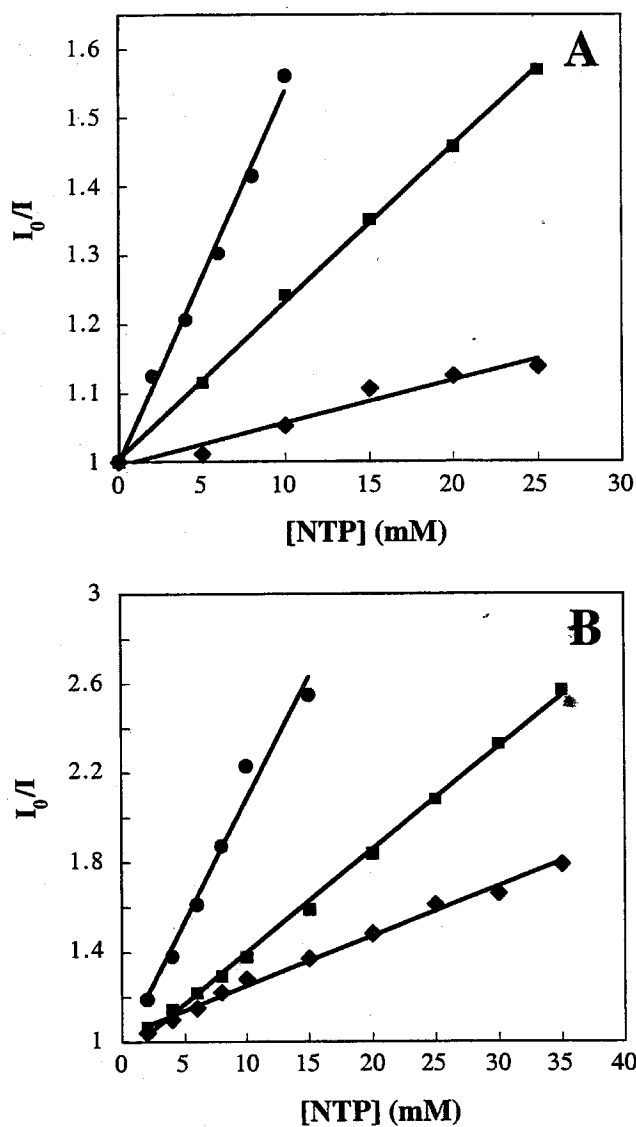
Figure 4.3 Stern-Volmer plots for fluorescence quenching titrations of A_2 (A) and $dA_\varepsilon TP$ (B) with dITP (◆), dGTP (■), and dZTP (●). The initial intensity (I_o) of solutions containing 100 μM A_2 or $dA_\varepsilon TP$, 100 mM sodium phosphate (pH 7) compared to those with increasing concentrations of quencher (I) were monitored by steady-state emission spectroscopy at 20°C. Excitation was performed at 335 nm for both fluorophores.

Transient absorption studies provide strong evidence for charge-separated products in these photoinduced reactions. Flash photolysis of aminopurine in the presence of dGTP produced long-lived transient absorption signals with the spectral profile expected for the neutral G radical (Figure 4.4).[15] The small yield of this species and slow kinetics of recombination suggest that the signals observed correspond to a small population of charge-separated species that have undergone cage escape. Nonetheless, the very striking correspondence between the spectral profile of this intermediate and the G radical provides strong evidence that A_2 and dGTP react via electron transfer.

Along with the lack of spectral overlap between these donors and acceptors, these data support electron transfer as the source of this fluorescence quenching. The similarity among the quenching constants obtained for these two different fluorescent bases show the reactions to have comparable driving forces, consistent with the excited-state potentials for A_2 and A_ε calculated from electrochemical measurements and spectral properties.

4.3.2 Distance-dependent electron transfer between DNA bases

Having identified base analogues that undergo photoinduced electron-transfer reactions, we could prepare DNA assemblies via chemical synthesis in which the positions of donor and acceptors were known precisely and varied systematically. DNA-mediated photooxidations of guanine by A_2 and A_ε were therefore examined in a series of 12 base-pair DNA duplexes at donor/acceptor separations of 3.4 - 13.6 Å. In the duplexes, the donor (G) and acceptor (A_2 or A_ε) were located on the same strand. The remaining heterogeneous sequences were composed of inosine-cytosine and adenine-thymine pairs which do not react with photoexcited A_2 or A_ε.
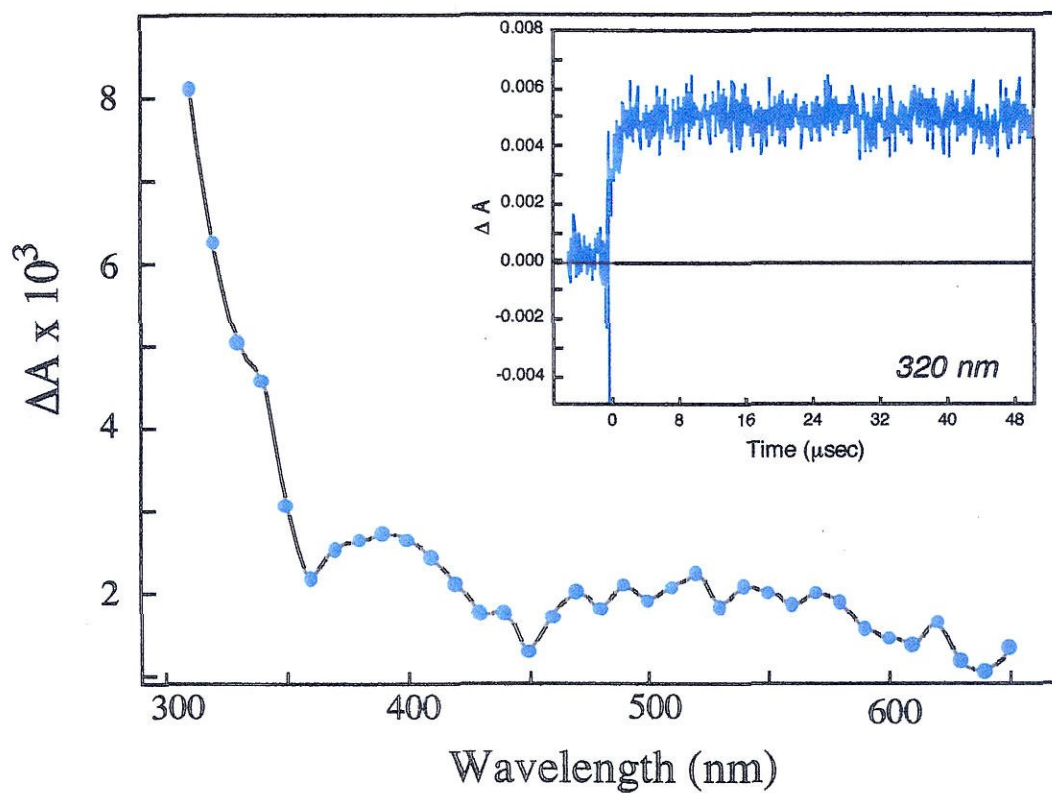
Figure 4.4 Wavelength dependence of long-lived intermediate observed upon flash photolysis ($\lambda_{exc} = 308$ nm) of 100 μM A$_2$, 50 mM dGTP in 100 mM sodium phosphate buffer, pH 7. (Inset) Transient absorption signal obtained at 320 nm.

Steady-state emission spectroscopy, reflecting the extent of electron transfer, reveals very different behavior with the two fluorescent bases (Table 4.1 and 4.2, Figure 4.5). Although both bases are highly quenched by G at the shortest donor-acceptor distance (F_q (3.4 Å): $A_2 = 0.93(3)$, $A_\varepsilon = 0.83(5)$) only aminopurine showed significant levels of electron-transfer quenching at larger separations (F_q (13.6 Å) = 0.21(1)). Indeed, ethenoadenine is only slightly reactive at 6.8 Å ($F_q = 0.21(6)$), and exhibits essentially no quenching at longer distances. As the fluorescence of A_2 is sensitive to its environment within the base stack, the quantum yields of unquenched inosine-containing duplexes were carefully monitored to delineate the effect of the subtle variations in sequence in the duplexes. The first duplex of the series consistently exhibited a higher quantum yield than the others of this series, presumably due to poorer stacking of A_2 with this modified base. However, throughout the rest of the series, constant quantum yields are obtained, indicating that (i) the environment of A_2 is essentially identical, and (ii) inosine-dependent reactions are not occurring.

It is noteworthy that the fluorescence spectra of the A_2/G duplexes contained a unique feature (Figure 4.5). A shoulder centered at ~400 nm was prominent in the most highly quenched duplexes. The intensity of this feature was pH dependent (Figure 4.6). Santhosh and Mishra[16] have proposed stable tautomers for aminopurine, and have calculated that all tautomeric structures would have lower excited-state reduction potentials than the predominant tautomer. Hence, the low-energy fluorescence feature observed here may reflect a small proportion of a minor tautomer with insufficient energy to oxidize G.

Time-correlated single photon counting (TCSPC) measurements revealed a striking difference in the rates of the G-dependent reaction for A_2 as compared to A_ε (Figure 4.7). At 3.4 Å, where donor and acceptor are located at adjacent positions within the DNA helix, A_2 undergoes ultrafast electron transfer manifested as static quenching (a decrease in initial intensity which indicates that the quenching reaction is

Table 4.1 Steady-state quantum yields and quenching efficiencies for ethenoadenine (ε)/guanine duplexes

	A_ε-Y distance (Å)	$\Phi_{Y=I}$[a]	$\Phi_{Y=G}$	F_q[b]
5'TAIε**Y**ITITTATIA ATCTCCACAATACT	3.4	0.26(4)	0.04(2)	**0.85(7)**
5'TAIε**AY**ITATTAIA ATCTTCCATAATCT	6.8	0.34(4)	0.28(4)	**0.18(4)**
5'TAIε**AAY**ITITTAIA ATCTTTCCACATCT	10.2	0.34(5)	0.34(4)	**0.01(1)**

[a]Quantum yields for 100 μM duplex samples in 100 mM phosphate (pH 7) were measured at 20°C relative to 100 μM AεTP, Φ = 0.60. Steady-state fluorescence intensities measurements were made at 20°C unless otherwise specified on an SLM 8000 spectrofluorimeter or a ISS K2 spectrofluorimeter. Samples were measured at a duplex concentration of 100 mM in 100 mM phosphate (pH 7). Sample excitation was performed with λ_{exc} = 335 nm, spectra were integrated from 355-525 nm. Normalized fluorescence spectra of quenched and unquenched samples were identical. [b] All fraction quenched (F_q = 1 - Φ_G/Φ_I) values obtained from steady-state fluorescence measurements were calculated from 4-6 sets of samples and least 3 independent oligonucleotide syntheses. Numbers in parentheses represent error values.

Table 4.2 Steady-state quantum yields and quenching efficiencies for aminopurine (A) -guanine/deazaguanine duplexes

	A_2-Y distance (Å)[a]	$\Phi_{Y=I}$[b]	$\Phi_{Y=G}$[c]	$\Phi_q(G)$[d]	$\Phi_{Y=Z}$[e]	$F_q(Z)$
5' TAI**AY**ITITTATIA ATCTCCACAATACT	3.4	0.067(3)	0.005(1)	**0.93(2)**	0.002(1)	**0.97(2)**
5' TAI**AAY**ITATTAIA ATCTTCCATAATCT	6.8	0.057(4)	0.016(2)	**0.72(2)**	0.009(1)	**0.84(4)**
5' TAI**AAAY**ITITTAIA ATCTTTCCACATCT	10.2	0.051(4)	0.027(3)	**0.47(2)**	0.028(5)	**0.47(6)**
5' TAI**AAIAY**ITATIA ATCTTCTCCATACT	13.6	0.055(4)	0.043(8)	**0.21(1)**	0.050(4)	**0.08(4)**

[a]Distances were calculated as described in Figure 4. [b]Quantum yields for 100 μM duplex samples in 100 mM phosphate (pH 7) were measured at 20°C relative to 100 μM A_2, Φ =0.32. Sample excitation was performed with λ = 325 nm, spectra were integrated from 340-500 nm. [c]The emission spectra of quenched A_2/G samples displayed a more prominent emission shoulder at ~ 400 nm than other samples, likely due to a tautomeric form of A_2 with a lower energy excited state that could not react with G. Therefore, emission intensities were determined by monitoring emission at 360 nm, the maximum of the main peak, for a 60 second interval. [d]F_q = fraction quenched. Numbers in parentheses represent error values. [e]The emission spectra of A_2/Z samples were distinctly sharper than others, again possibly due to a tautomeric form of A_2 with a lower energy excited state that is preferentially quenched. These spectral differences did not affect the quenching yields in this case more than 5%, and thus the entire spectrum was utilized.

Figure 4.5 Steady-state emission spectra for A_ε (**top**) and A_2 (**bottom**)

guanine-containing duplexes. For comparison, the spectrum of an

unquenched inosine-containing duplex is also shown.
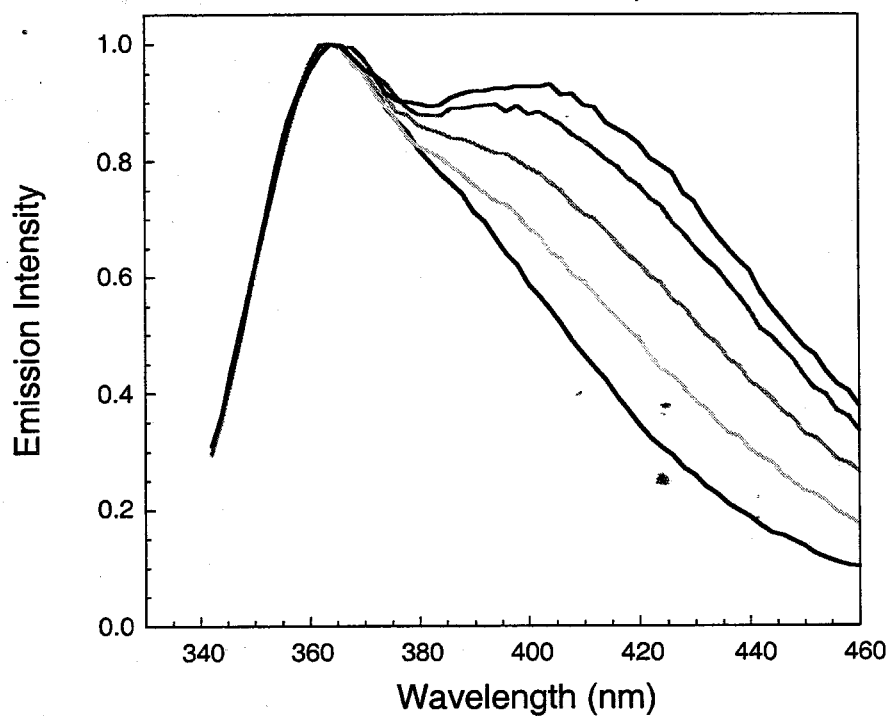
Figure 4.6 Normalized steady-state emission spectrum of A$_2$/G duplex obtained as a function of pH with λ_{exc} = 324 nm.. Spectra were obtained at pH 5.3, 6.4, 7.0, 7.4, 8.0. With increasing pH, the emission shoulder centered at 410 nm becomes more prominent. Longer excitation wavelengths also increase the intensity of this shoulder.
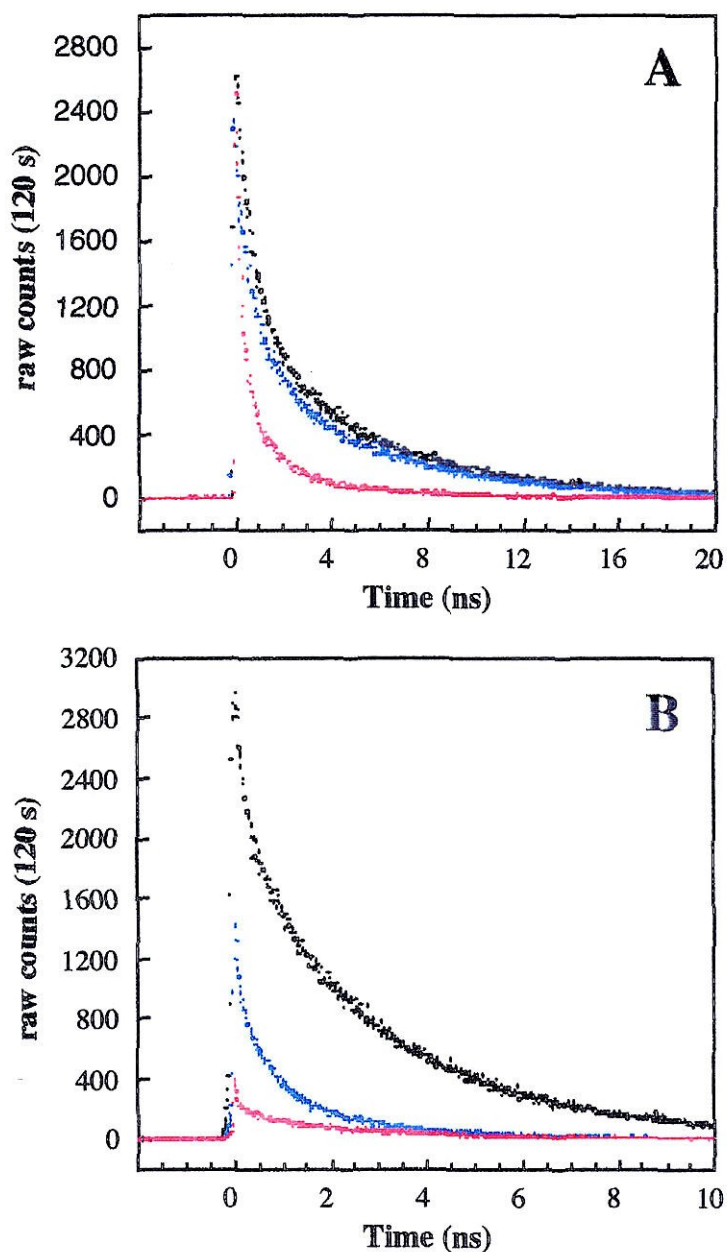
Figure 4.7 Fluorescence decay profiles for A_ε (**A**) and A_2 (**B**) obtained by TCSPC; data sets shown were obtained by collecting counts for 120 s under conditions of steady laser power. Data shown correspond to donor acceptor separations of 3.4 Å (red) and 6.8 Å (blue) compared to an unquenched inosine-containing duplex (black).

faster than the time scale measured by this apparatus ($k_{et} \geq 10^{10}$ s^{-1})). In contrast, decreases in the measurable fluorescence lifetimes for $A\varepsilon$ completely account for the quenching of this base by G, indicating that electron transfer takes place on a slower time scale ($k_{et} \sim 10^9$ s^{-1}).

As the decays of $A\varepsilon$ are multiexponential, as expected for a DNA-bound probe, the fits of the fluorescence decay profiles do not yield single rate constants for the electron-transfer reaction between $A\varepsilon$ and G (Table 4.3). However, the integration of the decay curves for the G-containing and I-containing duplexes provides a measure of dynamic quenching that is independent of any data fitting routine. These quenching yields are almost identical to those observed in steady-state measurements (F_q (3.4 Å): dynamic (TCSPC) = 0.76, overall (steady-state) = 0.85; F_q (6.8 Å): dynamic = 0.15, overall = 0.18. Moreover, if electron-transfer rates are approximated for each component of the decay, a distance dependence equivalent to that observed based on the steady-state quantum yields is obtained. Hence, since the quenching of $A\varepsilon$ is dynamic, the distance dependence of the $A\varepsilon$/G reaction provides a measure of β; based upon steady-state quantum yields, a value of 1.0(1) Å^{-1} is obtained for this parameter (Figure 4.8).

As the quenching reaction between A_2 and G occurs on a time scale faster than that predicted by a Stern-Volmer analysis (Table 4.4), the distance dependence of this reaction calculated from steady-state quantum yields is not purely a reflection of β. The distance dependences of this and other ultrafast reactions must therefore be interpreted within the context of a different model (*vide infra*).

4.3.3 Effects of reactant structure on electron transfer efficiency

The reactivities of A_2 and $A\varepsilon$, both adenine derivatives with similar electronic structures and electrochemical properties, are essentially identical in solution. However, in DNA, ultrafast electron transfer initiated by A_2 occurs over a range of distances, while with $A\varepsilon$, insulator-like behavior is observed. NMR studies of duplexes containing A_2[17] and $A\varepsilon$[18]

Table 4.3 Fluorescence decay lifetimes and evaluation of dynamic quenching in A_ε-G duplexes[a]

A_ε-G Distance	τ_1 (%)	τ_2 (%)	F_q(dynamic)[b]	F_q(total)[c]
3.4	2.0 ns (30%)	0.06 ns (70%)	0.76	0.85
6.8	6.9 ns (24%)	0.65 ns (76%)	0.15	0.18
6.8 (I)[d]	7.3 ns (27%)	0.77 ns (73%)	--	--

[a]Measured using TCSPC with λ_{exc} = 325 nm, λ_{em} = 350 nm in samples containing 100 μM duplex, 100 mM sodium phosphate, pH 7. [b]Calculated using the expression:

$$F_q \text{(dynamic)} = (((\tau_1 * c_1) + (\tau_2 * c_2))_q / ((\tau_1 * c_1) + (\tau_2 * c_2))_o) * (1 - (I_{init(q)} / I_{init(o)}))$$

where $I_{init(q)}$ and $I_{init(o)}$ are intensities at t= 0 obtained from data sets obtained under conditions of steady laser power for quenched and unquenched samples, respectively. $(1 - (I_{init(q)} / I_{init(o)}))$ is therefore the component of the fluorescence decay remaining after any fast electron transfer manifested as static quenching (not present in A_ε samples). [c]F_q (total) is the amount of fluorescence quenching observed with steady-state methods. [d]The fluorescence decays of all A_ε-I duplexes were similar, this data set is shown for comparison; no quenching was detectable by TCSPC at donor-acceptor distances greater than 6.8 Å.

128

Table 4.4 Fluorescence decay lifetimes and evaluation of intrastrand dynamic quenching in A_2-G duplexes[a]

Quencher	A_2-G/Z Distance	τ_1 (%)[b]	τ_2 (%)	F_q(dynamic)[c]	F_q(total)[d]
G	3.4	1.9 ns (46%)	0.070 ns (54%)	0.10	0.93
Z	3.4	2.5 ns(66%)	0.52 ns (34%)	0.10	0.97
G	6.8	1.3 ns (56%)	0.18 ns (44%)	0.26	0.72
Z	6.8	1.5 ns (28%)	0.14 ns (72%)	0.28	0.84
G	10.2	2.1 ns (52%)	0.19 ns (48%)	0.27	0.47
Z	10.2	1.7 ns (59%)	0.16 ns (41%)	0.28	0.47
G	13.6	2.8 ns (60%)	0.25 ns (40%)	0.15	0.21
Z	13.6	2.8 ns (65%)	0.25 ns (35%)	0	0.08
I[d]	6.8	2.3 ns (67%)	0.24 ns (33%)	--	--

[a]Measured using TCSPC with λ_{exc} = 325 nm, λ_{em} = 350 nm in samples containing 100 μM duplex, 100 mM sodium phosphate, pH 7. [b]The fluorescence decay of A_2 in G-containing duplexes could be satisfactorily fit to a biexponential, decays corresponding to Z-containing duplexes were better fit by a triexponential fit, but biexponential fit is shown here for comparison. [c]Calculated using the expression:

$$F_q \text{ (dynamic)} = (((\tau_1 * c_1)+(\tau_2 * c_2))_q / ((\tau_1 * c_1)+(\tau_2 * c_2))_o) * (1-(I_{init(q)}/I_{init(o)}))$$

where $I_{init(q)}$ and $I_{init(o)}$ are intensities at t= 0 obtained from data sets obtained under conditions of steady laser power for quenched and unquenched samples, respectively. $(1-(I_{init(q)}/I_{init(o)}))$ is therefore the component of the fluorescence decay remaining after the fast electron-transfer process manifested as static quenching. [d]F_q (total) represents the total amount of quenching quantitated in steady-state measurements. [e]The fluorescence decays of all A_2-I duplexes were similar, this data set is shown for comparison.

$$\beta = 1.0(1) \text{ Å}^{-1}$$
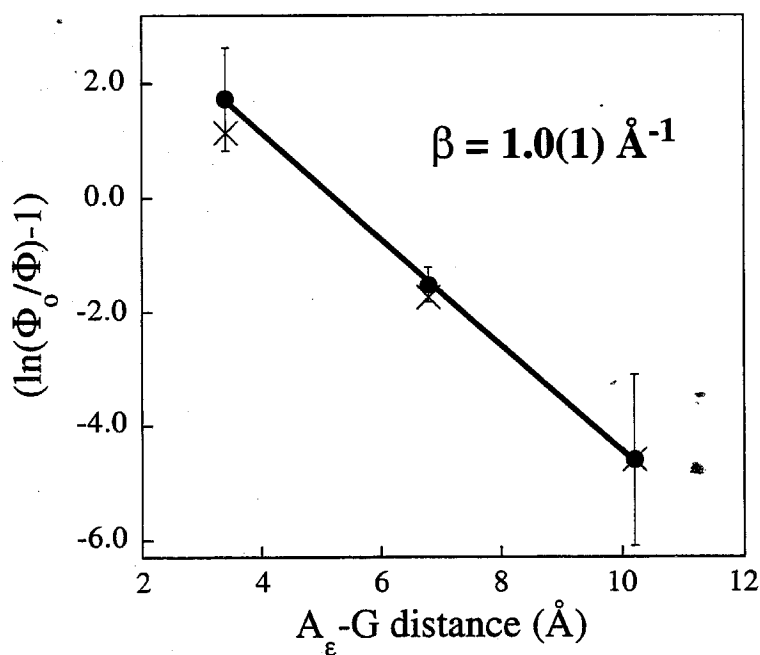
Figure 4.8 Distance dependence of electron transfer between A_ε and G.

Steady-state quantum yields for unquenched (Φ_0), inosine-containing

duplexes were compared to quenched (Φ), guanine-containing duplexes to

evaluate the dependence of this reaction on distance (●). For comparison,

data points obtained by quantitating quenching from the weight-averaged

lifetimes determined in TCSPC experiments are also shown (×).

provide insight into a clear difference between these modified bases: stacking within the DNA helix. A_ε is sterically bulky and does not pair with T; thus while it remains intrahelical, it is well-established that A_ε assumes a nonplanar orientation within the helix and is poorly stacked with the other DNA bases.[17] These features of the conformation of A_ε are consistent with characteristics of the duplexes we prepared.[17] Significant decreases ($\sim$ 5°C) in the thermal denaturation temperatures are observed for duplexes containing A_ε compared to adenine, and no hypochromism or transitions upon thermal denaturation in the 310 nm absorption associated with A_ε is detected. Moreover, very low steady-state fluorescence polarization values ($\sim$ 0.01) were observed for A_ε duplexes. All of these results, combined with information from structural studies, are consistent with a non-rigid, poorly stacked conformation for A_ε within the base stack.

In contrast, NMR studies of A_2[18] reveal that this base undergoes normal Watson-Crick pairing with thymine, and that A_2 is stacked within the DNA helix quite similarly to the natural bases. We find that A_2 exhibits much higher levels of steady-state polarization ($\sim$ 0.15) and a smaller destabilizing effect on duplex stability (1-2°C) compared to A_ε. Furthermore, thermal denaturation of A_2-containing duplexes can be monitored in the 310 nm absorption unique to this base, as this spectral feature is red-shifted when this base is within a hybridized duplex. This may result from a more nonpolar environment for the base, or as the result of hydrogen-bonding interactions. Thermal denaturation transitions can therefore be monitored at this wavelength, and are observed to occur 2-3°C before the transitions monitored at 260 nm corresponding to the melting of the entire duplex.

Thus, despite the fact that there are not large energetic differences in the reactions of A_ε or A_2 with guanine, the extent of stacking among these bases and the DNA base-pair stack dramatically affects the reaction kinetics and distance dependences of these electron-transfer processes mediated by the DNA helix. It is remarkable that such subtle distinctions in stacking lead to these vast differences in reactivity.

4.3.4 Intrastrand versus interstrand electron transfer

Base-base electron-transfer chemistry also provides an opportunity to examine coupling between donors and acceptors located on the same strand of DNA duplexes compared to that between reactants located on opposite strands (Figure 4.9). Table 4.4 shows steady-state emission results for assemblies in which the interstrand reaction analogous to the intrastrand reaction described above was studied. Here, at the shortest distance studied for the interstrand reaction of A_2, 5.0 Å, 52% of the emission intensity was quenched in a guanine-containing duplex. The yields of electron transfer are again attenuated with increasing donor-acceptor separation, but are much less sensitive to distance than for the intrastrand quenching reaction. Measurement of reaction kinetics by TCSPC revealed another important distinction between these reactions (Figure 4.10). The reaction kinetics were found to be significantly slower for the *interstrand* electron transfer compared to the *intrastrand* reaction. Indeed, while a large proportion of the quenching is unresolvable with 100 ps resolution for the intrastrand reaction, the electron-transfer quenching for A_2 and G localized on different strands is completely resolved on the time scale observable in this experiment. Thus, electron transfer occurs on a slower time scale for the bases in this orientation.

The fluorescence decay kinetics for A_2 are also multiexponential, and therefore make the determination of discrete electron-transfer rates difficult. However, the amount of lifetime quenching can be quantitated, and compared with steady-state quenching yields (Table 4.5). This analysis provides very good agreement for the interstrand electron-transfer reaction with F_q (5.0 Å): dynamic (TCSPC) = 0.52, overall (steady-state) = 0.52, F_q (7.8 Å): dynamic = 0.45, overall = 0.46, F_q (10.8 Å): dynamic = 0.34, overall = 0.34, F_q (13.9 Å): dynamic = 0.20, overall = 0.21. Since the distance dependence of this reaction results in measurable changes in electron-transfer rates, a value of 0.14(2) Å^{-1} for β can be determined for this interstrand reaction (Figure 4.9).
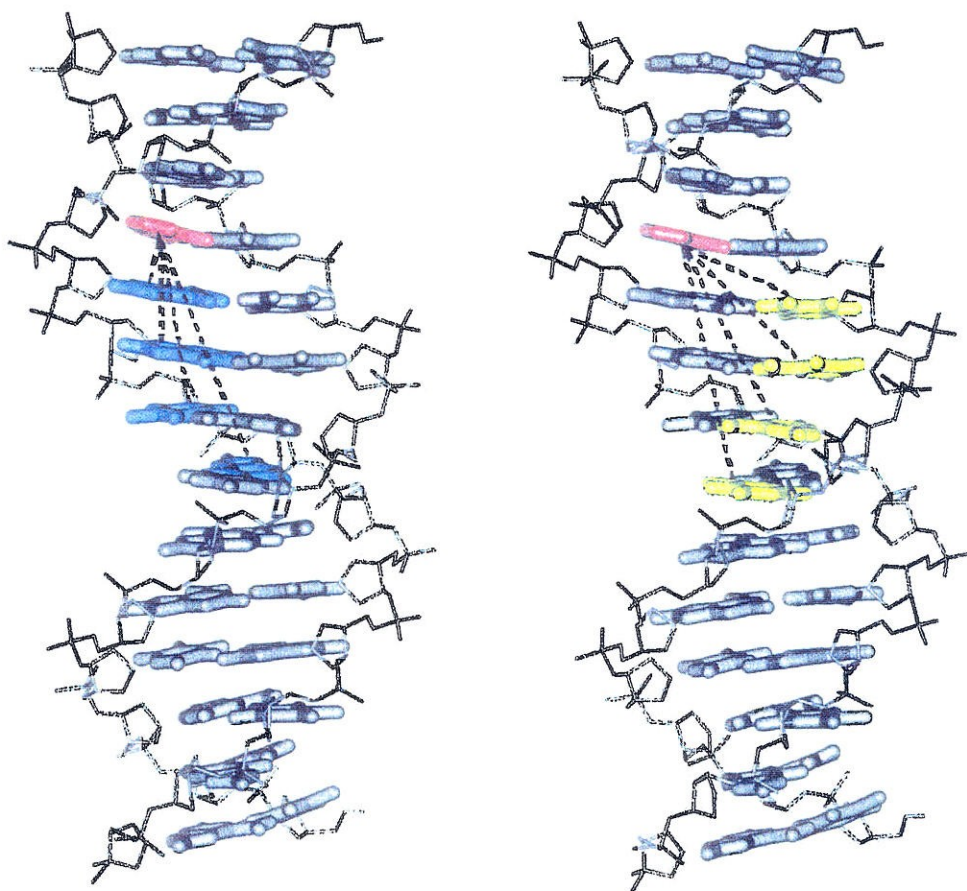
Figure 4.9 Assemblies used to evaluate intrastrand (left) and interstrand (right)
quenching reactions of A_2 by G.

Table 4.5 Steady-state quantum yields and quenching efficiencies for aminopurine (A₂) - guanine/deazaguanine duplexes

A₂-Y distance (Å)[a]	$\Phi_{Y=I}$[b]	$\Phi_{Y=G}$[c]	$F_q(G)$[d]	$\Phi_{Y=Z}$[e]	$F_q(Z)$
5'TAIAACITITTATIA ATCTTYCACAATACT	5.0	0.052(5)	0.025(3)	**0.52(4)**	0.017(4)	**0.68(6)**
5'TAIAAACITATTAIA ATCTTYCATAAATCT	7.8	0.057(3)	0.031(3)	**0.46(5)**	0.033(3)	**0.42(5)**
5'TAIAAACITITAIA ATCTTTYCACACATCT	10.8	0.061(3)	0.040(4)	**0.34(2)**	0.048(4)	**0.21(3)**
5'TAIAAIACITATIA ATCTTCTTYCATACT	13.9	0.059(7)	0.045(6)	**0.24(2)**	0.058(5)	**0.02(4)**

[a]Distances were calculated between 2-NH₂ of bases. [b]Quantum yields for 100 μM duplex samples in 100 mM phosphate (pH 7) were measured at 20°C relative to 100 μM A₂, Φ =0.32. Sample excitation was performed with λ = 325 nm, spectra were integrated from 340-500 nm. [c] The emission spectra of quenched A₂/G samples displayed a more prominent emission shoulder at ~ 400 nm than other samples, likely due to a tautomeric form of A₂ with a lower energy excited state that could not react with G. Therefore, emission intensities were determined by monitoring emission at 360 nm, the maximum of the main peak, for a 60 second interval. [d]F_q = fraction quenched. Numbers in parentheses represent error values. [d]The emission spectra of A₂/Z samples were distinctly sharper than others, again possibly due to a tautomeric form of A₂ with a lower energy excited state that is preferentially quenched. These spectral differences did not affect the quenching yields in this case more than 5%, and thus the entire spectrum was utilized.

Figure 4.10 Fluorescence decay profiles for duplexes containing A_2 and G on opposite strands obtained by TCSPC; data sets shown were obtained by collecting counts for 120 s under conditions of steady laser power. Data correspond to donor-acceptor separations of 5.0 Å (red) and 7.8 Å (blue) compared to an unquenched inosine-containing duplex (black).

Table 4.6 Fluorescence decay lifetimes and evaluation of interstrand dynamic quenching in A_2-G duplexes[a]

Quencher	A_2-G/Z Distance	τ_1 (%)[b]	τ_2 (%)	F_q(dynamic)[c]	F_q(total)[d]
G	5.0	1.5 ns (40%)	0.12 ns (60%)	0.52	0.55
Z[e]	5.0	2.0 ns (29%)	0.08 ns (71%)	0.35	0.72
G	7.8	1.8 ns (46%)	0.20 ns (54%)	0.45	0.47
Z	7.8	1.8 ns (52%)	0.13 ns (48%)	0.40	0.46
G	10.8	2.2 ns (60%)	0.18 ns (40%)	0.34	0.33
Z	10.8	2.1 ns (67%)	0.15 ns (33%)	0.22	0.25
G	13.9	2.8 ns (46%)	0.24 ns (54%)	0.20	0.20
Z	13.9	2.8 ns (60%)	0.26 ns (40%)	0.06	0.02
I[f]	7.8	2.2 ns (63%)	0.79 ns (37%)	--	--

[a]Measured using TCSPC with λ_{exc} = 325 nm, λ_{em} = 350 nm in samples containing 100 µM duplex, 100 mM sodium phosphate, pH 7. [b] The fluorescence decay of A_2 in G-containing duplexes could be satisfactorily fit to a biexponential, decays corresponding to Z-containing duplexes were better fit by a triexponential fit, but biexponential fit is shown here for comparison. [c]Calculated using the expression:

$$F_q \text{ (dynamic)} = (((\tau_1 * c_1)+(\tau_2 * c_2))_q/((\tau_1 * c_1)+(\tau_2 * c_2))_o) * (1-(I_{init(q)}/I_{init(o)}))$$

where $I_{init(q)}$ and $I_{init(o)}$ are intensities at t= 0 obtained from data sets obtained under conditions of steady laser power for quenched and unquenched samples, respectively. $(1-(I_{init(q)}/I_{init(o)}))$ is therefore the component of the fluorescence decay remaining after the fast electron-transfer process manifested as static quenching. [d]F_q (total) represents the amount of quenching quantitated from steady-state measurements. [e]This duplex was the only assembly containing donor and acceptor on opposite strands where static quenching was observed. [f]The fluorescence decays of all A_2-I duplexes were similar, this data set is shown for comparison.
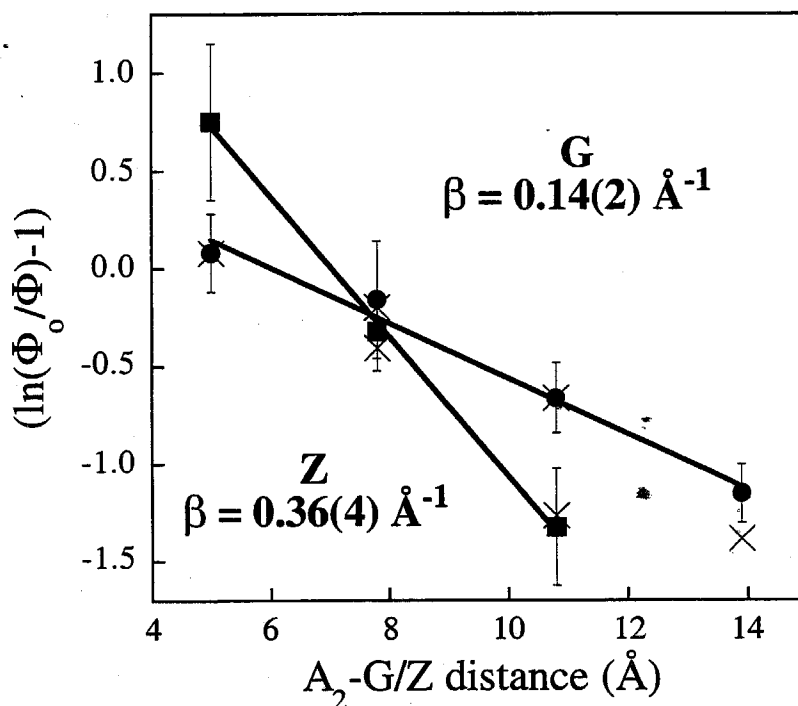
Figure 4.11 Distance dependence of electron transfer between A_2 and G or Z. Steady-state quantum yields for unquenched (Φ_o), inosine-containing duplexes were compared to quenched (Φ), guanine-containing duplexes to evaluate the dependence of this reaction on distance (●). For comparison, data points obtained by quantitating quenching from the weight-averaged lifetimes determined in TCSPC experiments are also shown (×).

For the intrastrand electron-transfer reaction, the same agreement is not observed because of the significant amount of static quenching: F_q (3.4 Å): dynamic = 0.10, static = 0.83, overall = 0.93, F_q (6.8 Å): dynamic = 0.26, static = 0.49, overall = 0.72, F_q (10.2 Å): dynamic = 0.27, static = 0.20, overall = 0.47, F_q (13.6 Å): dynamic = 0.15, static = 0.08, overall = 0.21. Therefore, as static quenching is observed even at the longest distances where the quenching is significantly attenuated, these quenching yields cannot be analyzed to extract β. The contribution from static and dynamic quenching observed over the entire series of duplexes may indicate that two different channels for electron transfer exist with different kinetics, or that the quenching rates are faster than can be fully resolved by this instrument, but slow enough to contribute somewhat to the observable fluorescence decay. Nonetheless, the data unequivocally demonstrate that interstrand and intrastrand electron transfer reactions occur on different time scales.

It is therefore apparent that electron transport proceeds preferentially down one strand in double-helical DNA, an unprecedented observation. Within B-form DNA, essentially only intrastrand stacking occurs.[19] Thus, when reactants are directly coupled through stacking along one strand, fast reaction kinetics result. If hydrogen-bonded base pairs must be traversed, the electron-transfer kinetics slow considerably. It is interesting that a shallow distance dependence with $\beta = 0.1$ Å^{-1} is observed nonetheless. Comparably low values of β have been observed only for fully conjugated systems.[20]

We also examined the effect of "cutting" a proximal interstrand connection by incorporating A_2 mispairs which lack hydrogen-bonding interactions. A_2 does not form a stable base pair with G; results of previous spectroscopic studies indicate a dynamic extrahelical conformation for the G of this pair.[21] Within the A_2-G mispair-containing duplexes, no red-shifted 320 nm absorption is observed for A_2. Furthermore, although the overall melting of the A_2-G duplex can be observed at 260 nm (T_m(260 nm) = 24°C (A_2-G); T_m = 30°C (A_2-T)), no transition can be detected in the A_2 absorption. It

therefore appears that A_2 is neither hydrogen-bonded nor well-stacked within the A_2-G mispair, consistent with photophysical studies. Furthermore, almost twofold increases are observed for the steady-state quantum yields of A_2-G duplexes compared to those with Watson-Crick pairs, again indicating that the fluorophore is not well-stacked within the duplex. The high quantum yields observed in these samples also indicate that G and A_2 do not participate in efficient electron transfer when incorporated within a mispair, and therefore do not interact strongly.

A comparison of quenching yields for the intrastrand and interstrand reactions for the Watson-Crick paired and mispaired fluorophore are depicted graphically in Figure 4.12. Quenching yields for the intrastrand reaction are decreased in the presence of an A_2-G mispair, but the overall distance dependence of the reaction is essentially identical to that observed with the A_2-T pair. In the A_2-G duplexes, intrastrand fluorescence quenching occurs even over the longest distance studied, 13.6 Å. However, for the interstrand reaction, the quenching yield is decreased by ~ 50% at the shortest donor-acceptor distance (5.0 Å), and quenching is barely detectable when only two base steps intervene between donor and acceptor (7.8 Å). Here, the overall distance dependence is dramatically increased ($\beta \sim 1.7$ Å^{-1}). It therefore appears that when the donor and acceptor are coupled through an intrastrand pathway, the direct stacking that facilitates the electronic interaction between the reactants is only slightly perturbed by the mispair, leading to decreased yields of fast electron transfer. For donors and acceptors coupled through an interstrand pathway, hydrogen-bonding contacts between strands are essential for long-range reactivity, and thus, the overall distance dependence is sharply attenuated by the presence of an A_2 base pair with limited hydrogen bonding. The efficiency of the interstrand reaction at 5.0 Å was also measured in the presence of A_2-C and A_2-A pairs, and the quenching yields for these pairs paralleled the strength of base-pairing interactions indicated by melting temperatures for the duplexes (Figure 4.13). These results implicate
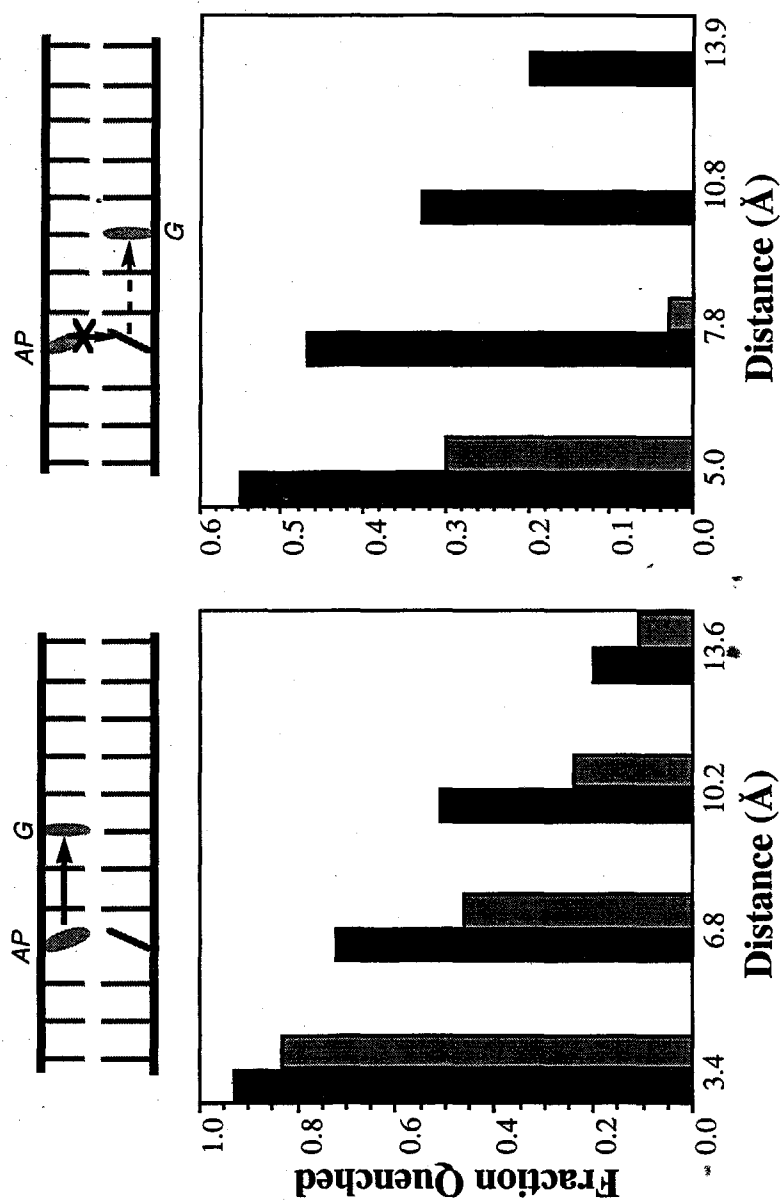
Figure 4.12 Comparison of quenching yields for intrastrand (left) and interstrand (right) quenching between A_2 and G when A_2 is paired with T (black) or G (gray). Duplexes used in this experiment were analogous to those shown in Table 4.2 and 4.3, with the exception of G being substituted for T across from A_2.

Table 4.7 Dependence of interstrand quenching on A_2 pairing

	T_m	F_q
5' X / TG	30°C	0.55(3)
5' X / GG	----	0.30(2)
5' X / AG	25°C	0.41(2)
5' X / CG	28°C	0.54(3)

the hydrogen-bond mediated interstrand connection between A_2 and its complementary thymine as an important component in the overall electron-transfer pathway for the interstrand reaction. The magnitude of the observed effect is somewhat surprising, as many other interstrand hydrogen bonds could potentially compensate for the disruption of the A_2 base pair; efficient interstrand reactions may require the excited state of A_2 to be directly coupled to the opposite strand.

4.3.5   Variation of reactant energetics

The effect of driving force and reactant energetics on DNA-mediated electron transfer has remained largely unexplored due to the difficulty of varying redox potentials without significantly changing the structure of synthetic assemblies. Base-base electron transfer chemistry offers a means to examine this issue as well. Here, by simply substituting deazaguanine for guanine as electron donor in the A_2^* assemblies, a change of one atom, the effect of lowering the oxidation potential of this reactant by ~ 300 mV can be monitored. In duplexes containing A_2 and Z either on the same or opposite strands, large amounts of fluorescence quenching were again observed (Table 4.2, 4.4). The quenching yields at short distances were higher than for the otherwise identical G-containing duplexes, consistent with the higher driving force for this reaction, but strikingly, the overall distance dependences for the A_2/Z reactions were steeper. The kinetic profiles for the intrastrand versus interstrand Z reactions were generally analogous to those observed for the G reaction, with large amounts of static quenching again observed for the intrastrand reaction, but full resolution of the quenching kinetics is achieved for the interstrand reaction with ~ 100 ps resolution. Although the decay profiles are complex, it is evident from these data that the kinetics of electron transfer for the interstrand A_2/Z reaction are faster those of the analogous A_2/G reaction, as expected for the higher driving force reaction.

Since the interstrand A_2/Z electron-transfer reaction results in measurable changes in the fluorescence decay dynamics, the distance dependence of this reaction represents β. Here, for the interstrand A_2/Z reaction, $\beta = 0.36(4)$ Å^{-1} (Figure 4.11).

The steeper distance dependence for the reaction of deazaguanine compared to guanine may confirm the importance of a parameter proposed in theoretical models for electron transfer: tunneling energy.[22] Since this DNA-mediated reaction, and most of the others studied to date, employ reactants with potentials close to those of the DNA bridge, a mechanism may be operative where the energetic gap between reactant orbitals and bridge orbitals, referred to as tunneling energy, becomes a crucial factor modulating the distance dependence of electron transfer. Indeed, by decreasing the donor oxidation potential here, we may increase this tunneling energy. These results may provide the first experimental demonstration of the importance of tunneling barrier effects in DNA-mediated electron transfer reactions.

Reactant energetics clearly play a role in modulating the distance dependence of electron transfer in DNA. However, these effects cannot completely explain the broad range of results obtained in systems employing different reactants. Many of the photoexcited acceptors utilized in different studies react selectively with G, indicating that these reactions have similar tunneling energies, yet markedly different distance dependences are observed ($\beta \sim 0.6 - 1.4$ Å^{-1}).[6,8] Moreover, the reactions of ethidium with deazaguanine or intercalators that have larger tunneling energies also have shallow distance dependences ($\beta \leq 0.1 - 0.4$ Å^{-1}).[2-3] In the studies described here, distance dependences differing by an order of magnitude are observed for the reactions of A_2 and A_ε, which have excited-state energies differing by no more that 100 mV. Therefore, although tunneling energies may somewhat modulate the efficiency of electron transfer through DNA, the strong stacking interactions between reactants and the DNA bases that are present in all of the systems with shallow distance dependences must also be essential.

4.3.7 Comparison of ultrafast DNA-mediated electron transfer reactions

The kinetics of the intrastrand reactions of A_2 with G or Z resemble the very fast reactions observed with intercalating reactants.[1-3] Static quenching, indicative of electron transfer with rates $\geq 10^{10}$ s^{-1}, dominates these reactions at all donor-acceptor distances. Hence, the attenuation of quenching yields as a function of distance does not appear to reflect only a competition between the rate of electron transfer and the excited state decay. We have previously proposed that base and reactant dynamics may effectively "gate" the yield of this reaction, thereby influencing this overall distance dependence since more intervening base pairs would result in a higher probability of a destacked duplex. Internal motions have been detected within DNA on picosecond time scales.[22] Therefore, if electron-transfer were to occur on this time scale or faster, only molecules in a limited range of conformations leading to the strong coupling required for this fast reaction may be active.

The distance dependences for the A_2/G and A_2/Z intrastrand reactions (Figure 4.13), 0.38(3) Å^{-1} and 0.59(2) Å^{-1}, respectively, therefore do not provide true measures of β, but because of the fast kinetics that are observed across a range of distances, these values may represent upper limits for β. The observation of steeper distance dependences for the fast intrastrand reactions compared to the slower interstrand reactions is consistent with the proposal that base destacking dynamics limit the efficiency of the faster reactions and contribute to the overall distance dependence. Interestingly, the distance dependences for the intrastrand reactions of A_2 with G as compared to Z display the same trend as for the interstrand reactions, again providing evidence that DNA-mediated reactions between stacked species are sensitive to reactant energetics.
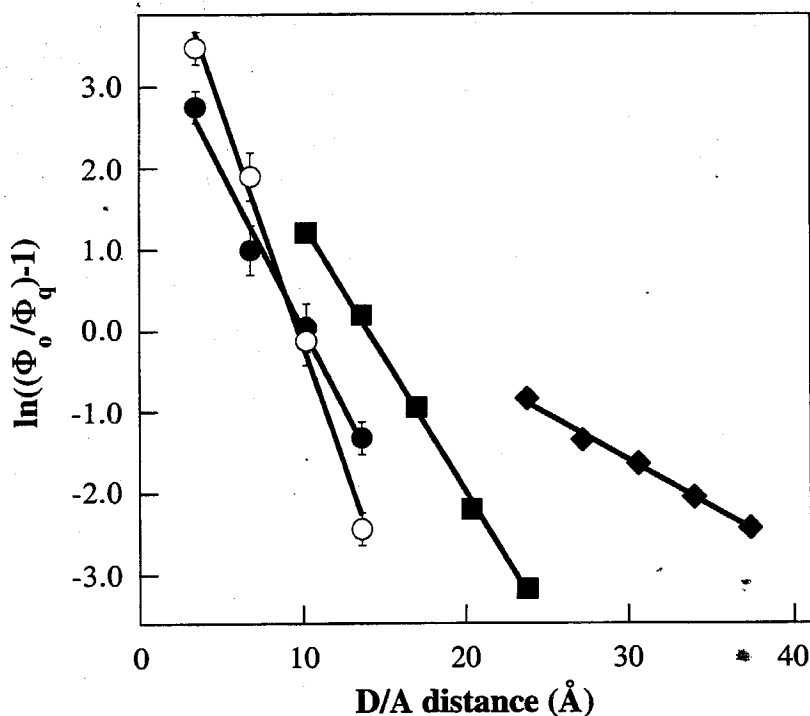
Figure 4.13 Distance dependences (γ) for intrastrand reactions between A_2 and G ($\bullet$) or Z (O). Quenching reactions for donors and acceptors localized on the same strand include significant contributions from fast, static quenching. Therefore, the distance dependence of these processes, just as those previously measured for oxidative quenching of ethidium by $Rh(phi)_2bpy^{3+}$ ($\blacklozenge$) and the photoxidation of deazaguanine by ethidium ($\blacksquare$), are not direct measurements of β. These distance dependences instead represent lower limits for this parameter, and include differing effects of stacking probabilities for reactants and the intervening DNA bases.

The distance dependences of the intrastrand A_2/G and A_2/Z reactions, referred to by the symbol γ, can be directly compared with those measured previously for the oxidative quenching of ethidium by a rhodium intercalator,[2] where $\gamma = 0.1$ Å^{-1}, and the photooxidation of deazaguanine by ethidium,[3] where values for γ from 0.2 - 0.4 Å^{-1} were measured (Figure 4.13). This range of distance dependences for these ultrafast reactions, where γ(intercalator/intercalator) < γ(intercalator/base) < γ(base/base), appears to reflect the different extents of interaction between these reactants with the DNA base stack, contributing either to stronger coupling between reactants, or higher reaction probabilities. Detailed kinetics studies including determinations of β for these systems will be necessary to make this distinction. Nonetheless, the compilation of these results illustrate that electron transfer on fast time scales occurring over significant distances is a general phenomenon that can be observed when intercalators and modified bases are utilized as reactants.

4.3.6 New perspectives on parameters governing electron transfer in DNA

Monitoring base-base electron transfer systematically in this structurally well-defined system demonstrates that electron transfer through double helical DNA can be exceedingly fast over long distances. Indeed, this reaction can be remarkably efficient between the moieties that would participate in this reaction *in vivo*: the DNA bases. However, electron transport can also be inefficient if a well-stacked pathway is not available through the DNA helix. The data presented clearly show: (i) strong reactant stacking is essential for ultrafast long-range electron transfer through DNA, (ii) electron transfer proceeds preferentially through directly stacked intrastrand pathways compared to interstrand pathways, and (iii) the distance dependence of electron transfer in DNA varies with donor energy.

Indeed, low values of β approaching 0.1 Å^{-1} can be observed for coherent, well-stacked pathways within the DNA helix; however, values of β approaching 1.0 Å^{-1} result when reactants are not directly coupled through strong stacking interactions. The observation of low values of β, and the measurement of such large range of values for this parameter within the same medium may in fact indicate that theoretical descriptions of nonadiabatic electron transfer are not the proper framework in which to consider these results. In addition, hopping mechanisms do not explain the fast, distance dependent reactions observed. Now that experimental studies have identified stacking and reactant energetics as important parameters, theoretical descriptions encompassing all features of the unique reactivity observed can be proposed to describe mechanisms of electron transfer through DNA.

We have now investigated electron transfer in a range of DNA assemblies where the intervening medium, the DNA base stack, was held constant. A striking range of reactivity (Table 4.7) was observed with distance dependences for electron transfer reflecting exponential changes in rates spanning a full order of magnitude. If such a range of results can be observed with reactants so similar, or even identical in structure but not in stacking orientation, the varying results observed in systems all employing different types of reactants can be understood as manifestations of the same sensitivity to stacking, orientation, and energetics.[1-8] The assessment of β in DNA, therefore, is not measured simply by monitoring the effect of distance, but requires the consideration of the range of parameters that are unique to this π-stacked molecular assembly. Paradigms developed to describe long-range electron transfer in σ-bonded systems such as proteins cannot be simply applied to describe the exquisite sensitivity of charge transport in DNA to π-stacking interactions and energetics.

Table 4.8 Summary of distance dependences for base-base electron-transfer reactions

Acceptor	Donor	Intrastrand/Interstrand	Distance Dependence		Conclusions
			β^a	γ^b	
A_ε	G	Intrastrand	1.0 Å^{-1}	--	weak coupling $k_{et} < k_{base\ dynamics}$
A_2	G	Intrastrand	--	0.4 Å^{-1}	direct coupling $k_{et} \geq k_{base\ dynamics}$
A_2	Z	Intrastrand	--	0.6 Å^{-1}	
A_2	G	Interstrand	0.1 Å^{-1}	--	indirect coupling $k_{et} < k_{base\ dynamics}$
A_2	Z	Interstrand	0.3 Å^{-1}	--	

[a]Calculated from steady state quantum yields; fluorescence decay profiles revealed expected changes in excited state lifetimes.
[b]Quenching for intrastrand reactions is mostly static ($k_{et} \geq 10^{10}$ s^{-1}), therefore these distance dependences do not solely reflect changes in electronic coupling with distance.

4.4 REFERENCES

1. Murphy, C. J.; Arkin, M. A.; Jenkins, Y.; Ghatlia, N. D.; Bossman, S.; Turro, N. J.; Barton, J.K. *Science* **1993**, *262*, 1025; Murphy, C.J.; Arkin, M.A.; Ghatlia, N.D.; Bossman, S.; Turro, N.J.; Barton, J.K. *Proc. Natl. Acad. Sci. U.S.A.* **1994**, *91*, 5315; Holmlin, R.E.; Stemp, E.D.A.; Barton, J.K. *J. Am. Chem. Soc.* **1996**, *118*, 5236; Arkin, M.R.; Stemp, E.D.A; Holmlin, R.E.; Barton, J.K.; Hörmann, A.; Olson, E.J.C.; Barbara, P.A. *Science* **1996**, *273*, 475.

2. Kelley, S.O.; Holmlin, R.E.; Stemp, E.D.A; Barton, J.K. *J. Am. Chem. Soc.* **1997**, *119*, 9861.

3. Kelley, S.O.; Barton, J.K. *Chem. & Biol.* **1998**, *5*, 413.

4. Kelley, S.O.; Barton, J.K; Jackson, N.M.; Hill, M.G., *submitted*.

5. Meade, T. J.; Kayyem, J. F. *Angew. Chem. Int. Ed. Engl.* **1995**, *34*, 352.

6. Lewis, F.D.; Wu, Taifeng; Zhang, Y.; Letsinger, R.L.; Greenfield, S.R.; Wasielewski, M.R. *Science* **1997**, *277*, 673; Lewis, F.D.; Letsinger, R.L. *JBIC* **1998**, *3*, 215.

7. Meggers, E.; Kusch, D.; Spichty, M.; Wille, U.; Giese, B. *Angew. Chem. Int. Ed.* **1998**, *37*, 460.

8. Fukui, K.; Tanaka, K. *Angew. Chem. Int. Ed.* **1998**, *37*, 158.

9. Marcus, R.A.; Sutin, N. *Biochim. Biophys. Acta* **1985**, *811*, 265.

10. Ward, D.C.; Reich, E.; Stryer, L. *J. Biol. Chem.* **1969**, *244*, 1228.

11. Barrio, J.R.; Secrist, J.A.; Leonard, N.J. *Biochem. Biophys. Res. Comm.* **1972**, *46*, 597; Secrist, J.A.; Barrio, J.R.; Leonard, N.J.; Weber, G. *Biochem.* **1972**, *11*, 3499; Spencer, R.D.; Weber, G.; Tolman, G.L.; Barrio, J.R.; Leonard, N.J. *Eur. J. Biochem.* **1974**, *45*, 425.

12. Holmen, A.; Norden, B.; Albinsson, B. *J. Am. Chem. Soc.* **1997**, *119*, 3114; Broo, A. *J. Phys. Chem. A* **1998**, *102*, 526.

13. Holmen, A.; Norden, B.; Albinsson, B. *J. Phys. Chem.* **1994**, *98*, 13460.

14. Seidel, C.A.M.; Schultz, A.; Sauer, M.H.M. *J. Phys. Chem.* **1996**, *100*, 5541; Steenken, S.; Jovanovic, S.V. *J. Am. Chem. Soc.* **1997**, *119*, 617.

15. Candeias, L.P.; Steenken, S. *J. Am. Chem. Soc.* **1989**, *111*, 1094; Stemp, E.D.A.; Arkin, M.R.; Barton, J.K. *J. Am. Chem. Soc.* **1997**, *119*, 2921.

16. Santhosh, C.; Mishra, P.C. *Spectrochim. Acta* **1991**, *47A*, 1685.

17. Kouchakdijan, M. et al. *Biochemistry* **1991**, *30*, 1820.

18. Norlund, T.M. et al. *Biochemistry* **1989**, *28*, 9095.

19. Saenger, W. *Principles of Nucleic Acid Structure* (Springer-Verlag, New York, 1984).

20. Woitellier, S.; Launay, J.P.; Spangler, C.W. *Inorg. Chem.* **1989**, *28*, 758.

21. Guest, C.R.; Hochstrasser, R.A.; Sowers, L.C.; Millar, D.P. *Biochemistry* **1991**, *30*, 3271.

22. Evenson, J.W.; Karplus, M. *Science* **1993**, *262*, 1247; Priyadarshy, S.; Risser, S.M.; Beratan, D.N. *J. Phys. Chem.* **1996**, *100*, 1767822.

23. Georghiou, L.; Bradrick, T.D.; Philippetis, A.; Beechem, J.M. *Biophys. J.* **1996**, *70*, 1909.

Chapter 5

Fabrication and Characterization
of DNA-Modified Surfaces and
Electrochemistry of Redox-Active Intercalators[‡]

5.1   INTRODUCTION

The discovery that thiol-containing compounds spontaneously assemble on gold surfaces has provided a new class of materials of great utility for the study of electron-transfer processes.[1] In particular, the development of well-ordered self-assembled monolayers formed by aliphatic alkanethiols of variable lengths on gold surfaces has allowed the application of electrochemical techniques to the study of electron transfer through σ-bonded media.[2] Because the construction of monolayers permits a redox-active species to be spatially separated by a well-defined distance from an electrode surface, the kinetics of electron transfer through the resulting films can be monitored as a function of distance. Studies of electron transfer through σ-bonded monolayers have confirmed evaluations of the electronic coupling ($\beta \sim 1$ Å^{-1}) in this medium obtained spectroscopically.[3]

The modification of surfaces with DNA appended to an alkanethiol tether provides another new class of materials potentially useful for the study of electron-transfer processes,[4] structural characterization of nucleic acids,[5] and biosensing applications (Figure 5.1).[6-10] Moreover, as the hydrophobic interior of DNA differs substantially from aqueous solution, DNA monolayers provide a convenient environment where the redox properties of molecules intercalatively bound to DNA may be monitored.

Electrochemical studies of small molecule/DNA complexes have focused primarily on solution-phase phenomena, in which DNA-induced changes in redox-potentials and/or diffusion constants of organic and inorganic species have been analyzed to yield association constants.[11-12] In addition, rates of guanine oxidation catalyzed by electrochemically oxidized transition-metal complexes have been used to evaluate the solvent accessibility of bases for the detection of mismatches or hybridization.[7-9]

Electrochemical signals triggered by the association of small molecules with DNA have also been applied in the design of other novel biosensors. Towards this end
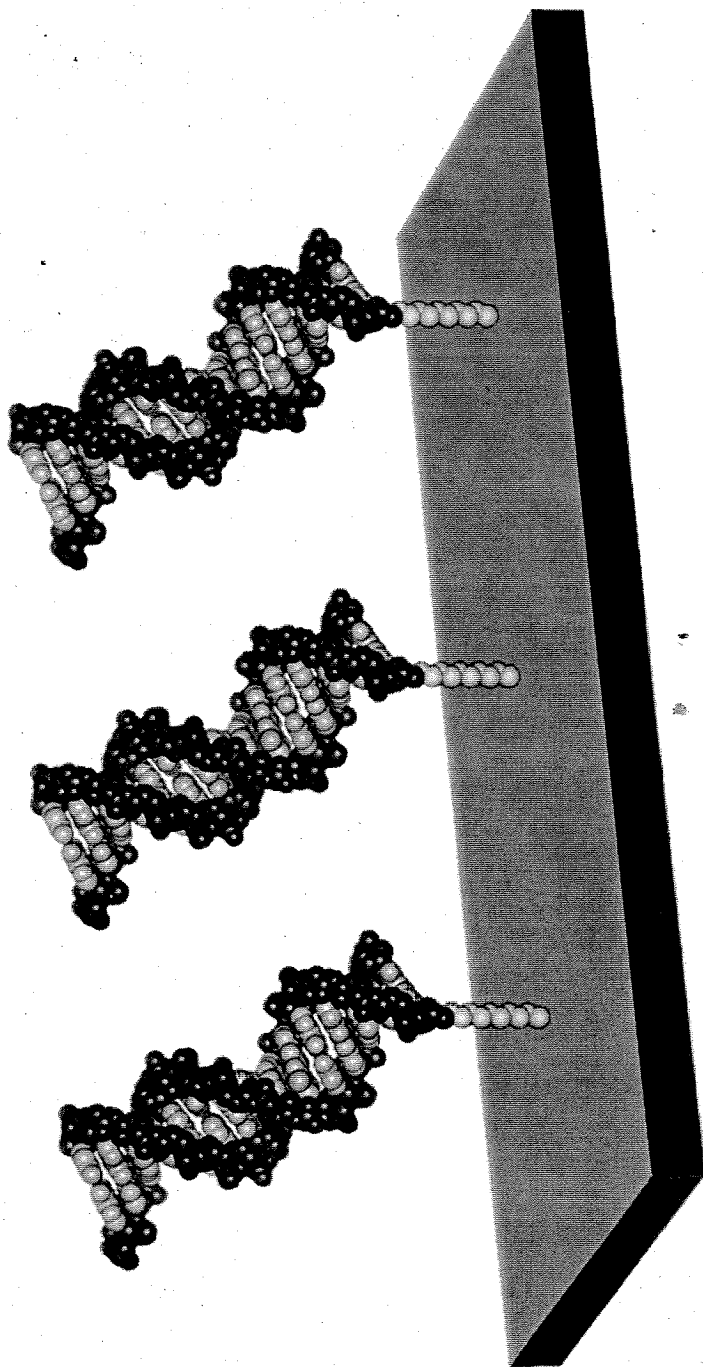
Figure 5.1 Schematic illustration of DNA monolayer immobilized on a gold surface.

oligonucleotides have been immobilized on electrode surfaces by a variety of linkages (*e.g.*, thiols on gold,[6b,10] carbodiimide coupling of guanine residues on glassy carbon,[6a] alkanebisphosphonate films on Al^{3+}-treated gold[8]) for use in hybridization assays. Both direct changes in mass (measured at a quartz crystal microbalance)[10] and changes in current[6a-b] or electrogenerated chemiluminescence signals[8] due to duplex-binding molecules have been used as reporters for double-stranded DNA. Gold surfaces modified with thiolated polynucleotides have also been used for the detection of metal ions and DNA-binding drugs.[13] Although surfaces modified with DNA have been reported, systematic studies investigating the surface structure and physical properties of these potentially useful substrates have not been performed.

This chapter describes the fabrication and characterization of DNA-modified surfaces, and our first electrochemical studies of a redox-active intercalator bound to these films. For the investigation of electron transfer through these films, it is crucial that the orientation and packing of the duplexes on the surface is established. We have therefore investigated the properties of DNA films with electrochemical and spectroscopic assays, and used atomic force microscopy (AFM) and radioactive tagging to quantitate surface coverage and explore surface morphology.

5.2 EXPERIMENTAL SECTION

Materials. Phosphoramidite reagents were obtained from Glen Research. Methylene blue (Sigma Chemicals), ferrocene carboxaldehyde, octadecyl mercaptan, carbonyl dimimidazole, diaminohexane, and 2-pyridyldithiopropionicacid N-succinimide ester (PDSP) (Aldrich) were used as received. Potassium ferrocyanide (Fisher) was recrystallized from aqueous solutions prior to use. [γ–^{32}P]dATP was obtained from NEN-Dupont.

Preparation of thiol-modified oligonucleotides. Oligonucleotides (synthesized by automated solid-phase synthesis)[14] immobilized on a controlled pore glass resin were treated in succession with carbonyldiimidazole and 1,6-diaminohexane (1g/10ml dioxane, 30 min./ea.) at the 5'-hydroxy terminus before cleavage from the resin.[15] After deprotection, a concentrated solution of amino-terminated oligonucleotides (typically 200 µl of a 10 mM solution) in 0.4 M HEPES buffer (pH 8) was mixed with PDSP (15 mg/100 µl) in acetonitrile to produce a disulfide.[16] After vortex agitation for 30 seconds, the reaction is essentially complete. Gel filtration (NAP-5 column, Pharmacia) removes excess PDSP, and sequences were purified by reversed-phase HPLC, converted to free thiols by incubation in 100 mM dithiothreitol for 30 min., and repurified before hybridization to their complements. Derivatized oligonucleotides were characterized by matrix-assisted laser desorption ionization time-of-flight mass spectrometry and HPLC retention times. Before deposition onto gold surfaces, the presence of free thiol was confirmed using a spectroscopic assay based on Ellman's reagent.[17]

Duplexes were hybridized in deoxygenated 5 mM phosphate, 50 mM NaCl (pH 7) by heating to 90°C followed by slow cooling to room temperature. Unprotected duplexes were stored frozen under Argon to prevent oxidation of the thiol.

Bulk gold electrodes were polished successively with 0.3 and 0.05 µm alumina (Buhler), sonicated for 30 min., and etched in 1.0 M sulfuric acid. Commercial Au(111) films on mica (Molecular Imaging) were prepared by flame annealing in hydrogen. Both types of surfaces were derivatized by incubation in 0.1 mM solutions of thiol-deriviatized DNA (50 mM phosphate buffer (pH 7), 0.1 M MgCl$_2$) for 1 - 12 hours. Samples were thoroughly rinsed in phosphate buffer before use. The deposition time required to obtain a desired surface coverage was somewhat batch-dependent, and longer times were typically required if the sample had not been made immediately before deposition. For the investigation of DNA-modified electrodes at high MB loadings, deposition of the thiol-

terminated DNA was performed in the presence of 0.6 mM MB; these electrodes were rinsed in 10 μM MB/buffer solutions. $CH_3(CH_2)_{17}SH$ modified electrodes were prepared by incubation in ethanol solutions for 48 hours.

Atomic Force Microscopy. All AFM images were collected using a MultiMode AFM running on the NanoScope IIIa controller (Digital Instruments, Santa Barbara, CA). A glass AFM electrochemistry chamber (Digital Instruments, Santa Barbara, CA) and a fluid volume of approximately 50 microliters were used for the experiments. Si_3N_4 cantilevers (spring constant, 0.06 N/m) with integrated, end-mounted oxide-sharpened Si_3N_4 probe tips were used. The applied vertical force of the AFM probe during imaging was minimized to beneath 200 pN. Continually adjusting the cantilever deflection feedback setpoint compensated for thermal drifting of the cantilever and a consistent, minimum force was maintained. Holes in the monolayer were prepared by decreasing the scan size to approximately 100-150 nm, increasing the scan rate to 24-30 Hz, and increasing the vertical force by advancing the setpoint several units. After about one minute, the scan size, scan rate, and setpoint were returned to their previous values, and images featuring a bare gold square were captured. All images captured for height-contrast analysis were recorded at minimum vertical tip forces. This was accomplished by decreasing the set-point until the tip disengaged from the surface, then reintroducing it with the minimum force required to achieve a stable image. In several cases, the film height was also measured in tapping mode, and gave the same result as the contact-mode experiments. AFM height calibrations were carried out on a NIST-traceable 180-nm height standard and then confirmed by measuring a single-atom step in the Au gold surface. The AFM images were recorded either in "Height" (constant force), or tapping mode. Potentials were controlled by a Princeton Applied Research Model 173 potentiostat/galvanostat, using silver and platinum wires for the pseudo reference and auxiliary electrodes, respectively.

Electrochemistry. All electrochemical experiments were performed with a Bioanalytical Systems (BAS) Model CV-50W electrochemical analyzer. Cyclic voltammetry (CV) and chronocoulometry (CC) were carried out at $20 \pm 2°C$ with a normal three-electrode configuration consisting of either a modified gold-disk working electrode or a hanging drop mercury electrode, and a saturated calomel reference electrode (SCE, Fisher Scientific). The working compartment of the electrochemical cell was separated from the reference compartment by a modified Luggin capillary. Potentials are reported versus SCE. Chronocoulometric measurements were corrected for double-layer charge as determined in buffer solutions. Heterogeneous electron-transfer rates were determined by cyclic voltammetry and analyzed as described previously.[18] The electron-transfer kinetics of several previously reported systems[19] (including benzo[c]cinnoline on gold and methylene blue on Hg) were investigated using this method with our instrumentation, and in each case, excellent agreement with the literature values was observed.

Ellipsometry. Optical ellipsometry ($\lambda = 632.8$ nm) was carried out on dried samples at 25°C using a Gaertner Model L116C ellipsometer.

[32]P labeling and quantitation. A 15-base pair oligonucleotide (5' CGCGAT GACTGTACT3') was 5' labeled with [γ-^{32}P]ATP and hybridized to a thiol-modified complement. Samples of Au(111) on mica (diameter = 0.41 cm) were treated with this duplex in the manner described above. After thorough rinsing in buffer solutions, dried samples were counted on a Beckman LS60001C scintillation counter, adjusted for attenuation by the presence of the mica, and compared to calibration standards that were prepared from known quantities of labeled oligonucleotide. The values obtained by scintillation counting and the surface areas of the modified mica were confirmed by analysis of the radioactivity of each sample by phosphoimagery (Molecular Dynamics).

5.3 RESULTS

5.3.1 Synthesis of thiol-modified DNA

The preparation of DNA-modified surfaces first required the development of a synthetic method that would produce thiol-modified oligonucleotides reproducibly in high yield. To accomplish this, a route based on a combination of established solid-phase[15] and solution-phase[16] methods was investigated for the synthesis of thiol-containing DNA (Figure 5.2). Oligonucleotides are synthesized using standard procedures, and while still attached to the controlled pore glass resin, an aliphatic, amino-terminated linker is attached. This portion of the tether can be synthesized with a variety of diaminoalkanes, but the preparation of DNA-surfaces with high surface coverages was found to be optimal when diaminohexane (as compared to diamaminononane, diaminobutane, and diaminopropane) was utilized. The pendant amino group is further reacted with an activated succinimide ester to yield disulfide-containing oligonucleotides. To ensure high levels of purity in the final product, disulfide oligonucleotides are purified first at this stage using reversed-phase HPLC. Upon reductive cleavage with DTT, thiol-terminated oligonucleotides are obtained, and purified again. Thiol-modified sequences were characterized by MALDI-TOF and electrospray mass spectrometry.

5.3.2 Characterization of DNA films by radiolabeling and ellipsometry

The surface coverage of DNA duplexes adsorbed on Au(111) was directly quantitated in a radioactive tagging (^{32}P) experiment. This assay yielded an average of $5.7(3) \times 10^{-12}$ moles of duplex DNA on a 0.14 cm^2 surface after 24 hours of modification. From this value and the cross-sectional area of DNA (3.14×10^{-12} cm^2), the surface coverage was calculated as $\Gamma = 4.1(2) \times 10^{-11}$ mol/cm^2, corresponding to a fractional coverage of 0.75(3). Ellipsometry of a 15-base-pair thiol-derivatized duplex on Au(111) was carried out and yielded an average monolayer thickness of 35 Å. As this
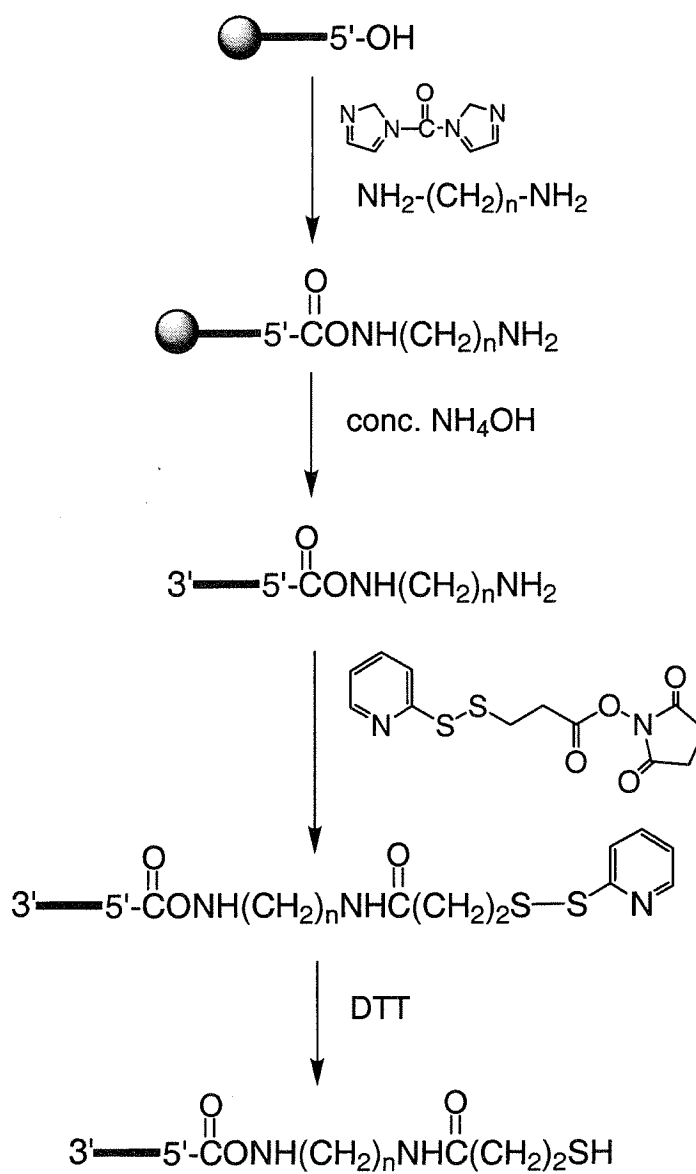
Figure 5.2 Synthetic strategy for preparation of thiol-terminated oligonucleotides.

measurement corresponds to an average thickness on the gold surface, it could reflect anywhere from 100% surface coverage with derivatized DNA duplexes stacked at an angle of 32° from the gold surface, to DNA helices oriented perpendicular to the surface with only 55% coverage, given a cylindrical DNA 15-mer duplex of 66 Å height (including the linker) and 20 Å diameter. It should be noted that both the ^{32}P labeling and ellipsometry experiments were performed without added magnesium (*vide infra*).

5.3.3 Electrochemical characterization of DNA-modified surfaces

The electrochemical window of 50 mM NaCl (pH 7) at DNA-modified gold extends from 0.70 V to -0.70 V (vs SCE), consistent with the known potential range over which thiol-gold linkages are stable. To probe the surface coverage of DNA on gold electrodes, the electrochemistry of ferrocyanide, an anionic species with a potential within the available window (~+200 mV vs NHE) was explored. Ferrocyanide does not bind to the DNA polyanion due electrostatic repulsion, therefore the electrochemical oxidation of this species is significantly attenuated at DNA-modified electrode. The differential responses of ferrocyanide at DNA-modified versus bare surfaces provides a means to follow the deposition kinetics of SH-DNA on gold. Figure 5.3A shows the cyclic voltammetry of this polyanion at electrodes modified with DNA for varying amounts of time. These voltammograms can be integrated to obtain the time course shown in Figure 5.3B. Interestingly, the addition of 100 mM $MgCl_2$ accelerates the deposition, and increases the overall surface coverage. It is not surprising that high concentrations are required in order for dense packing of the polyanionic duplexes on the surface to occur. In general, the derivatization proceeds quickly, with a high degree of surface coverage obtained within minutes. However, several hours are required for complete coverage, consistent with the deposition kinetics slowing dramatically once the surface density of duplexes is high enough for electrostatic repulsion between helices to become significant.
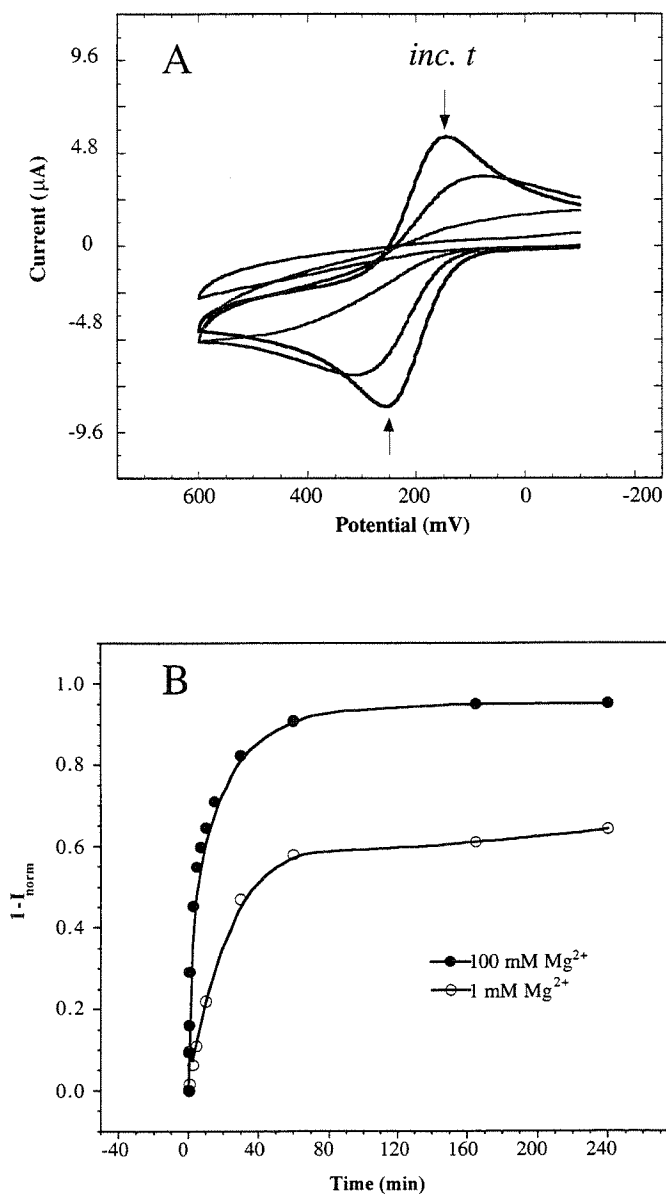
Figure 5.3 (A) Cyclic voltammograms for 0.1 mM $K_4[Fe(CN)_6]$ in 5 mM phosphate/50 mM NaCl (pH 7) at electrodes derivatized for 0 - 240 minutes with the oligonucleotide SH-5'-AGTACAGTCATCGCG + complement. (B) Integrated currents from cyclic voltammograms obtained when deposition was performed with 1 mM $MgCl_2$ (empty circles) and 100 mM $MgCl_2$ (filled circles). Scan rate $(v) = 100$ mV/s; electrode area $(A) = 0.02$ cm^2.

Gold surface waves (generated by the formation and stripping of gold oxide) at bare and derivatized electrodes were also compared as a qualitative measure of the surface coverage (Figure 5.4).[20] These results suggest a very high coverage (> 85%). However, thiol-gold linkages are known to undergo desorption at high potentials,[21] hence surface coverage is better evaluated by one of the methods described above.

5.3.4   Atomic force microscopy of DNA-modified surfaces

More detailed information concerning the morphology of the DNA films was sought using AFM. An AFM image of a DNA-modified surface prepared by our methods is shown in Figure 5.5. Several large, flat grains of the gold surface under the DNA film are clearly visible. While consistent with a well packed monolayer, no local order is evident; lateral force instabilities (typically on the order of 1 - 10 nN) associated with scraping the probe tip across a soft overlayer are well known to disrupt the local packing order.[22] The large structural anisotropy of the 15-base-pair DNA helices (20 Å in diameter vs. 50 Å in length), however, provides a convenient handle to gain indirect information concerning the orientation of the duplexes on the surface. A small patch of DNA was removed from the gold by applying a large vertical force with the AFM tip (Figure 5.6), and height-contrast measurements between the resulting square and the covered surface yield a monolayer depth of 45(3) Å. Including the dimensions of the tether, this corresponds to an average helical orientation of ~45° normal to the surface.

For simplicity, we have assumed that the thiol linker is both fully extended and colinear with the DNA. A molecular model of the tether yields a sulfur/DNA separation of 16.2 Å. However, as the self-assembly of these films is dependent on the much larger DNA helices, the exact conformation of the alkyl linker may vary somewhat. Depending on the effective length of the tether, the actual orientation of the DNA relative to the surface may deviate slightly from this 45° value.
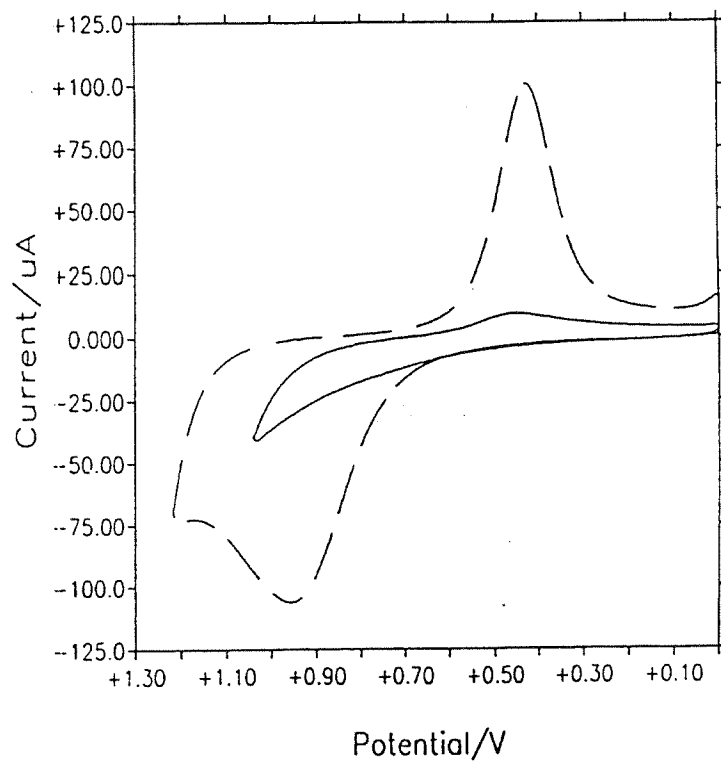
Figure 5.4 Cyclic voltammetry of bare (dotted line)

versus DNA-modified (solid line) gold electrodes in 50

mM sodium phosphate buffer, pH 7. $\nu = 100$ mV/s.
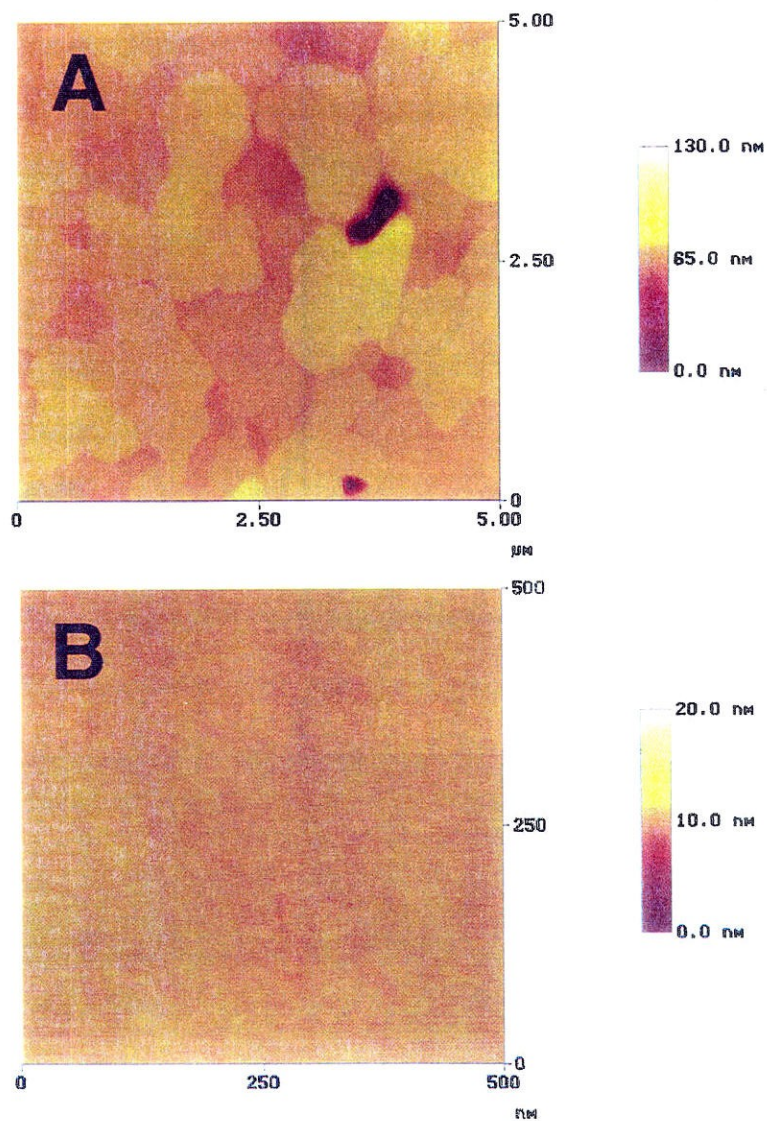
Figure 5.5 (A) 5x5 μm AFM image of DNA-modified gold (sequence: SH-5'-AGTACAGTCATCGCG) recorded under fluid solution (0.1 M sodium phosphate buffer, pH 7). (B) 500 x 500 nm image from same substrate area.
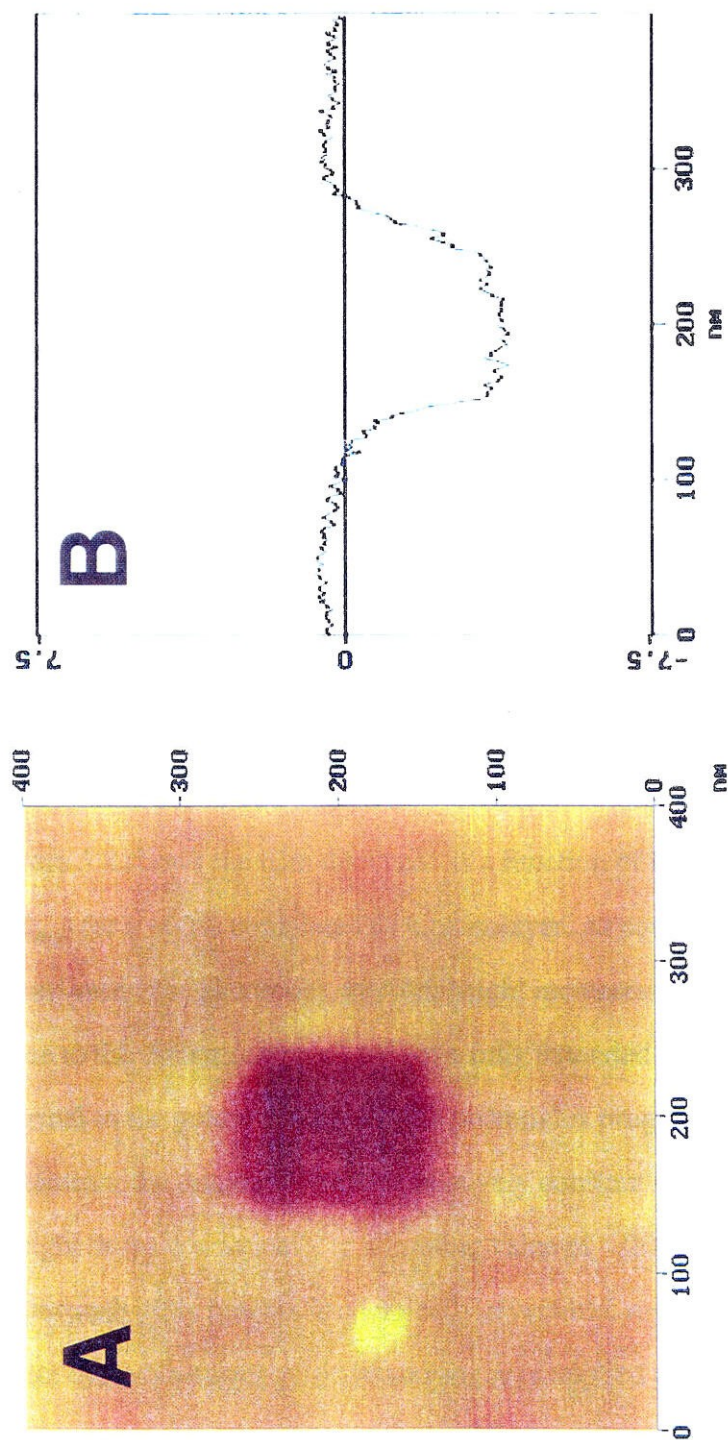
Figure 5.6 (A) AFM image of DNA-modified gold (sequence: SH-5′-AGTACAGTCATCGCG) after mechanical removal of a small square area (∼ 100 x 100 nm) of the monolayer. (B) Depth analysis of area shown in (A).

Although the film is very stable under open-circuit conditions, application of either large positive or negative potentials (-0.5 V $\leq$ E$_{app}$ $\geq$ 1 V vs Ag wire) results in rapid desorption of the monolayer (Figure 5.7), owing to redox reactions that occur at the gold-thiol linkages.[21] After removal of the film, the bare gold patch is no longer detectable, indicating that the mechanical scraping did not alter the structure of the metal within the resolution of this experiment.

We also investigated the effects of applied electric fields on the surface morphology.[23] Electrostatic effects have been shown[5b-c, 24] to modulate the surface coverages of charged species on gold electrodes polarized to either side of the potential of zero charge (pzc).[25] Consequently, a potential-dependent morphology change might be expected for the DNA monolayers: at potentials negative of the pzc, the duplexes would orient themselves normal to the surface in order to minimize electrostatic repulsion, whereas at potentials positive of the pzc, the duplexes would lie flat.

AFM studies performed under electrochemical control support the described model. Figure 5.8 shows the film thickness as a function of applied electrochemical potential (E$_{app}$) for a ~60% complete DNA monolayer. At potentials negative of ~ 0.45 V (vs a Ag quasi-reference electrode), the film height increases from its open-circuit value to ~ 55 Å (close to the dimension predicted for a fully extended duplex-linker conjugate oriented normal to the gold surface). As the potential is progressively scanned to more positive potentials, the thickness remains relatively constant until E$_{app}$ ~ 0.45 V, at which point the height drops dramatically to a limiting value of ~ 20 Å (the diameter of duplex DNA). Importantly, this process is chemically reversible; repeated switching (at least four complete cycles) between positive and negative applied potentials results in the formation of thin and thick monolayers, respectively.
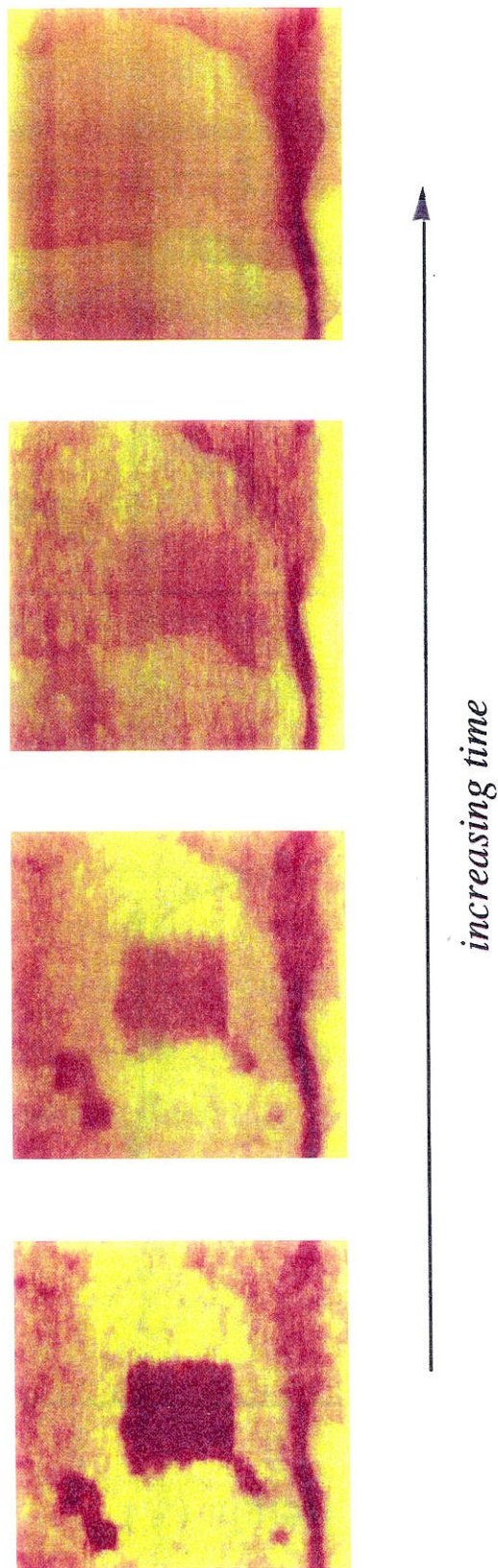
increasing time

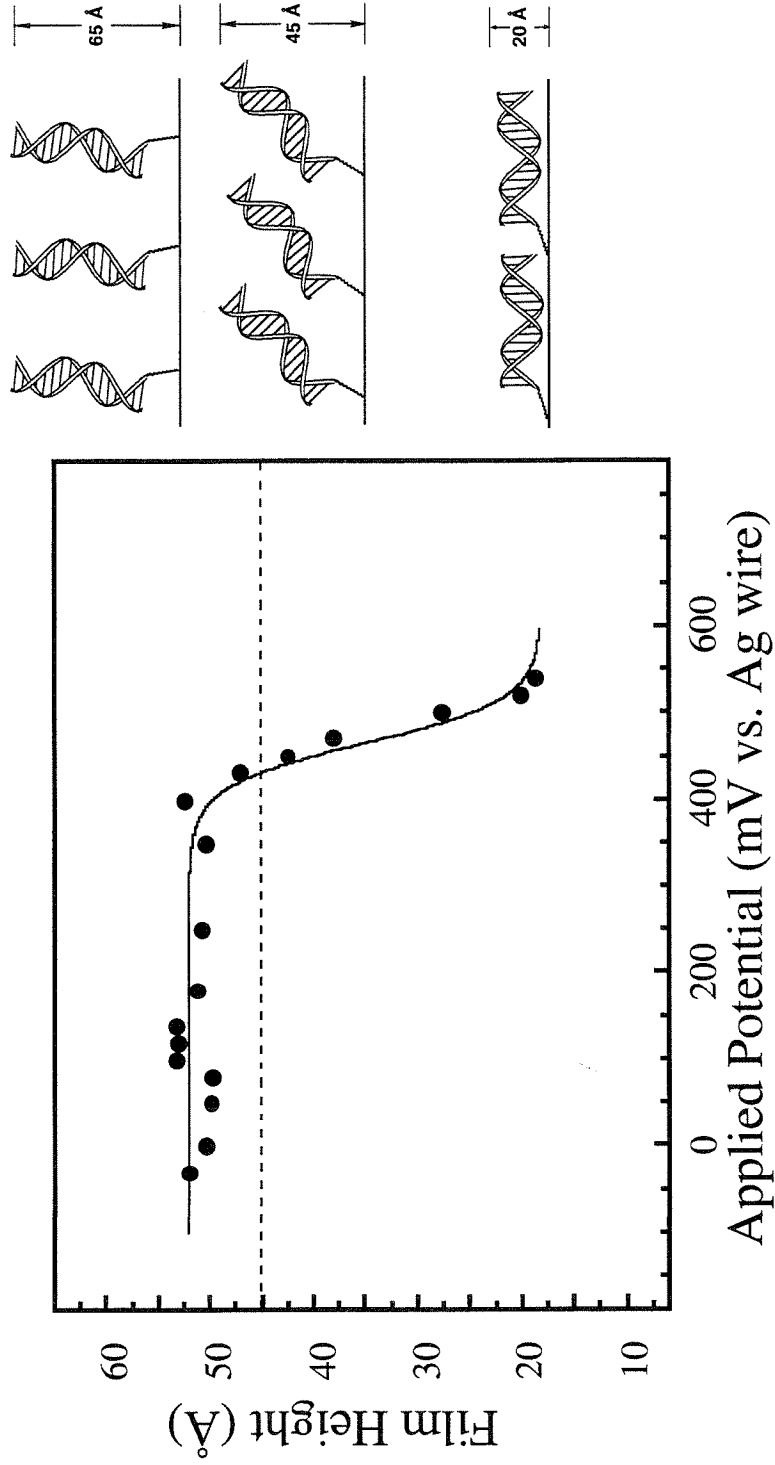**Figure 5.7** Oxidative desorption of DNA monolayer.

Figure 5.8 Electrochemical control of monolayer thickness as measured by AFM.

Because the Si_3N_4 probe tip possesses a slight negative charge in aqueous solution at pH 7,[26-28] we also considered the possible influence of surface/tip interactions on our film-height measurements. Bard and coworkers have also used AFM to measure double-layer forces between a silicon tip and bare- or chemically modified gold surfaces.[29-30] At small separations, they observe a roughly linear change in the electrostatic force between the tip and substrate over an ~800-mV range of applied potentials. For our system, we estimate that these tip/surface interactions are no more than 5 - 20 pN, or 5-10% of the total vertical force used to image our surface, and therefore do not significantly affect our results. This estimation is based on the dimensions of our silicon nitride tip (r ~ 5 - 20 nm) and the *maximum* electrostatic forces measured by Bard for a more highly charged silicon tip. We also note that the changes in DNA film height occur within a very narrow range of potentials (~75 mV), in sharp contrast to the monotonic response that characterizes electrostatic interactions between the tip and the surface. Finally, we have observed no measurable differences in film heights as a function of either pH (6.5 < pH > 7.5) or ionic strength (50 mM - 200 mM); both of these factors would be expected to affect our measurements if electrostatic forces at our tip were significant.

The (111) surface of gold is well known to undergo a reconstruction at high potentials[31] which results in changes of the gold surface on the order of ~ 3 Å. This effect cannot account for the substantial changes in depth we observe. Therefore, we conclude that the film-thickness variations result from an orientation change of the duplexes in the monolayer. Potential-dependent EC-AFM measurements on 100% complete monolayers are qualitatively similar to those shown in Figure 5.8; however, at potentials positive of ~ 0.45 V, the more densely packed monolayers reach a limiting thickness of only ~ 35 Å. As the DNA surface density in complete monolayers is too large to accommodate a horizontal orientation of the helices, it is likely that the observed 35-Å value represents the closest DNA/gold separation that is sterically possible.

5.3.5 Cyclic voltammetry of methylene blue

Having characterized the surface morphology of these films, we investigated the electrochemistry of methylene blue, a redox-active intercalator, at DNA-modified surfaces. The cyclic voltammetry of 1.0 μM MB at a DNA-modified electrode is shown in Figure 5.9. The pronounced electrochemical response at such a low concentration is strong evidence that MB binds tightly and is electronically well coupled to the modified electrode surface. The reduction potential of MB at the DNA-modified electrode is -0.25 V (vs SCE), compared to -0.22 V at bare gold. A plot of cathodic peak current (i_{pc}) versus scan rate (v) is linear (Figure 5.9), establishing that MB is strongly adsorbed to the DNA-modified surface.[25]

Qualitatively, ΔE_p (E_p = peak potential) increases as a function of scan rate (Figure 5.10), indicating measurable electron-transfer kinetics on the CV time scale.[19] For comparison, the peak separations are much less pronounced for MB adsorbed to a mercury surface, where the rate constant is reported as 1500 s^{-1};[32] at bare gold we observed essentially no peak splitting up to our fastest scan rates (50 V/s). Importantly, these measurements were all made at very low loadings of MB; thus artifacts due to lateral charge migration or ohmic (iR) drop were minimized (at the largest currents used, iR was less than 5 mV). These data indicate that the electron-transfer rate is attenuated by the intercalation of MB into the DNA monolayer, and that the rate is significantly faster at bare gold than the derivatized surface. Controls were also carried out to distinguish the binding charact-eristics of MB on different electrode surfaces. Coulometric experiments[33] on bare gold
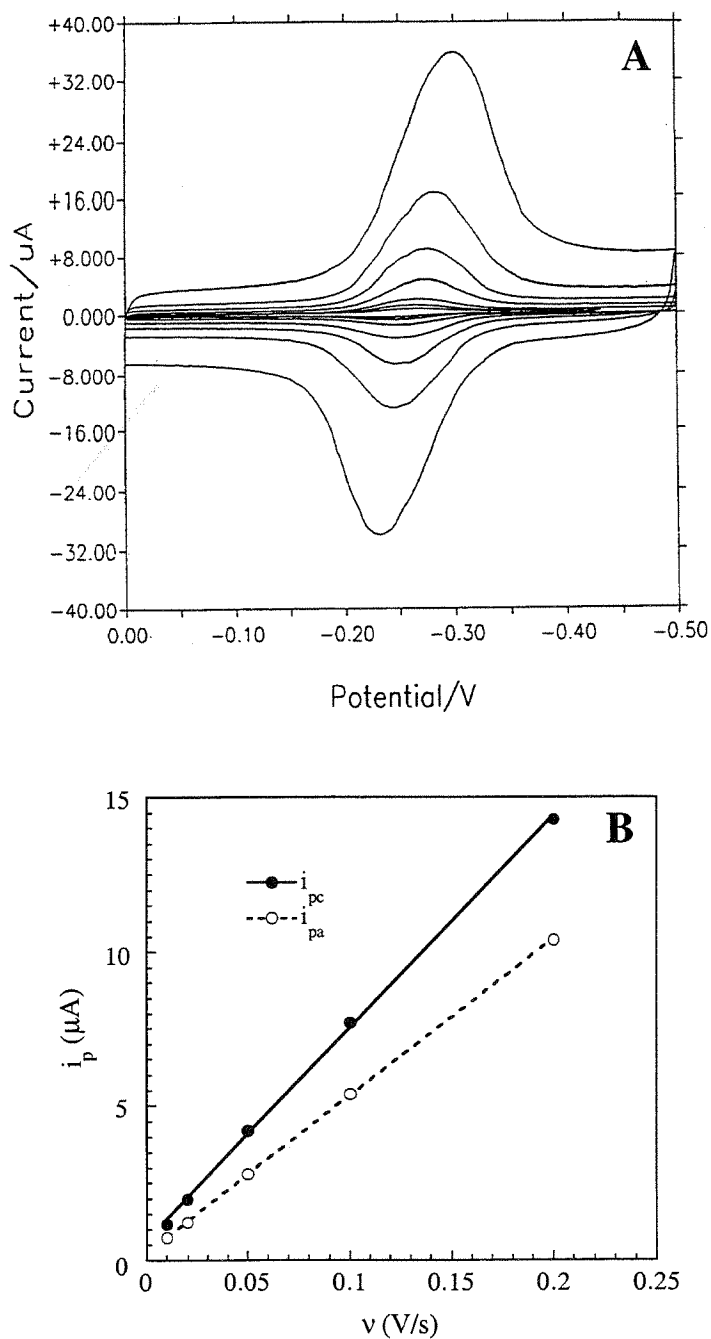
Figure 5.9 (**A**) Cyclic voltammetry of 1.0 μM MB in 50 mM phosphate

(pH 7) at a DNA-modified (SH-5'-AGTGCGAAGCTGCGT + complement)

electrode (A = 0.7 cm^2; ν = 5, 10, 20, 50, 100, 200, and 500 mV/s).

(**B**) Variation in peak current with scan rate.
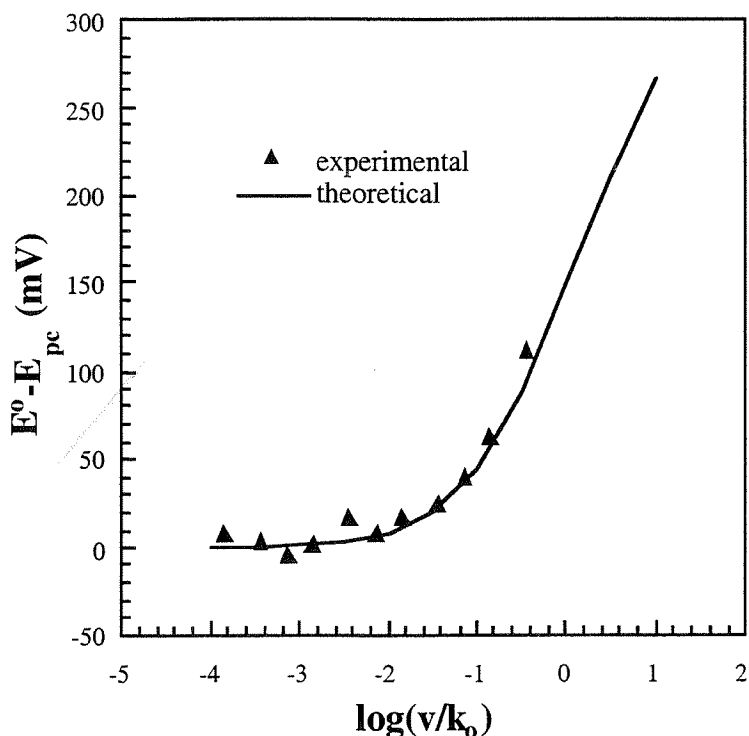
Figure 5.10 Plot of $E-E_{pc}$ vs $\log(v/k_o)$; comparison of theoretical curve (line) to data

for 0.1 μM MB at a gold electrode derivatized with SH-5'-AGTACAGTCATCGCG

hybridized to its complement (filled triangles) in 25 mM phosphate, 75 mM NaCl,

pH=7. The fit yields a value of k_o equal to 60(5) s^{-1}. We note that the formalism

described in reference 19 is based on Marcus theory and was derived for redox-active

species immobilized on electrode surfaces. In our case, the strong adsorption of MB to

DNA in both its oxidized and reduced states, and the adherence to a Langmuir isotherm

indicate that electron-transfer is not diffusion controlled. Additionally, in aqueous

solution at pH 7, MB undergoes a $2e^-$, $1H^+$ transfer *via* an ECE mechanism. Previous

work has shown that the follow-up reactions are fast, and we have assumed this to hold

for our system. Spectroelectrochemical experiments show isobestic conversion between

the oxidized and doubly reduced states. Therefore, we have treated this system

assuming a $2e^-$ transfer.

electrodes showed no evidence of adsorption of MB at sub-μM concentrations (Figure 5.11). In addition, electrodes treated with oligonucleotides lacking a thiol linker under the same conditions as those used for surface modification with the linker did not facilitate the subsequent adsorption of MB, and instead yielded irreproducible voltammetric responses that ranged from reversible to highly irreversible. Lastly, we contrast the behavior of MB at a DNA-modified electrode with that at a gold electrode modified with octadecanethiol (Figure 5.12). At the alkylthiol surface, cyclic voltammetry of MB reveals preferential binding to the surface in the reduced form, and a plot of i_{pc} versus $v^{1/2}$ is linear, consistent with diffusion of MB.

5.3.6 Electrochemical quantitation of small-molecule/DNA binding

MB reversibly binds to DNA-modified electrodes, as established by transfer experiments in which the electrochemical response of a derivatized electrode was monitored during sequential and repetitive immersions in MB and MB-free solutions. The affinity of MB for the DNA-derivatized surface was determined using chronocoulometry.[33] Figure 5.11 shows binding isotherms for MB at both DNA-modified (sequence = SH-5'-AGTACAGTCATCGCG) and bare gold electrodes. The data obtained at the DNA-modified electrode were fit according to Langmuir's model,[34] giving $K = 3.8$ (5) x 10^6 M^{-1} and Γ_{max} = 1.2 (1) x 10^{-12} mol, where K is the association constant per site and Γ_{max} is the maximum number of MB binding sites. The good fit obtained with this model confirms independent, non-cooperative binding sites for MB on the 15 base-pair duplexes. Comparable values for K and Γ_{max} were obtained for the sequence SH-5'AGTACAGTCATCAGT. It is noteworthy that the affinity of MB to a bare gold electrode is significantly lower (B, Figure 5.11).

The value of Γ_{max} corresponds to a stoichiometry of 1.4 (2) MB per 15-base pair DNA duplex based upon 75% coverage of this surface. Yet maximum stoichiometries of
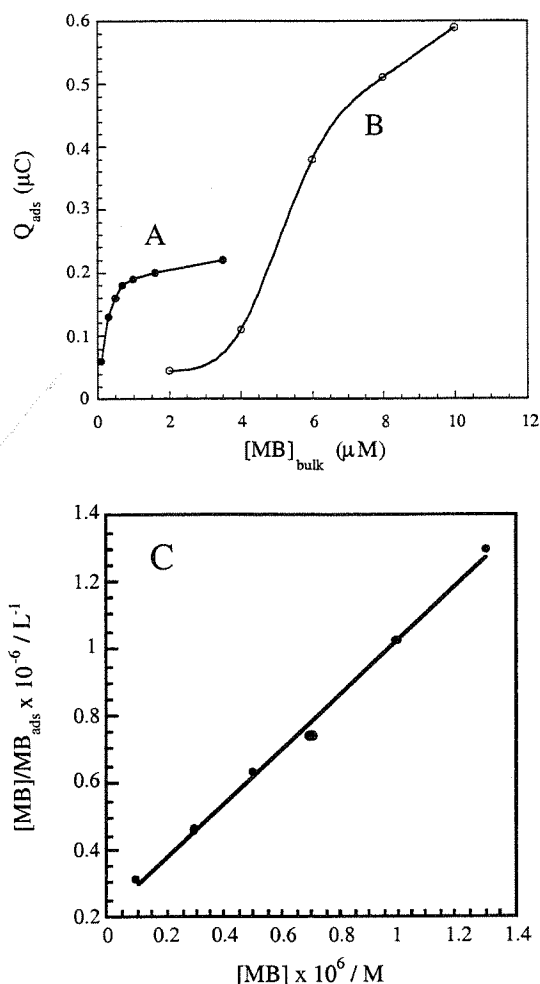
Figure 5.11 Adsorption isotherms for methylene blue (25 mM phosphate/75 mM NaCl, pH = 7) at an electrode modified with SH-5'-AGTACAGTCATCGCG hybridized to an underivatized complement (**A**) and a bare gold electrode (**B**). Surface concentrations were determined from the intercepts of Q versus $t^{1/2}$ curves obtained by chronocoulometry; A = 0.02 cm^2. (**C**) Fit of isotherm data shown in (A). Data were analyzed according to the expression:

$$[MB]/MB_{ads} = (1/\Gamma_{max})[MB] + 1/(K_o\Gamma_{max})$$

where [MB] is the concentration of methylene blue; MB_{ads} is the number of moles adsorbed on the surface; and Γ_{max} is the number of binding sites at saturation.
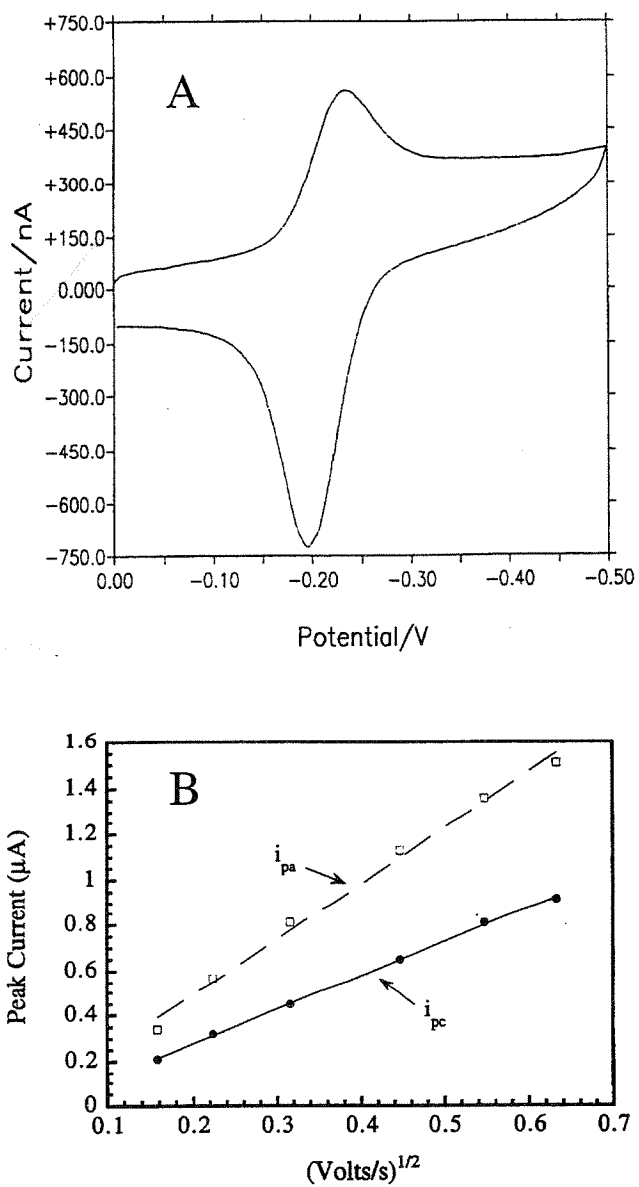
Figure 5.12 (**A**) Cyclic voltammograms of 0.1 mM MB at a octadecanethiol-
modified electrode. (**B**) Plots of i_{pc} and i_{pa} versus scan rate$^{1/2}$.

MB bound to DNA in solution are expected to approach 7 MB per 15 base-pair oligonucleotide duplex.[35] To test whether attachment of DNA to the electrode surface restricts access of MB, the electrochemistry of surfaces modified with duplexes pre-saturated with methylene blue was investigated. Figure 5.13 shows the cyclic voltammogram of 10 μM MB at an electrode derivatized with a 0.1 mM duplex solution that contained 0.6 mM MB (these conditions ensure that the DNA is almost entirely saturated, with a negligible concentration of MB free in solution). The very broad and cathodically shifted response is characteristic of interacting redox-active species. When this electrode was immersed in MB-free electrolyte, the response slowly decayed. Once the dissociation process was complete, the bulk concentration of MB was brought back to 10 μM, but a much smaller response was observed. Importantly, the signal with 10 μM MB was now identical to that observed for DNA-modified electrodes prepared in the absence of MB (i.e., not pre-saturated with MB). Integration of the currents shown in Figure 5.13 yields a 5:1 ratio, which is close to the ratio of saturation values expected for MB in solution versus that measured at the DNA-modified electrodes.

5.4   DISCUSSION

5.4.1   Adsorption of thiol-terminated DNA duplexes on gold

5'-thiol terminated DNA duplexes covalently modify gold surfaces. Importantly, duplexes that lacked the thiol linker showed little and irreproducible adsorption to gold under identical conditions. Very high surface coverages of gold by thiol-terminated DNA were confirmed by evaluating the accessibility of the modified electrode to diffusing species in solution, integrating the gold surface waves, quantitating the radioactivity of ^{32}P-labeled DNA electrodes, and examining the surface morphology via AFM. Indeed, the high density of oligonucleotides immobilized on the electrode appear to preclude an orientation of the helices where the long axis of the duplex would be parallel with the
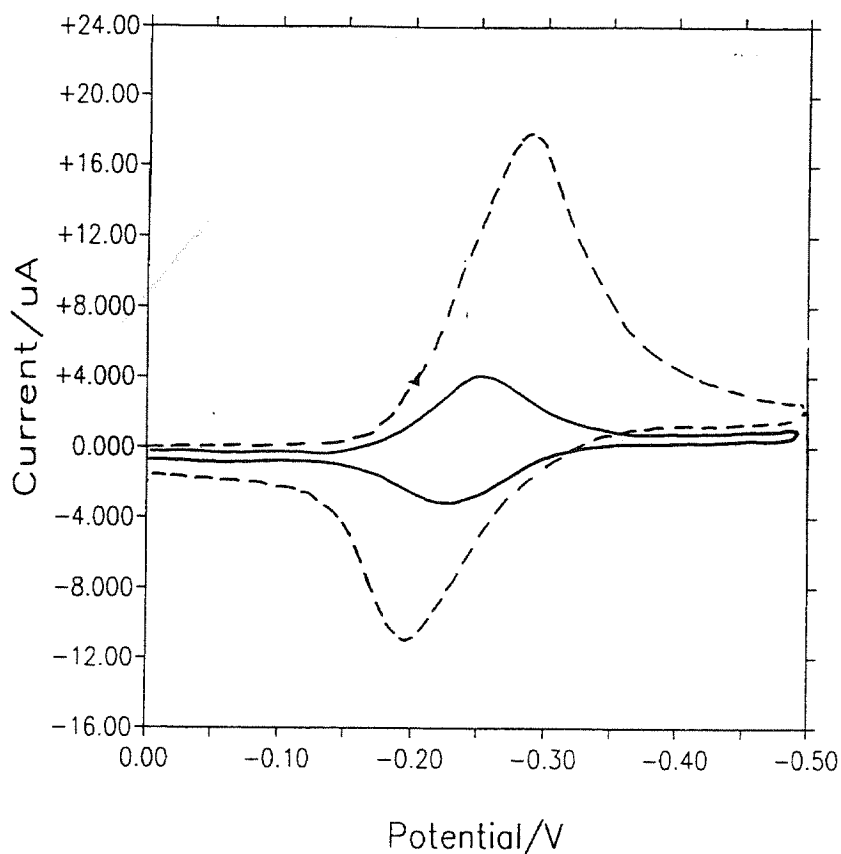
Figure 5.13 Cyclic voltammograms of 10 μM methylene blue in 50

mM phosphate (pH = 7) at a electrode (A ~ 0.7 cm^2) modified with a

solution containing 0.1 mM DNA (5' SH-AGTGCGAAGCTGCGT +

complement) and 0.6 mM MB (dotted line), and the same electrode

after buffer equilibration and subsequent restoration of the bulk

concentration to 10 μM MB (solid line).

electrode. Such a high loading of covalently bound duplexes on the surface would only be accommodated with the majority of DNA duplexes at a substantial angle from the surface. Moreover, since the duplexes are relatively short, representing 1.5 helical turns, they can also be considered quite rigid across the duplex. Ellipsometric measurements (albeit on dried samples), combined with electrochemical data, also suggest that the helices are stacked at an angle with respect to the surface. Hence the microscopic structure of the DNA-modified surface appears to involve a densely packed array of duplexes. However, to obtain information concerning the morphology of the surfaces, a more direct means to investigate the surface coverage is required.

5.4.2 Surface morphology of DNA-modifed surfaces

Atomic force microscopy has revealed interesting features of the surface morphology of these DNA films. AFM measurements demonstrated that the surfaces are densely covered with a monolayer 45 Å in thickness, indicating that the DNA helices are oriented at an angle of ~45° from the surface. We also explored the effect of applied potential on the orientation of the DNA monolayer to examine the influence of electrostatic forces on the monolayer. In these experiments (where the surface was modified with lower coverages) we found that when the electrode was positively charged, the polyanionic DNA appeared to be attracted to the metal surface, thereby compressing the monolayer thickness (~ 20 Å). In contrast, when a negative charge was induced, the monolayer thickness increased significantly (~ 50 Å). As these changes are reversible, this system effectively constitutes an electrochemical nanoscale "switch." The ability to modulate the thickness of a monolayer using only small changes in potential may provide a unique design feature for the construction of sensors and nanoscale electronic devices.

5.4.3 Electrochemistry of intercalated methylene blue

Micromolar solutions of MB yield well defined voltammetric responses at electrodes modified with thiol-derivatized DNA (Figure 5.9). The reduction potential for intercalated MB is cathodically shifted (-30 mV) from the value in aqueous solution. For comparison, the reduction potentials for MB in dimethylformamide, acetonitrile, and acetone are, respectively, -0.50, -0.52, and -0.48 V versus SCE (corrected for the junction potential, using ferrocenium/ferrocene as an internal standard). Wider variations in reduction potentials are observed in aqueous solution as a function of pH since the reduction is coupled to proton transfer. At low concentrations of MB (< 0.1 μM), the cyclic voltammograms exhibit full-widths-at-half-heights of ~ 55 mV. This value is slightly larger than the predicted 45 mV for a $2e^-$ Nerstian system. Starting at low loadings of MB, the voltammograms broaden until saturation in binding of MB to DNA is reached; the broadest cyclic voltammograms are observed at electrodes presaturated with MB. In each case, the cathodic and anodic peak splitting approaches zero at slow scan rates. The broadening (which depends directly upon loading of MB) therefore indicates a distribution of binding environments with slightly different reduction potentials.

Importantly, the binding affinity of MB for the DNA-modified electrode (SH-5'-AGTACAGTCATCGCG; K=3.8 x 10^6 M^{-1}) is comparable to that found for DNA in solution (K=10^6 M^{-1} in 50 mM NaCl).[36] A preference for GC-rich DNA has been noted in some studies; we do not observe a significant change in binding affinity with an electrode modified with the sequence SH-5'-AGTACAGTCATCAGT 3' which does not contain adjacent GC base pairs near its 3'-terminus.

While the equilibrium binding constants of MB to our DNA-modified electrodes are similar to those found for DNA in solution, the saturation values are not. Our observed Γ_{max} corresponds to roughly one MB per 15 base-pair duplex. This stoichiometry is significantly less than that of the MB:base-pair stoichiometry found in solution,[36] where MB may occupy many (>5) neighbor excluded[35] sites on a 15-mer duplex. Indeed, if the oligonucleotides are

presaturated with MB before attachment to the electrode surface, loadings of MB closer to that predicted by neighbor exclusion are detected electrochemically. However, once this presaturating MB dissociates from the surface (after immersing the electrode in pure buffer), subsequent binding of MB to the electrode surface is again restricted. These observations fully support the notion that the DNA helices on the gold surface are tightly packed, necessitating that MB binds at sites close to the DNA/solvent interface. Owing to dense DNA packing and to the high affinity of MB for DNA, diffusion down into the DNA monolayer may be severely inhibited.

Although available data suggest that MB binds to DNA that is densely packed at an angle from the electrode surface, we also considered the possibility that the DNA is lying flat on the electrode. If this were the case, we might expect the CV response to more closely resemble that of MB adsorbed directly onto gold; the significant difference in ΔE_p as a function of scan rate strongly argues against this possibility. Moreover, if a flat orientation were more favorable, we would expect to see similar behavior when the surfaces were modified with DNA lacking the linker. Instead, in experiments with DNA non-covalently associated with the electrode, we observe only very weak and irreproducible signals for MB.

One might also consider that the DNA merely facilitates delivery of MB to the gold surface. However, our adsorption isotherms clearly indicate that MB binds more strongly to DNA-modified electrodes than to bare gold. Therefore, appreciable dissociation of MB from DNA to the gold surface is highly unlikely. In this light, it is interesting that the ratio of the maximum surface coverages for MB and thiol-modified DNA on gold (18×10^{-11} and 6×10^{-11} mol/cm^2, respectively) corresponds roughly to the ratio of cross-sectional surface areas for methylene blue (1 nm^2)[32] and double stranded DNA (3 nm^2). Additionally, the electrochemistry of MB at an electrode modified with octadecanethiol provides further evidence against a channeling mechanism. At the alkylthiol surface, MB exhibits diffusional behavior and appears to bind more strongly in the reduced form. This is in stark contrast to the electrochemical response of MB at a DNA-modified electrode. The strength of the

interaction between DNA and methylene blue afforded by intercalation makes it much more energetically favorable for the intercalator to remain bound rather than to diffuse to the electrode.

5.4.4   Electron-transfer kinetics for the reduction of MB through a DNA film

These data may therefore be taken together in developing a model that describes the binding of MB to the DNA-derivatized surface. In this model (Figure 5.14), closely packed DNA helices are tethered to the gold surface via thiol linkages. Solution-borne MB binds reversibly to accessible duplex sites on the derivatized electrode, with an affinity comparable to that for duplex DNA in solution. Since the duplexes are tightly packed on the surface, however, access appears to be restricted primarily to those sites near the bulk solution. Our AFM results indicate that the helices are oriented at a substantial angle with respect to the electrode surface at negative potentials, hence the electron-transfer reactions of MB bound within the film would proceed *through* the DNA base stack. MB is therefore separated from the electrode by both the σ-system of the aliphatic linker (~ 15 Å) and the π-stacked base pairs (~ 50 Å), which lead to the intercalation site.

If this model is correct, our results lead to the suggestion that electron transfer through the double helix is remarkably efficient. For example, applying a decay constant (β) characteristic of σ-only arrays (1.0 Å^{-1}),[37] we would expect the electron-transfer rate to drop by more than 22 orders of magnitude through the π-stack alone. The almost reversible response observed at scan rates up to 500 mV/s for MB at DNA-modified gold rules out a rate constant of this small magnitude.

We stress, however, that if MB intercalates into sites evenly dispersed throughout the modified surface, the observed electrochemical response may not uniquely support long-range electron transfer through DNA. Specifically, if the decay rate of electron transfer

Figure 5.14 Schematic illustration depicting MB bound to 15-base-pair oligonucleotides attached to a gold surface. The lengths of the DNA helices and alkylthiol chains are shown to relative scale. Surfaces are realistically more heterogeneous than depicted.

through DNA were steep enough, in principle only MB bound at the first base steps from the aliphatic linker would give an electrochemical response. In this scenario, the observed rate of electron transfer would be attenuated essentially only by tunneling through the hexylthiol tether, as the rates of electron transfer to MBs intercalated further out would be too slow to measure. Although we cannot completely rule out this possibility, the electrochemical response of MB at pre-saturated DNA-modified electrodes (Figure 5.12) seems to indicate that intercalators bound throughout the double helix can contribute to the observed currents. Moreover, given a relatively large β, if the intercalators were distributed throughout binding sites along the entire helices, we would predict much less reversible voltammograms, as a wide range of rate constants would contribute to the overall currents.

Therefore, from the data now available, it appears that as long as the MB is intercalated into the DNA-modified electrodes (be it near the solvent-exposed terminus of the adsorbed DNA, or dispersed throughout the double helix), electron transfer over long distances through DNA is exceptionally efficient. Studies employing well-defined systems where the location of the intercalator is precisely determined will be required to assess quantitatively the electronic coupling mediated by the π-stack of DNA.

DNA-derivatized electrodes offer a valuable tool to examine the redox behavior of species within the DNA environment. Electrochemistry on DNA-modified surfaces provides a convenient method to determine equilibrium binding parameters of redox-active species and may represent an alternative means to investigate the dynamics of DNA-mediated electron-transfer processes.

5.5 REFERENCES

1. (a) Ullman, A. *An Introduction to Ultrathin Organic Films: From Langmuir-Blodgett to Self-Assembly,* Academic Press, Boston, **1991**. (b) Folkers, J.P.; Zerkowski, J.A.; Laibinis, P.E.; Seto, C.T.; Whitesides, G.M. *ACS Symp. Sers.* **1992**, *499*, 10. (c) Kumar, A.; Abbott, N.L.; Kim, E.; Biebuyck, H.A.; Whitesides, G.M. *Acc. Chem. Res.* **1995**, *28*, 219.

2. (a) Chidsey, C.E.D.; Bertozzi, C.R.; Putvinski, T.M.; Mujsce, A.M. *J. Am. Chem. Soc.* **1990**, *112*, 4301. (b) Finklea, H.O.; Hanshew, D.D. *J. Am. Chem. Soc.* **1992**, *114*, 3173. (c) Smalley, J.F.; Feldberg, S.W.; Chidsey, C.E.D.; Linford, M.R.; Newton, M.D.; Liu, Y. *J. Phys. Chem.* **1995**, *99*, 13141.

3. Bowler, B.E.; Raphael, A.L.; Gray, H.B. *Prog. Inorg. Chem.* **1990**, *38*, 259

4. Kelley, S.O.; Barton, J.K.; Jackson, N.M.; Hill, M.G. *Bioconj. Chem.* **1997**, *8*, 31.

5. (a) Cricenti, A.; Selci, S.; Felicic, A.C.; Generosi, R.; Gori, E.; Djaczenko, W.; Chiarotti, G. *Science* **1989**, *244*, 1226. (b) DeRose, J.A.; Lindsay, S.M.; Nagahara, L.A.; Oden, P.I.; Thundat, T.; Rill, R. *J. Vac. Sci. Technol. B* **1991**, *9*, 1166. (c) Lindsay, S.M.; Tao, N.J.; DeRose, J.A.; Oden, P.I.; Lyubchenko, Y.L.; Harrington, R.E.; Shlyakhtenko, L. *Biophys. J.* **1992**, *61*, 1570. (d) D. Rekesh, Y. Lyubchenko, L.S. Shlyakhtenko, S.M. Lindsay, *Biophys. J.* **1996**, *71*, 1079 (e) Mou, J.; Czajkowsky, J.; Zhang, Y.; Shao, Z. *FEBS Lett.* **1995**, 371, 279. (f) Allen, M.J.; Bradbury, E.M.; Balhorn, R. *Nucl. Acids Res.* **1997**, *25*, 1997.

6. (a) Millan, K.M.; Mikkelsen, S.R. *Anal. Chem.* **1993**, *65*, 2317-2323. (b) Hashimoto, K.; Ito, K.; Ishimori, Y *Anal. Chem.* **1994**, *66*, 3830. (c) Wang, J.; Cai, X.; Rivas, G.; Shiraishi, H.; Farias, P.A.M.; Dontha, N. *Anal. Chem.* **1996**, *68*, 2629. (d) Mikkelsen, S.R. *Electroanalysis* **1996**, *8*, 15. (e) Korriyoussoufi, H.; Garnier, F.; Srivastava, P.; Godillot, P.; Yassar, A. *J. Am. Chem. Soc.* **1997**, *119*, 7388. (f) Herne, T.; Tarlov, M.J. *J. Am. Chem. Soc.* **1997**, *119*, 8916. (g)

Souteyrand, E.; Cloarec, J.P.; Martin, J.R.; Wilson, C.; Lawrence, I.; Mikkelsen, S.; Lawrence, M.F. *J. Phys. Chem. B.* **1997**, *15*, 2980.

7. Napier, M.E.; Loomis, C.R.; Sistare, M.F.; Kim, J.; Eckhardt, A.E.; Thorp, H.H. *Bioconj. Chem.* **1997**, *8*, 906.

8. (a) Xu, X.-H; Yang, H.C.; Mallouk, T.E.; Bard, A.J. *J. Am. Chem. Soc.* **1994**, *116*, 8386. (b) Xu, X.-H; Bard, A.J. *J. Am. Chem. Soc.* **1995**, *117*, 2627.

9. Cheng, C.C.; Goll, J.G.; Neyhart, G.A.; Welch, T.W.; Singh, P.; Thorp, H.H. *J. Am. Chem. Soc.* **1995**, *117*, 2970.

10. Okahata, Y.; Matsunobu, Y.; Ijiro, K.; Mukae, M.; Murakami, A.; Makino, K. *J. Am. Chem. Soc.* **1992**, *114*, 8300.

11. (a) Carter, M.T.; Rodriguez, M.; Bard, A.J. *J. Am. Chem. Soc.* **1989**, *111*, 8901.
(b) Rodriguez, M.; Bard, A.J. *Anal. Chem.* **1990**, *62*, 2658-2662.
(c) Carter, M.T.; Bard, A.J. *Bioconjugate Chem.* **1990**, *1*, 257.

12. (a) Welch, T.W.; Corbett, A.H.; Thorp, H.H. *J. Phys. Chem.* **1995**, *99*, 11757.
(b) Kelly, J.M.; Lyons, M.E.G.; Van Der Putten, W.J.M. In *Electrochemistry, Sensors and Analysis*; Smyth, M.R.; Vos, J.G., Ed.; Elsevier: Amsterdam, 1986; pp 205-213. (c) Molinier-Jumel, C.; Malfoy, B.; Raymond, J.; Reynaud, J.A.; Aubel-Sadron, G. *Biochem. Biophys. Res. Comm.* **1978**, *84*, 441. (d) Berg, H.; Horn, G.; Luthardt, U.; Ihn, W. *Bioelectrochem. Bioenerg.* **1981**, *8,* 537. (e) Plambeck, J.; Lown, J.W. *J. Electrochem. Soc.* **1984**, *131*, 2556.

13. (a) Maeda, M.; Mitsuhashi, Y.; Nakano, K.; Takagi, M *Analyt. Sci.* **1992**, *8*, 83.
(b) Maeda, M.; Nakano, K.; Uchida, S.; Takagi, M. *Chem. Lett.* **1994**, 1805.

14. Beaucage, S.L.; Caruthers, M.H. *Tetrahedron Lett.* **1981**, *22,* 1859.

15. Wachter, L.; Jablonski, J.A.; Ramachandran, K.L. *Nucl. Acids Res.* **1986**, *14*, 7985.

16. Harrison, J.G.; Balasubramanian, S. *Bioorg. Med. Chem. Lett.* **1997**, *7*, 1041.

17. Riddles, P.W.; Blakeley, R.L.; Zerner, B. *Anal. Biochem.* **1979**, *94*, 75.

18. (a) Nahir, T.M.; Clark, R.A.; Bowden, E.F. *Anal. Chem.* **1994**, *66*, 2595. (b) Weber, K.; Creager, S.E. *Anal. Chem.* **1994**, *66*, 3164. (c) Tender, L.; Carter, M. T.; Murray, R. W. *Anal. Chem.* **1994**, *66*, 3173.

19. Laviron, E. *J. Electroanal. Chem.* **1975**, *63*, 254.

20. Sabatini, E.; Rubinstein, I.; Maoz, R.; Sagiv, J. *J. Electroanal. Chem.* **1987**, *219*, 365; Finklea, H.O.; Snider, D.A.; Fedyk, J. *Langmuir* **1990**, *6*, 371.

21. Widrig, C.A.; Chung, C.; Porter, M.D. *J. Electroanal. Chem.* **1991**, *310*, 335.

22. (a) Bustamante, C.; Keller, D. *Physics Today* **1995**, *48*, 32. (b) Hamers, R.J. *J. Phys. Chem.* **1996**, *100*, 13103.

23. (a) Ye, S.; Sato, Y.; Uosaki, K. *Langmuir* **1997**, *13*, 3157. (b) Cunha, F.; Tao, N.J.; Wang, X.W.; Jin, Q.; Duong, B.; D'Agnese, J. *Langmuir* **1996**, *12*, 6410.

24. Bretz, R.L.; Abruna, H.D. *J. Electroanal. Chem.* **1995**, *388*, 123.

25. Bard, A.J.; Faulkner, L.R. *Electrochemical Methods.* Wiley and Sons, New York. 1980.

26. Tsukruk, V.V.; Bliznyuk, V.N. *Langmuir* **1998**, *14*, 446.

27. Rotsch, C.; Radmacher, M. *Langmuir* **1997**, *13*, 2825.

28. Cjazkowski, D.; Allen, M.J.; Elings, V.B.; Shao, Z. *Ultramicroscopy*, in press.

29. Hillier, A.C.; Kim, S.; Bard, A.J. *J. Phys. Chem.* **1996**, *100*, 18808.

30. Hu, K.; Bard, A.J. *Langmuir,* **1997**, *13*, 5114.

31. Gewirth, A.A.; Niece, B.K. *Chem. Rev.* **1997**, *97*, 1129.

32. (a) Svetlicic, V.; Tomaic, J.; Zutic, V.; Chevalet, J. *J. Electroanal. Chem.* **1983**, *146*, 71. (b) Zutic, V.; Svetlicic, V.; Lovric, M.; Ruzic, I.; Chevalet, J. *J. Electroanal. Chem.* **1984**, *177*, 253. (c) Svetlicic, V.; Clavilier, J.; Zutic, V.; Chevalet, J. *J. Electroanal. Chem.* **1990**, *312*, 205. (d) Ju, H.; Zhou, J.; Cai, C.; Chen, H. *Electroanalysis* **1995**, *7*, 1165.

33. Christie, J.H.; Anson, F.C.; Lauer, G.; Osteryoung, R.A. *Anal. Chem.* **1963**, *35*, 1979.

34. Connors, K.A. *Binding Constants: The Measurement of Molecular Complex Stability*, Wiley-Interscience, New York, NY, **1987**.

35. Crothers, D.M. *Biopolymers* **1968**, *6*, 575.

36. (a) Bradley, D.F.; Stellwagen, N.C.; O'Konski, C.T.; Paulson, C.M. *Biopolymers* **1972**, *11*, 645. (b) Muller, W.; Crothers, D.M.; *Eur. J. Biochem.* **1975**, *54*, 267. (c) Nordén, B.; Tjerneld, F. *Bioploymers* **1982**, *21*, 1713. (d) Tuite, E.; Nordén, B. *J. Am. Chem. Soc.* **1994**, *116*, 7548. (e) Tuite, E.; Kelly, J.M.; *Biopolymers* **1995**, *35*, 419.

37. Marcus, R.A.; Sutin, N. *Biochim. Biophys. Acta* **1985**, *811*, 265.

Chapter 6

Single Base Mismatch Detection
Based on Long-Range
Charge Transduction Through DNA[‡]

6.1 INTRODUCTION

DNA sensors capable of detecting single-base mismatches are required for routine screening of genetic mutation and disease.[1] Conventional sequencing methods for mismatch detection involve expensive and time-consuming separations, rendering them impractical for diagnostic applications. More recently, sophisticated techniques that assay the hybridization of DNA target sequences to arrays of immobilized single-stranded oligonucleotides have been developed for highly parallel genomic sequencing and the detection of mutations.[2] As these techniques monitor the extent of hybridization between complementary target and probe sequences (typically employing fluorescent or radioactive reporters), their inherent sensitivity for point mutation detection depends ultimately on the small changes in base-pairing energy caused by single-base mismatches.

An alternative approach to mismatch detection based on charge transduction through DNA films can be envisioned (Figure 6.1). As described in Chapters 2, 3, and 4, long-range electron transfer between reactants intercalated into the base stack of DNA has been observed in a variety of photochemical systems.[3-7] The efficiencies of these processes are extremely sensitive to the coupling of the reactants into the base stack (thus the need for intercalating reactants), and depend upon the integrity of the base stack itself;[3,5,7] perturbations caused by mismatches or bulges greatly diminish the yields of DNA-mediated charge transport. While single-base mismatches may cause only subtle changes in duplex stability and structure, they induce significant perturbations in the electronic properties of the base stack. This inherent sensitivity to base mismatches may therefore be exploited in the design of new DNA sensors. However, a system useful for biosensing applications would utilize a reaction occurring at a solid surface, allowing a library of immobilized sequences to be addressed simultaneously.
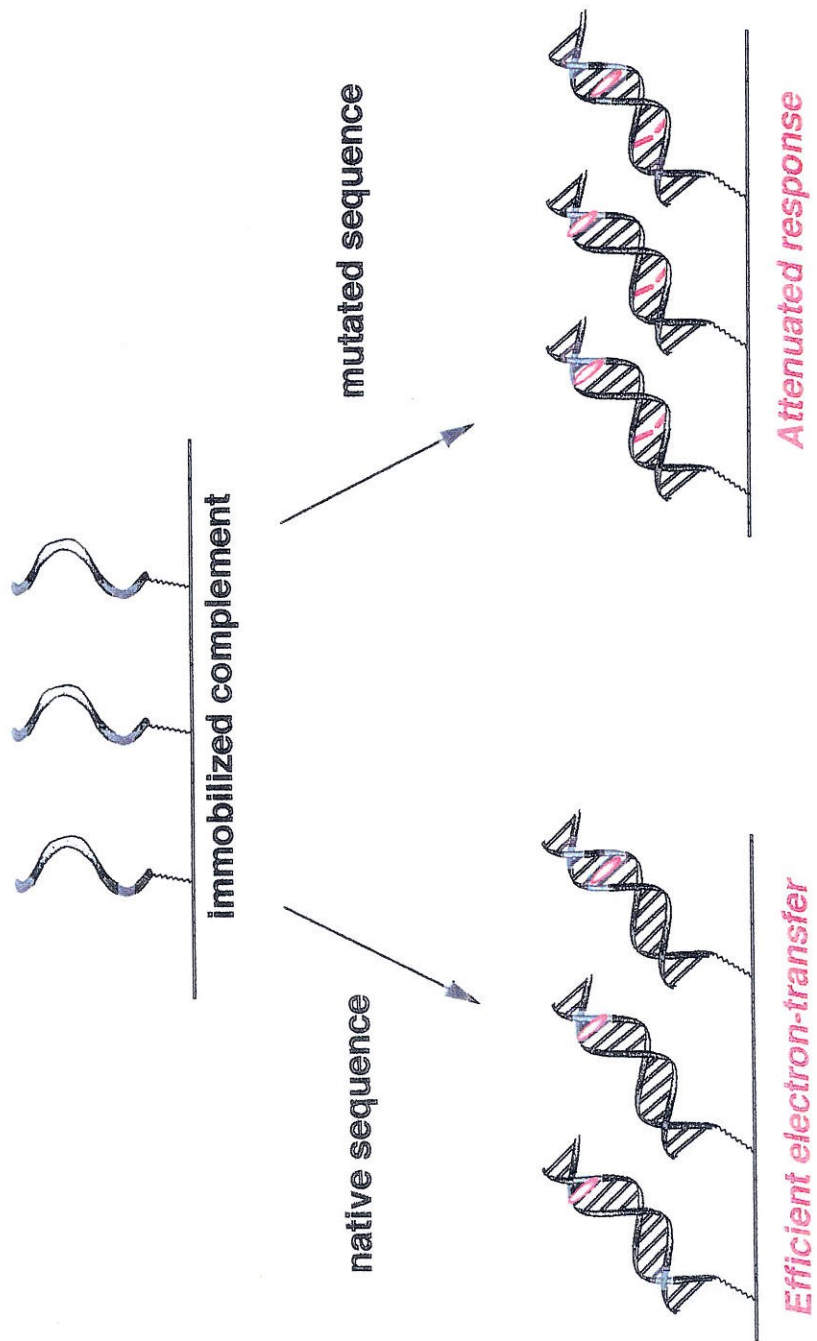
Figure 6.1 Strategy for detection of point mutations based on electron transfer through DNA films.

Hence, given the need for DNA sensors capable of detecting point mutations within DNA, and our interest in probing DNA-mediated electron transfer reactions using new methodologies, we further investigated the characteristics of charge transport through DNA films. In the previous chapter, techniques for fabricating and characterizing DNA films were described. We observed efficient electron transfer between the electrode and redox-active intercalators non-covalently bound to the helices.[8] Because the exact location of the intercalators within the duplexes was not fixed, however, these studies did not allow a systematic evaluation of the effect of distance on the rate of electron transfer through DNA. To study systematically the efficiency of electron transfer through the double helix using electrochemical methods, and to investigate the possibility of detecting base mismatches using this system, we have crosslinked daunomycin, a redox-active intercalator, to immobilized DNA duplexes. We investigated the electrochemistry of this intercalator at different separations from the gold surface, and probed the efficiency of electron transfer in the absence and presence of an intervening mismatch. The studies described in this chapter therefore provide further evidence supporting the notion that electron transfer can be facile through the well-stacked base pairs but is diminished with perturbations in π-stacking. On this basis, a versatile sensor capable of detecting DNA mismatches was developed.
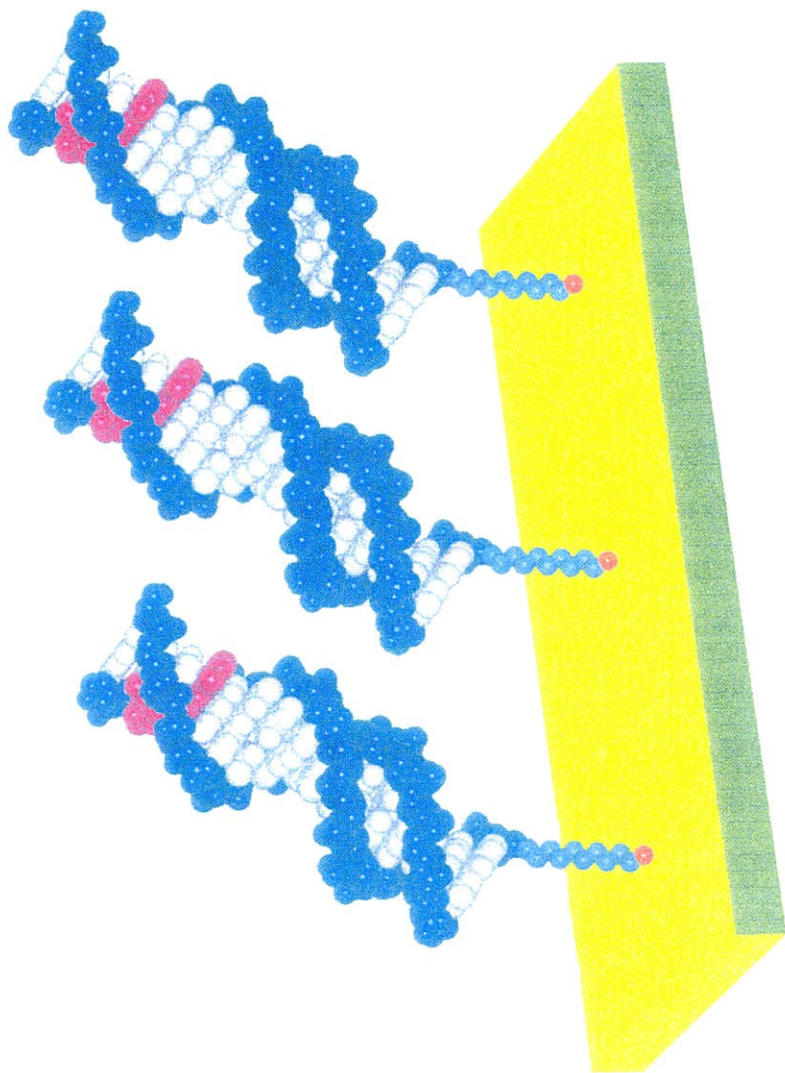
Figure 6.2 Schematic illustration of a gold surface modified with 15 base-pair thiol-modified duplexes, including the daunomycin-guanine crosslink (shown in red) incorporated into the DNA monolayer.

6.2 EXPERIMENTAL SECTION

Fabrication of DNA-Modified Surfaces. Thiol-modified oligonucleotides were prepared as described in the previous chapter. Thiol-terminated duplexes (0.1 mM) containing an adjacent pair of guanines were hybridized, incubated with 0.2% formaldehyde and 0.2 mM DM in 5 mM phosphate, 50 mM NaCl, pH 7 for 1 hour, and phenol extracted to remove excess daunomycin. Subsequently, samples were subjected to gel filtration chromatography and deposited on gold surfaces for 12-24 hours. DM-modified duplexes were characterized using mass spectroscopy and absorbance spectroscopy. For example, a duplex (SH-$(CH_2)CONH(CH_2)_6NHCO_2$-5'-ATCCTACTCATGGAC with its inosine complement) modified with daunomycin was analyzed by MALDI-TOF spectrometry. Mass-to-charge ratios (found/(calc)) of 5284/(5282) (DM + SH strand), 4541/(4540) (complement), and 4742/(4742) (SH strand) were detected. These values correspond to the calculated masses for fragments expected from this duplex. UV-visible absorption spectroscopy also revealed a 1:1 duplex/daunomycin stoichiometry based upon comparison of the duplex absorbance at 260 nm and the absorbance of intercalated daunomycin at 480 nm ($\varepsilon = 7.5 \times 10^3$ M^{-1} cm^{-1}). In the presence of 100 mM phosphate, 100 mM $MgCl_2$, and at pH 7, thermal denaturation studies of 5 mM duplexes (monitored by absorbance at 260 nm) revealed melting temperatures of 48 and 50°C for the native and daunomycin-crosslinked duplexes, respectively. A similar melting profile was obtained by monitoring hypochromicity at 482 nm for the daunomycin duplex.

Before deposition, electrode surfaces were prepared by mechanical polishing with alumina, sonication, and oxidative etching in acid solution. The surface structures of the DM-labeled films were determined using techniques in atomic force microscopy (AFM) as previously described.[9] To assess routinely the surface coverage of DM-derivatized DNA on gold, the electrochemical response of $Fe(CN)_6^{4-}$ (2 mM) was monitored. This negatively charged ion is repelled from the modified-electrode surface

by the polyanionic DNA, and exhibits essentially no response when the surface is well covered. While not a direct measure of surface coverage, this technique allows the convenient assay of individual electrodes for adequate modification. Significant fluctuations in the surface coverages of daunomycin-modified duplexes were observed. Therefore, only electrodes which exhibited both large integrated currents for the reduction of crosslinked daunomycin *and* an attenuated responses for the oxidation of ferrocyanide in solution were studied.

Electrochemical measurements: Cyclic voltammetry was carried out on 0.02 cm^2 polycrystalline gold electrodes using a Bioanalytical Systems (BAS) Model CV-50W electrochemical analyzer at (20 ± 2°C in 100 mM phosphate buffer, pH 7). A normal three-electrode configuration consisting of a modified gold-disk working electrode, a saturated calomel reference electrode (SCE, Fisher Scientific), and a platinum wire auxiliary electrode was used. The working compartment of the electrochemical cell was separated from the reference compartment by a modified Luggin capillary. Potentials are reported versus SCE. Heterogeneous rate constants were determined as previously reported.[8,10] Measurements were also carried out on modified gold(111) surfaces prepared either by vapor deposition of gold onto mica, or by melting the tip of a gold wire into a small (~ 2 mm in diameter) ball using a hydrogen flame. Other than a slight narrowing of the voltammetric peak widths (~ 5 – 10 mV), the signals were very similar for both polycrystalline and Au(111) electrodes.

6.3 RESULTS AND DISCUSSION

6.3.1 Electrochemistry of daunomycin crosslinked to DNA monolayers

To investigate charge transduction through DNA films, we site-specifically incorporated a redox-active intercalator, daunomycin (DM),[11] into the immobilized duplexes (Figure 6.3). DM undergoes a reversible reduction[12] within the potential window of the monolayers,[8] and covalent adducts of intercalated DM crosslinked to the 2-amino group of guanine[13] have been crystallographically characterized within duplex DNA.[14] We were therefore able to construct a series of oligonucleotides primarily containing A-T or inosine (I)-C pairs with discrete guanine binding sites to which DM was crosslinked. Moving the guanine site along the duplex resulted in a systematic variation of the through-helix DM/gold separation, and allowed an investigation of the effect of distance on the dynamics of charge transport through the monolayers (Figure 6.3). Based on molecular modeling, if DM is bound at the end of the duplex closest to the electrode, the through-helix DM-electrode separation is > 10 Å; if the intercalator is crosslinked to the end of the duplex farthest from the electrode, the DM-electrode separation is > 35 Å. Modified duplexes were characterized by mass spectrometry, ultraviolet/visible absorption spectroscopy, and thermal denaturation experiments, all of which were consistent with a 1:1 DM-duplex stoichiometry.

The DM-modified duplexes readily form self-assembled monolayers on gold. AFM studies of modified films reveal densely packed monolayers with heights greater than 45 Å at open circuit. Cyclic voltammograms of these surfaces show the reduction of DM at -0.65 V versus SCE (Figure 6.4). These films are extremely stable and exhibit responses characteristic of surface-bound species (*e.g.,* linear plots of peak current versus scan rate).[15]
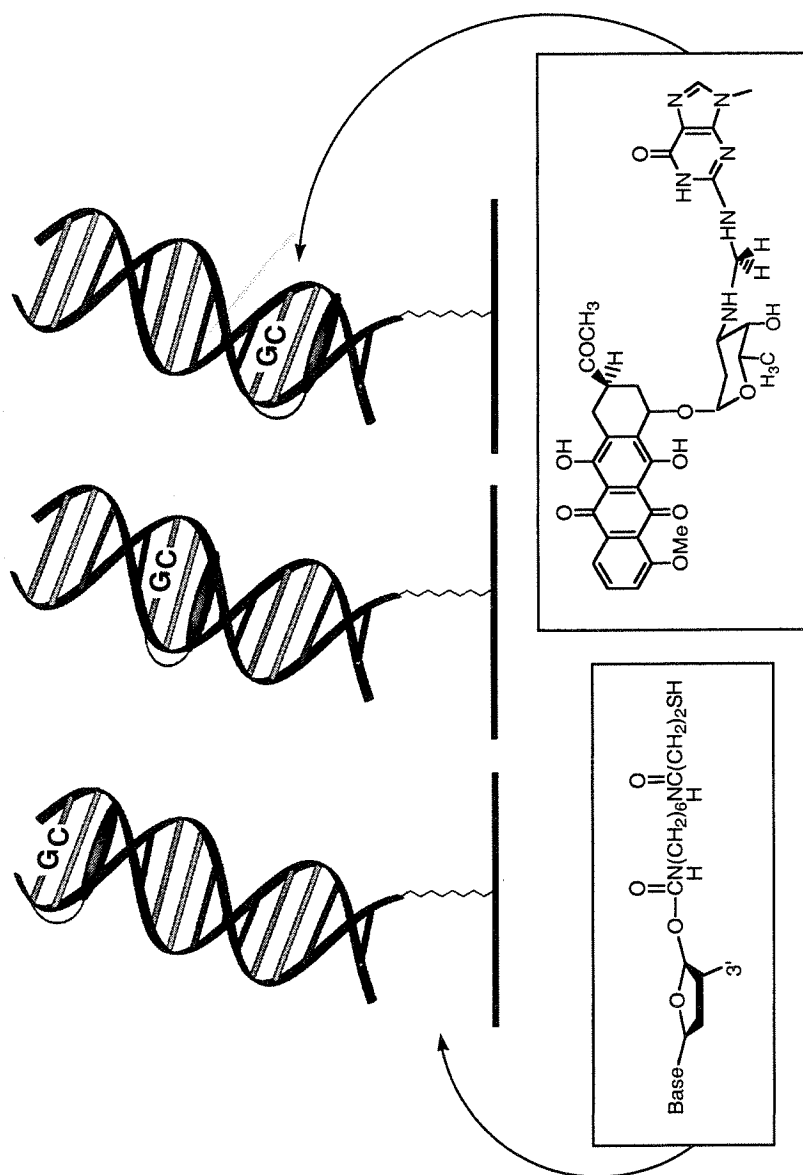
Figure 6.3 Schematic illustration of DNA duplexes used for study of distance-dependent reduction of daunomycin.

Integration of the electrochemical response yields a surface coverage (Γ) of electroactive daunomycin of $7.5(7) \times 10^{-11}$ mol/cm^2, a value in good agreement with the coverages of 15 base-pair duplexes previously measured via ^{32}P labeling.[8] Based the cross-sectional area of DNA (~ 3 nm^2) and the geometrical area of the gold electrodes (0.02 cm^2), the maximum surface coverage of DNA is calculated as $\sim 6 \times 10^{-11}$ mol/cm^2. The daunomycin value appears to exceed slightly the theoretical Γ for DNA, and likely results from additional electrode surface roughness.

Given a 1:1 stoichiometry of crosslinked daunomycin to DNA, these data indicate that all of the bound DM is electrochemically reduced. Doping these films with increasing percentages of DM-free duplexes resulted in a linear decrease in the observed electrochemical signals (as determined from coulometric assays), consistent with each of the bound intercalators being electrochemically active (Figure 6.4, inset).

6.3.2 Distance dependence of electron transfer through DNA films

Remarkably, efficient reduction of DM was observed regardless of its position along the 15 base-pair sequence (Figure 6.5). Not only were the intensities of the daunomycin signals the same for each of the duplexes studied, but the characteristic splittings between the cathodic and anodic waves as a function of scan rate were essentially invariant throughout the entire series (Figure 6.6). Clearly within the resolution of this experiment, increasing the through-helix DM/gold separation does not substantially affect the rate of electron-transfer.

If the electron-transfer pathway proceeds through the double helix, these results indicate exceptionally efficient charge transport through DNA, and imply that the rate-determining step may be tunneling through the σ-bonded linker. Such a shallow distance
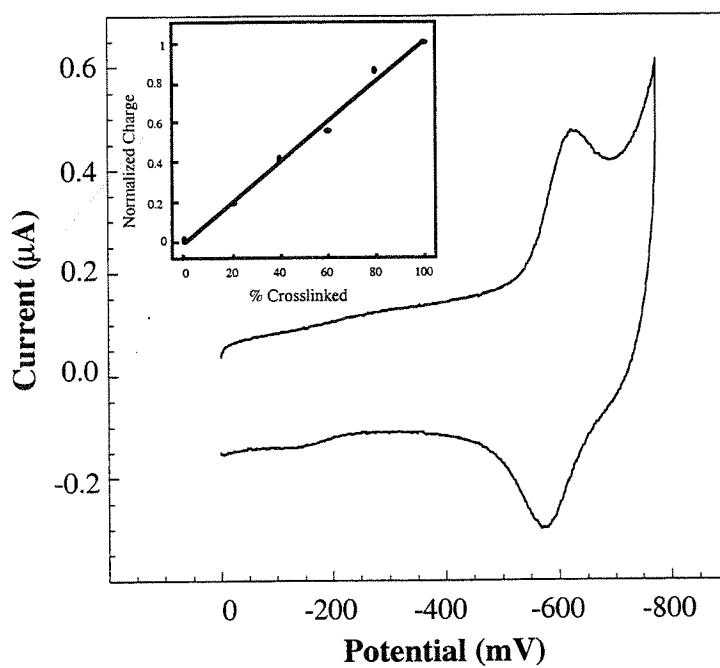
Figure 6.4 Cyclic voltammogram of DM-duplex immobilized on gold surface: $\nu = 100$ mV/s, A = 0.02 cm^2, sequence: SH-5'-ATAATATGCATTA. (inset) Variation in electrochemical response depending on ratio of DM-crosslinked duplexes:unmodified duplexes.
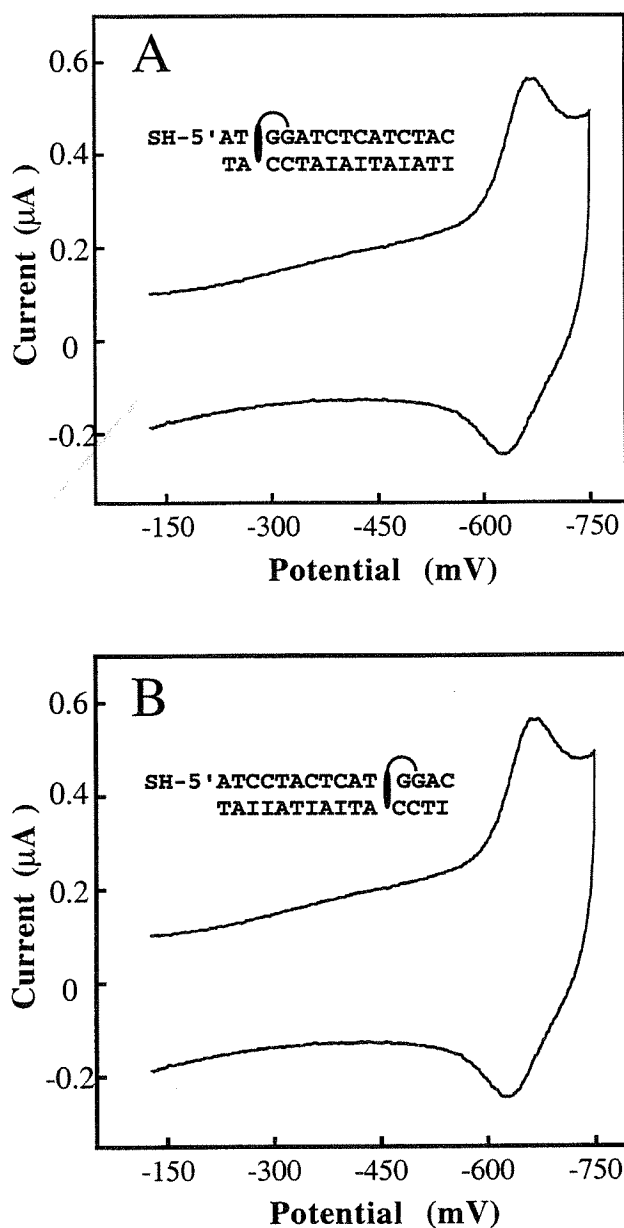
Figure 6.5 Cyclic voltammetry of gold electrodes modified with DM-crosslinked duplexes (**A**) SH-5'-AT**GG**ATCTCATCTAC + complement and (**B**) SH-5'-ATCCTACTCAT**GG**AC + complement, where the bold Gs represent the DM crosslinking site. ν = 100 mV/s; A = 0.02 cm^2.
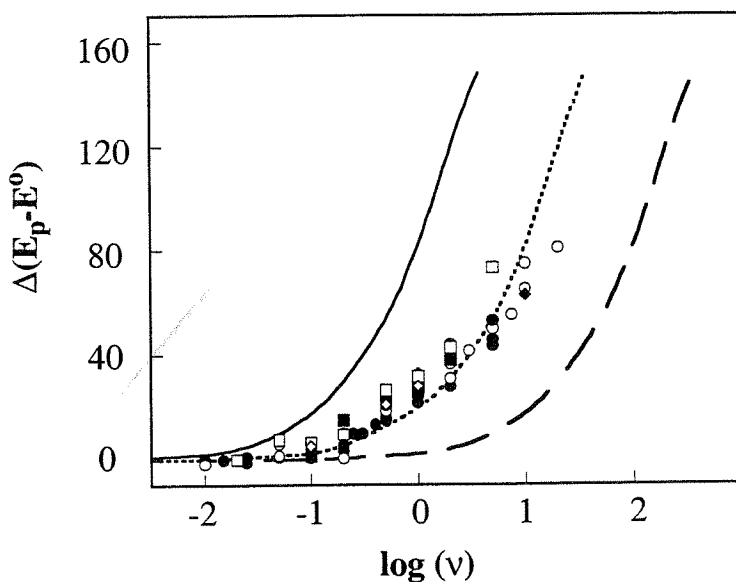
Figure 6.6 Plot of peak splitting ($\Delta E_{pc} = E_{pc} - E_o$) versus log($v$).

Measurements were obtained on the following sets of duplexes:

(●) SH-5'ATGGATCTCATCTAC (+ inosine complement),

(○) SH-5'ATCCTACTCATGGAC (+ inosine complement),

(▲) SH-5'GCATTATATAATTA (+ complement),

(□) SH-5'ATATGCTATAATTA (+ complement),

(◆) SH-5'ATTATATAGCATTA + complement,

(■) SH-5'ATTATATAATTGCT (+ complement).

For comparison, theoretical fits[10] corresponding to rate constants of 10 s^{-1} (solid line), 100 s^{-1} (dotted line), and 1000 s^{-1} (dashed line) are shown.

dependence through the base-pair stack would be consistent with the results of photoinduced electron transfer between intercalators or other well-stacked species[3-4] but is in sharp contrast to other studies of DNA-mediated electron transfer that report values for β (the decay of electronic coupling with distance)[16] ranging from 0.6 - 1.4 $\mathring{A}^{-1}$.[17] For example, a β value of 1.4 $\mathring{A}^{-1}$ would imply that the rate of electron transfer should drop by more than 15 orders of magnitude between the two sequences shown in Figure 6.5. Similarly, if β were 0.6 $\mathring{A}^{-1}$, these rates would differ by > 6 orders of magnitude. Clearly, these large changes would be easily resolved in our experiment. A β value of ~ 0.1 $\mathring{A}^{-1}$ would yield only one order of magnitude difference in the rates for these two assemblies, which may not be detectable by our analysis.

6.3.3 Effect of mismatches on the long-range reduction of daunomycin

Could an alternative gating mechanism be responsible for the lack of distance dependence observed in these experiments? We considered dynamical processes[18] that might bring the intercalated DM into direct contact with the metal surface, as well as diffusional mechanisms in which the charge might propagate laterally throughout the film from local "hot spots" (*e.g.*, defect sites) where the DM is close contact with electrode. To differentiate between these possibilities, we constructed a series of films featuring subtle intervening perturbations in the base stacks of the individual helices. A through-helix pathway should therefore result in significantly attenuated rates of electron transfer to the DM, whereas as dynamical or diffusional mechanisms would yield rates that were largely unaffected.

To accomplish this, a single site within the 15-base-pair duplex was mutated to produce a CA mismatch between the intercalated daunomycin and the electrode surface. CA mismatches are known to cause only local disruptions in the DNA base stack while remaining intrahelical,[19] yet have been shown to decrease the yield of photoinduced electron transfer through DNA.[1,20] Indeed, this one-base change in the duplex virtually

switched off the electrochemical response entirely (Figure 6.7). Significantly, sequences in which the positions of the daunomycin and CA mismatch were reversed (such that the mismatch was located above the daunomycin relative to the gold) showed no diminution in the electrochemical response. AFM measurements revealed monolayer thicknesses of ~ 40 Å at open circuit for both CA and TA containing duplexes; moreover the oxidation of ferrocyanide was similarly attenuated at both surfaces. Expected masses for daunomycin-crosslinked DNA duplexes (accounting for the one base change) were measured by mass spectrometry, and spectrophotometric assays revealed that the extent of crosslinking was identical in both fully paired and mismatched sequences.

To test for lateral charge propagation through these films, a series of monolayers were doped with increasing fractions of CA-mismatched helices: in all cases, the electrochemical signals decreased linearly with increasing percentages of mutated duplexes. This linear response indicates that electro*inactive* intercalators (presumably those molecules bound to the mismatched duplexes) are not reduced by the electro*active* species, as lateral charge diffusion is evidently very efficient.

The observation of an attenuated electrochemical response in the presence of a point mutation strongly implicates the stacked bases as the pathway for electron transfer displaying such a weak distance dependence. Moreover, we have demonstrated that point mutations may be detected based on DNA-mediated charge transport at a derivatized surface, an important finding for the development of DNA biosensors.

6.3.4 Mismatch detection based on charge transduction through DNA using non-covalently bound probes

In order to develop a general approach to test heterogeneous sequences that may possess more than one guanine-binding site, we investigated the electrochemistry of DM non-covalently intercalated into DNA-modified films. Coulometric titrations confirmed
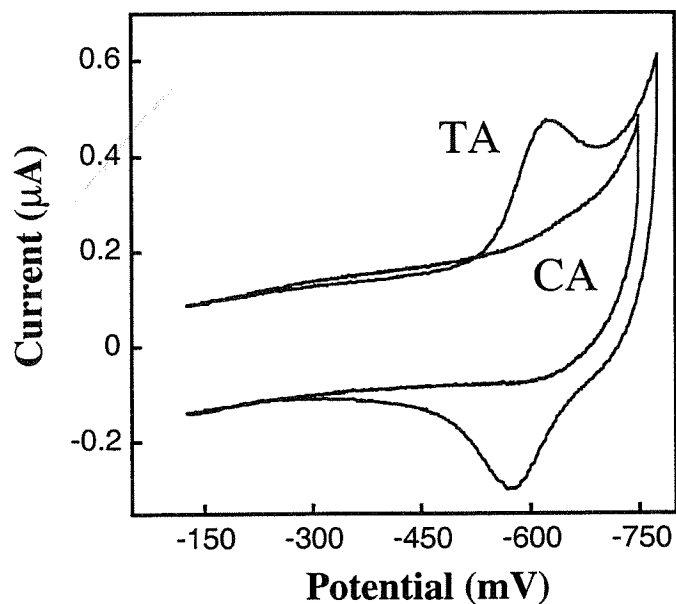
Figure 6.7 Cyclic voltammetry of gold electrodes modified with the DM-crosslinked thiol-terminated duplexes containing an intervening matched TA or unmatched CA base pair. Sequence: SH- 5'-ATTAT*A*TAATTGCT where complement contains either a T or a C opposite from the italicized A.

that DM strongly binds to surfaces modified with fully base-paired duplexes, and yielded affinity constants very similar to those determined for homogeneous solutions. At bulk DM concentrations ≥ 1 µM, the modified electrodes are saturated with intercalator, and hold approximately one intercalator per surface-confined duplex. In accord with the studies of covalently bound DM, incorporation of a single CA mismatch into these duplexes dramatically decreases the electrochemical response (Figure 6.8). Interestingly, the magnitude of this mismatch effect depends strongly on the location of the CA base step along the sequence: when the mutation is buried deep within the monolayer, the measured charge drops by a factor of 3.5(5) (relative to the Watson-Crick duplex), but by only 2.3(4) when it is located near the solvent-exposed terminus. These observations are consistent with DM occupying sites near the top of the densely packed monolayer, as suggested in earlier studies of methylene blue bound to these same surfaces.[8] The intensity of the electrochemical signals therefore not only reports the presence of the mismatch but also may describe the location of the disruption.

The fact that electrochemical signals are observed at all for DM non-covalently bound to mutated-DNA films may suggest that a fraction of the intercalator diffuses into the monolayer beneath the mismatch. This explanation would account for the dependence of these small responses on the position of the mismatch within the film.

Variation in mismatch composition. To explore the scope of this mismatch detection strategy, a series of different mutations was tested (Table 6.1). Coulometric analysis confirmed that the attenuation of the response was strongly dependent upon the identity of the mutation. In general, pyrimidine-pyrimidine and purine-pyrimidine mismatches caused marked decreases in the electrochemical signals; the one purine-purine pair studied (a GA mismatch, which is notoriously well-stacked within duplex DNA)[19] did not show a measurable effect. Surprisingly, a significant decrease was caused by a GT pair, which is not highly disruptive to the helix. This wobble base pair,
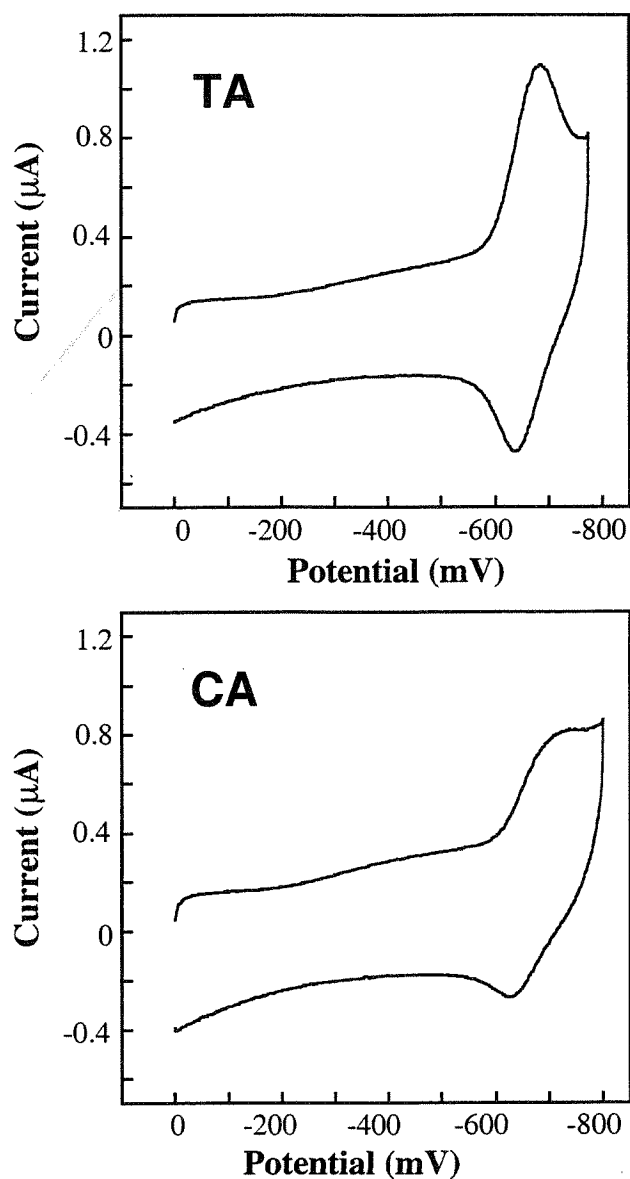
Figure 6.8 Cyclic voltammograms of 1.0 µM DM bound to DNA-modified

electrodes derivatized with the sequence SH-5'-AGTACAGTCATCGCG

where either a T (TA) or a C (CA) was paired with the A indicated in bold.

Voltammograms were obtained with v = 100 mV/s, A = 0.02 cm^2 in 100 mM

sodium phosphate buffer, pH 7.

Table 6.1 Electrochemical detection of base mismatches

	$Q_{c(int)}$ (nC)[b]	T_m (°C)[c]
SH–5'-AGTACAGTCATCGCG TCATGTCAGTAGCGC	165(37)	68
SH–5'-AGTACAGT**CAT**CGCG TCATGTCAG**C**AGCGC	56(15)	56
SH–5'-AGTACAG**T**CATCGCG TCATGTC**T**GTAGCGC	95(18)	57
SH–5'-AGTACAGT**C**ATCGCG TCATGTCA**CT**AGCGC	51(23)	56
SH–5'-AGTACAG**T**CATCGCG TCATGTC**GG**TAGCGC	49(30)	62
SH–5'-AGTACA**G**TCATCGCG TCATGT**AA**GTAGCGC	153(38)	60
SH–5'-AGTACAG**T**CATCGCG TCATGTC**C**GTAGCGC	93(17)	58

[a]Based on cyclic voltammograms measured for 1.0 μM daunomycin noncovalently bound to duplex-modified electrodes (0.1 M phosphate buffer, pH 7). Values are based on > 5 trials each, and results were comparable for experiments run side-by side, or from different sample preparation as long as electrodes exhibited high surface coverages. Electrodes with lower surface coverages yielded higher charges (> 1 DM/duplex), and decreased attenuations in the presence of mismatches. [b]Integrated background-subtracted cathodic charge. [c]Measured by monitoring duplex hypochromicity at 260 nm. Samples contained 10 μM duplex, 100 mM MgCl$_2$, 100 mM phosphate, pH 7.

although thermodynamically stable, appears to mediate electron transfer poorly. It is noteworthy that across a very narrow range of duplex thermal stabilities, large differences in the electrochemical response are observed: this assay is not hybridization-based. Overall, the electrochemical properties of films that possess the different mismatches appear to correlate with the degree of disruption to base stacking within the individual duplexes.

Variation in sequence composition. Importantly, this effect appears to be independent of DNA sequence and composition. As shown in Figure 6.9, the characteristic drop in coulometric signals for DNAs containing a single CA mismatch compared to fully-paired DNA films was essentially *invariant* across AT-rich to GC-rich sequences. A sequence-independent response is not achievable based upon differential hybridization. Indeed, as no special manipulation of conditions or sequence-dependent algorithms is required for detection, this feature highlights a unique and valuable aspect of the charge-transport methodology. These results underscore the sensitivity of this electrochemical assay to base stacking within DNA, and demonstrate the viability of detecting mismatches based upon charge transduction through thin films.

In situ detection. To extend this methodology to single-stranded targets, techniques for *in situ* hybridization were developed. Thiol-modified duplexes were deposited on the gold surface, heat denatured, thoroughly rinsed, then rehybridized with the desired target by incubation in ≥ 50 pmol of single-stranded oligonucleotide. The electrochemical properties of the resulting surfaces were identical to those described above, suggesting the suitability of this system for genomic testing.

To illustrate this approach, a 15 base-pair oligonucleotide was derivatized with a thiol-terminated linker, then hybridized both to its native complement and to a mutated complement that resulted in a CA mismatch (Figure 6.10). These duplexes were deposited on separate electrodes, at which DM exhibited electrochemical responses characteristic of fully base-paired and CA-mutated films, respectively. The surfaces were
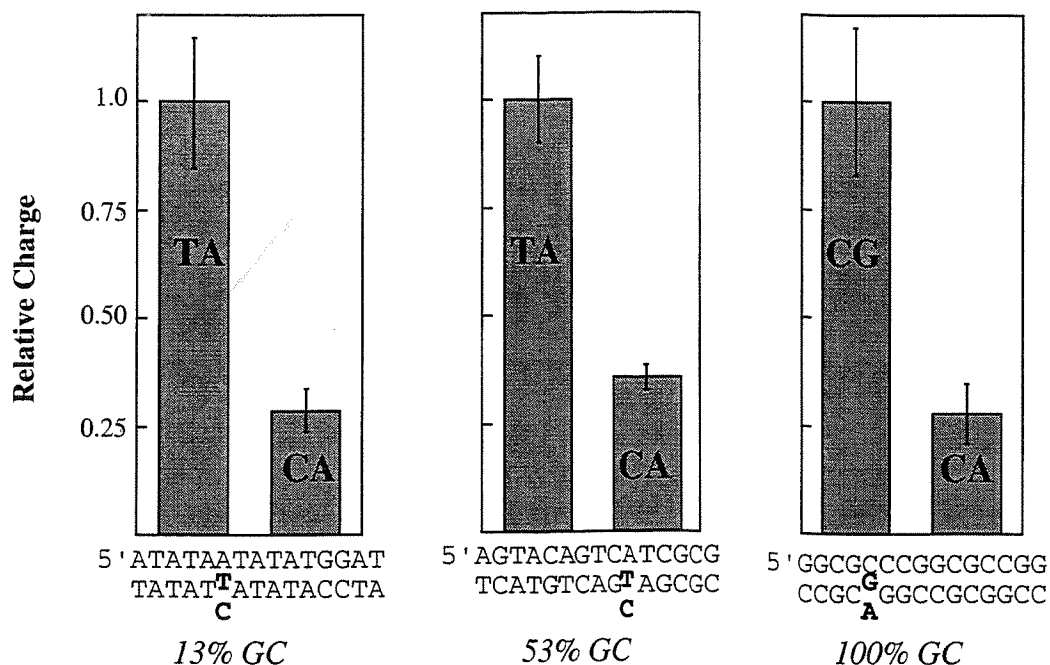
Figure 6.9 Charge obtained for DNA-modified electrodes in the presence of 1.0 µM DM. These duplexes, featuring varying percentages of GC content, were either fully base paired or contained a single CA mismatch. The melting temperatures for these duplexes, as determined by thermal denaturation measurements obtained for solutions containing 10 µM duplex, 100 mM sodium phosphate, and 100 mM $MgCl_2$ were (SH-5'ATATAATATATGGAT): TA = 47°C, CA = 32°C; (SH-5'AGTACAGTCATCGCG): TA = 68°C, CA = 56°C; (SH-5'GGCGCCCGGCGCCGG): GC = 82°C, CA = 69°C. Charge was quantitated from integrating background-subtracted cyclic voltammograms obtained at v = 100 mV/s and was corrected for electrode area.

209
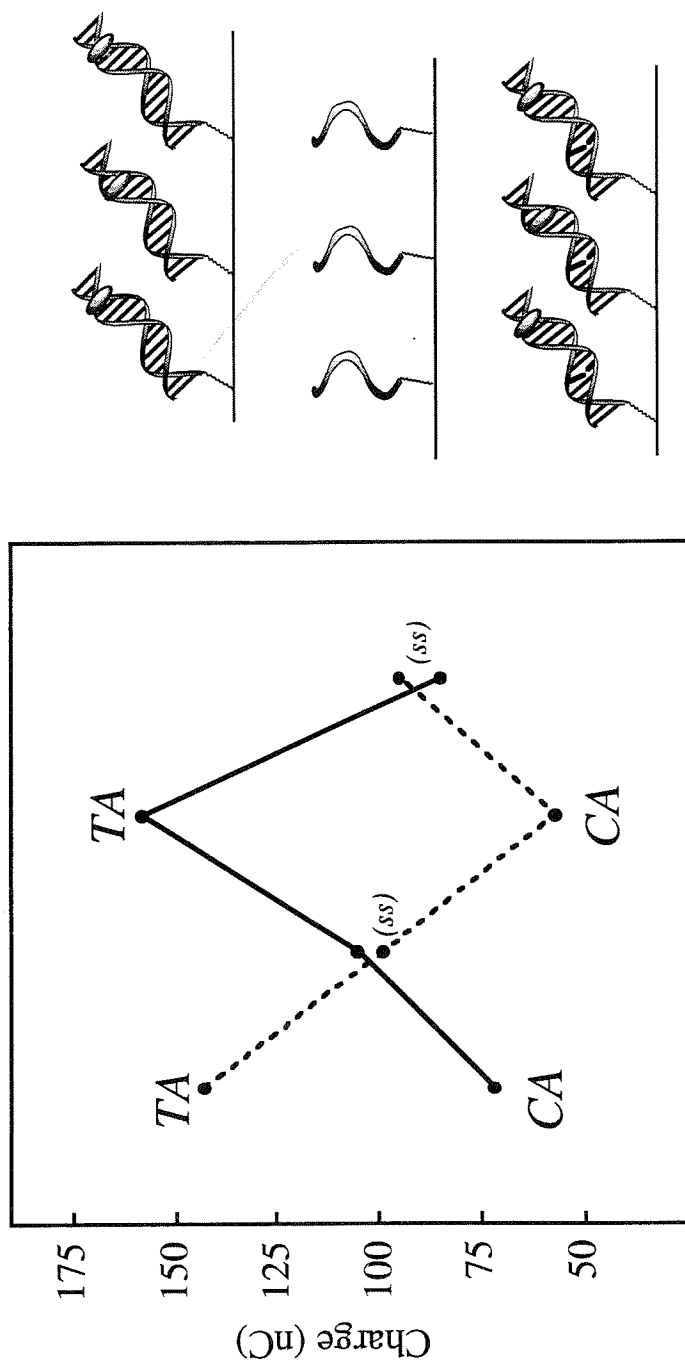
Figure 6.10 Charges (Q_C) measured during the *in situ* detection of a CA mismatch. Electrodes were derivatized with sequence SH-5'-AGTACAGTCATCGCG, where either a C or T was incorporated into the complement across from the italicized A. Using cyclic voltammetry ($v = 100$ mV/s, 1.0 μM DM), the electrochemical response of daunomycin non-covalently bound to duplex-modified electrodes was first measured for the intact TA- or CA-containing duplexes (*TA/CA*), then the electrodes were immersed in buffer at 90°C for 2 minutes, rinsed, and the charge was remeasured (*ss*). The electrodes were then incubated with 100 pmol of the opposite complement in the presence of buffered 100 mM MgCl$_2$, and the charge was again remeasured. Finally, electrodes were again heated and the response was quantitated. This detection limit is for a 1 hour hybridization period performed in the presence of 200 mM NaCl.

then denatured to yield single-stranded monolayers of identical sequence. Cyclic voltammetry of DM at these electrodes now revealed nearly identical responses, with the reduction appearing highly irreversible, broadened, and becoming smaller as a function of increasing scans. This may reflect the surface heterogeneity of electrodes containing disordered single strands. Importantly, the electrode that initially possessed the CA mismatch displayed a larger signal (for the first scan) after denaturation, while the reverse was true for the corresponding TA analog. New duplexes were formed where the complements were traded (TA → CA , CA → TA), and the electrochemistry at the duplex-modified films again showed the characteristic behavior expected for fully base-paired and CA-mutated films. Electrodes can be cycled through this sequence of events repeatedly, suggesting a practical means to detect point mutations within natural DNAs.

We have therefore demonstrated long-range charge transport through DNA-modified films, and have exploited this phenomenon in developing a mismatch sensor. The recent discovery of conductivity along the base-stacking direction of oriented DNA films, and now the observation of long-range electron transfer to a ground-state intercalated species, provide evidence that the DNA base stack may exhibit "wire-like" behavior. [21] The nature of DNA as an electron-transfer medium has been the subject of intense debate,[22] and the extent of charge delocalization within DNA has profound biological implications.[23] As shown here, this phenomenon and its sensitivity to base stacking can now be applied to the advance of biosensing technology. The characteristics of DNA-mediated electron transfer provide the basis for recognizing subtle changes within the genetic information stored within the double helix.

6.4 REFERENCES

1.   Skogerboe, K.J. *Anal. Chem.* **1993** *65*, 416; Southern, E.M. *Trends in Genetics* **1996**, *12*, 110.

2.   Chee, M.; Yang, R.; Hubbell, E.; Berno, A; Huang, X.C.; Stern, D.; Winkler, J.; Lockhart, D.J.; Morris, M.S.; Fodor, S.P.A. *Science* **1996**, *274*, 610; Eng, C.; Vijg, J. *Nat. Biotech.* **1997**, *15*, 422.

3.   Kelley, S.O.; Barton, J.K. *Chem. & Biol.* **1998**, *5*, 413; Kelley, S.O.; Barton, J.K. *submitted*, **1998**; Kelley, S.O.; Holmlin, R.E.; Stemp, E.D.A; Barton, J.K. *J. Am. Chem. Soc.* **1997**, *119*, 9861.

4.   Murphy, C. J.; Arkin, M. A.; Jenkins, Y.; Ghatlia, N. D.; Bossman, S.; Turro, N. J.; Barton, J.K. *Science* **1993**, *262*, 1025; Murphy, C.J.; Arkin, M.A.; Ghatlia, N.D.; Bossman, S.; Turro, N.J.; Barton, J.K. *Proc. Natl. Acad. Sci. U.S.A.* **1994**, *91*, 5315; Holmlin, R.E.; Stemp, E.D.A.; Barton, J.K. *J. Am. Chem. Soc.* **1996**, *118*, 5236; Arkin, M.R.; Stemp, E.D.A.; Holmlin, R.E.; Barton, J.K.; Hörmann, A.; Olson, E.J.C.; Barbara, P.A. *Science* **1996**, *273*, 475.

5.   Hall, D.B.; Holmlin, R.E.; Barton, J.K. *Nature* **1996**, *382*, 731; Hall, D.B.; Barton, J.K *J. Am. Chem. Soc.* **1997**, *119*, 5045.

6.   Arkin, M.R.; Stemp, E.D.A.; Barton, J.K. *Chem. & Biol.* **1997**, *4*, 389.

7.   Dandliker, P.J., Holmlin, R.E.; Barton, J.K. *Science* **1997**, *275*, 1465.

8.   Kelley, S.O.; Barton, J.K.; Jackson, N.M.; Hill, M.G. *Bioconj. Chem.* **1997**, *8*, 31.

9.   Kelley, S.O.; Barton, J.K.; Jackson, N.M.; McPherson, L.; Potter, A.; Spain, E.M.; Allen, M.J.; Hill, M.G. *Langmuir, in press*.

10.   Tender, L.; Carter, M.T.; Murray, R.W. *Anal. Chem.* **1994**, *66*, 3173.

11.   Arcamone, F., *Doxorubicin: Anticancer Antibiotics*, Academic Press, New York (1981).

12. Molinier-Jumel, C.; Malfoy, B.; Reynaud, J.A.; Aubel-Sadron, G. *Biochem. Biophys. Res. Comm.* **1997**, *84*, 441; Berg, H.; Horn, G.; Luthardt, U. *Bioelectrochem. Bioenerg.* **1981**, *8*, 537.

13. Leng, F.; Savkur, R.; Fokt, I.; Przewloka, T.; Priebe, W.; Chaires, J.B. *J. Am. Chem. Soc.* **1996**, *118*, 4732.

14. Wang, A.H.-J.; Gao, Y.-G.; Liaw, Y.-C.; Li, Y.-K. *Biochemistry* **1991**, *30*, 3812.

15. Bard, A.J.; Faulkner, L.R. *Electrochemical Methods,* Wiley and Sons, New York (1980).

16. Marcus, R.A.; Sutin, N. *Biochim. Biophys. Acta* **1985**, *811*, 265.

17. Meade, T. J.; Kayyem, J. F. *Angew. Chem. Int. Ed. Engl.* **1995**, *34*, 352; Lewis, F.D.; Wu, Taifeng; Zhang, Y.; Letsinger, R.L.; Greenfield, S.R.; Wasielewski, M.R. *Science* **1997**, *277*, 673; Fukui, K.; Tanaka, K. *Angew. Chem. Int. Ed.* **1998**, *37*, 158.

18. Feng, Z.Q.; Imabayashi, S.; Kakiuchi, T.; Niki, K. *J. Electroanal. Chem.* **1995**, *394*, 149.

19. Patel, D.J.; Kozlowski, S.A.; Ikuta, S.; Itakura, K. *FASEB* **1984**, *11*, 2664.

20. Ihara, T.; Takata, J.; Takagi, H. *Anal. Chim. Acta* **1998**, *365*, 49.

21. Okahata, Y.; Kobayashi, T.; Tanaka, K.; Shimomura, M. *J. Am. Chem. Soc.* **1998**, *120*, 6165.

22. Priyadarshy, S.; Risser, S.M.; Beratan, D.N. *J. Phys. Chem.* **1996**, *100*, 17678; Netzel, T.L. *J. Chem. Educ.* **1997**, *74*, 646.

23. Szent-Györgyi, A. *Nature* **1941**, *148*, 157.

Chapter 7

Summary and Outlook:
Sensitivity of DNA-Mediated Electron Transfer to
Distance, Sequence, Energetics, and Stacking

The possibility of efficient DNA-mediated charge transport has been debated essentially since the discovery of the double helix. For almost forty years, a diverse group of scientists, drawing upon the methods of physics, chemistry, and biology, have sought to understand the electronic structure of the DNA base stack. Interestingly, in almost every series of studies within a given discipline, conflicting assessments of the efficiency of charge transport have been obtained. As a consequence, DNA has been classified as both an insulator and a molecular wire. The challenge of understanding the properties of this material was therefore an ideal task for chemists, as it was clear that well-defined systems and unambiguous experiments were required to understand this phenomenon.

We first obtained intriguing results indicating that fast electron transfer could be mediated by the double helix in studies utilizing metallointercalators noncovalently bound to DNA.[1-2] These experiments hinted that subnanosecond electron transfer could occur over significant molecular distances, but the proposal that cooperative clustering[3] gave rise to these fast kinetics made a more well-defined system necessary for this notion to be given serious consideration. Synthesizing large quantities of duplexes containing two tethered metallointercalators proved difficult, thus we turned our attention towards finding other donors and acceptors more amenable to derivatization.

As described in this thesis, we have gained insight into the dependence of DNA-mediated electron-transfer reactions on distance, sequence, stacking, and energetics using organic intercalators and modified bases in conjunction with both spectroscopic and electrochemical methods. The following is a summary of the results obtained in terms of parameters that have been identified through this work as being important in modulating DNA-mediated electron transfer.

Distance. By employing new synthetic methodologies and exploring reactants other than intercalators, we have now obtained distance dependences for a variety of

electron-transfer reactions proceeding through the DNA helix. The most striking aspect of this collection of results is that *different distance dependences are measured for every system studied.* While it is expected that the measurement of electron transfer through one medium should yield a single distance dependence, we have now measured several which differ by a full order of magnitude. Our early studies provided evidence for a very weak sensitivity to distance,[4] but when these results were compared to much more pronounced, "protein-like" distance dependences, our observations were often dismissed as resulting from misinterpreted data. However, now that we have now been able to systematically vary parameters *other* than distance, we find that different dependences on donor/acceptor separation can be obtained in chemically identical systems that differ only in the *stacking or energetics of reactants.* Hence, it becomes clear that the DNA helix can exhibit behavior ranging from that of an insulator to a "molecular wire." This variability has intriguing implications for biological mechanisms that might limit access to this pathway *in vivo.*

Sequence. In considering the DNA helix as a medium for electron transfer, the presence of four different monomers within the π-stacked interior leads to questions concerning the sensitivity of electron transfer through this medium to sequence composition. Although we have not yet measured the difference in dynamics for electron transfer through an A-T as compared to a G-C base pair, we have observed that flanking sequence impacts the thermodynamic properties of a reactant incorporated within the base stack.[5] Indeed, as also discovered in studies of chemical oxidation reactions of the DNA bases,[6-7] sequence context strongly modulates the oxidation potential of a given site. This effect highlights the significant interactions between adjacent base steps, and may provide Nature with a means of concentrating base damage at thermodynamic sinks to simplify repair mechanisms.

Energetics. We identified that sequence effects could modulate the efficiency of DNA-mediated electron transfer as reflected in measures of the reaction efficiency. In studies where we could systematically vary energetics by employing two base analogues with slightly different potentials,[8] we determined that this factor not only governs the efficiency of a reaction at a given distance, but also affects the overall distance dependence. This observation indicated that these DNA-mediated reactions proceed in a different regime than the nonadiabatic, superexchange-dominated reactions monitored in σ-bonded systems. Here, as the available orbitals on the bridging aromatic DNA bases are much lower than those of aliphatic systems, reactions proceeding through the DNA base stack may operate through a regime with a low tunnelling barrier. Over the past few years, theoretical predictions of strong, energy-gap dependent coupling in low tunnelling barrier systems have been presented,[9] but the first experimental demonstration of the importance of this parameter only appeared very recently.[10] Hence, besides providing important insight into the factors modulating DNA-mediated electron transfer, these studies provide some of the first empirical evidence of this energetic regime.

Although reactant energetics may affect the overall efficiency of a given reaction, they cannot solely account for all of our observations and the disparate results reported in the literature. There are numerous examples of low tunelling energy systems with steep distance dependences,[11] and the electrochemically-intitated reactions of ground-state species also proceed over long distances through the double helix.[12] It is therefore clear that another parameter must dominate reactivity in DNA.

Stacking. In every system we have investigated, we obtained strong evidence that the behavior of the DNA helix as a bridge and reactant in electron-transfer processes is contingent upon stacking interactions within this structure. Base mismatches within the DNA base stack strongly attenuate the efficiency of reactions between donors and acceptors coupled through this medium.[13] The incorporation of reactants within base

mismatches also causes dramatic decreases in electron-transfer yields.[5] The observation of a proportion of unquenched reactants in many of our systems led us to propose that base dynamics within the double helix lead to a finite population of properly stacked duplexes that can facilitate ultrafast electron transfer.[5,13] However, the effect of stacking is most profoundly exhibited in the overall distance dependence of DNA-mediated reactions. Reactants within flanking sequences composed of varying proportions of purines and pyrimidines exhibit different distances trends, with a more shallow dependence observed for a site where stronger stacking interactions would be predicted.[5] Even more striking is the example of electron-transfer reactions in two analogous sets of duplex assemblies differing only in the stacking of the acceptor (as deduced from NMR structures) where distance dependences differing by a full order of magnitude are observed.[8] These results underscore that the stacking interactions of reactants with the DNA bases is critical for access to a pathway facilitating remarkably fast, long-range electron transfer. Moreover, studies reported in the literature revealing different distance dependences can be reconciled within this context, as systems employing reactants that do not interact strongly with the base stack tend to exhibit the most pronounced sensitivity to distance.[11,14]

Outlook. The studies described in this thesis have qualitatively identified parameters important in understanding DNA as a medium for electron transfer. However, a great deal of further investigation will be required to quantitate the effects described above and to establish the mechanism of these reactions. The capability to monitor electron transfer dynamics on ultrafast timescales will provide an important tool in delineating systematic trends. Moreover, the further variation of temperature and sequence will provide information essential in determining the mechanistic pathway of DNA-mediated electron transfer reactions and elucidating the relationship between base dynamics and reaction kinetics.

We have exploited the weak sensitivity of electron transfer through DNA to distance and the strong sensitivity of this phenomenon to base stacking to develop an approach applicable in DNA-based biosensors. Our charge-transport based method differs dramatically from any current available, and should provide a powerful tool in the detection of deleterious genomic mutations. The challenges ahead in this area include the investigation of our detection strategy at microelectrode arrays, and the detection of point mutations within heterogeneous biological samples.

The past five years of research in this area have included a renaissance in the development of new techniques and systems to monitor charge transport through the DNA helix. Biochemical assays monitoring the products of chemical reactions effected by long-range electron transfer have strengthened the connection between this area of research and biological function.[6-7] Recent experimental accomplishments, and the emergence of unifying explanations for previous conflicting results, may soon propel this field out of a period hampered by controversy towards creative assessment of the fundamental and biological ramifications of the finding that efficient electron transport proceeds through the interior of one of the most essential biological materials

Since the established biological function of DNA involves the transmission of information based upon the structural characteristics of the DNA bases within the double helix, we might now imagine that this function might be influenced also by the electronic properties of these stacked bases. Could nature access the pathway for electron transport through DNA for the communication of information? Moreover, just as we can so accurately detect the presence of base mismatches by the attenuation of electron transfer, might mutagenic changes in the genomic code be identified in this manner *in vivo*? The questions now presented are endless.

References

1. Murphy, C.J.; Arkin, M.A.; Ghatlia, N.D.; Bossman, S.; Turro, N.J.; Barton, J.K. *Proc. Natl. Acad. Sci. U.S.A.* **1994**, *91*, 5315.

2. Arkin, M.R.; Stemp, E.D.A.; Holmlin, R.E.; Barton, J.K.; Hörmann, A.; Olson, E.J.C.; Barbara, P.A. *Science* **1996**, *273*, 475.

3. (a) Olson, E.J.C.; Hu, D.; Hörmann, A.; Barbara, P.F. *J. Phys. Chem.,* **1997** *101*, 299; (b) Lincoln, P.; Tuite, E.; Norden, B. *J. Am. Chem. Soc.,* **1997** *119*, 1454.

4. Murphy, C. J.; Arkin, M. A.; Jenkins, Y.; Ghatlia, N. D.; Bossman, S.; Turro, N. J.; Barton, J.K. *Science* **1993**, *262*, 1025.

5. Kelley, S.O.; Barton, J.K. *Chem. Biol.* **1998**, *8*, 413.

6. Hall, D.B.; Holmlin, R.E.; Barton, J.K. *Nature,* **1996**, *382*, 731.

7. Arkin, M.R.; Stemp, E.D.A.; Barton, J.K. *Chem. & Biol.,* **1997**, *4*, 389.

8. Kelley, S.O.; Barton, J.K. *Science* **1998**, *in press.*

9. (a) Reimers, J.R.; Hush, N.S. *J. Photochem. Photobiol. A: Chem.* **1994**, *82*, 31; (b) Evenson, J.W.; Karplus, M. *Science* **1993**, *262*, 1247.

10. Davis, W.B.; Svec, W.A.; Ratner, M.A.; Wasielewski, M.R. *Nature* **1998**, *396*, 60.

11. (a) Lewis, F.D.; Wu, Taifeng; Zhang, Y.; Letsinger, R.L.; Greenfield, S.R.; Wasielewski, M.R. *Science* **1997**, *277*, 673; (b) Fukui, K.; Tanaka, K. *Angew. Chem. Int. Ed.* **1998**, *37*, 158.

12. Kelley, S.O.; Jackson, N.J.; Hill, M.G.; Barton, J.K. *Angew. Chem.* **1998**, *in press.*

13. Kelley, S.O.; Holmlin, R.E.; Stemp, E.D.A; Barton, J.K. *J. Am. Chem. Soc.* **1998**, *119*, 9861.

14. Meade, T. J.; Kayyem, J. F. *Angew. Chem. Int. Ed. Engl.* **1995**, *34*, 352.